Pinned, Driven and Confined Colloidal Supercooled Liquids and Glasses

A Thesis
Submitted for the Degree of
Doctor of Philosophy

by

K Hima Nagamanasa

Chemistry and Physics of Materials Unit
Jawaharlal Nehru Centre for Advanced Scientific Research
(A Deemed University)
Bangalore – 560 064

MARCH 2015

Dedicated to my parents

DECLARATION

I hereby declare that the matter embodied in the thesis entitled "**Pinned, Driven and Confined Colloidal Supercooled Liquids and Glasses** " is the result of investigations carried out by me at the Chemistry and Physics of Materials Unit, Jawaharlal Nehru Centre for Advanced Scientific Research, Bangalore, India under the supervision of **Dr. Rajesh Ganapathy** and that it has not been submitted elsewhere for the award of any degree or diploma.

In keeping with the general practice in reporting scientific observations, due acknowledgment has been made whenever the work described is based on the findings of other investigators. Any omission that might have occurred by oversight or error of judgement is regretted.

K Hima Nagamanasa

CERTIFICATE

I hereby certify that the matter embodied in this thesis entitled "**Pinned, Driven and Confined Colloidal Supercooled Liquids and Glasses** " has been carried out by **Ms. K Hima Nagamanasa** at the Chemistry and Physics of Materials Unit, Jawaharlal Nehru Centre for Advanced Scientific Research, Bangalore, India under my supervision and that it has not been submitted elsewhere for the award of any degree or diploma.

Dr. Rajesh Ganapathy
(Research Supervisor)

Acknowledgements

While this thesis is an outcome of the scientific pursuit of a few people over the last five years, in reality there are many more who contributed to it indirectly. I am grateful for this opportunity to thank all the people without whom this thesis would have not been possible.

Needless to say, I am thankful to my parents for their unflinching support for all my decisions and for nurturing my dreams and ambitions. My happiest moments have been to see pride in their eyes for every accomplishment of mine.

I would like to express my deepest gratitude to my advisor Dr. Rajesh Ganapathy for his guidance and encouragement all through my PhD. Although I was naively trained for experiments during my graduation days, I learned to think, plan and execute an idea from him. Being the first student I got an opportunity to learn experimental techniques first hand from him. I can still remember those days when I was not very comfortable in handling sophisticated instruments all by myself, he used to come in the middle of the night to help me whenever I encountered a problem. The most important thing I have learned in due course of my PhD from him is to be the most severe critique of your own work. Working with Rajesh has also provided me a wonderful opportunity to work in close collaboration with one of the eminent scientists, Prof. Ajay K Sood (IISc, Bangalore). The discussion meetings with Sood sir are always scientifically enriching and cherishing. Most of the times I used to be astonished by his knowledge about vastly different subjects and the connections he makes between disparate topics of condensed matter physics.

I express my thanks to Prof. C. N. R Rao, FRS, for providing excellent research facilities and for being a constant source of inspiration. I would like to thank Prof. Balasubramanian and Prof. Kulkarni, present and past chairmen of CPMU. I thank Prof. Rahul Pandit (IISc, Bangalore), Prof. Santosh Anshumali (EMU), and Prof. Shobhana Narasimhan (TSU) for their guidance during the course work. I am also thankful to Prof. Srikanth Sastry (TSU) for his stimulating discussions. I am also thankful to Mr. Sharrif (IISc, Bangalore) and Mr. Arokianathan for helping me in fabricating desings vital for my experiments as and when needed.

Throughout my PhD, I worked in close collaboration with Shreyas Gokhale (IISc, Bangalore). The scientific discussions and his sound theoretical understanding are something which I am going to miss the most. He is one of the best examples of how well planned we ought to be in our pursuit of science.

One of the projects with confocal-rheometer was solely possible because of V. Santosh and his ingenuity in instrumentation. Though I spent only an year with him in the lab, the moments spent are always cherishing. He is simplicity personified in true sense. I owe a lot to my other lab mates Chandan, Srishti, Amritha and Neelima. This thesis would not have seen the light of the day without their support and encouragement. They provided me a perfect atmosphere to work in the lab. It does not mean that we did not have fun. During the time when me, Chandan, Srishti and Amritha were around, we used to dine outside frequently (now I realize where all my stipend went!) ans such outings were always refreshing and recharging. The love and affection I got from Srishti was what one would expect from a younger sister. Very few people know me the way Chandan does. He would look at my face and predict what's going on in my mind. Of course there were times when we would argue for silly things and go on without talking to each other for a couple of days, and then we would realize we were being stupid! Needless to say, how much I have learned from our scientific discussions. I am also thankful to my other lab mates Mamtha, Vikram, Rajiv, Dibyashree, Divya, Rakul, Jyoti, Krishna, Aishwarya and Pawan.

Apart from my labmates, I am also grateful to find two very good friends Shiwani and Garima at JNC. I always knew that I need not think twice before sharing anything with Shiwani. I know a very few people who can be as hard working as Garima. Both of them stood with me throughout my stay at JNC, in all my highs and lows (esp. lows). Since all three of us were from different branches of science, I also got an oppurtunity to learn new things from them. One thing which I will miss the most is Sunday morning tea where we used to disccuss about each others work and of course gossip about all other nonsensical things as well.

It is not only the Sunday morning tea that I will miss, but also everyday evening tea with Ashvini, Shiny, Palak, Shiwani, Garima, Chandan, Srishti and Amritha. During this time, we used to acquaint ourselves with the latest gossips of JNC. Our discussion topics would range from who is dating whom to politics to mythology and ofcourse science. Garima has this talent of putting life and expression into every story she shared with us and of course with a bit of her own *masala* and we eventually named this sort of story telling after her as 'Garima effect'. I am also thankful to my other JNC friends Manjusha, Loukya, Nandini, Arjun, Ramana, Gangaiah, Renu, Padma, Moumita and Manoj.

During the last year of my stay at JNC, I met a marvelous person in Diwakar. I am fortunate to have the kind of support, encouragement and patience which I always wished for. I would also take this opportunity to thank a few people from my college days. If it was not for my college lecturers, Ms. Sumati, Ms. Subha and Ms. Charukesi, I would have been marketing the products whose physics I investigated in the lab. I am also thankful to friends I made at different stages of life Himaja, Sravya, Harini, Shravan and Shanti for being with me throughout. Last but not the least, I am grateful to my aunt from whom I have learned how to look at life positively. I am thankful to my brother, Praneeth for being with me whenever need.

I appreciate and thank all the efforts of JNC staff- academic, administrative, library, technical and hostel for making my stay at JNC comfortable.

Preface

Colloidal systems are used to investigate a multitude of fundamental condensed matter phenomena like liquid-solid phase transitions, nucleation and growth of crystals, super heating of crystals and solid-solid phase transitions. Their large sizes($\sim \mu$m) and slow dynamics ($\sim$ms) make them ideal test beds to probe dynamics with single-particle resolution and hence gain insight into the microscopic underpinnings of various processes. In this thesis, using colloids as model systems, we address questions pertaining to nature of the glass transition, deformation of amorphous solids and defect dynamics in polycrystals. The organization of the thesis is as follows.

Chapter 1 presents a general introduction to the glass transition, theories developed to understand it, amorphous solids and polycrystals. This chapter also contains an overview of the how colloids have served as models to understand these phenomena.

Chapter 2 consists of colloid synthesis protocols followed by a description of the techniques used, which include confocal microscopy, confocal-rheometery and holographic optical tweezers.

Chapter 3 aims at understanding the nature of the glass transition, one of the oldest yet unresolved puzzles of condensed matter physics. Over the last few decades there has been a growing debate on whether glass transition is associated with an underlying thermodynamic phase transition or it is a purely kinetic process. Here, by freezing an amorphous wall of particles using a holographic optical tweezers in a 2D colloidal glass-forming liquid, we provide direct evidence for a few key predictions of Random First Order Transition Theory (RFOT), a popular thermodynamic theory of glass transition. We have successfully extracted a growing static length scale vis-a-vis amorphous order on approaching glass transition. Remarkably, we observe a non-monotonicity in dynamic correlations with increasing supercooling. We show that this non-monotonicity arises as a result of the change in the morphology of cooperatively rearranging regions (CRRS), manifestations of relaxation events, from string-like to compact. Strikingly, such a change in the morphology of CRRS is also consistent with the fuzzy sphere model which explains relaxation mechanisms within RFOT. Together, our observations suggest a thermodynamic paradigm of glass transition.

In chapter 4 we provide a direct evidence for a non-equilibrium phase transition associated with yielding of an archetypal soft solid - a colloidal glass. From hard to soft systems, most materials yield and flow plastically when subjected to stresses beyond a threshold namely, the yield stress. By combining confocal microscopy with rheometery, we simultaneously quantified single-particle dynamics and bulk rheological response and established direct connections between microscopic processes and macroscopic mechanical properties. Quantifying single particle dynamics reveal that the fraction of local irreversible events behave as an order parameter for this transition. The time taken for the system to reach a steady state also diverges in the vicinity of the yield strain. Accompanying this diverging time scale, we identified a length scale, associated with the clusters of particles having high local Debye-Waller factor, which exhibits a maximum in the vicinity of the yield strain. Collectively, these observations show that yielding shows signatures of a phase transition.

Chapter 5 discusses our results where we show that the dynamics of grain boundaries share similarities with supercooled liquids. Grain boundaries (GBs) are thin disordered interfaces

which separate two adjacent crystallites in a polycrystal. A GB is characterised by its misorientation angle, the angle with which one crystallite is rotated with respect to the other. It is well known that the properties of a GB depend crucially on its misorientation angle. Further, over decades there exists a debate if high angle grain boundaries (HAGBs), GBs with mosorientation angle greater than $\sim 15^{\circ}$, posses characteristics of supercooled liquids. By probing single particle dynamics at GBs, we reveal that HAGBs indeed display hallmark features of glass forming liquids such as slowing down of particle dynamics, non-Gaussian probability distribution of displacements and the existence of string-like cooperative rearrangements. We observe that with increasing misorientation angle the width of the boundary increases and hence the dynamics becomes faster. Thus, our studies show that GBs behave as confined supercooled liquids and their misorientation angle dependent properties stem from misorientation angle dependent geometric confinement.

Chapter 6 gives a brief summary and future outlook about the work discuused in this thesis.

List of Figures

List of Tables

Contents

Chapter 1

Introduction

1.1 Disordered Materials

In Nature, disorder is more prevalent than order. In the realm of condensed matter, the most common form of disorder we encounter is structural disorder. The epitome of structural disorder is a glass, although crystals also possess some degree of disorder in the form of point defects, dislocations and grain boundaries. In crystals, however, scientists have developed methods to intelligently utilize these imperfections to enhance the functionality of materials. One such striking example is the development of super plastic materials (Nieh *et al.* 2005). These materials are achieved by engineering the architecture of grain boundaries, thin disordered interfaces that separate crystallites of different orientations in a polycrystal. The characteristic attributes of any material stem from its structure. For instance in the context of crystallization, at high temperature the system is a fluid and does not posses any long-range order. However, once it crystallizes, the onset of long range order leads to the development of rigidity. Further, the degree of disorder dictates the mechanical properties of crystals. But as always, Nature surprises us by providing exceptions to a general premise. One such popular example of matter is 'glass' which possess a liquid like structure but is rigid like a crystal. Despite decades of research very little is known about glasses, how they form and what gives rise to rigidity. Numerous theories have been formulated to understand amorphous solids. In this process, many new concepts arose which have significantly contributed to other fields like protein folding (Bryngelson & Wolynes 1987) and computer science (Kirkpatrick *et al.* 1983) as well. However, the lack of understanding of glasses did not hinder their utility. About 500 years ago, it was discovered that glasses offer useful properties like high wear resistance, high fracture toughness, high porosity and many more. Amorphous solids are therefore used routinely for numerous applications ranging from window panes to artificial implants . Their extensive use has also provoked scientists to discover new glassy materials. One such recent development is ultra stable glasses (Swallen *et al.* 2007; Daisman *et al.* 2013; Singh *et al.* 2013). As the name suggests, unlike ordinary glasses, they are ultra stable in the sense that they posses very high strength and toughness. Most importantly, the study of such glasses is expected to shed light on mechanisms that lead to glass formation, one of the unsolved puzzles of condensed matter physics. Interestingly, existence of structural disorder is not just limited to hard materials like silica and metallic glasses, it is also found in soft materials like emulsions, gels and foams. Most products we use in our day-to-day life from food items (van der Sman 2012; Ubbink *et al.* 2008) to cosmetics (Genzer & Groenewold 2006) are soft materials (Quake & Scherer 2000; Bates & Fredrickson 2008). Given the wide range of applications of disordered materials, it is imperative to develop a unified understanding of these systems. Moreover, it is possible that knowledge gained from studying amorphous solids can help understanding disorder in crystals as well.

The holistic understanding of any phenomenon is attained from a synergistic combination of experiments, simulations and theoretical approaches. Knowledge about the bulk properties like elasticity or yield strength can be estimated by measuring stress-strain curves either by compressing or extending materials or more recently by nanoindentation. With regard to structure, it can be probed on a global length scale using X-ray diffraction and locally using techniques like Transmission Electron Microscopy (TEM). In fact, experiments on crystals have revealed collective motion of dislocations at the onset of plasticity (Miguel *et al.* 2001) and cooperative rearrangement of particles at grain boundaries (Merkle *et al.* 2002). In spite of these advances in atomic experiments, there exists limitations in probing dynamics with atomic resolution. These limitations are compounded in amorphous solids, where disorder precludes the characterization of local packing and hence hinders the development of structure-property relations. Therefore for such studies one relies on computer simulations, in particular for glasses, to gain insights into the local structure as well as to study dynamics. While our understanding of many phenomena has greatly benefited from simulations, they are also limited to small system sizes and small time scales. One way to circumvent these limitations, is to use colloidal suspensions as models to investigate atomistic phenomena. This is possible mainly because colloidal systems exhibit phase behaviour similar to that of atomic and molecular systems. Moreover, unlike atoms, colloidal particles owing to their large size and slow dynamics enable study of motion down to the single-particle level in real-space. In addition, colloidal particles can be easily manipulated by external forces like shear, magnetic and electric fields. More importantly, the size, shape as well as their interactions can be tuned with exquisite precision. This combination of properties make colloidal suspensions valuable model systems and hence powerful probes to understand fundamental condensed matter phenomena (Poon 2004). Over the last few decades, studies on colloidal systems have contributed immensely to the understanding of crystals as well as glasses. More recently, synthesis of inorganic active particles has led to developments where these active colloids are used to model biological systems from bacterial suspensions to bird flocks (Schweitzer 2007; Romanczuk *et al.* 2012; Golestanian 2012).

1.2 Colloids

Colloids belong to a class of materials known as soft matter (Jones 2002; Israelachvili 2010) which also include gels, emulsions and polymers. Colloidal suspensions consist of particles of sizes raging from $\sim$100nm to $\sim$5μm dispersed in a solution. The defining property of these systems is that they exhibit Brownian motion. Common examples of colloidal suspensions include milk, blood, paints, etc. Colloids find applications (Cosgrove 2010) in ink-jet printing, e-book readers and are used for making protective coatings and photonic band gap materials (Singh *et al.* 2010; Kim *et al.* 2011; Vlasov *et al.* 2001). The use of colloids is not restricted to industries, they also form excellent model systems to probe the microscopic underpinnings of numerous statistical mechanical phenomena (Poon 2004). Colloidal suspensions are therefore instrumental even from a purely academic perspective. This field of using colloids as models started with suspensions of simple spherical colloidal particles with isotropic short-range repulsive or nearly hard-sphere like interactions. Currently, owing to the enormous strides in colloidal chemistry, there exists protocols through which the size, shape and interaction of particles can be controlled accurately

(Glotzer & Solomon 2007; Sacanna & Pine 2011; Li *et al.* 2011) and few such examples are shown in Fig. 1.1. Over the last decade, scientists have successfully synthesized particles with different shapes such as ellipsoids (Snoeks *et al.* 2000), cubes (Rossi *et al.* 2011), dimples (Sacanna *et al.* 2010), rods (van Kats *et al.* 2004), clusters of spheres (Meng *et al.* 2010) and many more (Johnson *et al.* 2005; Kraft *et al.* 2008; Hong *et al.* 2008; Ahmadi *et al.* 1996; Greyson *et al.* 2006; Zhang *et al.* 2005). In addition to the shape, strategies to introduce directional interactions have also been developed. Examples for this include patchy particles (Pawar & Kretzschmar 2010; Hong *et al.* 2006; Pawar & Kretzschmar 2009; Kraft *et al.* 2009; Cayre *et al.* 2003) and coating particles with DNA (Huo *et al.* 2006; Xu *et al.* 2006). More recently, Pine and co-workers (Wang *et al.* 2012*a*) have devised methods for synthesizing colloids with valence which are more analogous to atoms. Here, they achieved directional interaction using DNA patches. Further they have shown that these colloids can assemble into structures that resemble molecules with different multivalent sp hybridized orbitals such as methane and ethylene molecules. Such systems are particularly useful to realize complex phase transitions like liquid-liquid phase transition (Smallenburg *et al.* 2014) as well as to study protein crystallization (Fusco & Charbonneau 2013). This precise control over various properties make colloids potential building blocks to realize exotic self-assemblies and model complex molecular systems. While there exists well established approaches to make complex colloids, utilizing them to model molecular processes is still limited and in-fact is one of the future directions of the field. Nevertheless, even using simple isotropic spherical colloids scientists have provided insights into a large number of atomistic phenomena such as nucleation, growth (van Blaaderen *et al.* 2003), pre-melting (Alsayed *et al.* 2005), super heating (Wang *et al.* 2012*b*) and crystal-crystal transitions (Peng *et al.* 2015).

The property of colloids which make them ideal to model the atomistic phenomena is the similarity in the interaction potential they share with Hard-sphere (HS) systems. HS potential, U_{HS}, is given by

$$U_{HS} = \infty \quad \text{if} \quad 0 < r < \sigma \tag{1.1}$$

$$U_{HS} = 0 \quad \text{if} \quad r > \sigma \tag{1.2}$$

This potential is used extensively in simulations to investigate a multitude of atomistic phenomena. Here, r is the distance between the colloids and σ is the diameter of the particles. In contrast to the Lennard-Jones potential (Fig. 1.2a), which best describes the interactions between neutral atoms in real atomic systems, the HS potential is a steep repulsive interaction (Fig. 1.2b). Despite ignoring long range attractions, systems with just HS interactions are known to exhibit striking similarities with real systems, in particular at high densities. This is because of the fact that in dense systems, it is the rapidly changing short range repulsive forces that govern the structure and dynamics and not the slowly varying long range ones (Andersen *et al.* 1976; Weeks *et al.* 1971). In dense systems, each particle be it atoms, molecles or colloids is surrounded by many particles and hence any local rearrangement is governed by the short-range repulsive part of the potential. Since long rang attractive interactions vary slowly with distance it can be thought of as a mean-field contribution. It is therefore possible to use just nearest-neighbour or short range repulsive forces to model realistic systems. The importance of the interactions due

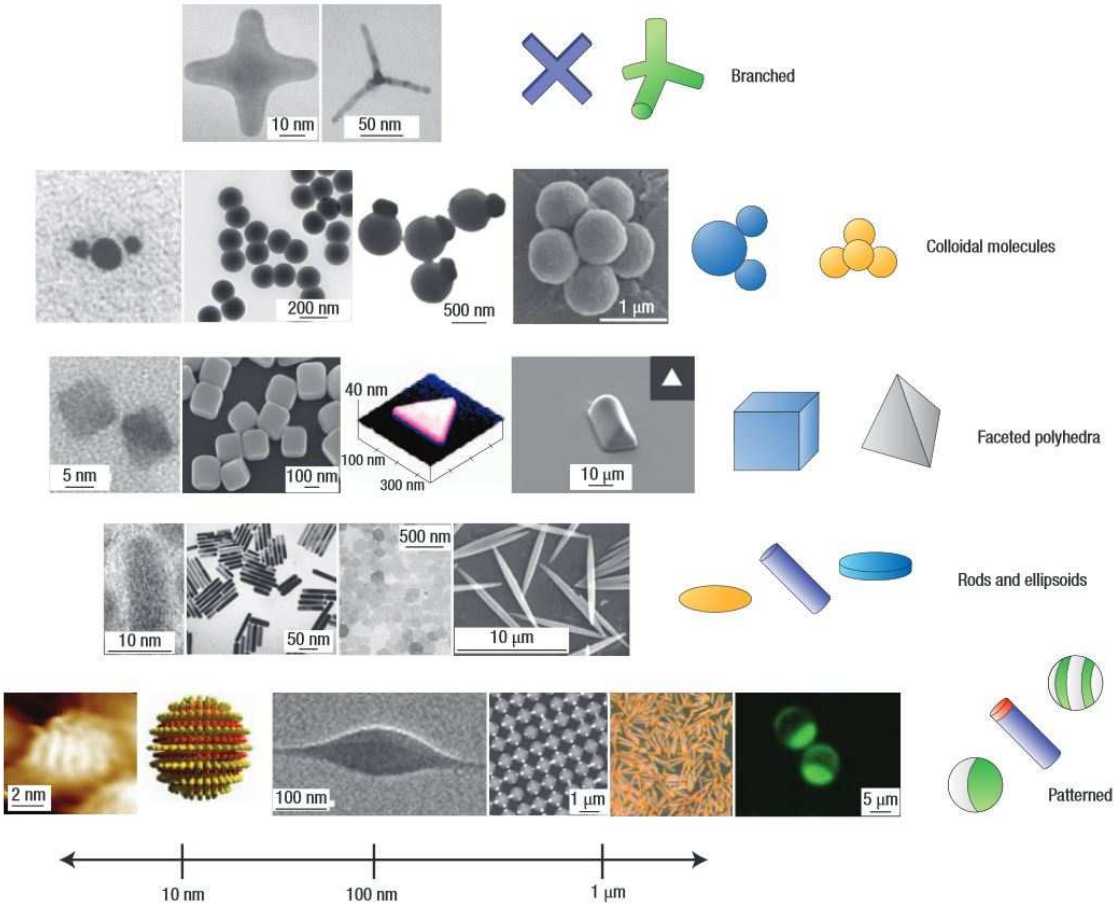

Figure 1.1: Representative examples of colloidal particles with various shapes and interactions. Particles are classified in rows based on their anisotropy type. The first three rows correspond to particles of various shapes and the last row consists of examples of patterned particles. The last row from left to right include striped spheres, biphasic rods, patchy spheres with valence, Au-pt nanorods and Janus spheres. Adopted from (Glotzer & Solomon 2007).

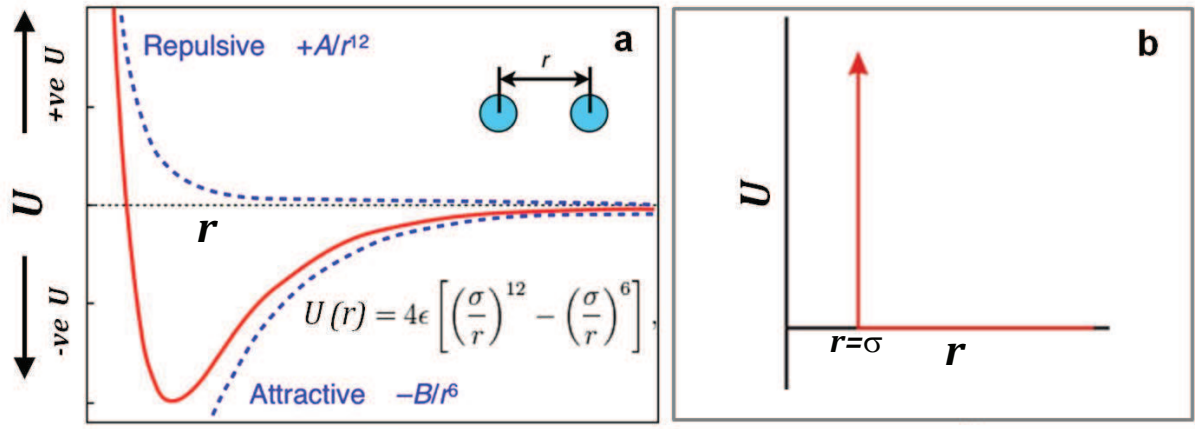

Figure 1.2: (a) Schematic of Lennard-Jones potential as a function of r distance between the particles. The solid curve represents the net potential and the dotted curves correspond to the repulsive and attractive parts of the potential. Adopted from *http://www.cmbi.ru.nl/redock/Glossary.php* (b) Schematic of Hard-Sphere potential (red lines) as a distance between the particles r. σ corresponds to the diameter of the particles.

to the repulsive part of the potential was realized as early as van der Waals, and around 1960's computer simulations (Alder & Wainwright 1957, 1960) and theoretical calculations (Percus & Yevick 1958; Thiele 1963; Wertheim 1963) were able to verify this premise. Estimation of the structure factors for systems with both kind of interactions indeed confirmed that HS interactions are sufficient to model the dynamics of dense real systems. Owing to its analytical tractability and a fewer parameters needed to describe the system, the HS potential is invaluable in theory and simulations that probe various condensed matter phenomena. However, the real-space experimental realization of a truly HS like system came into light from the experiments by Pusey and van Megen (Pusey & van Megan 1986). This triggered the burgeoning field of colloids as model atoms which is also the driving force behind using complex colloids to model molecules.

From the above discussion, it is evident that it is the nature of interactions between colloidal particles that make them invaluable as model systems, we will now focus on the forces present between colloidal particles in a suspension.

Forces at Work

Typically the force between two colloidal particles is attractive due to van der Waals interaction. This attractive force can result in aggregation when two particles collide either due to gravity or Brownian motion or other forces. It is therefore necessary to stabilize the particles against coagulation by introducing some form of counteracting forces. One way to realize this is by using charged colloidal particles where the electrostatic forces provide the necessary repulsive forces and the other is to modify the surface by adsorbing polymers on to it where steric interactions prevent aggregation of colloidal particles.

Electrostatic Stabilization: The interaction potential between two charged colloids is well described by Derjaguin, Landau, Verwey and Overbeek (DLVO) theory (Fig. 1.3a) (Israelachvili 2010). According to DLVO theory, the stability is a result of balance of van der

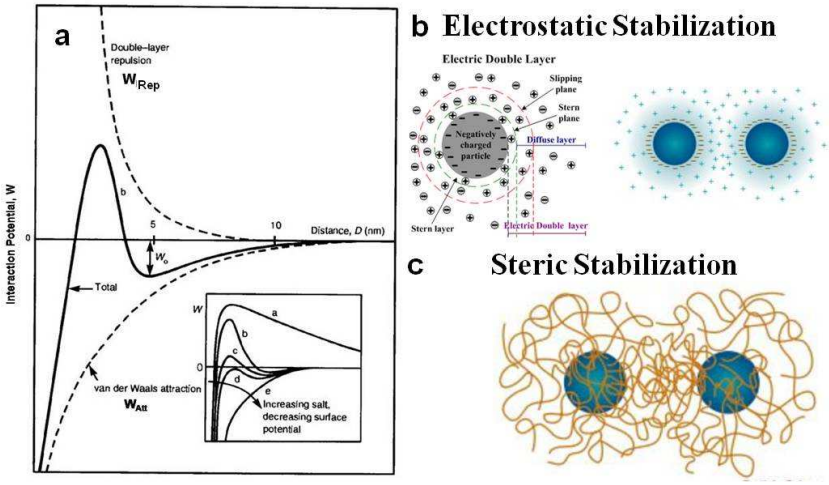

Figure 1.3: (a) Schematic of DLVO potential W. Inset shows the variation of W with the salt concentration. Adopted from (Israelachvili 2010). Image showing (b) Electrostatic stabilization. The left side image demonstrates the distribution of counter ions around a charged spherical particle. (c) Steric stabilization. In (b) and (c), the filled circles correspond to the particles. In (c) the curves represent the polymers tethered to the sphere.

Waals attraction and electrostatic repulsion. Given two spherical colloids of size R separated by a distance D the net interaction is given by

$$W = W_{Att} + W_{Rep} = -\frac{AR}{12\pi D} + \frac{64\pi k_B T n_o R \gamma^2}{\kappa} e^{(-\kappa D)} \tag{1.3}$$

Here, A is called Hamaker constant, κ is known as the Debye screening length, k_B is the Boltzmann constant, n_o is the ion density, and γ is the surface potential.

In Eqn. 1.3, W_{Att} is the van der Waals attractive contribution to the force. W_{Rep} is the repulsive part of the potential which is obtained by using a linearized Poisson-Boltzmann equation for describing electrostatic interaction at the mean-field level and the Gouy-Chapman model approximations for spherical particles. From Eqn. 1.3, it is clear that the parameter which governs the range of interaction. Further, κ is given by

$$\frac{1}{\kappa} = \left(\frac{k_B T}{\sum 2e^2 Z^2 n_o} \right)^{1/2} \tag{1.4}$$

To understand this, consider charged objects dispersed in an electrolyte. It is now well known that when charged particles are suspended in an electrolyte, the surface charge is balanced by the counter ions present in the solvent which will result in a concentrated double layer of charges around the particle (Fig. 1.3b). Physically, κ is a measure of the thickness of this double layer. Therefore, the stability of the suspension is also governed by κ. From Eqn. 1.4 it can be seen that κ solely depends on the number of ions present in the solvent and hence κ can be easily tuned by changing the salt concentration in the suspension (Inset Fig. 1.3a). Examples of charge stabilized colloidal suspensions include silica and polystyrene suspensions to name a few.

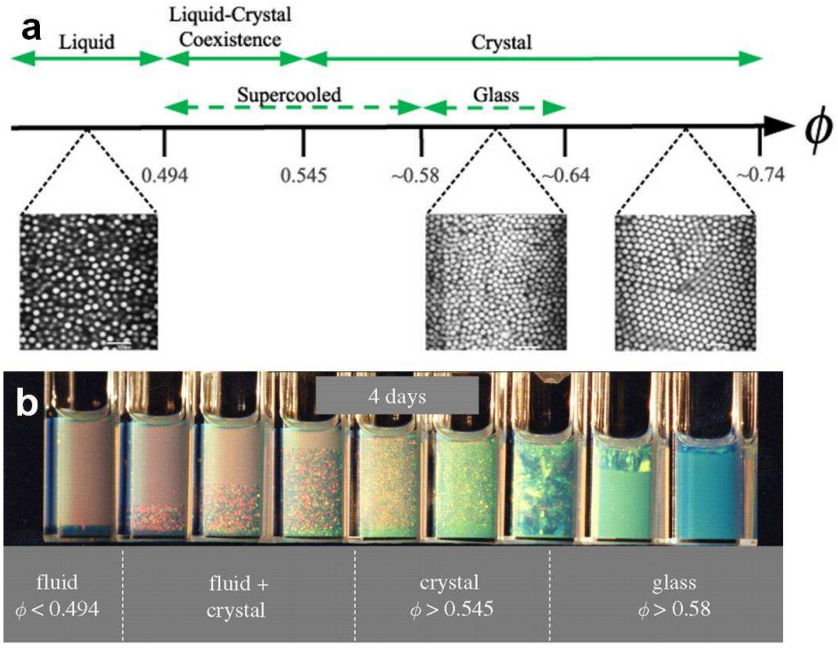

Figure 1.4: (a) Phase Diagram of a system with Hards Sphere potential. Adopted from (Hunter & Weeks 2012). (b) Experimental observation of phase diagram of colloidal suspensions. Adopted from (Pusey & van Megan 1986).

Steric Stabilization:

Another way to introduce repulsive forces is by attaching small polymers either physically or chemically on the surface of the particles (Fig. 1.3c). The overlap of these adsorbed polymers gives rise to a steric repulsion either due to osmotic repulsion or entropic repulsion thus resulting in stable suspensions. The stability in this case is controlled by thickness as well as the density of the adsorption layer. This interaction is typically short-ranged. Examples of colloidal systems which are stabilized in this manner include Poly methyl methacrlyate (PMMA) colloidal suspensions.

Regardless of the way colloidal suspension are stabilized, these particles exhibit nearest neighbour interactions and are the closest mimics of the HS potential. Thus like in HS system, the parameter which controlled the phase diagram is volume fraction, ϕ (Fig. 1.4).

For a HS potential,

$$\phi = \frac{4}{3}\pi\sigma^3\frac{N}{V} \tag{1.5}$$

Here, σ is the radius of the particle, N is the number of particles and V is the volume of the suspensions.

Phase Diagram of HS systems Given U_{HS} (Eqn. 1.2), Helmholtz free energy, F is

$$F = U - TS = -k_B T\, lnZ \tag{1.6}$$

$$Z = \sum_{config.} \exp\left(-\sum_{i,j\ bonds}\frac{U_{i,j}}{k_B T}\right) \tag{1.7}$$

$$\tag{1.8}$$

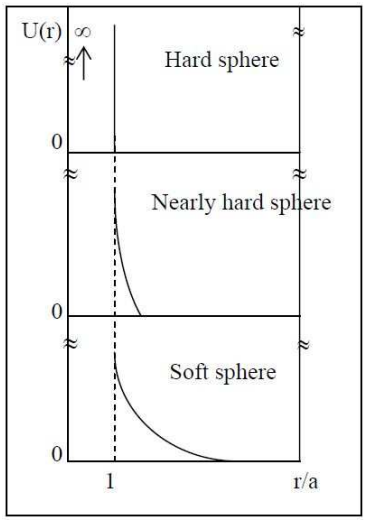

Figure 1.5: Schematic of (a) Perfectly Hard Sphere potential. (b) Nearly Hard Sphere potential. (c) Soft Sphere potential. Here, r is the distance and a is the size of the particle. Adopted from (Liu 2003).

$$\exp\left(-\frac{\sum_{i,j\ bonds} U_{i,j}}{k_B T}\right) = 0 \quad \text{if} \quad 0 < r < \sigma \tag{1.9}$$

$$\exp\left(-\frac{\sum_{i,j\ bonds} U_{i,j}}{k_B T}\right) = 1 \quad \text{if} \quad r > \sigma \tag{1.10}$$

$$\tag{1.11}$$

where T is the temperature, U is the internal energy and S is the entropy. F (Eqn. 1.7) clearly shows that phase diagram is controlled by S which is in-turn governed by density or equivalently ϕ.

Although colloidal suspensions and HS systems share striking similarities in their phase behavior, in reality colloidal suspensions are not perfect hard spheres (Royall *et al.* 2013) (Fig. 1.5a). They posses intrinsic softness and therefore they are conventionally called as nearly Hard-Sphere like (Fig. 1.5b). In steric interactions, the polymer attached on the surface makes them nearly HS like. On the other hand in electrosaticaly stabilized system, typically $\kappa > \sigma$. Moreover, tuning κ also enables one to tune the softness of the potential. Thus, charge stabilized systems can be used as nearly HS like as well as soft sphere like depending on κ (Fig. 1.5b).

For the experiments discussed in this thesis, we use nearly hard sphere electrostatically stabilized colloids to study nature of the glass transition, and microgel particles which are soft sphere like to investigate deformation of glasses and dynamics of grain boundaries. The rest of Chapter 1 gives a comprehensive introduction to each of these topics.

1.3 Glasses and Glass Transition

In a vast majority of liquids that are cooled rapidly to temperatures below their melting point, T_M, crystallization is suppressed and the liquid enters the supercooled regime (Fig. 1.6 red lines) (Debenedetti & Stillinger 2001; Cavagna 2009). In this regime, while the liquid-like structure is preserved the relaxation time (τ) increases by many orders of magnitude even for small changes

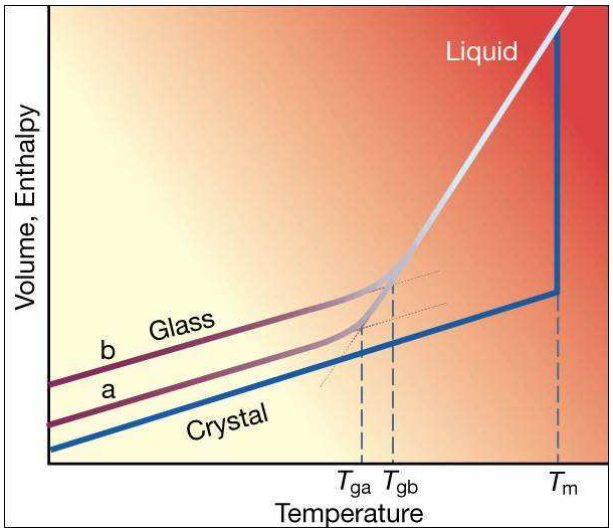

Figure 1.6: Temperature dependence of volume or enthalpy. T_M is the melting temperature. Lines a and b correspond to glasses obtained by different cooling rates. The red line corresponds to crystallization path. Adopted from (Debenedetti & Stillinger 2001).

in temperature (Berthier & Biroli 2011; Biroli & Garrahan 2013). For instance, in molecular glasses τ at T_M is of the order of picoseconds but it increases by about 14 orders of magnitude to about 100s when the temperature decreases to only $2/3T_M$. Eventually beyond a characteristic temperature, T_g identified as the experimental glass transition temperature, τ becomes larger than any observable time scale. Below T_g, the liquid does not flow and the system develops a finite yield stress. This amorphous state is termed as 'glass'. Intriguingly, unlike crystallization, where the development of the yield stress is associated with the development of long range order, the liquid-glass transition is not associated with any apparent change in the structure. Although the system behaves as a solid at temperatures below T_g, unlike equilibrium phase transitions, T_g itself depends on the cooling rate (Fig. 1.6 red lines a and b). This mixture of solid and liquid like properties of glasses make the development of a holistic understanding of this transition a formidable task. Any theory developed to explain the glass transition should explain satisfactorily the four characteristic features listed below, termed as 'stylized facts' by Biroli and Garrahan (Biroli & Garrahan 2013).

- Slowing down of dynamics with increasing supercooling without any apparent change in the structure (Fig. 1.7a).
- Heterogeneous dynamics - fast moving regions are spatially separated from slow moving regions (Fig. 1.7b).
- Anomalous thermodynamic response such as the difference in the temperature variation of specific heat in the heating and the cooling cycle (Fig. 1.7c).
- Onset of rigidity - developments of a yield stress while still being disordered (Fig. 1.7d).

While a precipitous increase in τ on approaching T_g is common to all glass forming liquids, the rate of change of τ with T is material dependent. This material dependent property called fragility is best captured by a plot of logτ or viscosity(η) versus T_g/T (Fig. 1.8). Such a

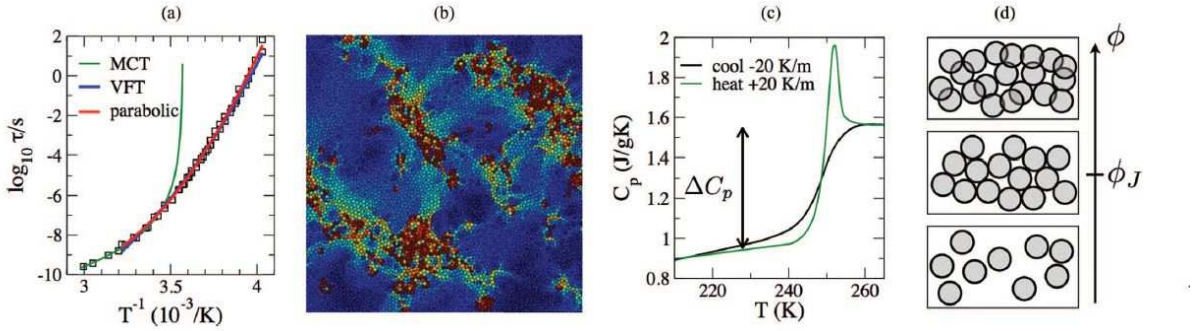

Figure 1.7: Stylized Facts. (a) relaxation time τ versus inverse temperature T^{-1}. The symbols correspond to the data taken from (Richert & Angell 1998). The blue and the red lines are VFT and parabolic fits to the data.The green line is the MCT fit. (b)Dynamic Heterogeneities. The particles are colour coded based on their mobility with maroon being particles with displacement greater than their diameter and dark blue corresponds to regions that did not move. (c) Temperature variation of heat capacity of ortho-terphenyl in heating and cooling cycles. (d) Jamming at zero temperature. The system is fluid like below jamming density ϕ_J, mechanically stable at ϕ_J and particles would overlap for densities greater than ϕ_J. Adopted from (Biroli & Garrahan 2013).

classification of materials based on fragility was put forth by Angell and hence is known as Angell plot (Angell 1995; Richert & Angell 1998). From Fig. 1.8, it is clear that some glass formers exhibit Arrhenius dependence and are termed as strong glasses while others show super Arrhenius behaviour and are known as fragile glasses. Fragility index, m, defined as $m = \frac{d(\log \tau)}{d(T_g/T)}$ quantifies the deviation from the Arrhenius behaviour. For fragile glass formers, the τ dependence with T is captured by the empirical Vogel-Fulcher-Tammann, (VFT) relation (Vogel 1921; Fulcher 1925; Tammann & Hesse 1926).

$$\tau(T) \propto \tau_o \ \exp\left(\frac{E}{T - T_0}\right) \tag{1.12}$$

Here, T_0 is the temperature at which τ diverges and $T_0 < T_g$ and E is the activation energy barrier. The VFT relation can be reconciled within the thermodynamic theories such as Random First Order Transition theory (RFOT) and Adam Gibbs (AG) theory which advocates a finite temperature ideal glass transition.

Surprisingly, the dependence of τ on T can also captured by other forms such as Bässlers law (Bässler 1987) which yields a divergence only at $T = 0$K.

$$\tau(T) = \tau_o \ \exp\left[K\left(\frac{T_{onset}}{T - T_{onset}}\right)^2\right] \tag{1.13}$$

Here, T_{onset} is the onset temperature for supercooling. Interestingly, this parabolic form is motivated by a purely kinetic theory namely, Dynamic facilitation theory (Elmatad *et al.* 2009).

Interestingly, both thermodynamic and kinetic approaches predict functional forms that describe the dependence of τ on T with reasonable accuracy. From Fig. 1.7a it is clear that just from these observables it is impossible to predict the nature of the glass transition. Discovering the true nature of the glass transition is mainly hindered by the range of temperatures that

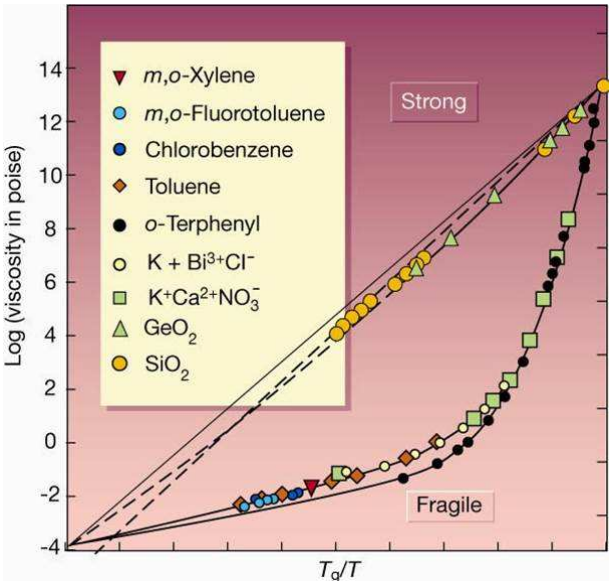

Figure 1.8: Viscosity, η, as a function of T/T_g for various glass formers. Adopted from (Debenedetti & Stillinger 2001).

can be accessed in simulations and experiments. Thus, the postulated critical behavior which occurs at $T < T_g$ cannot be tested. This makes it immensely difficult to understand the glass transition and hence it continues to remain one of the long standing puzzles in condensed matter physics. In spite of these difficulties numerous theoretical approaches have been proposed which successfully explain various attributes of the glass transition phenomenon. Before we go further, we will give a brief introduction to the various theories of glass transition that are relevant to the results discussed in this thesis.

1.3.1 Theories of the Glass Transition

Adam Gibbs Theory

The Adam-Gibbs theory (AG) put forth in the 1960's is one of the first thermodynamic theories of glass transition (Adam & Gibbs 1965). A key assumption here is that at low temperatures relaxation proceeds through correlated motion of a localized region of particles, namely the cooperatively rearranging regions (CRRs). As per AG theory, a CRR can rearrange independent of its surroundings with the only constraint being that it must exist at least in two configurations. As per AG theory, different CRRs interact only weakly. Thus, if N is the total number of particles and n the number of particles in a CRR then the number of states in which the system can exist, is given as $\mathcal{N} = \Omega^{(N/n)}$. Here, Ω is the number of states each CRR can exist and does not depend on temperature. Accordingly, the configurational entropy of the system, S_c, is

$$S_c = \frac{1}{N}\log(\mathcal{N}) = \frac{1}{n(t)}\ \log\Omega \tag{1.14}$$

$$\text{hence} \quad S_c(T) = \frac{\log\Omega}{n(t)} \tag{1.15}$$

According to this theory, the system undergoes a thermodynamic transition into a glassy state at a characteristic temperature T_K, namely the Kauzmann temperature (Kauzmann 1948). T_K is the temperature at which supercooled liquid's configurational entropy goes to zero. It is clear from Eqn. (1.15) that at the transition, the vanishing of S_c is associated with a diverging size of CRRs. This is yet another important postulate of AG theory.

AG theory also assumes that the energy barrier for a CRR to rearrange solely depends on the size of the CRR i.e, the number of particles $n(t)$ and consequently, the activation energy barrier is given by $\Delta \sim n \sim \frac{1}{S_c}$. Using these postulates in combination with the Arrhenius dependence gives τ to be

$$\tau = \tau_o \exp\left(\frac{B}{TS_c(T)}\right) \qquad \text{where B consists of all constants factors} \tag{1.16}$$

This relation between τ and S_c is one of the most important outcomes of this theory. Further, to obtain precise dependence of S_c on T at low T, $S_c(T)$ is identified with the excess entropy $S_{exc}(T)$. $S_{exc}(T)$ is the liquid entropy minus the crystal entropy at a given temperature. Using the relation between entropy and specific heat capacity, c_p, we can get

$$\Delta S_c = \Delta\left(S_{liquid} - S_{crystal}\right) = \Delta c_p \tag{1.17}$$

$$S_c(T) - S_c(T_K) = \int_{T_K}^{T} \frac{\Delta c_p}{T} dt \tag{1.18}$$

Within the approximation that the liquid-crystal specific heat capacity is independent of temperature and using $S_c(T_K) = 0$, we have $S_c(T) = \Delta c_p \log \frac{T}{T_K}$. Expanding the logarithm finally gives $S_c(T) = \Delta c_p \dfrac{T - T_K}{T_K}$. Substituting this in Eqn 1.16 gives

$$\tau = \tau_o \exp\left(\frac{B}{T - T_K}\right) \tag{1.19}$$

Identifying T_K in Eqn (1.19) with T_0 in Eqn (1.12), it is clear that the VFT relation can be recovered from the AG equation. While the AG theory successfully captures the T dependence of τ observed in simulations as well as experiments, this theory contains a few draw backs. To enumerate a few, it proposes the existence of CRRs but does not provide a prescription to identify them. The assumption that CRRs rearrange independent of each other is also repeatedly questioned and in fact interaction between them is one of the aspects of Random First Order Transition theory. Also, the assumption regarding the number of configurations each CRR can take has also been questioned (Dyre *et al.* 2009; Bouchaud & Biroli 2004).

Mode Coupling Theory

Mode Coupling Theory (MCT) is one of the most popular dynamic approaches that is used to explain the slow dynamics of supercooled liquids (W. Götze & Zinn-Justin 1991; Götze & Sjogren 1992; Götze 2008; Bengtzelius *et al.* 1984; Leutheusser 1984). Unlike AG theory, where slowing down is due to thermodynamics, within MCT the non-linear feedback mechanisms in microscopic dynamics at low temperatures results in the structural arrest of the system. MCT aims at solving the equations of motion for density fluctuations with appropriate approximations

whose time dependent solutions correctly describe the dynamics of supercooled liquids.

The dynamics of the liquid is usually described by the self-intermediate scattering function, $F_s(q,t)$ defined as follows

$$F_s(q,t) = \frac{1}{N}\sum_{i=1}^{N}\langle \exp\{i\mathbf{q}.\left[\mathbf{r}_i(t+t_o) - \mathbf{r}_i(t_o)\right]\}\rangle \tag{1.20}$$

Here, $\bar{\mathbf{r}}_i(t)$ is the position of i^{th} particle at time t and $\mathbf{q}$ is the wave vector. The starting equation of motion for $F(q,t)$ for an isotropic system is given by

$$\ddot{F}(q,t) + \Omega^2(q)F(q,t) + \int_0^t \left[M^0(q,t-t') + \Omega^2(q)m(q,t-t')\right]\dot{F}(q,t')dt' = 0 \tag{1.21}$$

Here, $\Omega^2(q) = q^2k_BT/\mathrm{m}S(q)$ where $S(q)$ is the structure factor, m is the mass and k_B is the Boltzmann's constant. The kernal $M^0(q,t)$ gives relevant contribution only at temperatures in the vicinity of triple point and hence only $m(q,t)$ becomes important for supercooled liquids. In order to solve these equations, they were simplified by neglecting a few terms (Bengtzelius *et al.* 1984) which were thought to be irrelevant at low temperatures and by using a quadratic function of $F_s(q,t)$ for m. The form of m used is $m(\Phi) = \lambda_1\Phi + \lambda_1\Phi$ with $\lambda_i > 1$ and $\Phi = F(q_0,t)/S(q_0)$. The self consistent equations with these approximations are called mode-coupling equations. In $m(\Phi)$ used, λ is the coupling parameter whose strength governs the behaviour of the solution. Here, λ corresponds to temperature in real systems. From the graphical representation of the numerical solutions of the mode-coupling equations (Götze & Sjogren 1988) as shown in Fig. 1.9a, it is clear that if λ is increased beyond a certain value the function does not decay and this characteristic value of λ and the equivalent temperature (T_{MCT}) is identified as the glass transition temperature in the context of this theory. Thus, the full solutions of these equations give the relevant temperature dependent dynamics of supercooled liquids just by using structure factor as the input. Owing to the complexity in solving these equations, here we do not go into the details and we refer the reader to the following review articles (Kob 1997; Reichman & Charbonneau 2005; Das 2004), but below we state the key predictions of this theory.

Predictions of MCT

- One of the most important predictions of this theory is the power-law divergence of the relaxation time, τ, at temperatures close to mode coupling transition temperature T_{MCT}. T_{MCT} is the characteristic temperature across which there is a transition from an ergodic state to a non-ergodic state.

  $$\tau \propto (T - T_{MCT})^{-\gamma} \text{ where } \gamma \text{ is a system dependent constant.} \tag{1.22}$$

  Interestingly, the predicted power-law behaviour of τ with T is observed in simulations and experiments on supercooled liquids (Kob & Andersen 1995; Kob 1999; Zheng *et al.* 2011; Mishra *et al.* 2013).

- The other remarkable prediction of this theory is the existence of three relaxation processes (Fig. 1.9b). The short time behaviour (regime I) is relaxation on the microscopic time

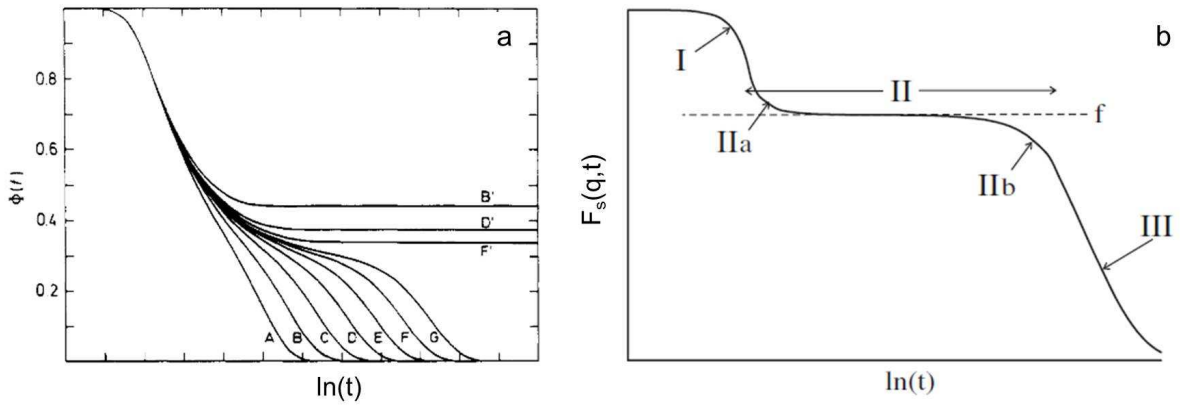

Figure 1.9: (a) Numerical solutions for MCT equations for supercooled liquids. $\phi(t)$ versus ln(t) and it is to be noted that $\phi(t)$ exhibits a behaviour analogous to $F_s(q,t)$. Curves A-G correspond to supercooled liquid for $T > T_{MCT}$ and B', D' anf F' correspond to $T < T_{MCT}$. Adopted from (Kob 1997). (b) Schematic of a typical $F_s(q,t)$ profile showing three relaxation regimes. Adopted from (Reichman & Charbonneau 2005).

scale and hence depends on the microscopic details of the system. For instance, it is ballistic for atomic liquids and diffusive for colloidal glass formers. The intermediate time regime (II) (Fig. 1.9b) is the one where particles are caged by their neighbours which results in the development of a plateau and is known as the β-regime. Here, according to MCT predictions the initial decay of plateau (IIa) can be described using a Critical power law given by

$$F_s(q,t) = f_q + h_q \frac{t}{t_\sigma} \tag{1.23}$$

where f_q and h_q are plateau height and the amplitude and $t_\sigma = \frac{t_0}{|\sigma|^{1/2a}}$ with t_0 being a system dependent constant, a is the power-law exponent and σ is the separation parameter given by

$$\sigma = C(T - T_{MCT}) \tag{1.24}$$

The final decay of the plateau (IIb) is characterized by von Schweilder law which reads as

$$F_s(q,t) = f_q - h_q t^b \tag{1.25}$$

where b is the von Schweilder's exponent. Moreover, $\gamma = \frac{1}{2a} + \frac{1}{2b}$. Furthermore at long times, namely the α-regime, the decay is well described by a stretched exponential (Kohlrausch 1854; Williams & Watts 1970)

$$F_s(q,t) \propto \exp\left(-(t/\tau)^\beta\right) \tag{1.26}$$

with τ being the relaxation time and β being the characteristic exponent.

Thus, simply by plotting $F_s(q,t)$ and fitting the above stated functional forms various parameters like a, b, τ and γ can be determined. Knowing these parameters at different Ts, one can plot $\tau_\alpha^{1/-\gamma}$ versus T whose X-intercept gives an estimate of T_{MCT}. Thus far, this theory has been used extensively in simulations as well as in experiments to extract T_{MCT} and understand relaxation

processes. Moreover, the stretched exponential at long times in $F_s(q,t)$ is an indirect evidence for heterogeneous dynamics, a characteristic property that is unique to supercooled liquids (Ediger 2000). Later, simulations have provided direct evidence for such heterogeneities and also insights into their structure and cooperative nature as predicted by the AG theory.

The two step relaxation captured by $F_s(q,t)$ is also captured by the mean squared displacement, MSD, which is defined as follows (Kob 1999)

$$MSD = \langle r^2(t)\rangle = \frac{1}{N}\sum_{i=1}^{N}\langle |r_i(t) - r_i(o)|^2\rangle \tag{1.27}$$

Analogous to $F_s(q,t)$, at intermediate times, MSD starts developing a plateau which is a signature of caging of particles by their neighbors. The height of the plateau provides an estimate for the cage size. With time, the MSD shows an upturn indicating escape of the particles from their respective cages, followed by diffusive behavior at long times. This happens typically in the vicinity of τ_α. Since the long time behavior is related to τ_α, the time at which MSD becomes diffusive increases with $1/T$. Moreover, the fourth moment of $r(t)$, α_2, can also be used to characterize heterogeneous dynamics (Kob *et al.* 1997).

$$\alpha_2 = \frac{\langle r^4(t)\rangle}{3\langle r^2(t)\rangle^2} - 1 \qquad \text{for} \quad d = 2 \tag{1.28}$$

α_2 quantifies the deviation from Gaussian dynamics and hence the time corresponding to the maximum in $\alpha_2(t)$ is the characteristic time, namely cage breaking t^*, where the dynamics is maximally heterogeneous.

To conclude, MCT has been exceptionally successful in describing the relaxation mechanisms of real glass formers in the supercooled liquid regime. Additionally, the solutions of MCT equations are fully consistent with what is observed in simulations and experiments (Kob & Andersen 1994, 1995). More importantly, it can predict novel glass transitions. Striking example of which include the existence of reentrant glass transitions in colloidal systems with short range attractive interactions (Dawson *et al.* 2000; Pham *et al.* 2002; Mishra *et al.* 2013). Although this theory predicts a transition into a non-ergodic state at T_{MCT}, it is to be noted that $T_{MCT} > T_0$, T_0 being the ideal glass transition. Therefore MCT best captures the dynamics in the supercooled regime $T > T_{MCT}$. In the vicinity of T_{MCT} it is now believed that hopping process become important and hence idealized version of MCT cannot be used. Instead an extended version of MCT which takes these hopping processes into account has to be used (Kob 1997; Götze & Sjögren 1987; Das & Mazenko 1986). Moreover, parameters a, b, and β which are predicted to be constant is completely valid only when $\dfrac{T - T_{MCT}}{T_{MCT}} \ll 1$. Care should be taken when applied in the limit where $\dfrac{T - T_{MCT}}{T_{MCT}}$ is not small (Reichman & Charbonneau 2005; Kob 2003).

Dynamic Facilitation Theory

Dynamic Facilitation (DF) theory is another important dynamic approach towards understanding the glass transition (Garrahan & Chandler 2002, 2003; Whitelam *et al.* 2004; Berthier & Garrahan 2003; Chandler & Garrahan 2010). One of the primary postulates of DF theory is that

system relaxes solely through the propagation of mobile defects termed as 'Excitations'. A key assumption of this theory is that defects cannot emerge spontaneously anywhere in the space but will only be created in the vicinity of the existing defects due to transfer of mobility. Thus in DF these defects or excitations trigger mobility and facilitate relaxation in their neighborhood. In addition, these defects are localized in space and time and hence any long time relaxation event like a cooperative rearrangement of particles is purely due to facilitated dynamics.

The main predictions of the DF theory are captured by a class of dynamical models called the kinetically constrained models (KCM) (Ritort & Sollich 2003; Jäckle & Eisinger 1991). KCMs were first introduced by Fredrickson and Andersen and have been studied in the context of glasses with an aim to explain the dynamical features of glass forming liquids (Fredrickson & Andersen 1984). The characteristic feature of these models is that they have a trivial Hamiltonian which is free of a thermodynamic phase transition but the constraints on their dynamics give rise to a dynamic transition. Also, these models exhibit complex behavior reminiscent of glass forming liquids like slow dynamics and dynamic heterogeneities. Another interesting feature displayed by these models is that, some KCMs exhibit a strong glass like behavior while other show fragile or super Arrhenius dependence of τ on T. All in all, there are many possible KCMs and each of which has its own set of constrains with dictate their dynamics. Two basic models of KCMs include the one dimensional Fredrickson-Anderson spin model (FA) model (Fredrickson & Andersen 1985) and the East model (Evans 2002). Both these models are lattice models with N sites and each site n_i can be 1 or 0 depending on whether it is occupied by an excitation or not. It has been recently demonstrated by Chandler and co-workers that East like KCMs are a good model for studying atomic glass formers. Therefore here we will discuss briefly the dynamics of the East model. In this model there is no interaction between two sites and hence the Hamiltonian is simple and is given by

$$E = \sum_{i=1}^{N} n_i \tag{1.29}$$

and using the detailed balance one can find the equilibrium concentration of excitations, c, to be

$$c = \langle n_i \rangle = \frac{1}{1 - e^{\beta}} \quad \text{with } \beta \text{ being the inverse temperature} \tag{1.30}$$

It is clear from the Eqn (1.30) that c decreases with decreasing T which consequently gives rise to a large relaxation time. Now we move on to dynamics, where the FA and East model differ. In the East model (Fig. 1.10) an excitation $n_i = 1$, can facilitate relaxations only to a neighbour to its east, i.e, n_{i+1} where $i = 1, 2, ...N$. Interestingly, this simple constraint is enough to gives rise to slowing down of dynamics with decreasing temperature with τ dependence on T described by Bässlers law with a dynamic transition at T=0.

Although DF can explain slowing down dynamics observed in KCMs, owing to the lack of an appropriate definition for identifying a mobile defect or an excitation in particulate systems, its application to atomic glass formers has been hindered. It was only in 2011 that Chandler and co-workers devised a protocol to identify excitations in particulate systems and validated

Figure 1.10: Shematic of 1D East model. The dotted squares correspond to the ones that can be excited.

this picture for atomic glass formers (Keys *et al.* 2011). These predictions have also been tested experimentally in colloidal glass formers (Gokhale *et al.* 2014). In ref (Keys *et al.* 2011), an event is defined to be excitation depending on the displacement made by the particle. A particle is said to be associated with an excitation of size 'a' if it makes a displacement a in a time Δt and persists in its initial and final position for at least a time interval Δt (Fig. 1.11a). Here, Δt is called the instanton time. Further, by studying excitation dynamics Chandler and co- workers have observed that atomic glass formers exhibited many features similar to those displayed by East like KCMs.

Firstly, they found that these excitations are localized in space and time and are hierarchical. They observed that the concentration of excitations increases with decreasing T (Fig. 1.11b) following

$$c_a \propto \exp\left[-J_a\left(\frac{1}{T}-\frac{1}{T_o}\right)\right] \quad \text{for } T > T_o \tag{1.31}$$

with T_o being the onset temperature. Further, the authors have shown that CRRs emerge hierarchically over time from facilitated dynamics with excitations being the primary objects. Analogous to the size of CRRs, they have extracted a dynamic length scale $l_a = c_a^{1/d_f}$ where d_f is the fractal dimension of the clusters of excitations of size a. However, a direct connection between l_a and the size of CRRs is yet to be established. More importantly, they have shown that the relaxation time for an excitation of size a (τ_a) obeys

$$\tau_a = \tau_o \exp\left[J^2\left(\frac{1}{T}-\frac{1}{T_o}\right)^2\right] \text{ for } T > T_o \tag{1.32}$$

$$\text{here, } \quad J = J_a\sqrt{\frac{\gamma}{d_f}} \tag{1.33}$$

Furthermore they showed that relaxation times thus estimated, for an excitation of size $a = \sigma$, σ being the particle diameter, are in excellent agreement with those obtained from the conventional self-intermediate scattering function $F_s(q,t)$ for $q = \sigma$. Remarkably, they have validated their predictions by probing five different glass formers which include both 2D and 3D as well as glass formers of different fragility indices (Keys *et al.* 2011).

To summarize, DF can reproduce many striking features of glass forming liquids like growing dynamic correlations (Chandler *et al.* 2006), relaxation times and even the anomalous behavior of specific heat (Keys *et al.* 2013). However, like other theories DF also has a few limitations. One of the questions is about how the first excitation is created. More importantly, the presence of growing non-trivial static correlations with relaxation time which are seen in simulations and experiments are not intrinsic to facilitation picture.

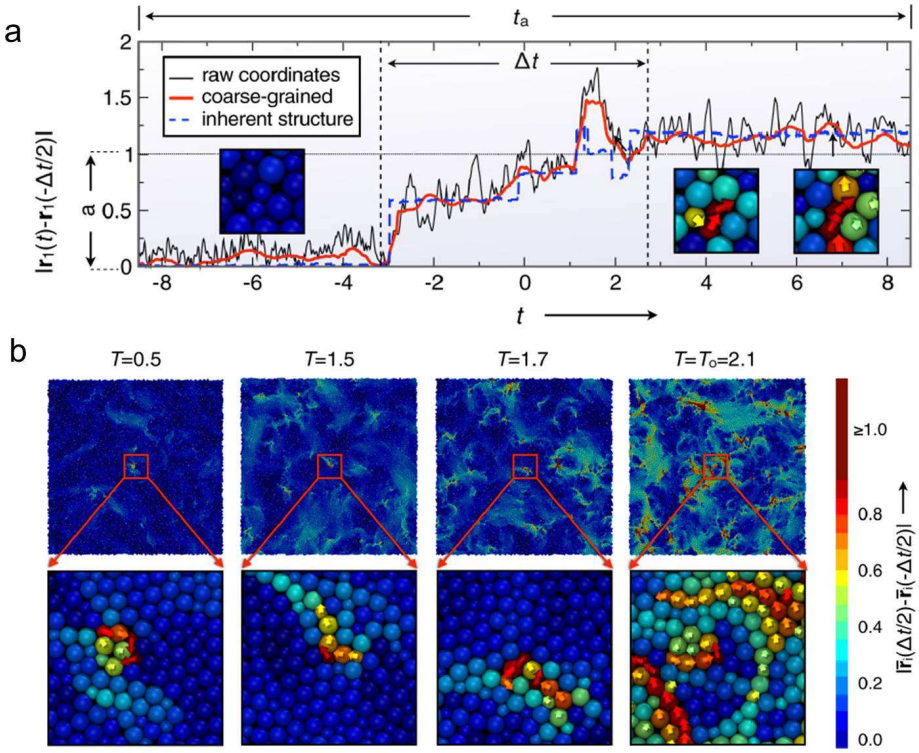

Figure 1.11: (a) Representative trajectory of a particle with the protocol for identification of an excitation. a is the excitation size and Δt is the instanton time and $t_a = 3\Delta t$. (b) Visualization of excitation concentration dependence on T. The particles are colour coded based on their displacement. Here, maroon corresponds to displacement larger that a and blue represent no motion over Δt. Increasing maroon regions with increasing T is a signature that c_a decreases with T. Adopted from (Keys *et al.* 2011).

Random First Order Transition Theory

Random First Order Transition theory (RFOT) (Kirkpatrick *et al.* 1989; Lubchenko *et al.* 2007; Biroli & Bouchaud 2012; Xia & Wolynes 2001), unlike DF is a thermodynamic theory of the glass transition. RFOT is qualitatively similar to AG but offers a much more detailed theoretical description of the glass transition. Within RFOT, there exists an ideal glass transition at a finite temperature T_0 which is of thermodynamic origin. As per RFOT, at low temperatures the systems can be described as a mosaic of metastable states. In such a scenario, the glass transition is associated with a diverging length scale which is of entropic origin and is related to size of mosaic. In addition to a thermodynamic transition, there also exists a dynamic transition which shares similarities with the one predicted by MCT, at a temperature larger than the ideal glass transition temperature(Kirkpatrick & Thirumalai 1987*a*). Further, in finite dimensions the divergence associated with the dynamic transition becomes a cross over. Moreover, through analytical calculations it has been shown that activated events dominate relaxations close to ideal glass transition and also the mechanism of relaxation changes across T_{MCT}, which is manifested in the shapes of cooperatively rearranging regions.

RFOT is motivated from spin-glass physics (Binder & Young 1986) and specifically a class of spin models namely, the p-state Potts model. In 1987, Kirkpatrick, Thirumalai and Wolynes discovered that p-spin glass models share striking similarities with the structural glass transition (Kirkpatrick & Wolynes 1987*a*,*b*; Kirkpatrick & Thirumalai 1987*a*,*b*). This model has two phase transitions, one at a high temperature T_s, which is now identified with T_{MCT}, where $F_s(q,t)$ plateaus implying that system remains in stable states for extended periods of time. The number of these states decreases with decreasing T and finally below a critical temperature now identified with ideal glass transition temperature, T_0, only a nonextensive number of them remain and hence the configurational entropy vanishes. It is this picture that inspired the real space thermodynamic description of supercooled liquids and glass transition.

Going from spin-glass systems to structural glass theory, Wolynes and coworkers hypothesized that for $T_0 < T < T_{MCT}$ the system consists of mosaic of sub-regions each of which is characterized by a metastable state (Lubchenko *et al.* 2007; Biroli & Bouchaud 2012). As suggested by Bouchaud and Biroli (Bouchaud & Biroli 2004), a very small sub-region will not have enough internal degrees of freedom to make a transition to another metastable state and on the other hand a very large one will break into smaller ones. Therefore the mosaic will have a characteristic size (ξ) at a given T and the time it takes to transform is assumed to be the structural relaxation time τ. To explain this better and estimate ξ and τ, they used a formulation based on nucleation of entropic droplets of metastable states. Accordingly, the critical size of the domain is given by the competition between surface tension and bulk free energy. If there exists two states α and β then the energy cost for the interface is given by

$$\Delta F = Y R^{\theta} \tag{1.34}$$

Here, R is the linear dimension of the droplet size and $\theta \leq d-1$ where d is the spatial dimension and Y is the generalized surface tension. Given that the correct order parameter for this transition is not known and the nature of interface between amorphous states is unknown, θ could be

less than $d-1$. Thus the only assumption is that if two surfaces are in contact there is a free energy cost given by Y. The difference between a conventional first order transition and this transition is that, in the former there is an energy mismatch between the states but in the latter the two states can have roughly the same free energy. Since the state β is unspecified i.e., there could be multiple metastable states of same energies, the droplet gains entropy from the number of possible states it can exist which is the driving force. Thus, the free energy contribution is from the total configurational entropy available to that region which is given by

$$\Delta F_{gain} = -TS_c R^d \tag{1.35}$$

The critical size of the droplet is obtained by balancing these two energies (Eqn 1.34 and 1.35) which is given by

$$\xi = \left(\frac{Y(T)}{TS_c(T)}\right)^{\left(\frac{1}{d-\theta}\right)} \tag{1.36}$$

For super cooled liquids although the value of θ cannot be determined experimentally, renormalization group theory have suggested this value to be 3/2 for $d = 3$ (Kirkpatrick *et al.* 1989; Villain 1985). This reduces Eqn 1.36 to the one which is similar to that of AG equation for the length scale. Using the free energy barrier, once again obtained from two competing forces, and the Arrhenius relation the relaxation time comes out to be

$$\tau = \tau_o \exp\left(\frac{Y(T)^{\frac{d}{d-\theta}}}{T\left[TS_c(T)\right]^{\frac{\theta}{d-\theta}}}\right) \tag{1.37}$$

Further, by substituting $S_c \sim T - T_K$ and $\theta = 3/2$ for $d = 3$ the AG relation or VFT relation for relaxation time can be retrieved.

To sum up, some of the main predictions of RFOT are as follows:

- There exist an ideal glass transition at a temperature T_K where the configurational entropy goes to zero with VFT like increase in relaxation time with $1/T$.
- The mosaic size or ξ is the characteristic static length scale which quantifies the growing amorphous order on approaching the glass transition. Interestingly, Biroli and Bouchaud have shown analytically that point-to-set correlations can give an estimate of ξ (Bouchaud & Biroli 2004) which was also computed in recent simulations by Biroli and coworkers (Biroli *et al.* 2008).
- Dynamics of supercooled liquids can be explained by MCT equations for $T > T_{MCT}$ and for $T < T_{MCT}$ activated hops become important (Stevenson & Wolynes 2010). In addition analytical studies have also shown that there is a change in the relaxation mechanism across this dynamical cross over, T_{MCT} (Stevenson *et al.* 2006).

From the brief summary of various theories it is clear that some general phenomenology can be rationalized within all of them. Most theories can rationalize the observed qualitative trends in the observables that characterize the transition and reproduce quantitative features

at the expense of adjustable parameters. From an experimental or simulation perspective, the difficulty in investigating the nature of the glass transition is because the observed experimental glass transition is undoubtedly a kinetic one and other striking properties of supercooled liquids which include slowing down of dynamics, cooperative dynamics are also attributes of dynamics. Nevertheless, this does not rule out the existence of a thermodynamic transition at the ideal glass transition temperature as predicted by thermodynamic theories. Although lack of a clear evidence for a diverging static length scale thus far supports that dynamic nature of the glass transition, these theories overlook the rapid decrease in the configurational entropy which on the other hand is intrinsic to thermodynamic theories. Thus, despite enormous efforts that have been put in understanding the glass transition, even today the underlying mechanism for this transition is not clear and continues to remain a central issue of condensed matter physics. As stated by G Tarjus "Predictions that do not involve any additional assumptions and could be crisply checked in experiments" are necessary to unambiguously validate different theories of glass transition (Berthier *et al.* 2011).

1.3.2 Colloids as Models to Study Glass Transition

Over the course of time, numerous theories have been formulated to solve the glass transition puzzle (Berthier & Biroli 2011; Biroli & Garrahan 2013). Decades ago, methods and concepts developed were predominantly based on complex energy landscapes in configuration space (Angell *et al.* 2000; Debenedetti & Stillinger 2001). However, with the observation of dynamic heterogeneities (Ediger 2000; Glotzer 2000; Andersen 2005) the importance of real space fluctuations was realized and from then the development of real space concepts and methods has taken precedence (Lubchenko *et al.* 2007; Chandler & Garrahan 2010; Berthier & Biroli 2011; Biroli & Garrahan 2013). The fact that real space predictions can be directly tested in simulations and experiments is also responsible for this paradigm shift in the perspective. While atomic experiments can provide indirect evidence of dynamic heterogeneities through the decay in $F_s(q,t)$, investigating properties such as their structure and spatial arrangement necessitates access to single particle dynamics. Quantification of dynamics down to single particle resolution in experiments is possible only in colloidal systems and hence they are ideal to study and test predictions of various theories of the glass transition (Hunter & Weeks 2012; Duplantier *et al.* 2011).

For colloidal systems, increasing the volume fraction, ϕ, beyond the melting volume fraction, ϕ_M, gives rise to a glass (Duplantier *et al.* 2011). For $\phi > \phi_M$, the system becomes crowded which results in caging of the particles by their neighbours which hinder the relaxation processes. This results in increasing relaxation time with ϕ. The existence of a glass in hard sphere systems was originally suggested by sphere packing experiments by Scott (1960) (Scott 1960) and Bernal and Mason (1960) (Bernal & Mason 1960). However, it was only after mode coupling theory calculations by Gotze and Sojlender (Götze & Sjögren 1987) and experiments on hard-sphere like colloids (Pusey & van Megen 1989, 1987) that the study of colloidal glasses started gaining attention. Experiments on colloidal systems composed of PMMA particles have witnessed the existence of a supercooled liquid state for $0.46 < \phi \lesssim 0.58$ and an experimental glassy phase beyond $\phi \gtrsim 0.58$. Measuring relaxation times from the decay of $F_s(q,t)$ using light scattering

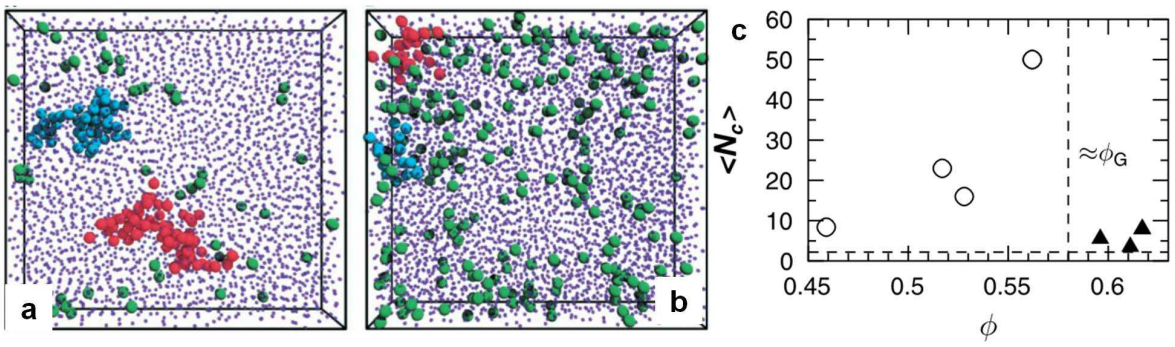

Figure 1.12: (a) Representative images of dynamic heterogeneities for $\phi = 0.56$. The blue and red spheres correspond to CRRs. (b) Average CRRs size $\langle N_c \rangle$ as a function of ϕ. Adopted from (Whitelam *et al.* 2004).

techniques at various supercoolings revealed that the system has indeed undergone a transition from an ergodic state to a non ergodic one across $\phi >\sim 0.58$ (Pusey & van Megen 1987). Slowing down of dynamics was also demonstrated by real space video microscopy experiments on colloidal glass forming liquids by Weitz and coworkers where they have computed MSD from individual particle positions at various times (Weeks *et al.* 2000). Remarkably, these experiments provided the first real-space visualization for heterogeneous dynamics in the form of cooperatively rearranging regions (Fig. 1.12a) (Weeks *et al.* 2000) . Further, with slowing down of dynamics they observed a concomitant increase in the size of these cooperatively rearranging regions with supercooling (Fig. 1.12c).

Numerous real space studies directed towards the understanding of the glass transition followed this seminal work (Pham *et al.* 2002; Ghosh *et al.* 2010; Nugent *et al.* 2007; Zhang *et al.* 2011; Fris *et al.* 2011). One interesting study in this regard is the realization of fragile and strong glass formers even in colloidal systems (Mattsson *et al.* 2009). By simply tuning the interaction systematically from soft sphere to hard sphere like, the fragility of colloidal liquids increases systematically (Fig. 1.13). This is captured in a plot of η versus ϕ which shows that soft colloids behave like strong glasses whereas hard colloids form fragile ones.

All the studies discussed thus far are for spherical colloids. However, recent advances in chemistry led to development of protocols for synthesis of particles with complex shapes and interactions. These systems provide an opportunity to study glasses which mimic real glass formers more closely. In this context, works by Zheng et.al (Zheng *et al.* 2011, 2014) led to experimental visualization of orientational glass transition in addition to the translational one in systems of ellipsoidal particles. More interestingly, using ellipsoids of aspect ratio 2.1, Mishra et.al showed that there exists a re-entrant transition with increasing attraction in translational degree of freedom and no such re-entrace in dynamics is found in the orientational degree of freedom (Mishra *et al.* 2013). However, most recent studies were aimed at quantifying various dynamic length scales, cooperative rearrangements and understanding glasses with exotic shapes and interactions. There exist very few studies which focus on testing predictions of various theories which might help in distinguishing theories of glass transition. In this context, only recently Gokhale et al. (Gokhale *et al.* 2014) have provided first experimental verification for a few aspects of DF theory by using the procedure developed by Chandler and Garrahan for particulate systems

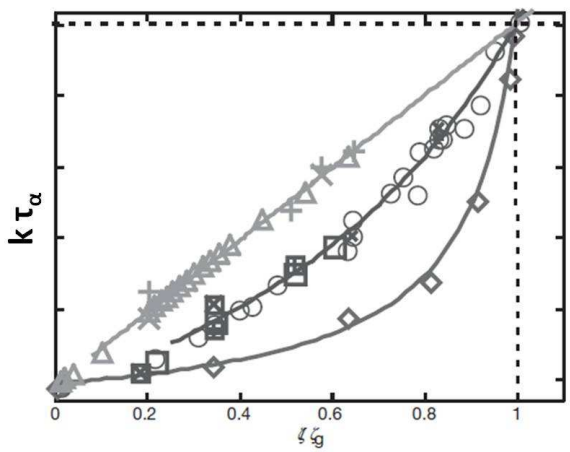

Figure 1.13: Relaxation time scaled by the stiffness of the particle $k\tau_\alpha$ versus Normalized effective volume fraction ζ/ζ_g. ζ_g is the volume fraction of the system for which $\tau_\alpha = 100$s. Different symbols correspond to different stiffness values. Stiff particles (◇), intermediate stiffness (○, □) and soft microgel particles (X , △). Adopted from (Mattsson *et al.* 2009).

(Fig. 1.14a-b) (Keys *et al.* 2011). Consistent with simulations, they have shown that excitations exist and are localized in time and space. Remarkably, the authors observed a decrease in the concentration of excitations with subsequent increase in the facilitation volume with increasing area fraction leading to a slowing down of dynamics (Fig. 1.14b). Interestingly, they showed that even in the presence of random pinning, the concentration of excitations systematically decreased with increasing pinning i.e, on approaching the random pinning glass transition. Most remarkably, by extending the formalism to more complex colloids like ellipsoids, the authors have shown that facilitation theory can also be used to predict re-entrant transition in ellipsoids with attractive interactions (Mishra *et al.* 2013). These studies clearly tilts the balance in favor of DF theory.

However, in facilitation studies on spherical particles, the authors observed that maximum in mobility transfer function (M_{max}), parameter which quantifies the importance of facilitation as a mechanism for relaxation, increases at low area fractions but starts decreasing beyond a given area fraction (Fig. 1.15). The peak in M_{max} is thought to be either due to finite size effects or due to dominance of activated events over facilitated dynamics (Gokhale *et al.* 2014; Elmatad & Keys 2012) and activated hoping is a primary mechanism of relaxation close to glass transition is one of the key predictions of RFOT. Given that proof for neither of these reasons exist, it is crucial to test predictions of RFOT in experiments before drawing conclusions about the nature of the glass transition. In this thesis (Chapter 3, Nagamanasa *et al.* (2014*a*)), we provide direct evidence for a growing static length scale and a change in morphology of CRRs on approaching the glass transition, two key microscopic predictions of RFOT (Biroli *et al.* 2008; Stevenson *et al.* 2006). More importantly, our studies suggest that facilitation might be an important mechanism of relaxation upto T_{MCT} beyond which activated events, primary relaxation processes according to RFOT, dominate structural relaxation (Stevenson *et al.* 2006; Stevenson & Wolynes 2010). Thus our studies provide evidence in favor of thermodynamic nature of glass transition.

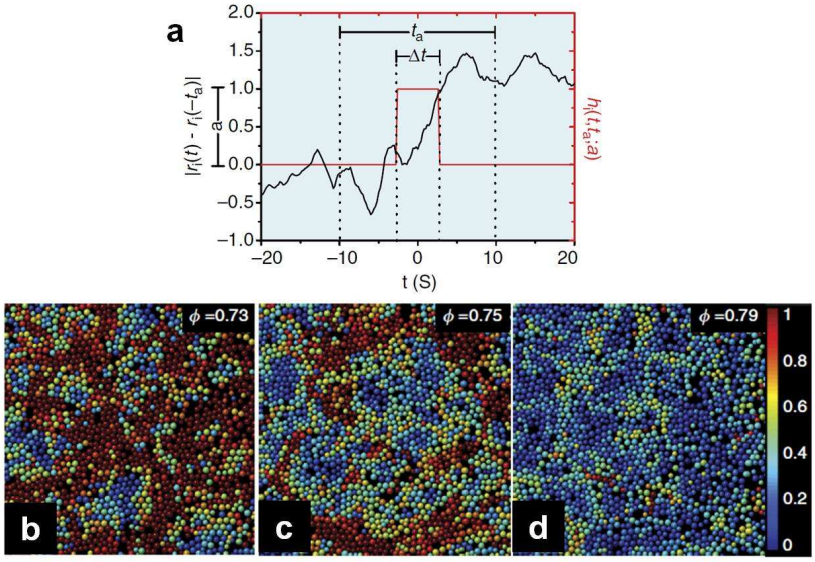

Figure 1.14: (a) Representative trajectory of an excitation from colloid experiment. Here, a is the size of the excitation and Δt is the instanton time. (b)- (d) Experimental visualization of decreasing concentration of excitation with increasing volume fraction. The particles are colour coded based on the displacement as shown by the colour bar. Maroon corresponds to particles which made a displacement greater than a. Adopted from (Gokhale *et al.* 2014).

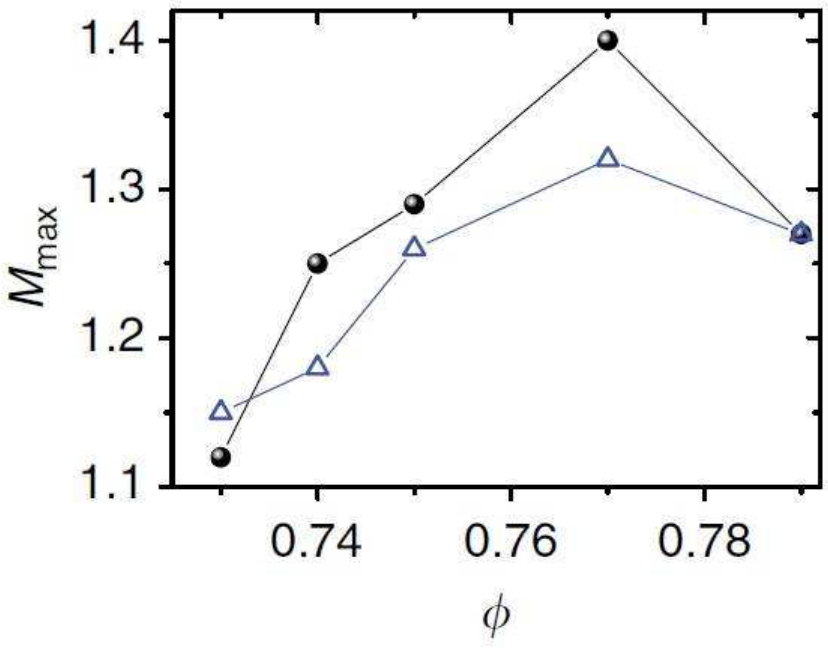

Figure 1.15: Maximum in Mobility Transfer Function M_{max} as function of area fraction ϕ for small (△) and big particles (●). Adopted from (Gokhale *et al.* 2014).

1.4 Deformation of Glasses

Glass transition is associated with the onset of rigidity. Like crystals, glasses also yield and flow plastically when subjected to a stress beyond a threshold value, namely the yield stress (Fan *et al.* 2013). Despite having disparate structural attributes, the bulk mechanical response of crystals and glasses share remarkable similarities (Fig 1.16 a & b). This similarity is not limited to atomic crystals and glasses i.e, hard solids, the ones characterized by large elastic moduli such as metals, it extends to soft materials as well (Fig 1.16 c & d). If differences in the absolute value of applied stresses to deform soft and hard materials are neglected, the bulk mechanical response of hard and soft solids also share striking similarities (Berthier *et al.* 2011). Conventionally, study of flow behaviour of soft materials is called Rheology (Deshpande *et al.* 2010). Given the ubiquity of yielding and plasticity, it is necessary to develop a holistic understanding of these phenomena.

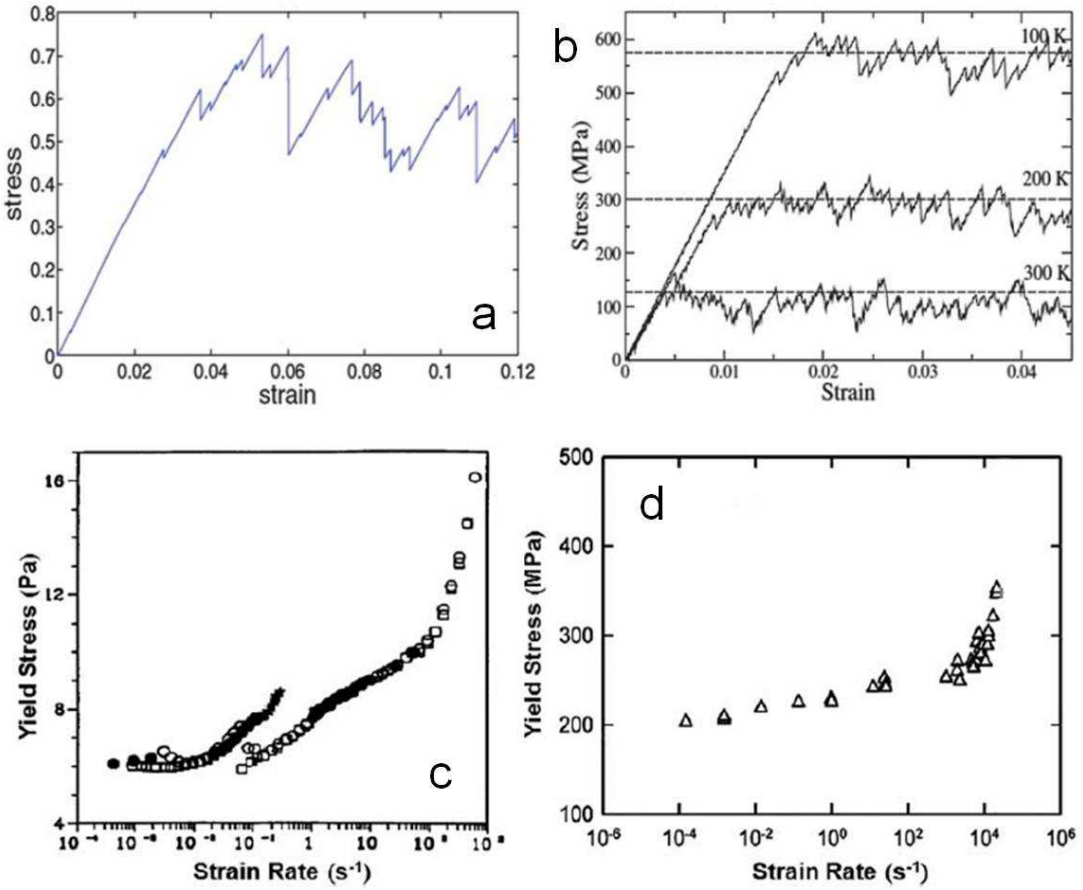

Figure 1.16: (a) Stress-Strain curve from MD simulation results on a glassy systems. (b) Stress-Strain curve from MD simulations on Al single crystal. (c) Yield stress behaviour of a colloidal suspension. (d) Yield stress behavior in copper. Adopted from (Fan *et al.* 2013).

When compared to amorphous plasticity, crystal plasticity is relatively well understood owing to their ordered structure. In crystals, it is now well established that deformation proceeds via the motion and interaction of the well-defined topological defects such as dislocations and grain boundaries (Alava *et al.* 2014). Experimental studies on crystal plasticity have observed that the local plastic events do not occur independently but occur collectively. This is demonstrated by

intermittent dislocation bursts or avalanches which eventually lead to the formation of complex dislocation patterns like cellular structures (Fig. 1.17a) (Miguel *et al.* 2001). This collective behavior was originally quantified experimentally through acoustic emission experiments, where energy signals showed large fluctuations and the size distribution of these avalanches showed a power-law behaviour with exponent 1.5 (Fig. 1.17b) (Miguel *et al.* 2001; Weiss & Grasso 1997; Weiss & Marsan 2003; Richeton *et al.* 2005). Such a power-law behaviour is an evidence for the presence of spatio-temporal correlation between events. However, whether these power-laws are universal or system dependent is yet to be understood. On a macroscopic scale, these intermittent bursts of plastic events manifest themselves as steps in the stress-strain curves, plots used to quantify the flow behaviour of materials. Thus, if the phenomenon is universal, one would expect that the power law exponents for stress size distributions should be identical to the ones obtained from acoustic emission experiments. While stress-strain curves of macroscopic samples can give rise to smooth profiles due to incoherent superposition of deformation bursts, the step profile can be visible for samples of small sizes (Alava *et al.* 2014; Uchic & Dimiduk 2005; Uchic *et al.* 2004; Dimiduk *et al.* 2005; Brinckmann *et al.* 2008). Exploiting this fact, Dimiduk et al. performed compression experiments on micron scale samples using a nano indentation device (Dimiduk *et al.* 2006). Remarkably, they observed step profiles in stress-strain curves and more interestingly the distribution of stress bursts turned out to be a power-law with an exponent of $\sim$ 1.5 (Fig. 1.17c). More strikingly, even experiments with colloidal crystals show that dislocations occur as intermittent bursts and form cellular structures when deformed plastically (Fig. 1.17d). By quantifying the motion of individual dislocations, they have estimated the velocities of these bursts and have observed that the distribution of velocities once again follows a power-law with an exponent that is identical to the one observed for atomic crystals (Fig. 1.17d) (Pertsinidis & Ling 2005). All these results clearly demonstrate the universality associated with crystal plasticity (Tsekenis *et al.* 2013). Apart from experimental studies, even theoretical studies propose that yielding transition has features reminiscent of a self-organized critical behaviour (SOC). On the other hand, it is known that in general SOC can be connected to a non-equilibrium critical phenomenon if a steady state can be attained (Dickman *et al.* 2000). Taking these into account, there are propositions that yielding transition could be associated with a non-equilibrium phase transition. In-fact there are theoretical studies which suggest that yielding in crystals can be thought of as a pinning and depinning transition (Ispánovity *et al.* 2014; Zaiser *et al.* 2005).

Now we move to amorphous plasticity whose study is difficult due to lack of well defined defects. Since the macroscopic deformation of these solids share similarities with crystals, it is natural to quantify stress-strain curves and check for the universality in exponents. In this regard, compression experiments performed on amorphous solids exhibit phenomenology similar to that of crystals (Shan *et al.* 2008; Wang *et al.* 2009; Antonaglia *et al.* 2014; Demkowicz & Argon 2005). In addition atomistic simulations of amorphous materials displayed strain bursts similar to those observed in crystalline materials (Maloney & Lemaitre 2004; Lin *et al.* 2014). However, consensus on the universality class associated with the scaling is yet to emerge (Alava *et al.* 2014; Budrikis & Zapperi 2013; Salje & Dahmen 2014).

Stress-strain relations emerge from a homogeneous continuous medium description. However,

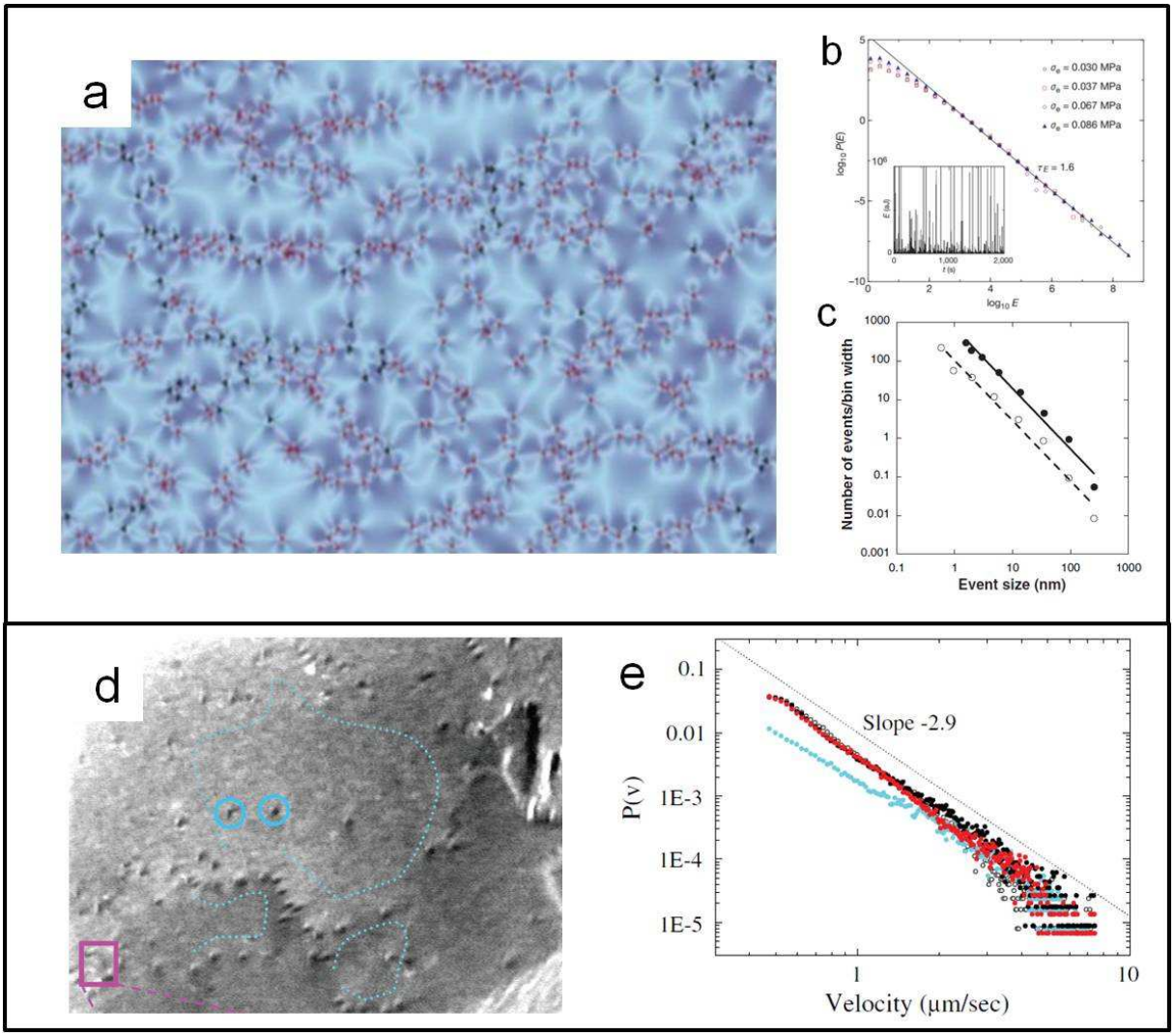

Figure 1.17: (a)-(c) Results from experiments probing atomic crystal plasticity. (a) Visualization of cellular structure of dislocations from experiments on ice crystals. (b) Power-law behaviour of dislocation avalanches resulted from acoustic emission experiments. (a)-(b) Adopted from (Miguel *et al.* 2001). (c) Power-law behaviour of stress distributions from nano indentation experiments on micron sized crystals. Adopted from (Uchic *et al.* 2004). (d)-(e) Results from experiments on colloidal crystals. Adopted from (Pertsinidis & Ling 2005). (d) Video microscopy image of dislocation bursts. Cellular structures are outlined by dotted blue lines (e) Power-law behaviour of velocities of dislocation bursts. Different symbols represent data from different parts of the image.

from a microscopic perspective, one of the important aspects is identification of local events which play the role of dislocations in crystals and hence underly the macroscopic behaviour. It is now believed that there exists elementary events 'shear transformations' which govern plastic deformation in amorphous materials (Argon & Kuo 1980; Falk & Langer 1998). Most modern theories are based on the idea that plasticity is a result of accumulation of these local events which are nothing but weak regions of about ~ 10 particle diameters which are susceptible to collective rearrangements when subjected to external stress, analogous to dislocation in crystals. Before going further, we will give a brief overview of the development of microscopic theories of amorphous plasticity (Berthier *et al.* 2011).

1.4.1 Theories of Amorphous Plasticity

Early theories on sheared amorphous solids were developed by Eyring (Eyring 1936), Turnbull and Cohen (Turnbull & Cohen 1970) and Argon (Argon 1979; Argon & Kuo 1980; Argon 1982). According to Eyring's theory, the flow proceeds through hopping of individual molecules across energy barriers to the free spaces created by their adjacent ones which eventually gives rise to a macroscopic strain. In theories which followed this, the individual hops were replaced by collective motion of particles. According to Argon, these collective events called as shear zones are like inclusions that are weakly coupled to the surrounding medium. For the weak zone to make a rearrangement, it has to over come a small free energy barrier. His model is based on the idea that zone flips are thermally activated and the effect of the external stress is to reduce the free energy barrier thus causing more rearrangements. In addition, a zone can flip if the zone is deformed upto a critical strain, namely yield strain. The main draw backs of these theories are that they assume these zone flips or hops are independent and also ignore the fact that energy barriers could be broadly distributed instead of being a constant for all zones. Nevertheless, Argon's theory introduced the notion of weak zones which is the basis of most theories now. But this theory does not focus on where these flips occur and it relies on them only weakly. Accordingly, plasticity is because of large number of such local rearrangements which can occur anywhere in the systems. On the other hand, the theoretical formulation which is based on the dynamical equations for the density of these weak zones is the Shear Transformation Theory developed by Falk and Langer (Falk & Langer 1998, 2011). It is after the development of this theory that these weak zones are termed as 'shear transformation zone (STZ)'. The major difference between STZ theory and the above mentioned theories is that this theory takes STZs in a important way. According to this theory STZs are well defined objects and hence one can write dynamical equations for their densities. One of the main additions made by Falk and Langer to the preceding theories is that STZs have internal degrees of freedom. Using these postulates, without going into the details, we wish to mention that many features of a deformation process could be explained by the mean field theory of Falk and Langer. However, simulations revealed that there exists phenomena which can be rationalized only by considering correlations between STZs. These were taken into account in the elasto-plastic theories developed by Bulatov and Argon (Bulatov & Argon 1994a,b,c,d). They postulated that these zones are embedded in an elastic medium and whenever an STZ transforms, it modifies the stress field at long distances which in-turn can given rise to a new STZ. They also pointed that the transformation happens

via a mechanism similar to that of Eshelby inclusions (Eshelby 1957) and this is the key for modern theories of plasticity. Remarkably, the presence of STZ and the accompanying Eshelby like quadrupolar fields has been shown in simulations by Lemaître and co-workers (Maloney & Lemaitre 2006; Lemaître & Caroli 2009). More interestingly, they have seen correlations in the strain fields which eventually give rise to avalanches of flips (Bailey *et al.* 2007), consistent with elasto-plastic theories. All the aforementioned theories are developed mostly in the context of hard amorphous solids, the theory which is used extensively to study rheological properties of soft materials is soft glassy rheology (SGR) (Sollich *et al.* 1997; Sollich 1998). According to SGR model, the system is collection of elements l each of which is trapped in a state of energy E. When the system is strained each element can deform upto a critical value l_y and each local element yields when the strain energy $1/2kl_y^2$ becomes equal to the energy of the trap. Here, k is the spring constant. Once an element yields, l is reset to zero. The first important ingredient of this theory is that all elements do not have same E but have a distribution of energies, that is each yield event has an energy of its own. After yield the element picks a new E from the distribution. The second ingredient is the concept of effective temperature. This is primarily to take into account interactions between elements. Thus, yielding here is governed by the effective temperature. Taking these two features into account and solving dynamical equations for strain distribution functions $\mathcal{P}(E, l, t)$, probability of an element having yield energy E and a local strain l at a time t, this theory can explain various rheological features like flow curves, stress overshoots, rejuvenation and overaging observed in experiments on soft systems. While it could successfully explain many features of deformation of soft materials, it does not offer any spatial information about stress distribution or non-affine displacement. Also, it does not explain how effective temperature is linked to material parameters. Further it does not offer any information on the length scale of the elements.

1.4.2 Experimental Studies on Deformation of Soft Glasses

While the existence of local plastic events is predicted by amorphous plasticity theories and are shown by simulations, their experimental evidence came from colloidal glasses (Schall *et al.* 2007). Unlike crystalline defects, these 'shear transformations' do not possess a specific structure and hence they are usually identified by measuring local strain fields or local elastic moduli. However, there is no universal prescription for the same. First experimental evidence for the existence of shear transformation zones was provided by Weitz and co-workers (Schall *et al.* 2007). By quantifying the strain fields in a 3D sheared colloidal glass they have revealed the presence of localized regions which possess large negative and positive strain fields as compared to their neighboring regions and more importantly these are the regions which undergo flips (Fig. 1.18a). Remarkably, studies by Schall and co-workers have shown that the strain fields around an STZ indeed possess a quadrapolar symmetry with Eshelby-like inclusions (Fig. 1.18b) (Chikkadi *et al.* 2011; Chikkadi & Schall 2012). Computing spatial correlations of the strain field further show power-law correlations which span system sizes at plastic deformation which is consistent with simulations (Fig. 1.18c). Similar results were also observed in experiments on indenting colloidal glasses (Rahmani *et al.* 2013, 2014). All the above discussed experimental results and simulations strongly suggest correlations in local yield events analogous to the ones

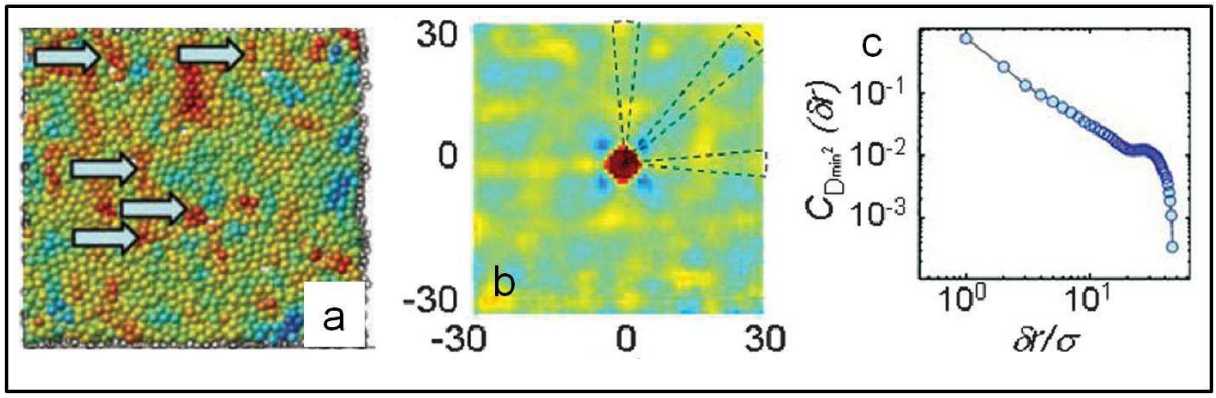

Figure 1.18: (a) Experimental evidence for shear transformation zones (STZ) in a 3D colloidal glass. Reb and Blue spheres corresponds to particles associated with negative and positive strain, respectively. Adopted from (Schall *et al.* 2007) (b) Evidence for quadrapolar fields around an STZ in a 3D colloidal glass. The image is colour coded based on the strain fields with red for extreme positive and blue for extreme negative. (c) Long range strain correlations observed in 3D colloidal glass. Adopted from (Chikkadi *et al.* 2011).

observed in crystalline materials indicating the presence of a non-equilibrium phase transition. However, no direct evidence for such a transition and hence the nature of the transition exist.

Towards this end, recently there is a large volume of work trying to establish the existence and hence the nature of the phase transition underlying yielding of amorphous solids. It is to be noted that most of these studies are motivated by recent experiments on periodically driven non-Brownian suspensions by Pine and co-workers (Pine *et al.* 2005; Corte *et al.* 2008; Corté *et al.* 2009). Briefly, through a set of experiments and simulations on dilute non-Brownian suspensions, in ref (Pine *et al.* 2005) they have observed that for these suspensions there exists a threshold strain for the onset of irreversibility. Using a periodic strain has enabled them to probe steady states at all applied strains which in-turn allowed them to extract the time taken to reach a steady state, τ. By plotting τ as a function of applied strain γ, they observed a divergence in τ close to the γ associated with the onset of irreversibility. Accompanying this diverging τ, they have observed an order parameter like behaviour for fraction of irreversible or active particles f_A. Similar results were also obtained from their simulations (Corte *et al.* 2008). More interestingly, from the relaxation time exponent and the order paramter exponent, they conclude that this transition falls into a category of non-equilibrium critical phenomena called Absorbing-phase transitions (Corte *et al.* 2008).

Absorbing Phase Transitions (APT) Absorbing Phase Transition is a non-equilibrium phase transition where the systems goes from an inactive steady state to an active steady state beyond a critical driving force (Hinrichsen 2000; Jensen 1993). Such transitions are typically associated with a critical-like behaviour. Examples of such transitions are found in epidemics (Dickman 2002), heterogeneous catalysis (Ziff *et al.* 1986), flow through porous media (Bouchaud 1990) and turbulence (Pomeau 1986) to name a few. In the context of experiments with non-Brownian suspensions, below the critical strain (γ_y) the system settles into a steady state which does not undergo any irreversible rearrangements, even on the application of strain cycle. Such a steady state is termed as 'absorbing state' (Fig. 1.19a). On the other hand for $\gamma > \gamma_c$, the

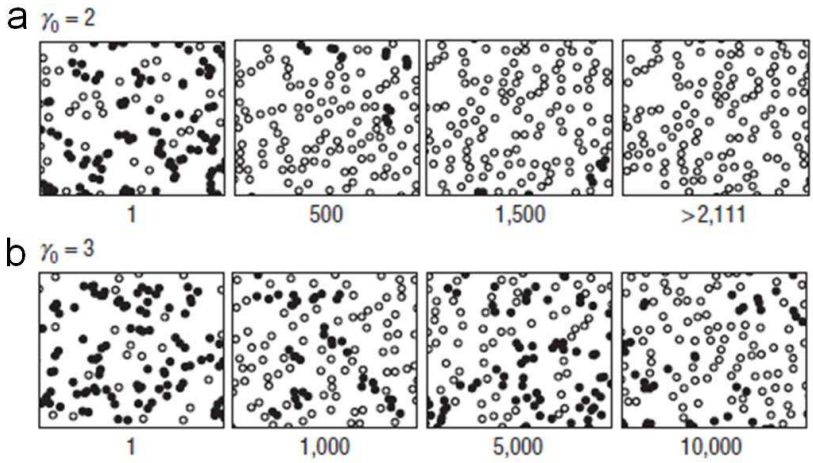

Figure 1.19: Simulations of 2D model. Snapshots of particle distributions for different cycle numbers for (a) $\gamma < \gamma_c$ and (b) $\gamma < \gamma_c$. The black filled particles correspond to active particles and the hollow circles represent irreversible particles. Adopted from (Corte *et al.* 2008)

system settles into a steady state which has a finite number of active or irreversible events and this state is termed as 'active' state (Fig. 1.19b). Also, the steady state fraction of active or irreversible events increase with increasing strain (Corte *et al.* 2008). More interestingly, in ref (Pine *et al.* 2005), the authors observed that the threshold strain for the onset of irreversibility decreases with increasing volume fraction of the non-Brownian suspension.

Colloidal glasses do not posses quenched disorder and hence it is unlikely that yielding in these systems would be associated with pinning-depinning like crystals but simulations suggest the existence of SOC like crystals (Sun *et al.* 2010; Salje & Dahmen 2014). Given that an Absorbing phase transition is one of the paths towards self-organized criticality (Dickman *et al.* 2000) it is tempting to speculate that yielding here is associated with an underlying absorbing phase transition. Furthermore, since yielding is associated with the onset of irreversibility (Hébraud *et al.* 1997; Petekidis *et al.* 2002) and also studies suggest the existence of phase transition in its vicinity (Budrikis & Zapperi 2013), it is natural to use methods developed by Pine and co-workers to probe this transition.

Applying the protocols developed by Pine and co-workers to amorphous solids, Keim et al. (Keim & Arratia 2013) and Fiocco et al., as well as Mohan et al.(Mohan *et al.* 2013; Fiocco *et al.* 2013) via experiments and simulations, respectively, have provided evidence suggesting the existence of critical phenomenon associated with plasticity. Nevertheless, the nature of the phase transition and the proof that it is associated with bulk yielding is yet to be established. In this thesis (Chapter 4, Nagamanasa *et al.* (2014*b*)) we discuss experiments, where by simultaneously quantifying the bulk mechanical response as well as single particles dynamics in periodically driven prototypical amorphous solid - colloidal glass, we have investigated yielding phenomenon. Our studies provide evidence for an absorbing phase transition underlying yielding and also establish a direct connections between microscopic and macroscopic irreversibility.

In this section we have discussed studies where insights originating from studying crystals were used to investigate amorphous solids. On similar lines, since crystals have disordered interfaces - grain boundaries, we attempt to understand these amorphous interfaces using the

concepts developed for glasses. We provide the details of the results in Chapter 5 but here we give an overview of polycrystals and how colloids can be used to investigate them.

1.5 Grain Boundaries and Polycrystals

Most metals when cooled slowly from a high temperature to a low temperature crystallize (Fig. 1.6 blue line) (Kelton & Greer 2010; Callister & Rethwisch 2007). However, entropic effects favor the formation of imperfections and hence perfect single crystals are rare and most often annealing results in the formation of polycrystals. A polycrystal is a collection of crystallites of different orientations separated by disordered interfaces namely grain boundaries (GB). The thermal and mechanical properties of polycrystalline materials are governed by their microstructure which is composed of defects such as dislocations and grain boundaries.

1.5.1 Crystal Defects

Crystal defects are typically classified based on their geometry as point, line and surface defects (Fig. 1.20) (Mrowec & Marcinkiewicz 1980).

Point Defects

In a perfect crystal, all lattice sites contain atoms, however, in reality there could be missing atoms namely vacancies or an atom may occupy a non-lattice site called as self-interstitial (Fig. 1.20a). In addition, a lattice position and an interstitial site can also be replaced by a foreign atom (Fig. 1.20b). All such imperfections are termed as point defects.

Line Defects

Dislocations (Fig. 1.20c) are missing half-plane of atoms which causes lattice distortion in their vicinity (Hull & Bacon 1984; Nabarro & Duesbery 2002). The nature of the lattice distortion is best described by a Burgers circuit and a Burgers vector (**b**). **b** is the additional vector needed to complete the Burgers circuit, obtained by joining atoms around a dislocation when compared with a similar circuit in a defect free crystal. Based on the relative directions of **b** and the dislocation line, dislocations are classified as edge and screw type. In the former, **b** and the dislocation line are perpendicular to each other whereas in the latter they are parallel. Fig. 1.20c shows schematic of a edge and a screw dislocations along with **b** and dislocation lines. While there exists two kinds of dislocations, in reality more often one observes mixed dislocations which are partly edge and partly screw type. The motion of the dislocations play a key role in deformation of single crystals. In-fact the preliminary evidence for the existence of dislocations is a result of attempts to reconcile theoretical and experimental values of the shear stress needed to deform single crystals.

Grain Boundaries

Grain boundaries (GB) are thin disordered interfaces which separate two adjacent crystallites of different orientations in a polycrystal (Howe 1997; Lejcek 2010; Gottstein & Shvindlerman 2009; Rollett *et al.* 2004) (Fig. 1.20d). GBs are characterized by five parameters. These parameters essentially give a quantitative measure of how much one crystallite is rotated with respect to the

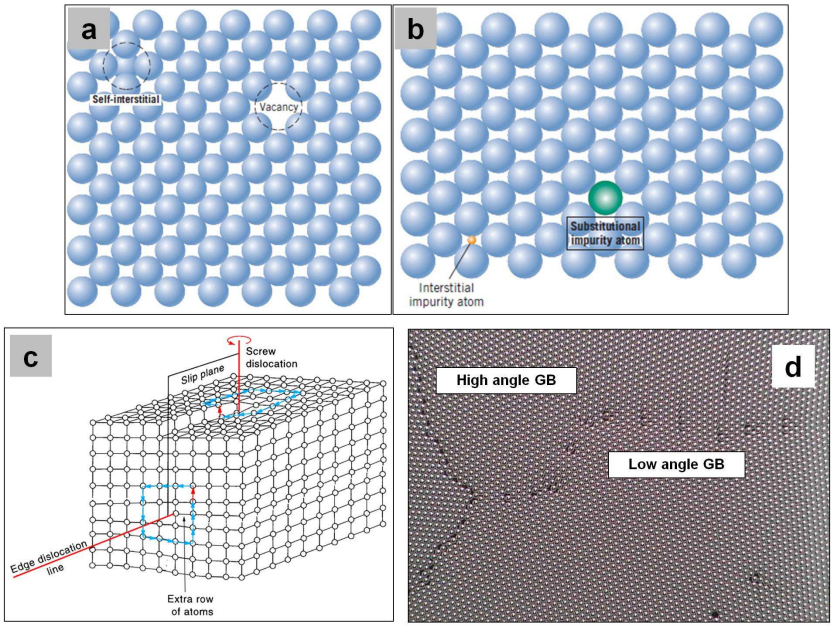

Figure 1.20: Point Defects (a) Schematic of vacancy and self-interstitial (b) Substitutional impurity atom and interstitial impurity atom. (a)-(b) Adopted from (Callister & Rethwisch 2007) (c) Edge and Screw dislocations with respective Burgers vector, Burgers circuit and dislocation line. Adopted from *https://courses.eas.ualberta* (d) Grain Boundaries both LAGB and HAGB. Adopted from *http://homepages.cae.wisc.edu*

other. Out of these five crystallographic parameters, three correspond to the angles of rotation with respect to the three orthogonal axes (Φ_1, Φ_2, π), termed as misorientation angles, and the remaining two correspond to the vectors normal (n_1, n_2) of the two crystal surfaces. Angles Φ_1 and Φ_2 which are in the plane of the grain boundary and are called tilt angles and π is the rotation about an axis normal to the GB plane and is known as a twist angle.

Classification of GBs

If two adjacent grains of a GB are mirror images of each other, such boundaries are termed as symmetrical GBs. GBs are typically categorized based on the misorientation angles. A GB is called a tilt boundary if π is zero, a twist boundary if Φ_1 and Φ_2 are zeros and mixed boundary if all three angles are non-zero. In addition to the aforementioned classification, they are also divided based on their atomic structure, which in turn depends on the value of the misorientation angle as Low and High angle boundaries (Fig. 1.20d). This classification of GBs is important, since the characteristic properties like boundary energy and mobility depend crucially on value of Φ_1, Φ_2 or π (Fig. 1.21b) (Gottstein & Shvindlerman 2009).

Low angle boundaries Low angle boundaries (LAGB) also known as small angle boundaries, are GBs for which the misorientation angles are small and hence are composed of a periodic array of discrete dislocations (Fig. 1.20d). Edge dislocations result in tilt boundaries and twist boundaries are formed from screw dislocations. For LAGBs, the number of dislocations per unit area or the dislocation density, n, can be directly estimated from the value of θ. Here, θ could be Φ_1, Φ_2 or π. If $\mathbf{b}$ is the Burgers vector, and D is the distance between two adjacent dislocations, $\sin\frac{\theta}{2} = \frac{|\mathbf{b}|}{2D}$. For small θ, $\sin\frac{\theta}{2} = \frac{\theta}{2}$ and hence $n = \frac{1}{D} = \frac{\theta}{|\mathbf{b}|}$. Further, the energy also depends

on the misorientation angle and is given by the Read-Shockley model (Read & Shockley 1950). According to this model, grain boundary energy (γ_{GB}) is

$$\gamma_{GB} = E_o\theta\,(A_o - \ln\theta) \tag{1.38}$$

$$\text{with } E_o = \frac{Gb}{4\pi(1-\nu)} \text{ and } A_o = 1 + \ln\frac{b}{2\pi r_o}$$

Here, G is the shear modulus, ν is Poisson's ratio and r_o is the radius of the dislocation core. The dependence of GB energy on θ as estimated by Read-Shockley model is shown in Fig. 1.20a. Remarkably, the estimated values were found to be in good agreement with the measured values. However, this dislocation model fails for boundaries with $\theta \gtrsim 15°$, where individual dislocations loose their identity and the dislocation cores start overlapping.

High angle boundaries: High angle boundaries, (HAGBs), unlike LAGBs, are continuous interfaces and typically have $\theta \gtrsim 15°$ (Fig. 1.20d). Owing to the difficulty in quantifying their structure, there exist no universal theory to describe the energy or the mobility of these boundaries and therefore HAGBs are relatively less understood. HAGBs can be further divided into special or Σ boundaries, vicinal and general grain boundaries. Special boundaries are ones which are composed of a repeating structural unit. These boundaries are described using the coincidence site lattice model (CSL). Coincidence sites are the ones where the atomic positions of the grain boundary coincide with the ideal positions of the two adjacent crystals. GBs for which all its atoms are at the coincidence site possess repetitive structural units and such boundaries are termed as special or CSL boundaries (Brokman & Balluffi 1981). The basic unit of CSL is a polyhedra and is larger than unit cell of the lattice. The CSL boundary is characterized by density of its coincidence sites, defined by Σ.

$$\Sigma = \frac{\text{volume of elementary CSL cell}}{\text{volume of elementary unit of crystal lattice}} \tag{1.39}$$

General boundaries are the ones which contain more than one repetitive structural unit overlapped and hence do not posses a well-defined structure. On the other hand vicinal boundaries consist a structural unit combined with one or more sets of dislocations. Interestingly, the energies of HAGBs do not show a monotonic dependence on θ as in the case of LAGBs but contains a few cusps (Yip 2007; Gottstein *et al.* 2001). It is now well understood that the minima correspond to the special boundaries which owing to a defined structure posses lower energy (Fig. 1.21b). However, only a few specific θs result in Σ boundaries. A complete understanding of dynamics of other types of HAGBs is still lacking.

It is to be noted that GB architecture and its migration govern processes such as plastic deformation, grain growth and recrystallization (Lejcek 2010; Gottstein & Shvindlerman 2009; Rollett *et al.* 2004). Given that HAGBs are poorly understood and possess complex structure, one of aims of materials research is to understand the dynamics and migration of HAGBs (Randle 2010; Yip 2007).

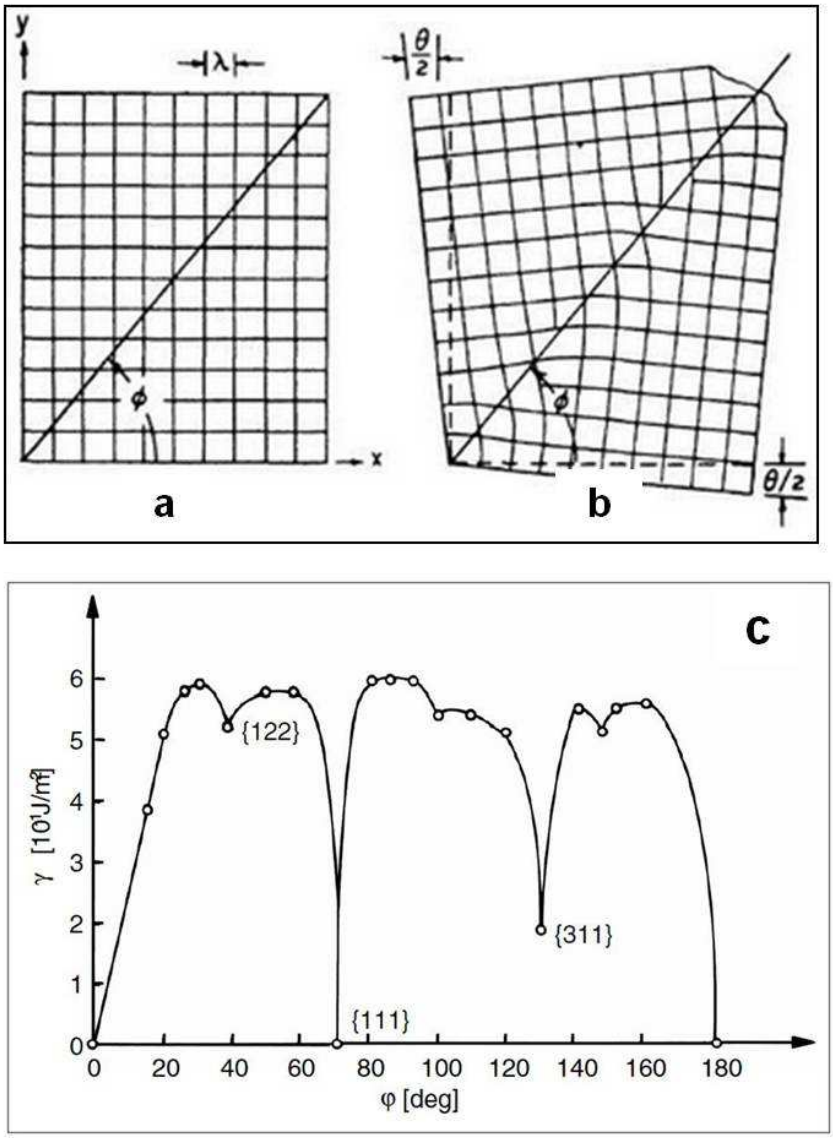

Figure 1.21: (a)-(b) Read-Shockley model for a low angle boundary. Here, θ is the misorientation angle and λ is the lattice constant. Adopted from (Read & Shockley 1950). (c) Grain Boundary energy, γ, as a function of misorientation angle, ϕ. Adopted from (Goux 1974)

1.5.2 Colloidal Crystals as Models for Atomic Crystals

Colloidal systems have been used as models to understand a wide variety of processes in crystals including dislocation dynamics (Schall *et al.* 2004, 2006), pre-melting (Alsayed *et al.* 2005), grain growth (Palberg *et al.* 1995; Gokhale *et al.* 2012), impurity segregation (Yoshizawa *et al.* 2011; Ghofraniha *et al.* 2012) and super heating (Wang *et al.* 2012*b*). After the discovery of a liquid-crystal transition in simulations on hard sphere systems by Wood and Jacobson (Wood & Jacobson 1957) and Alder and Wainwright (Alder & Wainwright 1957) in 1957, the experimental evidence for the same was provided only in 1986 by using colloidal systems (Pusey & van Megan 1986; Pusey *et al.* 1989). Numerous studied followed this seminal work where colloids were used to realize complex self assembled structures (Velikov *et al.* 2002; Shevchenko *et al.* 2006; van Blaaderen *et al.* 2003; Dziomkina & Vancso 2005) as well as to investigate microscopic underpinnings of physical processes (Ganapathy *et al.* 2010; Kaya *et al.* 2010; Peng *et al.* 2015).

In the context of complex crystal structures, for example, by using a mixture of positively and negatively charged particles van Blaaderen and co-workers have achieved self-assembled structures analogous to NaCl and CsCl crystals (Leunissen *et al.* 2005). Even more complicated structures, like Kagome lattice were also realized experimentally by Chen et.al. using tri-block Janus particles, particles with three patches (Chen *et al.* 2011). In addition, using micropatterend templated surfaces in combination with sedimentation, one can direct crystallization (Vogel *et al.* 2012; Yin *et al.* 2001; Dziomkina & Vancso 2005). Such a technique was used to grow crystals of different lattice constants and crystal symmetries (Ramsteiner *et al.* 2010; Savage *et al.* 2013). On the other hand, pioneering work using colloids to investigate microscopic processes in crystals was carried out by Weitz and co-workers (Schall *et al.* 2004, 2006; Suresh 2006). By combining laser diffraction microscopy and confocal microscopy, a real space visualization of dislocation, nucleation and their dynamics (Fig. 1.22a-c) has been achieved. In a following work, by indenting a colloidal crystal with a sewing needle, a technique analogous to nano indentation technique used for atomic crystals, they have studied the formation of dislocations, mapped the associated strain field and also quantified the dislocation nucleation rate (Fig. 1.22d-f)(Schall *et al.* 2006). Remarkably, these works have provided evidence that the defects dynamics in these systems can be well described by the continuum approach which is used to describe defect dynamics in atomic crystals (Cotterell 1953; Frank 1950). These studies have set the stage for using colloids to probe phenomena that are prohibitively difficult to study in atomic experiments.

Colloids are also used routinely to explore polycrystals (Gokhale *et al.* 2013). The first systematic study of grain growth was carried out by Palberg et al (Palberg *et al.* 1995). far, systems have been developed where the average size of a crystallite or a grain can be tuned by changing the inter particle interactions (Palberg *et al.* 1995), external fields like electrical and shear (Palberg *et al.* 1992, 1995; Gokhale *et al.* 2012), addition of impurities (de Villeneuve *et al.* 2005, 2009; Yoshizawa *et al.* 2011; Ghofraniha *et al.* 2012) as well as cooling rate (Gokhale *et al.* 2012). In addition to growth, one can also address issues regarding melting of crystals. The mechanisms by which crystals melt has been predicted over a century ago (Dash 1999; Dash *et al.* 1995; Löwen 1994) and simulations and theoretical studies suggest that melting begins from defects (Lipowsky 1986; Pluis *et al.* 1987; Dahmen *et al.* 2004). Strikingly, Yodh and co-

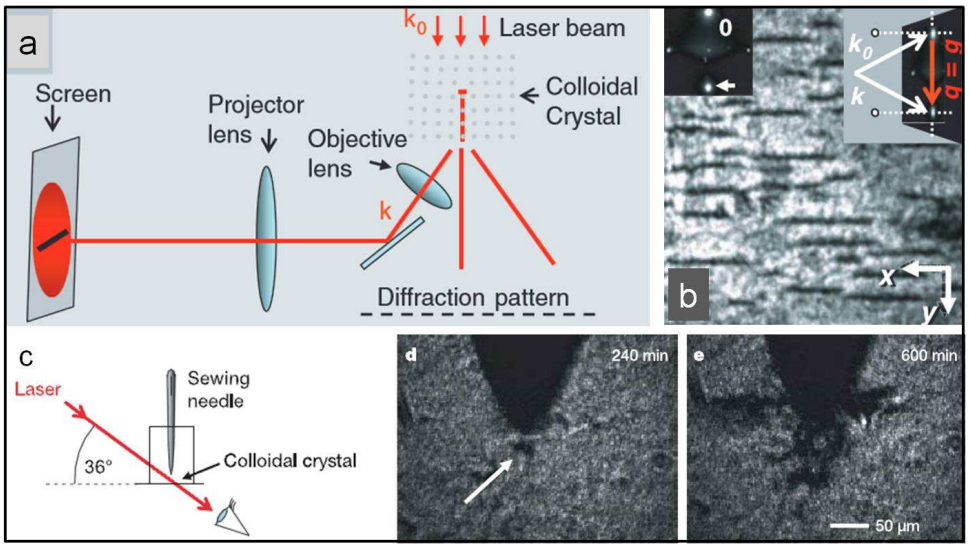

Figure 1.22: (a) Schematic of Laser Diffraction Microscopy (LDM) set-up. (b) LDM image of colloidal crystal. The dark regions correspond to dislocations. (c) Schematic of the indentation configuration. (a)-(c) Adopted from (Schall *et al.* 2004) (d) LDM image showing dark region that correspond to dislocation nucleated because of indentation. (e) Final dislocation structure after 600 min. (d)-(e) Adopted from (Schall *et al.* 2006)

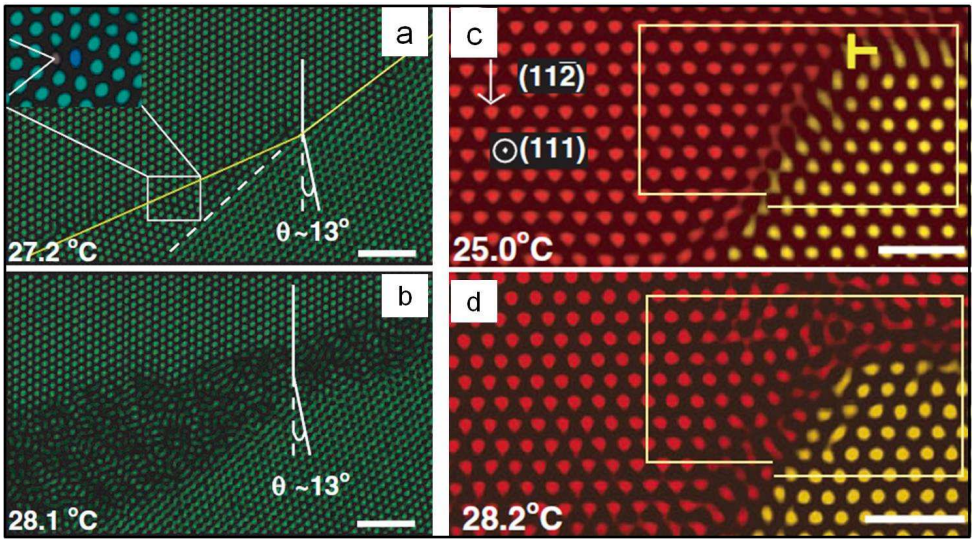

Figure 1.23: Pre-melting of crystal at GB (a) and (B) Bright field image of the GB at different temperatures. Pre-melting from dislocation (b) and (d) Bright field image of Shockley partial dislocation at different Ts. Adopted from (Alsayed *et al.* 2005)

workers using temperature tunable colloids have provided experimental evidence for pre-melting at dislocations and grain boundaries (Alsayed *et al.* 2005). They have also shown that the extent of pre-melting also depends crucially on the nature of the defects (Fig. 1.23).

Given that GBs play a crucial role in grain growth and melting, it is necessary to study them down to the single particle level which is feasible only in colloidal polycrystals. In this regard, Skinner et al. (Skinner *et al.* 2010) and Gokhale et al (Gokhale *et al.* 2012) have quantitatively extracted parameters like stiffness (Γ), quantity related to interfacial tension, and mobility (M) from GB interface fluctuations using capillary fluctuation method (Foiles & Hoyt 2006; Trautt & Upmanyu 2005).

Thus far we discussed studies where the emphasis is on grain growth and GB interfaces. In this thesis, by studying dynamics of particles in GBs, we have shown that HAGBs exhibit properties that are strikingly similar to that of supercooled liquids (Chapter 5, Nagamanasa *et al.* (2011)). Later, it was shown that these results are independent of the dimensionality of the system (Skinner *et al.* 2011).

Chapter 2

Experimental Details

The development of novel instrumentation techniques and protocols to synthesize colloidal particles of various shapes, sizes and interactions have helped unraveling the microscopic underpinnings of diverse phenomena. In this chapter, we discuss protocols followed for synthesizing various colloidal particles used for our studies. We also describe the experimental set-up developed to probe the nature of the glass transition, yielding of glasses and dynamics of grain boundaries.

2.1 Synthesis Protocols

2.1.1 Synthesis of PNIPAm Particles

PNIPAm particles are charge stabilized soft microgel particles. Microgel particles generally contain a network of cross-linked polymers with the interstitial spaces filled with solvent. The characteristic property of these polymers is that they undergo a transition from a lyophilic to lyophobic state in water across a critical temperature namely the lower critical solution temperature (LCST) (Alsayed 2006). This transition on the particle scale manifests as a change in its size with temperature i.e. the particles deswell at high temperatures and with decreasing temperature below LCST their size increases. In addition, the size of these particles can also be varied by changing the pH of the solution with particles being in their swollen state at neutral pH and going to their shrunken state in acidic pH (Wu *et al.* 2003). To synthesize these particles we employed a protocol based on the free-radical polymerization technique. All the chemical for the synthesis were procured from Sigma Aldrich.

The protocol we followed is described below (Wu *et al.* 2003) . We first dissolved 3.8 g of monomer N-isopropylacrylamide (NIPA), 0.066 g of cross-linker N,N′-methylenebisacrylamide (BIS) and 0.11 g of acrylic acid (AA), each in 50 ml of water. These solutions were added into a 500 ml 3 necked round bottom flask (RB), in the same order as mentioned above and subsequently the solution was diluted to 250 ml with water (TQ instruments, 18MΩ). Prior to stating the reaction, the RB was purged with excess nitrogen to remove traces of air. The RB was then left for stirring at 300 rpm under Nitrogen atmosphere at 70 °C. Then 0.166 g of 1% aqueous solution of initiator potassium persulphate (KPS) was added. The solution was then left for stirring for 4 h. Care should be taken that the nitrogen is supplied continuously, rpm is constant at 300 and the temperature is kept at 70 ± 1 °C. The particles thus obtained were purified using dialysis membranes (Spectra/Por Mol.Wt. 10,000) in aqueous environment for one week to remove unreacted chemicals. The water was changed every 10-12 h. To enable confocal imaging, we have added aqueous solution of flurophore Rhodamine 6G externally.

The size of these particles can be varied by adding various amounts of surfactant, sodium

salt of dodecyl sulphate (SDS), along with the NIPA monomer. We find that with increasing concentration of SDS the size of the particles decreases (Table. 2.1). We also observe that a decrease in concentration of AA decreases LCST and increases the intake of Rhodamine 6G (Table. 2.1). To estimate the particle size, the colloids were allowed to crystallize using depletion interaction and subsequently the lattice constant was measured. For crystallizing as synthesized dilute suspension, we used the following composition

NIPA: 100μl in 1ml
Dye: 40μl of 2mg/ml in 1ml
Depletant: 20μl of 2mg/ml in 1ml
We have used sodium carboxyl methyl cellulose (NaCMC, Fischer Scientific, Mol.Wt. 700,000) as the depletant.

Table 2.1: Protocols for Synthesizing PNIPAm Particles

S.No	NIPA monomer (gm)	BIS (gm)	AA (gm)	SDS (gm)	KPS (gm)	Total Reaction Volume (ml)	Size (nm)	LCST (°C)
1	3.8	0.066	0.11	0.1	-	250	1000	60
2	3.8	0.066	0.11	0.1	0.166	250	600	-
3	3.8	0.066	0.11	0.14	0.166	250	440	-
4	3.8	0.066	0.022	0.016	0.166	250	620	34
5	2.5	0.043	0.0144	none	0.109	164.5	780	34
6	2.5	0.043	0.0197	none	0.036	164.5	890	34
7	2.5	0.043	0.0197	none	0.012	164.5	950	34

The volume fraction ϕ of as synthesized suspensions is $\sim 20\% - 30\%$ and hence we have to concentrate them to $\phi \sim 70\%$ at T=26 °C, where the particles self-assemble into hexagonally closed packed crystal structure. Unlike silica or polystyrene particles, PNIPAm particles are density matched with water. Therefore, these suspensions were concentrated by evaporating the excess water at T$\sim$ 60 °C. However, the particles do not swell to their original size even after cooling the suspension to room temperature. In-order to regain the original size of the particles, small volumes of aqueous sodium hydroxide (NaOH, Merck) solution was added. It is to be noted that the amount of NaOH added should be optimized for individual synthesis. For our system, the optimized samples' composition to get polycrystals is as follows:

PNIPAm : 48 μl of $\phi \sim 70\%$ at T=26 °C
Rhodamine 6G : 1 μl of 2mg/ml
NaOH : 1 μl of 100mM

The optimized sample is fluid at T=38 °C and polycrystalline at T=26 °C. Here, ϕ can be tuned in-situ by changing the temperature. Interestingly we observe that, analogous to atomic crystallization, the annealing rate governs the average grain size (Fig. 2.1). Given that average grain size is crucial in dictating the properties of crystalline materials (Hansen 2004; Chok-

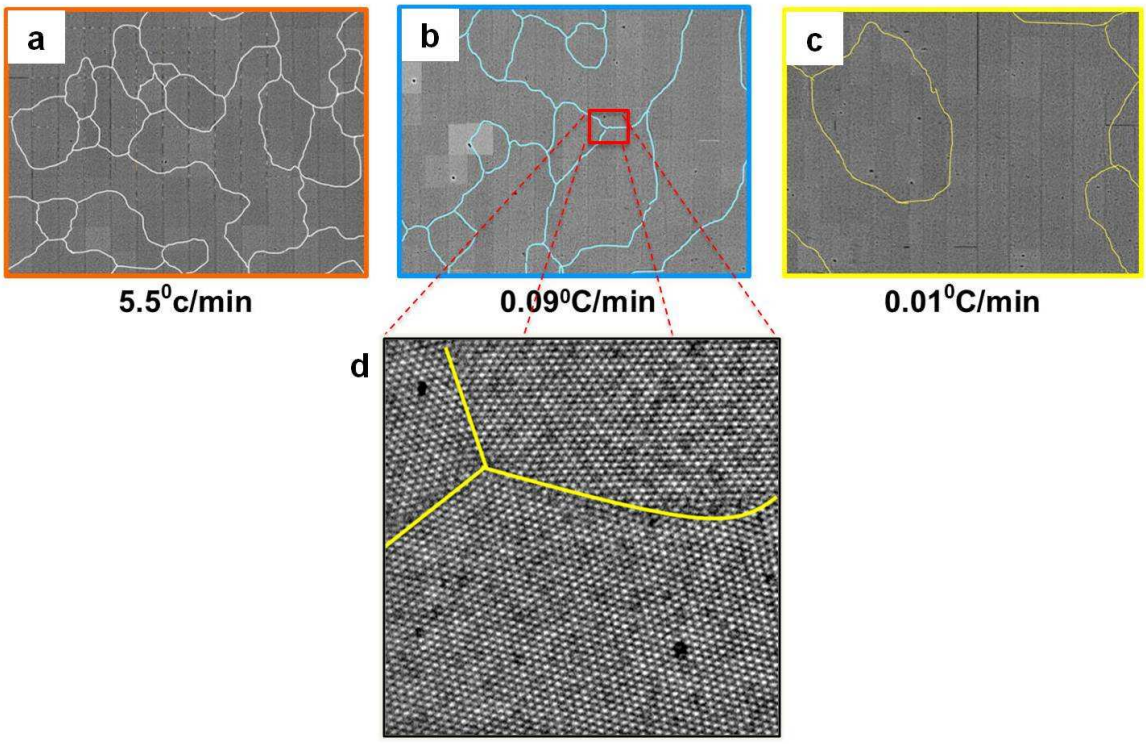

Figure 2.1: (a)-(c) Average grain size for three different annealing rates (a) 5.5 °C/min, (b) 0.09 °C/min (c) 0.001 °C/min. (d) Single confocal slice of a polycrystal with three grain boundaries and a triple junction. Images in (a)-(c) were obtained by tiling ∼ 300 such images. The solid curves represent grain boundaries.

shi *et al.* 1989), this system is best suited for investigating grain size dependent properties of polycrystalline materials.

2.1.2 Synthesis of Fluorescent PNIPAm Particles

While PNIPAm particles obtained using the above protocol enable confocal imaging, the dye absorbed by them is insufficient to image particles deep into the sample for long times, in particular, in dense disordered systems. To circumvent this problem, we synthesized particles using protocols developed to attach dye during synthesis itself (Lawrence *et al.* 2007). To synthesize these particles, we have added polyfluor 570 (methacryloexethyl thiocarbonyl rhodamine B, Polysciences) in addition to the components mentioned in Table. 2.1. The synthesis protocol followed is identical to the one described above. Here, by varying the concentrations of AA, SDS and dye, we have synthesized particles of different sizes and dye concentrations (Table. 2.2). Inorder to maximize the flurophore molecules that are incorporated into the particles, we also performed syntheses where dye saturated solution of water (∼50mg/ml) was used as the reaction medium. The particles obtained were once cleaned using dialysis membrane (Section 2.1.1). Unlike PNIPAm particles, fluorescent PNIPAm can be concentrated using centrifugation.

We want to use these particles to investigate glasses under shear. To avoid crystallization, a binary system of 1 μm and 2.5 μm fluorescent PNIPAm were used. The composition of the sample used is as follows:

Table 2.2: Protocols for Synthesizing Fluorescent PNIPAm Particles

S.No	NIPA monomer (gm)	BIS (gm)	AA (gm)	SDS (gm)	Dye (mg)	KPS (gm)	Volume of water (ml)	Size (nm)
1	2.5	0.044	0.31	0.0065	0.65	0.109	157.9	600
2	2.5	0.043	0.0197	-	32.5ml of 0.65 mg/ml	0.012	164.5	2500 slightly polydisperse
3	1.9	0.033	0.0149	0.01	-	0.0091	125 dye saturated solution	2500
4	1.9	0.033	0.0149	-	-	0.06825	125 dye saturated solution	polydisperse
5	1.9	0.033	0.0149	0.0013	-	0.0091	125 dye saturated solution	1200 polydisperse
6	1.9	0.0335	0.24	0.005	-	0.027	125 dye saturated solution	1050

Composition for big particles:
PNIPAm : 160 μl of $\phi \sim 64\%$ at T=26 °C
Rhodamine 6G : 8 μl of 2mg/ml
NaOH : 4 μl of 100mM

Composition for small particles:
PNIPAm : 105 μl of $\phi \sim 64\%$ at T=26 °C
Rhodamine 6G : 9 μl of 2mg/ml
NaOH : 4 μl of 100mM

For realizing a binary glass, the big and the small particles of the above suspensions were mixed in the ratio 1:1.38 (Fig. 2.2).

2.1.3 Synthesis of PS-PNIPAm Core-Shell Particles

In addition to the above described PNIPAm particles, we have also synthesized core-shell particles where the core is polystyrene particle the shell is composed of PNIPAm. The core was synthesized following the protocol given by Hellweg *et al.* (2004). It is to be noted that to grow a PNIPAm shell using PS particles as seeds, it is necessary to use PS particles which consist of small amounts of PNIAm as well. We have used 450 nm PS particles as seeds and have grown PNIPAm shell around them following the procedure given by Berndt & Richtering (2003). Core-shell particles synthesized in the lab are listed in Table. 2.3. These core-shell particles are particularly suited to study melting in the presence of pinning. Here, PNIPAm shell provides

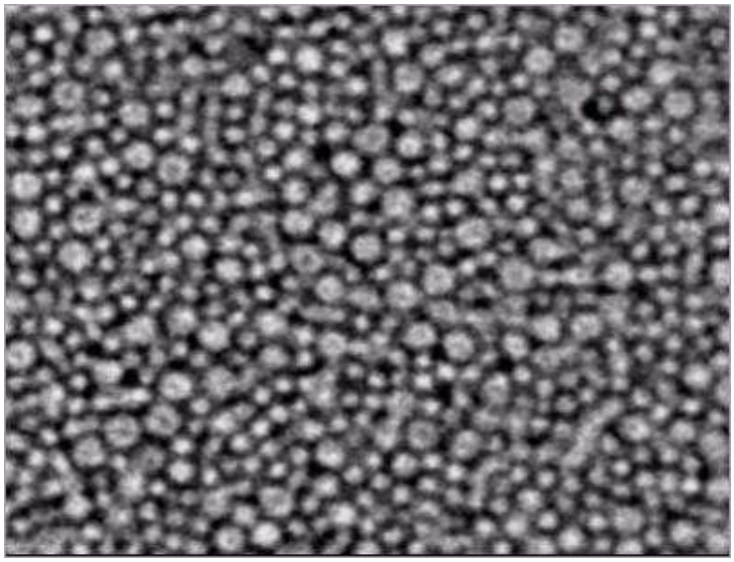

Figure 2.2: Confocal slice of binary glass composed of fluorescent PNIPAm particles.

the temperature sensitivity and PS particles facilitate pinning using optical tweezers.

Table 2.3: Protocols for Synthesizing Core-Shell Particles

S.No	PS-PNIPAm core (gm)	NIPA monomer (gm)	BIS (gm)	AA (gm)	Dye (mg)	KPS (gm)	Volume of water (ml)	Size (nm)
1	1.2	0.76	0.0134	0.096	-	0.0108	50ml	1600
2	1.2	0.76	0.0134	0.016	8ml of dye saturated solution	0.0108	50ml	1600

2.2 Instrumentation

2.2.1 Holographic Optical Tweezers

Optical tweezers are one of the important tools used to probe soft systems at the microscopic level non-invasively. As the name suggests, it uses the electro-motive force of a focused laser beam to hold and manipulate particles. This was demonstrated for the first time by Arthur Ashkin in 1970 (Ashkin 1970). A focussed Argon laser was used to push micron sized latex spheres. During the course of experiment it was realized that some particles were being pulled towards the center of the laser beam. Exploiting this pulling force, a single beam gradient trap was realized for the first time in 1986 (Ashkin *et al.* 1986). Further, this technique was used to even trap single cells (Ashkin *et al.* 1987). Since then, this technique is being applied to a variety of interdisciplinary fields. In a very short span of time, optical tweezers have gained immense popularity and have been used to study biopolymers (Brower-Toland *et al.* 2002; Kerssemakers *et al.* 2003), chromosomes (Ojeda *et al.* 2006), bacteria (Ashkin *et al.* 1987), yeast cells (Ashkin *et al.* 1987), motor proteins (Fazal & Block 2011) and colloidal (Grier 1997) as well nano (Hansen *et al.* 2005) particle systems to name a few. The applications of this technique are many-fold. Tweezers are not just limited for trapping particles, it is also used extensively to measure and apply local forces (Smith *et al.* 1996; Nugent-Glandorf & Perkins 2004). Forces as small as piconewton (pN) can be applied and measured with great precision making this tool important for applications in biology, chemistry and physics. In order to understand the principle behind trapping and to calculate the forces numerous theories have been developed (Harada & Asakura 1996; Ashkin 1992; Mazolli *et al.* 2003; Neto & Nussenzveig 2000).

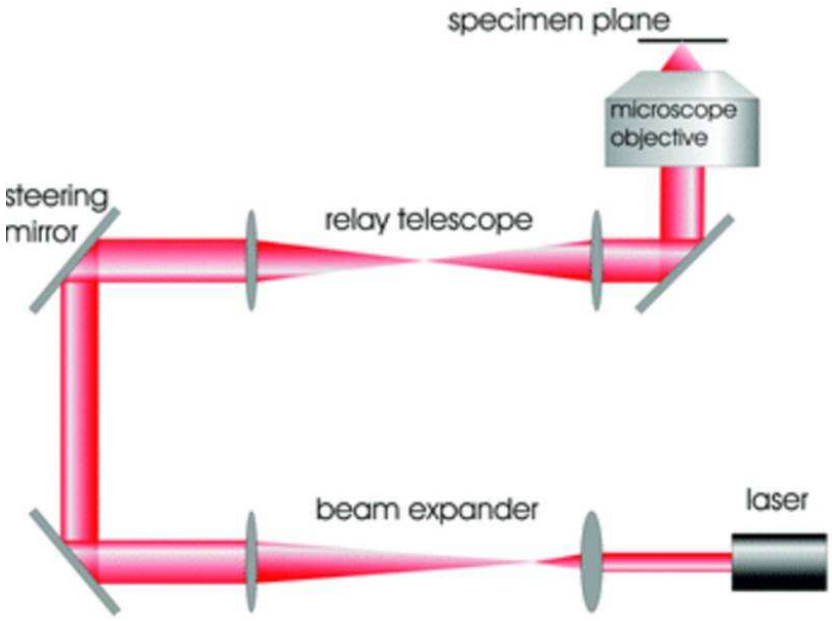

Figure 2.3: Schematic of the set-up for assembling a single trap optical tweezers. Adopted from (Rodrigo *et al.* 2004).

Schematic for single-trap optical tweezer is shown in Fig. 2.3 (Rodrigo *et al.* 2004). Here, the beam steering mirror is used to change the position of the trap laterally. However, increasing

use of tweezers has led to the development of novel techniques to manipulate multiple particles simultaneously (Grier 2003; Moffitt *et al.* 2008; McGloin 2006). This can be achieved by using single beam combination techniques, scanning or holographic techniques. The first attempt to trap multiple particles was by using single beam combination techniques where one laser beam is split into two using a beam splitter cube thus generating dual traps (Fällman & Axner 1997). Another way to create multiple traps is to time share a single trap. Here, by scanning the laser beam rapidly across different trap positions, by spending only a fraction of time at each of them, multiple particles can be trapped. To use this technique, the time taken for the beam to return to a given trap position should be much smaller than the diffusive time scale of the particle. Thus, this technique necessitates devices like acousto-optic deflectors (AOD) which can scan at kilohertz (kHz) rates (Vossen *et al.* 2004). More recently, three dimensional holographic optical tweezers based on diffractive optics, have been developed to trap multiple particles. Here, a hologram or a diffractive element is placed in the conjugate plane to back focal plane of the microscope. This produces an intensity distribution in the focal plane of the sample, which is a Fourier transform of the pattern imposed by the element. This gives rise to multiple beams at required positions. Trapping particles using a diffractive element in the path of the light was pioneered by Fournier et.al (Fournier *et al.* 1995). Fournier et.al used a static glass hologram to generate multiple traps. However, this technique gained momentum following the work done by Grier's group where they used glass etched holograms to study dynamics of colloids (Dufresne & Grier 1998). Further, replacing the diffraction element by spatial light modulator (SLM) led to the development of dynamically movable computer controlled traps (Reicherter *et al.* 1999; Liesener *et al.* 2000; Rodrigo *et al.* 2004; Eriksen *et al.* 2002; Schmitz *et al.* 2005). Holographic optical tweezers (HOT) have been used to create crystal structures (Ganapathy *et al.* 2010), dislocation in a crystal (Irvine *et al.* 2013), microfludics (Ladavac & Grier 2004; Padgett & Leonardo 2011), optical potential landscapes (Lee *et al.* 2005) and to hold cell assays (Rodrigo *et al.* 2004) to name a few.

Spatial Light Modulator, SLM

One of the primary components of the modern day HOT set-up is the Spatial Light Modulator (SLM). SLM is a device which can change the phase or the intensity of the light. SLM when used with optical tweezers allows the users to dynamically create and manipulate multiple traps. SLMs typically contain liquid crystalline molecules (LCs) which control the output phase or intensity of the light. The optical anisotropy of liquid crystals, the refractive index dependence on the axes of the molecule, is exploited to modulate intensity or phase of the light. There exists a variety of LC molecules but typically ferro electric LCs and nematic LCs are used in SLMs. While ferroelectric LC devices are known to have high operating speeds, nematic ones offer better dynamic range and hence allow complex holograms. In addition, these devices can be operated either by using electric fields or optical fields and can work in a reflective or transmissive mode. Here, we have used an electrically addressed phase controlled, nematic LCs, reflective SLM (XY phase series 512 X 512 pixels) from Boulder Non-linear systems (BNS) (Fig. 2.4a).

Electrically controlled SLMs contain LC molecules sandwiched between a transparent electrode and a silicon substrate (Fig. 2.4b). SLMs are mostly computer controlled and hence the silicon substrate is manufactured as an array of electrically-addressable pixels (Fig. 2.4c). The

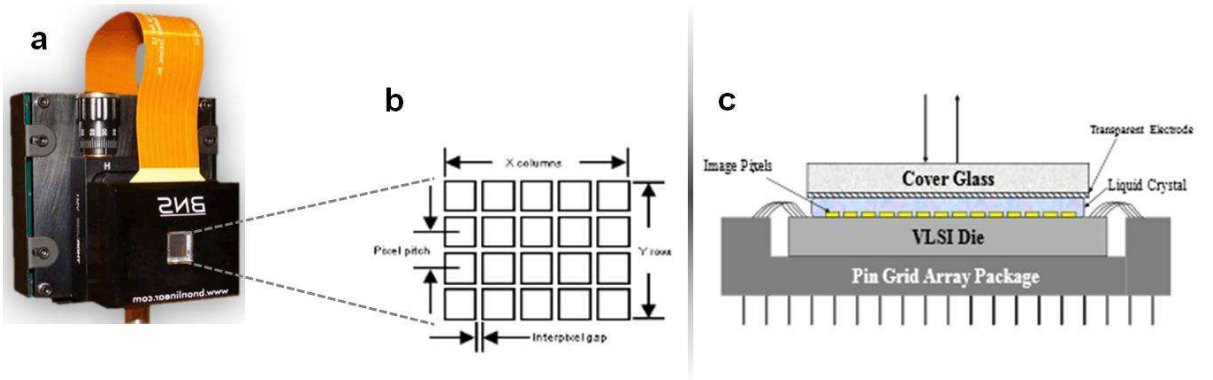

Figure 2.4: (a) Picture of a BNS SLM. (b) Schematic of pixel representation on the SLM (c) Cross section of the SLM. Adopted from *http://bnonlinear.com*

pixel value in an 8-bit gray scale image is appropriately converted to the voltage that needs to be applied across each pixel. Applying a voltage sets up an electric field which subsequently rotates the LC molecules which eventually result in a change in the effective refractive index and hence the effective path length. This further manifests as a phase change thereby creating traps at the required positions. While SLMs facilitate computer control of the traps, being pixelated devices one of their main limitations is a finite resolution.

To use an SLM to create multiple traps, one also needs to generate holograms that are to be fed into the SLM. Thus, using SLMs efficiently also necessitates development of efficient algorithms to produce holograms.

Algorithm for Generating the Hologram

Since there is a Fourier relation between the plane of hologram on SLM and the focal plane, the desired geometry of traps at the focal plane can be reconstructed using Fourier transform of the hologram at SLM. Analogously, the hologram can be obtained by an inverse Fourier transform of the trap patterns. If optical beam incident is

$$u_i = a \exp(i\phi) \tag{2.1}$$

with a being the amplitude and ϕ being the phase, the beam exiting out of the SLM will be

$$u_h = a \exp[(\phi + \phi_h)] \tag{2.2}$$

All algorithms used to generate holograms precisely generate the phase pattern ϕ_h. A number of iterative and non-iterative algorithms have been developed over the last few years (Leach *et al.* 2006; Leonardo *et al.* 2007; Curtis *et al.* 2002; Meister & Winfield 2002; Liesener *et al.* 2000). Examples include gratings and lenses, direct binary search and Gerchberg-Saxton algorithm. For the purpose of our experiments we have used gratings and lenses algorithm to generate phase only hologram in order to create desired trap patterns.

Gratings and lenses is one of the simplest algorithms. It is non-iterative and hence it is computationally faster when compared to iterative algorithms like Gerchberg-Saxton. In this, the inverse Fourier transform of the trap pattern is determined using mathematical analogues of

optical components which include gratings or prisms and lenses (Leach *et al.* 2006). The lateral shift in the traps is achieved by gratings and the axial one using lenses. While this algorithm is fast, it becomes increasingly slower for large number of traps. Also, it is known that this algorithm can produce uneven intensity between traps and ghost traps which result from higher order diffraction peaks produced by the grating. The problem of ghost traps and unintended intensity variations can be reduced using iterative algorithms for calculating phase holograms. However, for the the purpose of this thesis, gratings and lenses algorithm efficiently trapped the colloidal particles in a desired geometry. Having discussed the SLM and algorithm used for trapping, we now discuss the construction of our HOT set-up.

Construction

The basic elements for assembling a HOT are similar to the ones needed for single trap optical tweezers (Fig. 2.5). The main difference is that, for HOT, the steering mirror in Fig. Fig. 2.3 is replaced by an SLM. For our HOT set-up (Fig. 2.5), we have used an Excelsior diode pump solid state linearly polarized continuous wave laser (Spectra Physics) of wavelength $\lambda = 1064$ nm, TEM_{00} mode profile with $M^2 < 1.1$ and power 800 mW. M^2 gives a measure of the deviation of the output beam profile from an ideal Gaussian shape beam. The wavelength chosen is well separated from the excitation and emission wavelengths of the fluorescent dyes which can be used with our confocal microscope. However, for the work reported in this thesis we have used only an optical microscope. Further, since absorption at this wavelength is minimum for water, it best suited for biological and water based samples. Therefore, laser of $\lambda = 1064$ nm is routinely used with tweezer set-up. The laser is first aligned such that it is along the optic axis of the microscope. Once the height, tilt and the position of the laser are fixed, we arrange other components in between the laser and the microscope as describe hereafter. The collimated infrared laser beam is first passed through a half wave plate, W. Half-wave plate is used to rotate the plane of polarization of the linearly polarized light thereby changing the relative power of the vertically and the horizontally polarized light. The output from W is directed using mirror M_1 on to the beam expanding optics. For this, we used lenses L_1 & L_2 of focal lengths f_1 =5 cm and f_2 =10 cm, respectively. This combination of focal lengths expands the beam such that it slightly overfills the mirror of the SLM. The expanded beam is then directed into the polarizing beam splitter cube C, which separates the horizontally and the vertically polarized light. Thus, W and C together help in controlling the power of the traps. C is placed such that the vertically polarized light coming out from it impinges on to the SLM. The light reflected from the SLM is now directed into the back aperture of the microscope and subsequently into the objective. The horizontally polarized light, the light transmitted through C, is stopped using a beam blocker. To further direct the beam into the microscope, we have used a pair of mirrors M_2 and M_3 and two lenses L_3 & L_4 of focal lengths f_1 =50 cm and f_2 =40 cm, respectively. The distance between SLM and the objective is twice $f_1 + f_2$ which is the $4f$ arrangement. The $4f$ imaging system ensures that the SLM is imaged onto the back focal plane of the objective lens. The lenses L_3 & L_4 also expand the beam such that it fills the back aperture of the microscope. This beam finally goes through a 100X, oil immersion objective of NA 1.4. A high NA objective lens is used to ensure that the gradient force is larger than the scattering force.

Using this tweezers set-up, we have trapped particles in an amorphous wall configuration

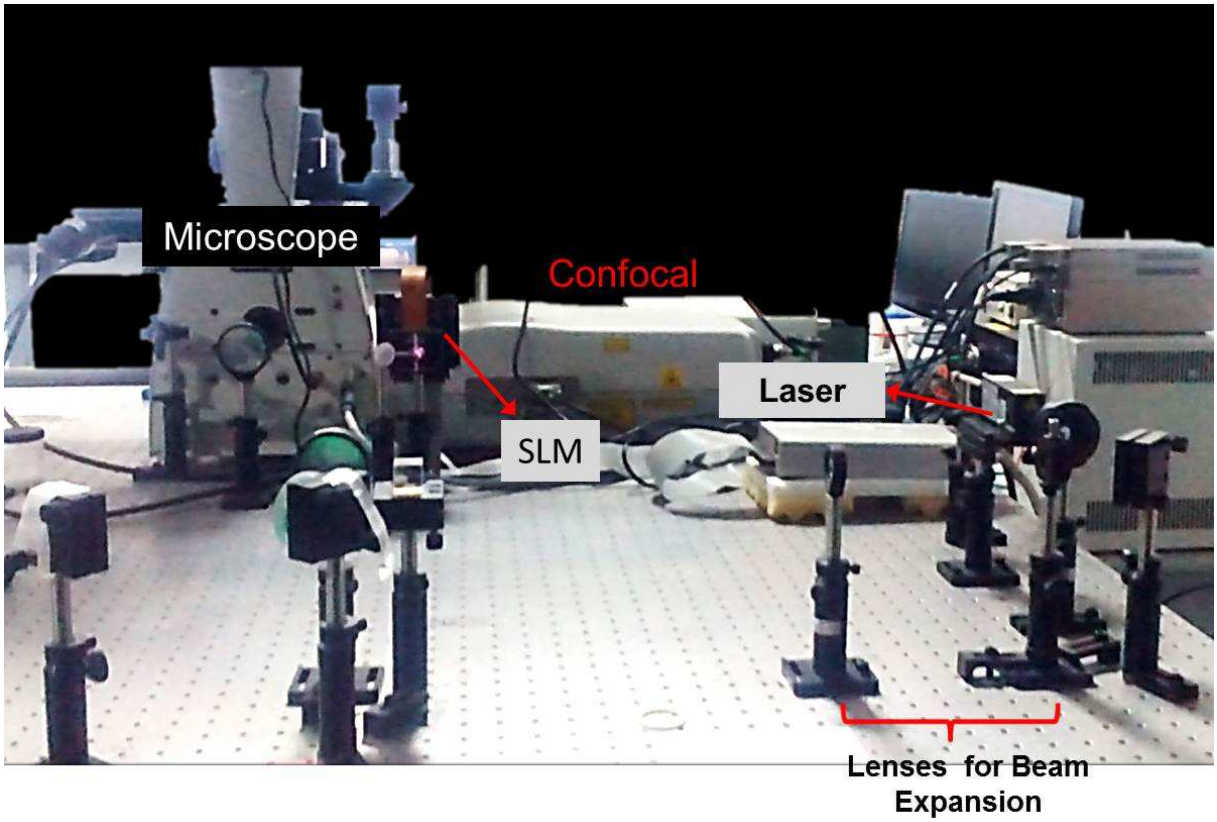

Figure 2.5: Image of the Holographic optical tweezers set-up.

along one side of the field of view. To freeze the particles in an instantaneous configuration of the dense colloidal liquid, the trap positions were obtained from the particles coordinates extracted from the bright field image captured just then. In addition to the traps created along the wall, there exists a central trap (zeroth order diffraction spot) which precludes study of dynamics at different distances from the wall. Further, owing to large number of traps (∼100) needed, the laser powers used are high. This further increases the region influenced by the central trap. Hence, to eliminate the influence of the central trap, we moved it away from the field of view and blocked it using a beam blocker. Our beam blocker consists of 5 to 6 pencil leads (0.7 mm diameter) glued along the longer side on a coverslip (Electron Microscopy Sciences). Thus, we trapped ∼100 particles along a wall in a given configuration and were able to study dynamics at different distances away from the wall. This enabled us to probe the nature of the glass transition, the results of which are discussed in Chapter 3.

2.2.2 Confocal Microscope

The size of the colloids used is such that they can be viewed using simple optical microscopy techniques. Confocal microscopy is a slightly advanced optical imaging technique, when compared to bright field optical microscope, which provides increased contrast and allows for a 3D re-construction of the volume. These additional features of the confocal microscope are because the illumination and collection/detection are limited to a point. The principle of confocal microscopy was developed by Marvin Minsky in as early as 1957 (Minsky 1988), however it was

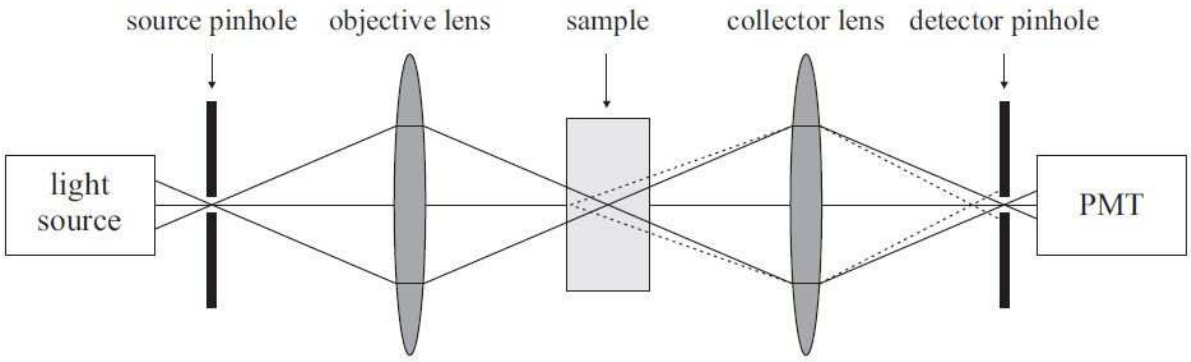

Figure 2.6: Ray optics representation of the confocal microscope set-up used by Minsky. The dotted lines represent the out-of-focus light and the solid line corresponds to the light in the focal plane.

only after the development of lasers that the technique of laser scanning confocal microscopy became commercially available (Sheppard & Shotton 1997; Semwogerere & Weeks 2005). For a long time, this technique was used extensively only for biological samples but now it is widely used to study other soft systems such as colloids. The principle behind the working of a confocal microscope can be easily understood from ray optics representation of the set-up used by Minsky (Fig. 2.6). The point source of the light is produced by using a pin hole in front of the source. This light is focused by an objective lens onto the specimen. The light coming from the sample is then focused by another objective lens to a second pinhole which is at the same focal distance as the first one implying that the pinholes are confocal. This confocality ensures that only the in-plane light enters the detector and blocks the light from all the other out-of-focus planes which results in enhanced contrast.

Modern confocal microscopes retain the main elements of Minsky's microscope. However, owing to the advances in optics, electronics and chemistry, developments have been made in the methods employed to illuminate and scan the specimen as well as to store the data. One of the main differences between Minsky's microscope and the present day is the scanning procedure. Minsky moved the specimen to illuminate the whole sample and get a 2D optical section, whereas current day confocal scan the laser beams across the sample (Fig. 2.7a). Thus, it is the scanning speed which governs the frame rate at which the data can be acquired. For the experiments discussed in this thesis, we have used a VisiTech VT-eye confocal scanner with a Leica DMI 6000B inverted optical microscope. This confocal scanner can scan as fast as 300 fps at a field of view of 340 X 340 pixels. This system uses a galvanometer mirror for scanning in Y-direction and an acoustic-optic deflector (AOD) for the orthogonal direction. It is this scanning technique that facilitates high frame rates. Moreover, present day confocal scanners use fluorescence to image the samples. Here, the incident and the emitted light have different wavelengths and they are separated using dichroic mirrors. Therefore, unlike in Fig. 2.6, the present day confocal scanners use only one objective to illuminate and well as to collect the fluorescence from the sample (Fig. 2.7a). Moreover, since only one objective is used, conventionally scanning and de-scanning are done by same optical components (Fig. 2.7a). Since AODs are sensitive to the wavelength of the light incident on them, only the galvanometer mirror is used for de-scanning. Therefore, the pin hole in the path of the emitted light is replaced by a slit. This emitted light

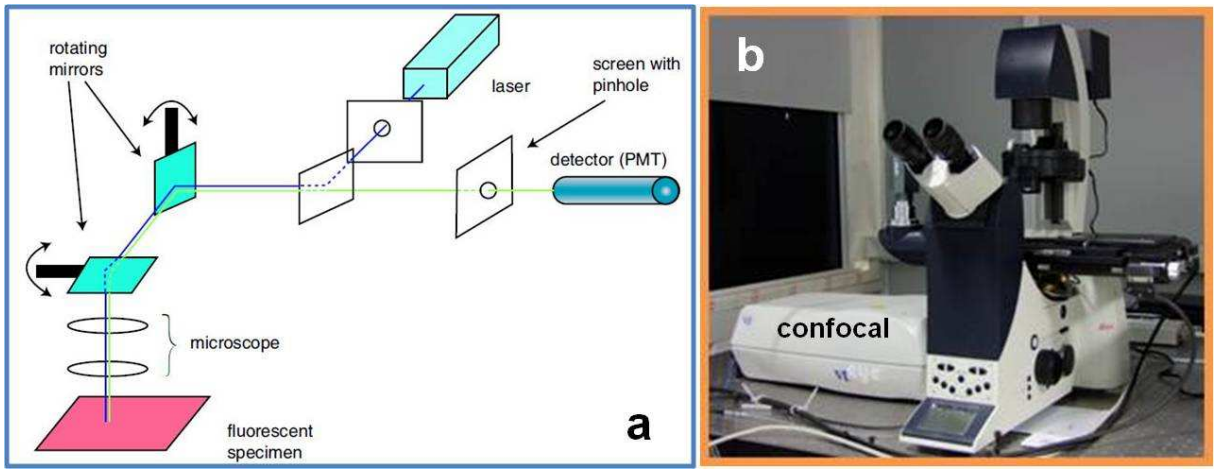

Figure 2.7: (a) Schematic of a basic confocal set-up. The blue and the green light correspond to the incident and the fluorescence light from the sample. The sample is scanned by the two oscillating galvanometer mirrors. Adopted from (Prasad *et al.* 2007). (b) Picture of the confocal laser scanner with the optical microscope which was used to investigate grain boundary dynamics.

from the slit is collected by the photo multiplier tube. The picture of the instrument used to study grain boundary dynamics (Chapter 5) is shown in Fig. 2.7b.

2.2.3 Confocal Rheometer

More often than we think, we subject materials to external mechanical forces which eventually lead to their deformation. The study of the relation between applied force and its mechanical response is called rheology (Macosko & Larson 1994; Larson 1998). Rheological properties of complex fluids like colloidal suspensions and polymers are all the more complex because of their viscoelastic nature i.e. their mechanical properties are in between Hookean solid and that of a Newtonian fluid.

For these materials, shear stress σ is given by

$$\sigma = G\gamma + \eta\dot{\gamma} \tag{2.3}$$

where the first term corresponds to the elastic component and the second one to the viscous component. Here, G is the elastic modulus, γ is the strain, η is the viscosity and $\dot{\gamma}$ is the shear rate.

The mehanical properties, stress-starin relations, of these materials are probed using a rheometer by applying either a steady or an oscillatory shear. Since oscillilatory rheology allows one to quitifiy both viscous-like and elastic-like properties of materials in different time regimes, it is best suited to quantify the structural and the dynamical properties of these materials. For an oscillatory measurement, a sinusoidal shear deformation $\gamma(t)$ is applied and the corresponding stresses are measured.

$$\gamma(t) = \gamma_0 \sin(\omega t) \tag{2.4}$$

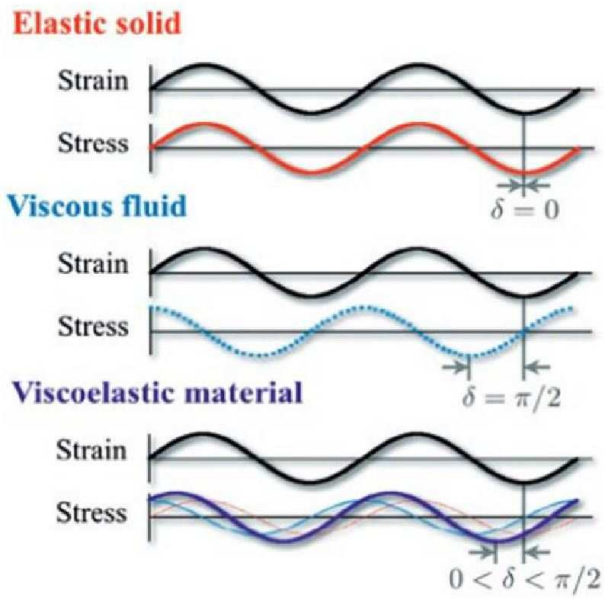

Figure 2.8: Phase relation between stress and strain for different materials.

Here, γ_0 is the amplitude of the applied strain and ω is the oscillation frequency which determines the probing time scale. While for a Hookean solid the applied stress is in phase with strain ($\sigma(t) = G\gamma_0 \sin(\omega t)$), for a Newtonian fluid it is out of phase by $\pi/2$ $\left(\sigma(t) = \eta\gamma_0\omega \sin\left(\omega t + \frac{\pi}{2}\right)\right)$. However for a viscoelastic material, the phase shift between γ and σ could be in range $0 \leq \delta \leq \pi/2$ ($\sigma(t) = \gamma_0 \sin(\omega t + \delta)$) (Fig. 2.8). This equation on expansion gives,

$$\sigma(t) = \gamma_0 \left[G'(\omega) \sin(\omega t) + G''(\omega) \cos(\omega t)\right] \tag{2.5}$$

From above equations it is clear that while $G'(\omega)$ is the elastic contribution to the stress and is termed as storage modulus, $G''(\omega)$ is the viscous contribution and is called as loss modulus. From the Eqn. 2.4, it is clear that two kinds of oscillatory measurements can be performed, one where ω is held constant and γ_0 is be varied or vice versa. Conventionally, the former is called an amplitude sweep (Fig. 2.9a) and the latter is called a frequency sweep (Fig. 2.9b). In any oscillatory rheological measurements we measure G' and G'' to charecterize the mecahnical response of soft systems.

It is well known that change in mechanical properties can lead to changes in the microstructure. To probe these structural changes in-situ while shearing, originally light scattering techniques were integrated with rheology (Panine *et al.* 2003; Sasa *et al.* 2010; Porcar *et al.* 2011). Scattering techniques investigate only average structural properties like phase behavior in micellar systems (Ganapathy & Sood 2006; Liberatore *et al.* 2006) but do not provide any information about the local structure. This information can be obtained by combining a shearing device with real-space imaging techniques like optical or confocal microscope. This has driven many scientists to couple home-made shearing devices with microscopy (Wu *et al.* 2009; Cheng *et al.* 2011; Boitte *et al.* 2013). However, to enhance the precession and the resolution with which mechanical responses can be quantified and to estimate stress and strain simultaneously, we have coupled a commercially available rheometer (Anton Paar MCR 301) with the confocal microscope (Vis-

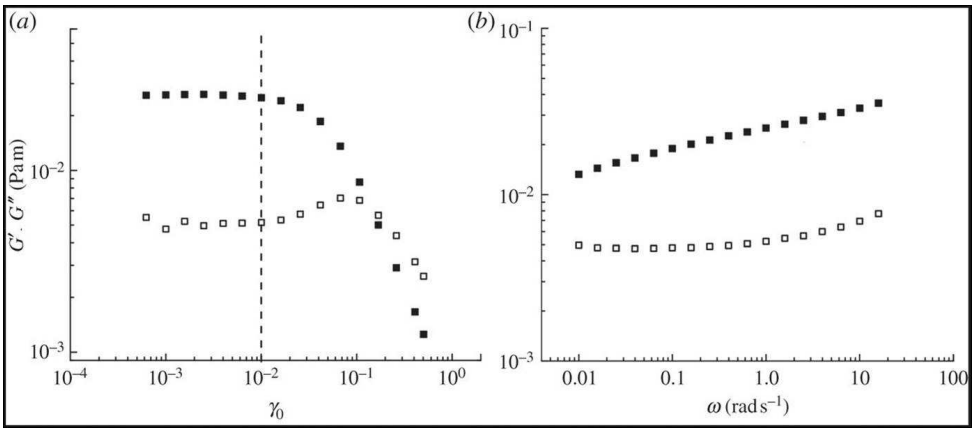

Figure 2.9: Examples of oscillatory strain measurement (a) Amplitude sweep measurement which clearly shows a change from elastic-like ($G' > G''$) behaviour to viscous-like behaviour ($G' < G''$). (b) Frequency Sweep measurement. This shows the relaxation time of the system which exhibits a soft glassy rheological behaviour. Adopted from (Jaishankar & McKinley 2013)

iTech VT-eye confocal scanner with a Leica DMI 6000B optical microscope) (Dutta *et al.* 2013). This combination enables simultaneous quantification of bulk elastic modulus (G') and viscous modulus (G'') as well as the local structure. The picture of the set-up used is shown in Fig 2.10.

For coupling these two instruments, a movable aluminum stage was fabricated in-house on which the rheometer was mounted. A steel rod is attached to the optical table along which the rheometer can slide. This design allows us to use the rheometer independently or in combination with the microscope. As shown in Fig 2.10, to combine the two instruments, the rheometer is moved such that the axis of the rheometer is aligned with the objective. To enable this coupling, we have used a customized rheometer such that the conventional front control panel was relocated to one side and the bottom of the front section is detachable. Since our rheometer bottom plate does not allow for microscopy imaging, we have designed a sample chamber with coverslip at the bottom as shown in Fig. 2.11a. In addition, we have attached metal tubes at the bottom and top of the glass plate which allows us to regulate the temperature by circulating water through them as seen in (Fig. 2.11b-c).

In order to do a measurement it is necessary to ensure that the bottom plate is parallel to the plane of the rheometer. For this we exploited the normal force exerted by the rheometer spindle itself. We fabricated a holder with a pointed tip which can be attached to the spindle and is off-centered (Fig. 2.11d). Now, by bringing the rheometer down such that the tip just touches the coverslip we measure the normal force. Measuring the normal force at different positions on the coverslip gives an estimate of the tilt. This tilt can be adjusted by using the three screws (Screws A, B and C Fig. 2.11a) present on the top of the sample chamber. Thus, we align the bottom plate parallel to the rheometer plane. Using this set-up (Fig. 2.10), we have investigated grain growth under shear (Gokhale *et al.* 2012) and yielding of colloidal glasses (Chapter 4, Nagamanasa *et al.* (2014*b*)).

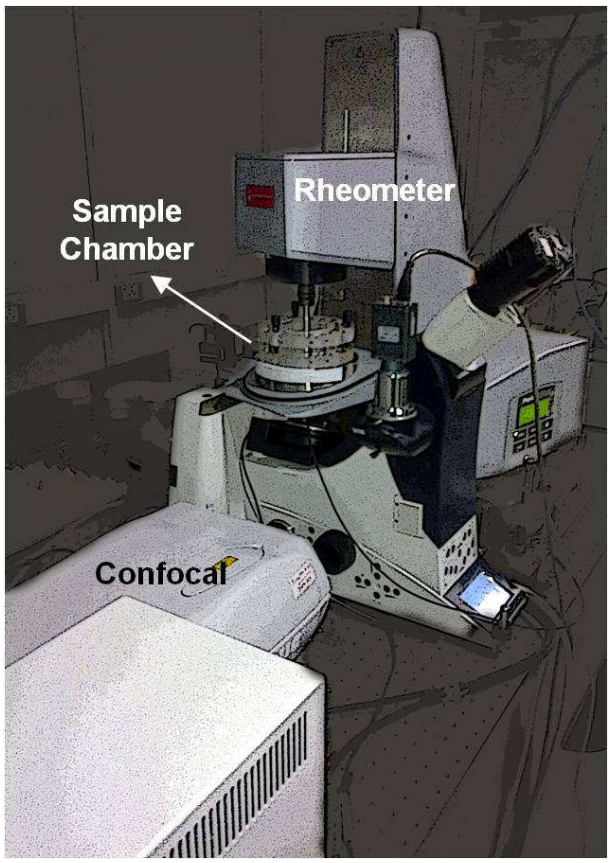

Figure 2.10: Picture of the confocal rheometer set-up used for shearing colloidal glasses.

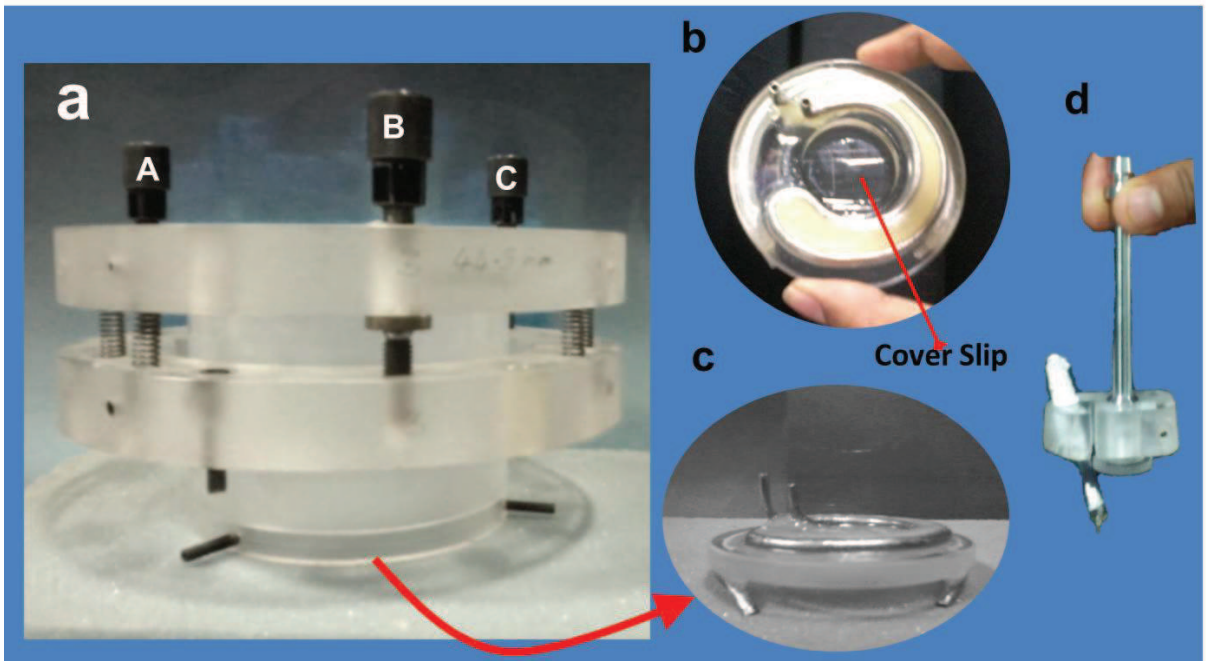

Figure 2.11: (a) Image of the sample chamber. Screws A, B and C used to adjust the tilt of the bottom glass plate. (b) Top view of the glass pate with coverslip attached at the center. (c) Side view of the glass pate which clearly shows arrangement for controlling the sample temperature. (d) The holder with a pointed tip used for aligning the bottom plate.

Chapter 3

Experimental Evidence for Growing Amorphous Order and Non-Monotonic Dynamic Correlations in Colloidal Glass-Forming Liquids

3.1 Introduction

While the transformation of flowing liquids into rigid glasses is omnipresent, it is as yet unclear whether the glass transition has a thermodynamic or a dynamic origin (Berthier & Biroli 2011; Debenedetti & Stillinger 2001). Numerous theoretical perspectives such as Random First Order Theory (RFOT) (Kirkpatrick *et al.* 1989; Biroli & Bouchaud 2012; Lubchenko *et al.* 2007), Dynamic Facilitation Theory (DF) (Chandler & Garrahan 2010; Keys *et al.* 2011), Mode Coupling Theory (MCT) (Götze & Sjogren 1992) and Geometric Frustrated models (Tarjus *et al.* 2005) have been developed to understand the glass transition problem. Both thermodynamic and kinetic approaches predict increasing dynamic correlations in the form of size of cooperatively rearranging regions (CRRs), dynamic susceptibility ξ_4 and various other measures on approaching the glass transition. However, according to thermodynamic theories, the growing dynamic length scale is due to an underlying growing static length scale. Unfortunately, the routinely used two-point measures of structure such as the structure factor $S(q)$ with q being the wave vector or the radial pair correlation function which is a Fourier transform of $S(q)$, do not show any change across the glass transition. Therefore, one of the primary aims of the thermodynamic theories is to find the right static measure associated with this transition, if there exists any. Hence, a variety of growing static length scales have been identified and computed in numerical simulations. Some of them depend on the inherent structure of the system under study (Tanaka *et al.* 2010; Malins *et al.* 2013*a*,*b*) and others are measures of amorphous order (Cammarota & Biroli 2012*b*; Dunleavy *et al.* 2012; Karmakar *et al.* 2012). Of these different length scales proposed thus far, the one which is consistent with one of the well developed thermodynamic theories, RFOT, and is order agnostic is the point-to-set length scale, ξ_{PTS} (Berthier & Kob 2012; Hocky *et al.* 2012). Within RFOT, the supercooled liquid freezes into a mosaic whose domains correspond to configurations of the metastable minima and ξ_{PTS} is thought to follow directly from the mosaic size. A systematic procedure to extract the mosaic size from point-to-set correlations has been established by Bouchand and Biroli (Bouchaud & Biroli 2004) and

hence ξ_{PTS} is crucial and is thought to serve as a direct measure of the mosaic size. In addition, it has been shown analytically that a diverging relaxation time is indeed associated with diverging ξ_{PTS} (Montanari & Semerjian 2006). Practically, ξ_{PTS} can be extracted by freezing a subset of particles in the liquid's equilibrium configuration and examining their influence on the remaining free particles. This method was first implemented by Biroli and coworkers (Biroli *et al.* 2008) where they extracted ξ_{PTS} by freezing particles outside a spherical cavity and examined the configurations of the free particles inside the cavity. This ξ_{PTS} is thought to provide an estimate of domain size or mosaic size. Subsequently, simulations have shown the existence of a growing ξ_{PTS} for various other pinning geometries and glass formers as well (Berthier & Kob 2012; Hocky *et al.* 2014). More importantly, in addition to the growing static length scale, different pinning geometries were also useful in testing other predictions of RFOT. The existence of a finite temperature ideal glass transition, one of the important predictions of RFOT, was shown by randomly pinning particles (Cammarota & Biroli 2012*a*). In this work it was shown that the glass transition can also be driven by biasing the thermodynamics by randomly pinning particles instead of increasing supercooling. They observe that for a moderately supercooled liquid, with increasing pining density the relaxation time grows and at a critical pinning density the systems freezes into an ideal glass. The authors also propose that probing the transition by freezing a part of the system might be a promising avenue of research and might help distinguishing between various theories of the glass transition. Another interesting and useful geometry is pinning particles along a single amorphous wall and examining the dynamics of free particles at different distances from the wall (Kob *et al.* 2012). In recent simulations on this geometry in addition to ξ_{PTS}, dynamic length scale, ξ_{dyn} was also computed. Intriguingly, they have shown a non-monotonic evolution of ξ_{dyn} before the mode coupling theory (MCT) cross over (Kob *et al.* 2012). This behavior of ξ_{dyn} is consistent with the dynamic cross over which is thought to occur within RFOT around MCT cross over temperature. It was surmised that this also reflects a change in morphology of CRRs from sting-like to compact on approaching the glass transition which is yet another important prediction of RFOT (Stevenson *et al.* 2006; Stevenson & Wolynes 2010). However, these predictions remain untested in experiments.

Here, we set out to test the predictions of RFOT by using holographic optical tweezers to freeze a wall of particles in an equilibrium configuration of the supercooled liquid in a 2D binary colloidal glass-former.

3.2 Experimental Section

We performed optical video microscopy experiments on a binary mixtures of polystyrene colloidal particles of diameters $\sigma_S = 1.05$ μm and $\sigma_L = 1.4$ μm, respectively. The size ratio $\sigma_L/\sigma_S = 1.33$ and the number ratio $N_S/N_L = 1.23$ were chosen to provide sufficient frustration against crystallization or phase separation. Dilute samples of both sizes were loaded into a wedge shaped cells and desired area fraction was attained by sedimentation of particles into a monolayer thick region of the cell. Since large particles sediment faster, the relative concentrations of the small and the large particles that are to be loaded into the cell should be determined carefully to avoid phase separation and crystallization of either of the species. After loading the sample, the particles were left for sedimentation for about $4-5$ days so that the monolayer thick region

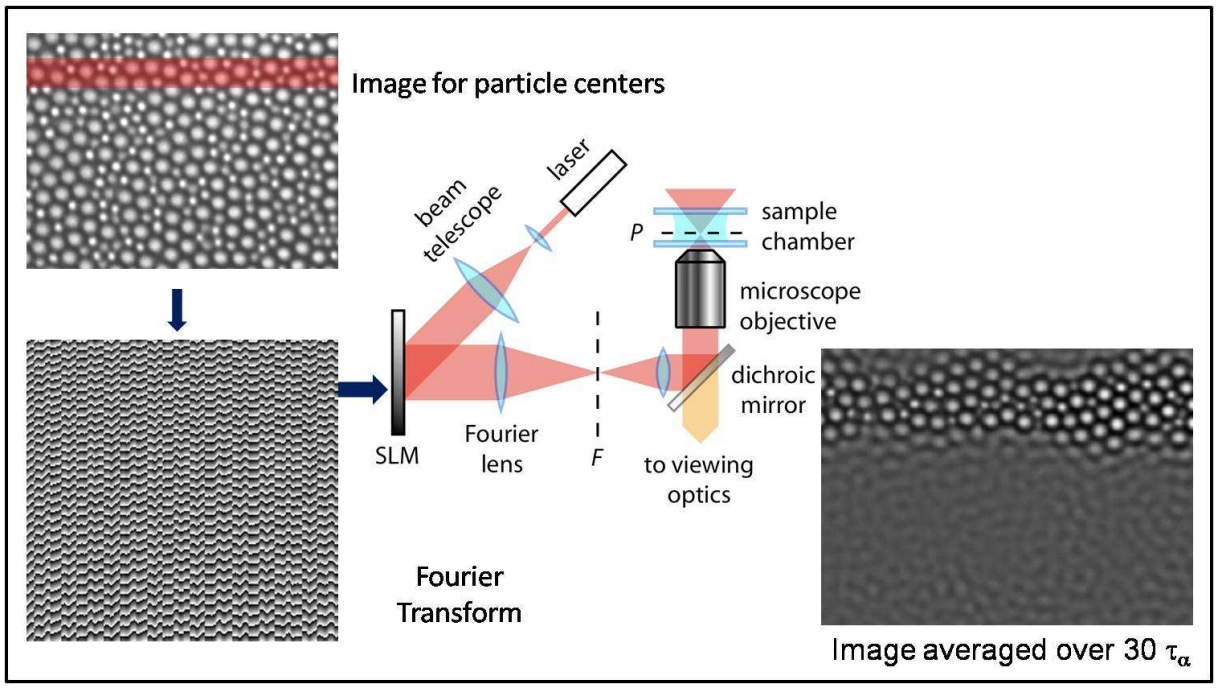

Figure 3.1: Schematic of the set-up.

attains a desired area fraction ϕ. Before collecting the data, we observed a waiting time of about $10 - 12$ hrs. This waiting time ensures that the sample is equilibrated for the ϕs studied and also minimizes the sample drift. We observed that over the experimental duration the typical drift is as small as $\sim 0.5\sigma_L$ in x-direction and $\sim 0.1\sigma_L$ in z-direction. It is to be noted that the presence of the wall does not allow for sample drift corrections and hence minimizing the drift is necessary for these experiments. For all these experiments, we also glued the sample cell to the stage plate of the microscope. We observed that this further helps in reducing the drift. Moreover, since a wedge shaped cell is used, the thickness is different at different regions and hence to ensure that all the experiments are performed at the same thickness, it is important to collect the data in the same 2D region of the cell. Gluing the cell and not moving the stage through out the experimental duration, indeed ensures that we are imaging the same region of the cell for all ϕs.

To measure ξ_{PTS} and ξ_{dyn}, it is necessary to freeze particles in an equilibrium configuration of the supercooled liquid. We have pinned multiple particles simultaneously using a holographic optical tweezers (Chapter 2, Gokhale *et al.* (2014); Irvine *et al.* (2013)). To pin the particles in a nearly equilibrium configuration, we first captured a bright field image of the sample and extracted particle coordinates within a strip of width $\sim 2\sigma_L$ along the longer dimension of the field of view. These coordinates were used to compute the necessary hologram. This hologram was then fed onto to the spatial light modulator (SLM) which in turn created traps at the desired positions (Fig. 3.1). The time taken for the whole process is about 30s which ensures that configuration pinned is nearly in an equilibrium configuration. To check if the particles are indeed a part of the liquid's equilibrium configuration, we superimposed the coordinates of these particles on time averaged images of the sample in the presence of the amorphous wall, for two different area fractions ϕ (Fig. 3.2). Particles forming the wall owing to their negligible

mobility appear brighter in the time-averaged images and can be easily identified. Further, we have computed the distance between the initial set of input particle coordinates and the centres of pinned particles acquired from the time averaged images. It is evident from (colored spheres in Fig. 3.2) these distances are smaller than the cage size, which shows that particles forming the amorphous wall are pinned in an equilibrium configuration of the colloidal liquid.

For each experiment, we have pinned an amorphous wall following which images were captured at 3.3-5 fps for 1-1.5 hours depending on the value of ϕ. The size of the viewing region is 44σ X 33σ with $\sigma = (\sigma_S + \sigma_L)/2$. In addition, for every ϕ, we have captured images in the absence of the pinning, immediately after capturing the data in the presence of a pinned wall. Standard Matlab algorithms were used to generate particle trajectories and subsequent analysis was performed using codes developed in-house. The particle tracking resolution is 0.08μm and the mean squared displacement curves for all ϕ lie above the tracking resolution (Fig. 3.3) confirming that the results are not affected by tracking resolution.

3.3 Results and Discussion

3.3.1 Static Length Scale

We first extracted ξ_{PTS} by calculating the total overlap function, $q_c(t, z)$, at various distances z from the pinned wall (Kob *et al.* 2012). Here, we have used a two-dimensional analogue of $q_c(t, z)$ developed for three-dimensional systems. We divided the field of view into boxes of size $0.25\sigma_S$ and computed $q_c(t, z)$ at different z using the following equation

$$q_c(t, z) = \frac{\sum_{i(z)} \langle n_i(t) n_i(0) \rangle}{\sum_{i(z)} \langle n_i(0) \rangle} \tag{3.1}$$

where $\langle\rangle$ correspond to time averaging, i is the box index, $n_i(t) = 1$ if the box contains a particle at time t and $n_i(t) = 0$ otherwise. The box size $0.25\sigma_S$ was chosen to be larger than the cage size, $\sim 0.14\sigma_S$, to avoid spurious overlap fluctuations due to cage rattling. Moreover, the chosen size is small enough to provide sufficient spatial resolution for the computation of ξ_{PTS}. $q_c(t, z)$ at various z for $\phi = 0.74$ is shown in Fig. 3.4a. $q_c(t, z)$ is intensive to particle exchanges and measures the overlap between configurations at two different times at a given distance away from the wall. Thus, in the long time and long distance limit it should attain a finite asymptotic bulk value $q_{rand} = q_c(t \to \infty, z \to \infty)$. As shown in Fig. 3.4a, consistent with simulations we observe that for each z, $q_c(t, z)$ exhibits a decaying profile with time and attains an asymptotic value $q_c(t \to \infty, z)$ labeled as $q_\infty(z)$. $q_\infty(z)$ is estimated by averaging the saturation value of the overlap function over a 5-10 min time window (Charbonneau & Tarjus 2013). We find that within the experimental duration, asymptotic value is not reached for a few zs very close to the wall and hence we have not considered these zs to compute the length scale. As expected, we observe that $q_\infty(z)$ decreases with increasing z and does not show any perceptible change beyond a particular value of z (Fig. 3.4a). $q_\infty(z)$ corresponding to these z gives an estimate of the bulk overlap value identified as q_{rand}. We find that, consistent with simulations, $q_\infty(z)$ - q_{rand} decays

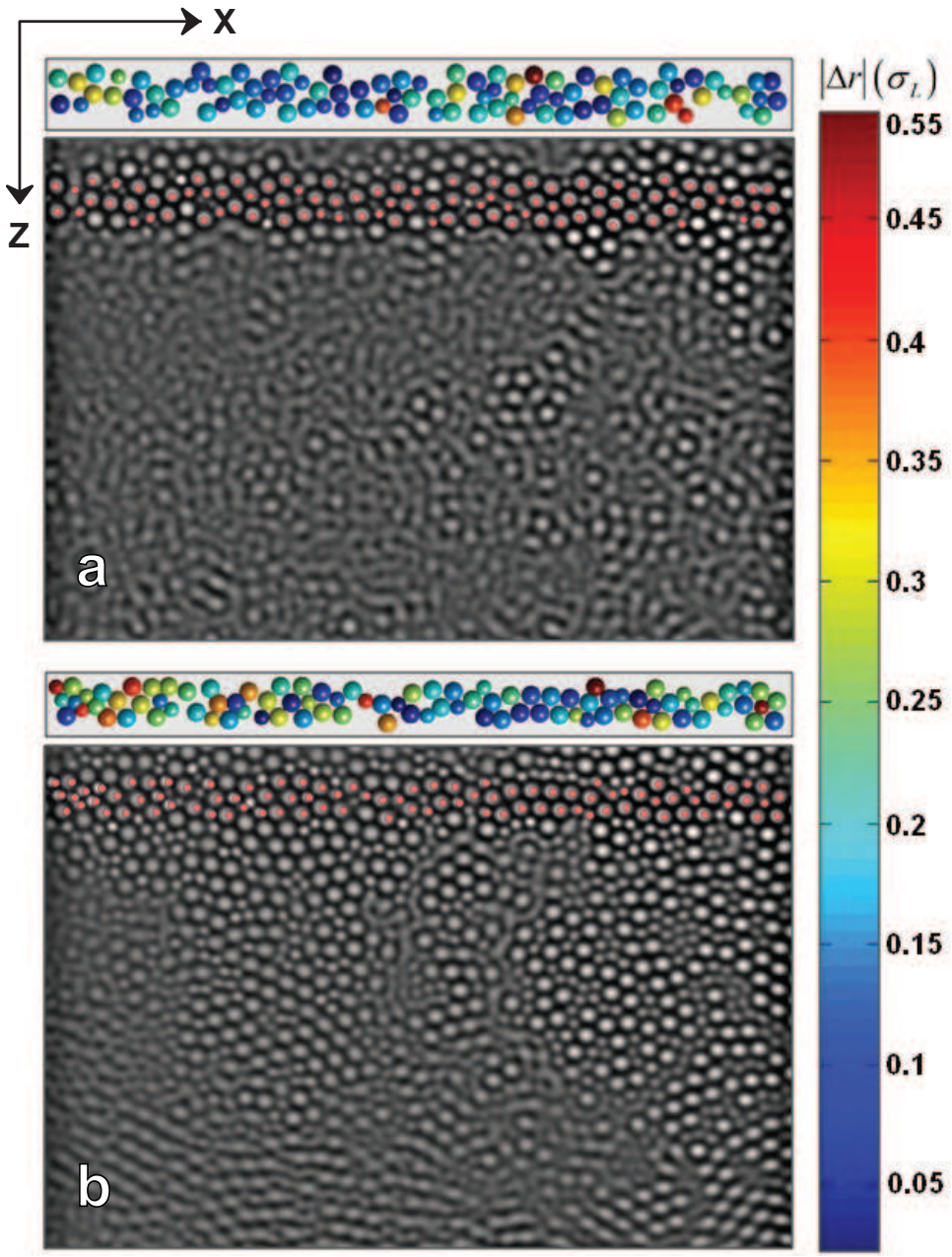

Figure 3.2: Visualization of amorphous wall. The underlying grey scale images have been generated by time-averaging snapshots over $30\tau_\alpha$ for $\phi = 0.68$ (a) and $\phi = 0.76$ (b). The red circles correspond to the coordinates of the trapped particles that form the amorphous wall. The spheres at the top of the images in (a-b) constitute the pattern whose fast Fourier Transform was fed into the spatial light modulator (SLM). Spheres are colour coded according to the displacement between the input coordinates for creating traps and time-averaged particle positions in units of σ_L.

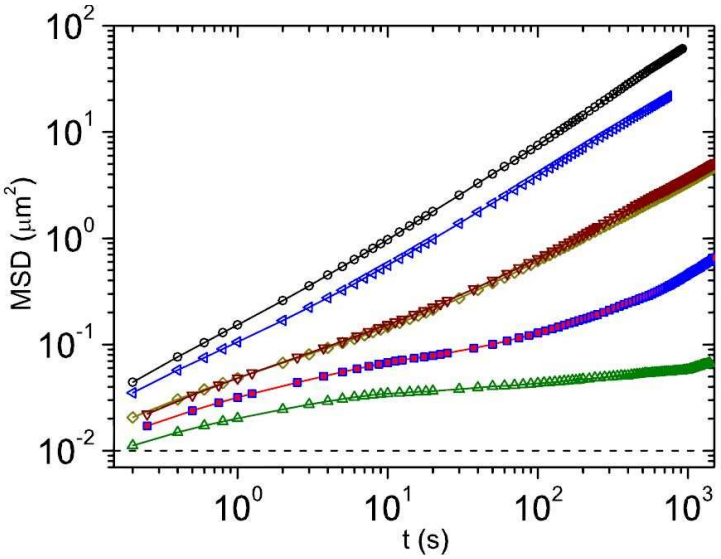

Figure 3.3: Mean squared displacement, MSD. MSD for $\phi = 0.68$ (○), $\phi = 0.71$ (◁), $\phi = 0.74$ (▽), $\phi = 0.75$ (◇), $\phi = 0.76$ (■) and $\phi = 0.79$ (△). The horizontal dotted line corresponds to the tracking resolution.

exponentially with z (Fig. 3.4b). This allowed us to extract ξ_{PTS} using the following relation

$$q_\infty(z) - q_{rand} = B \exp(-z/\xi_{PTS}) \tag{3.2}$$

$q_\infty(z)$ can also be estimated by fitting a stretched exponential to $q_c(t,z)$ (Kob *et al.* 2012). To ensure that the value of $q_\infty(z)$ and hence ξ_{PTS} do not depend on the protocol chosen, we have extracted $q_\infty(z)$ also by fitting a stretched exponential to $q_c(t,z)$.

$$q_c(t) = A\left(\exp\left[-t/\tau\right]^{-\beta}\right) + q_\infty(z) \tag{3.3}$$

Here, $A, \tau, \beta, q_\infty(z)$ are fitting constants. Since we do not have data at very short times we only fit the long time limit and estimated $q_\infty(z)$ (Fig. 3.5 solid symbols). For the low ϕs, where the fits are reasonable, we observe that ξ_{PTS} thus obtained is nearly identical to the one extracted using the procedure described above (Fig. 3.5 hollow symbols). Since the functional form used for fitting has four free parameters and we have data only for a limited duration, the fits become progressively worse for large ϕs as well as regions close to the wall. Hence, we could not estimate $q_\infty(z)$ from the fits for the two largest ϕs studied, nevertheless we estimated $q_\infty(z)$ for all ϕs by averaging the saturation value.

3.3.2 Dynamic Length Scale

Next, we computed ξ_{dyn} from the self-part of the overlap function, $q_s(t,z)$

$$q_s(t,z) = \frac{\sum_{i(z)} \langle n_i^s(t) n_i^s(0)\rangle}{\sum_{i(z)} \langle n_i^s(0)\rangle} \tag{3.4}$$

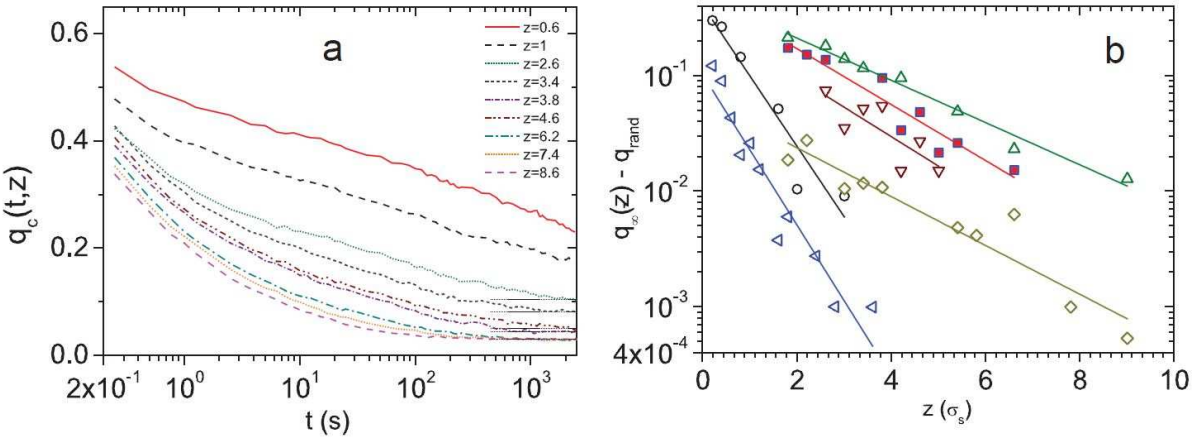

Figure 3.4: Total overlap function. (a) The total overlap $q_c(t, z)$ for $\phi = 0.74$. Different colours represent different z. The black dashed lines indicate $q_\infty(z)$, the value at which $q_c(t, z)$ saturates. (b) $q_\infty(z) - q_{rand}$ versus z for $\phi = 0.68$ (○), $\phi = 0.71$ (◁), $\phi = 0.74$ (▽), $\phi = 0.75$ (◇), $\phi = 0.76$ (■) and $\phi = 0.79$ (△). The solid lines are exponential fits of the form given in Eqns 3.2.

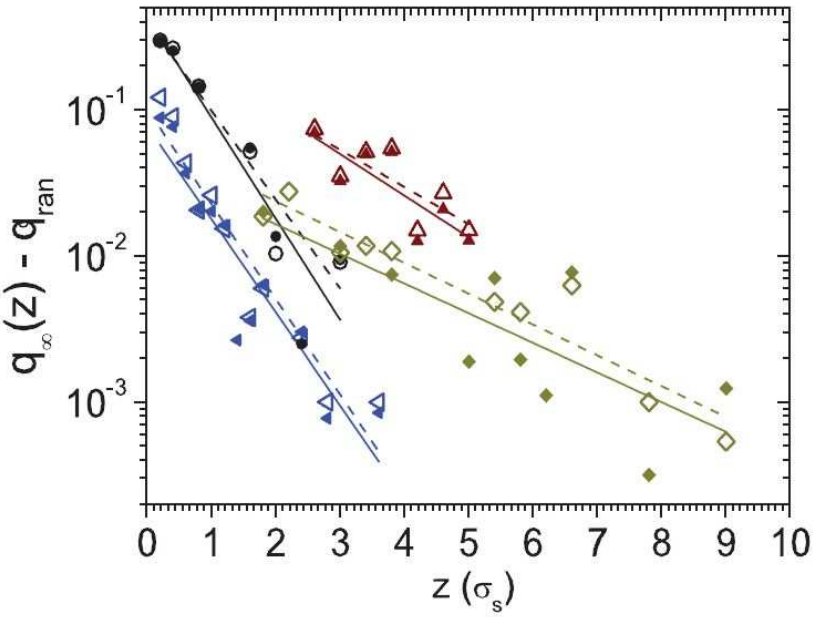

Figure 3.5: $q_\infty(z) - q_{rand}$ obtained by fitting a stretched exponential to $q_c(t, z)$ (solid symbols) and from the saturation value of $q_c(t, z)$ (hollow symbols) for $\phi = 0.68$ (black circle), $\phi = 0.71$ (blue left triangle), $\phi = 0.74$ (brown down triangle), $\phi = 0.75$ (yellow diamond). The dashed lines are exponential fits to the data represented by hollow symbols whereas the solids lines are exponential fits to the data represented by solid symbols.

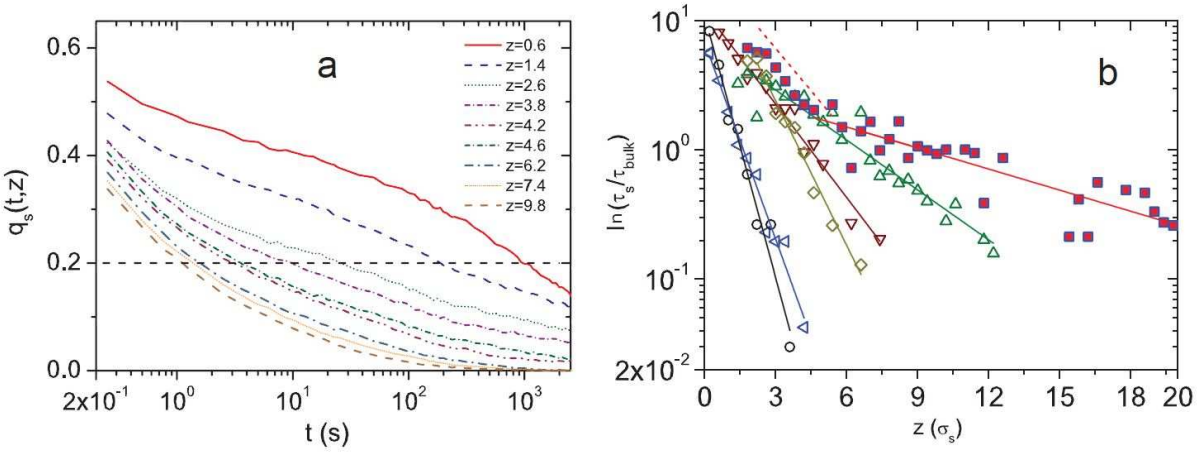

Figure 3.6: Relaxation time. (a) The self overlap $q_s(t,z)$ for $\phi = 0.74$. Different colours correspond to different z. (b) $\log(\tau_s(z)/\tau_s^{bulk})$ as a function of z, for $\phi = 0.68$ (○), $\phi = 0.71$ (◁), $\phi = 0.74$ (▽), $\phi = 0.75$ (◇), $\phi = 0.76$ (■) and $\phi = 0.79$ (△). The solid lines are exponential fits of the form given in Eqn 3.5. In (b) for $\phi = 0.76$ (■), ξ_{dyn} was extracted from the asymptotic slope (Kob *et al.* 2012). The red dashed line is a guide to the eye.

Here, $n_i^s(t) = 1$ if the box is occupied by the same particle at time t and $n_i^s = 0$ otherwise (Kob *et al.* 2012). Unlike $q_c(t,z)$, $q_s(t,z)$ is sensitive to particle exchanges and reaches zero at long times, when all the particles undergo a displacement larger than the box size. $q_s(t,z)$ is similar to the self-intermediate scattering function calculated for the wave vector corresponding to the box size. Owing to its similarity with the self-intermediate scattering function, $q_s(t,z)$ yields relaxation times $\tau_s(z)$ at different distances z from the wall (Kob *et al.* 2012). Due to the limited temporal resolution in our experiments, we defined $\tau_s(z)$ as the time taken for $q_s(t,z)$ to decay to 0.2 (Starr *et al.* 2013). Fig. 3.6a shows $q_s(t,z)$ at various z values for $\phi = 0.74$. As expected, $\tau_s(z)$ approaches its bulk value τ_s^{bulk} for large z. In accordance with simulations (Scheidler *et al.* 2002; Kob *et al.* 2012), we find that the dynamic length scale ξ_{dyn} (Fig. 3.6b) can be extracted from the equation

$$\ln(\tau_s(z)) = \ln(\tau_s^{bulk}) + B_s \exp(-z/\xi_{dyn}) \tag{3.5}$$

.

Having extracted ξ_{PTS} and ξ_{dyn} for various ϕs, we have investigated their dependence on ϕ. In complete concord with simulations, we observe that ξ_{PTS} increases with ϕ over the entire range of ϕs studied (Fig. 3.7). From Fig. 3.4b it is clear that the prefactor B also changes with ϕ. To ensure that the trend is ξ_{PTS} is not influenced by this variation in B we extracted another static length scale, $\xi_{PTS-Int} = B\xi_{PTS}$. This definition is adopted from ref. Kob *et al.* (2012) and as in their simulations, we also find this length scale increasing with ϕ (Fig. 3.7). This is the first experimental evidence for the existence of a growing amorphous order on approaching the glass transition.

On the other hand, strikingly, we find a non-monotonic evolution of ξ_{dyn} with ϕ (Fig. 3.7). Most dynamic length scales reported thus far were seen to grow with ϕ (Weeks *et al.* 2000; Berthier *et al.* 2005; Flenner & Szamel 2012). Such a non-monotonicity was observed till now only in simulations with pinned wall (Kob *et al.* 2012). Having a pinned wall therefore appears to be crucial for this observation. It is to be noted that simulations show that the maximum in

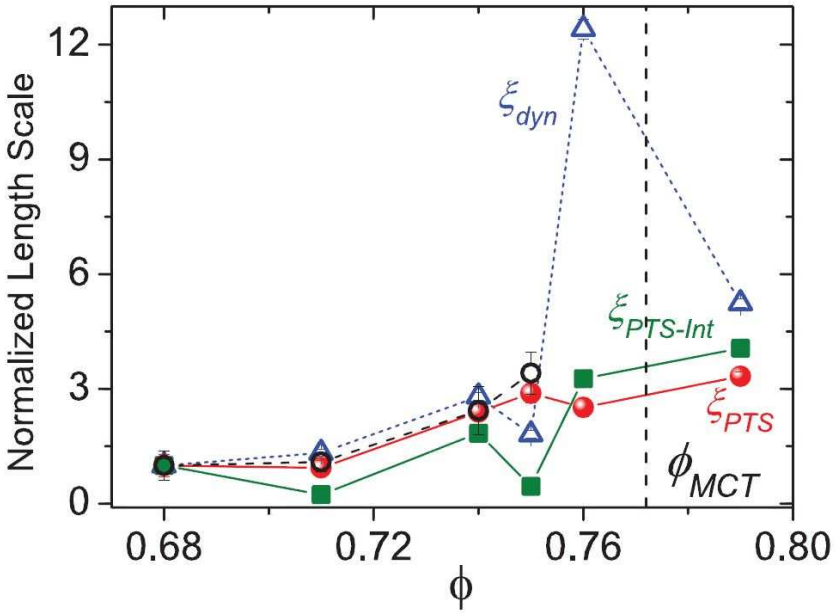

Figure 3.7: Normalized length scales. Point-to-set length scale ξ_{PTS} (●), $\xi_{PTS-Int}$ (■) and dynamic length scale ξ_{dyn} (△) normalized by their respective values at $\phi = 0.68$. The absolute values of ξ_{PTS}, $\xi_{PTS-Int}$ and ξ_{dyn} for $\phi = 0.68$ are $1.64\sigma_s$, $0.67\sigma_s$ and $1.48\sigma_s$ respectively. (○) correspond to ξ_{PTS} estimated from $q_\infty(z) - q_{rand}$ obtained by fitting a stretched exponential to $q_c(t, z)$ (solid symbols in Fig. (3.5)) normalized by $1.44\sigma_S$, its value at $\phi = 0.68$. The error bars have been obtained from the exponential fits. The dashed black line indicates the mode coupling crossover ϕ_{MCT}.

ξ_{dyn} occurs in the vicinity of the mode coupling theory (MCT) crossover. According to MCT, the mode coupling crossover corresponds to the ϕ beyond which the systems becomes non-ergodic (Kob *et al.* 2012). This transition from ergodic to non-ergodic is typically captured by plotting the self intermediate scattering function, $F_s(q, t)$ for various ϕs. It is known that $F_s(q, t)$ decays for an ergodic system and exhibits a non-decaying profile for a non-ergodic one. Thus to see if the ξ_{dyn} peaks in the vicinity of the mode coupling area fraction ϕ_{MCT}, we have computed $F_s(q, t)$ for all ϕs. To avoid the influence of the wall, we have computed $F_s(q, t)$ for the data in the absence of wall. From Fig . 3.8 it is clear that in our experiments ϕ_{MCT} should lie in between $\phi = 0.76$ and $\phi = 0.79$. This indicates that ξ_{dyn} indeed peaks in the vicinity of MCT crossover.

To further confirm this, using MCT scaling analysis, we have estimated ϕ_{MCT} quantitatively. According to MCT, the relaxation time τ_α diverges on approaching ϕ_{MCT} as

$$\tau_\alpha(\phi) \propto (\phi_{MCT} - \phi)^\gamma \tag{3.6}$$

where $\gamma = \frac{1}{2a} + \frac{1}{2b}$. Here, a and b are exponents obtained from the critical decay law and von Schweilder law (Götze & Sjogren 1992; Mishra *et al.* 2013; Zheng *et al.* 2011), respectively. In our experiments, we obtained $b = 0.885$ by fitting von Schweilder law, $F_s(q, t) = f_q - h_q t^b$, where f_q and h_q are plateau height and amplitude respectively. Because of poor temporal resolution, we could not extract a from our data but we obtained $a = 0.377$ from ref. Götze & Sjogren (1992); Mishra *et al.* (2013). These values of a and b yield $\gamma = 1.89$. We have then plotted $\tau_\alpha^{(-1/\gamma)}$

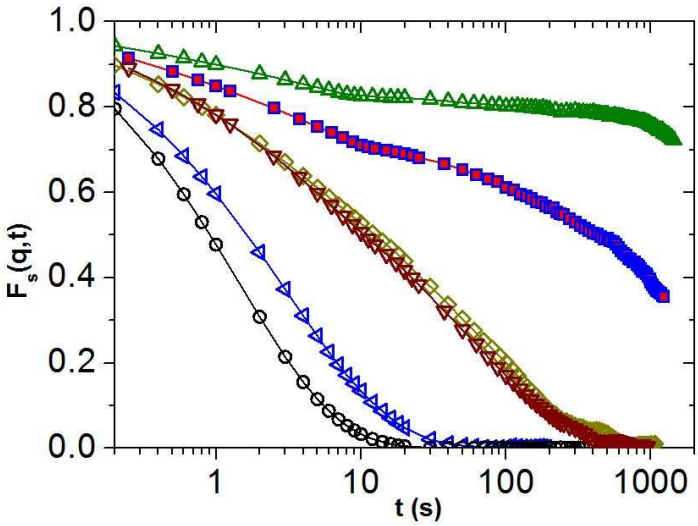

Figure 3.8: Self-intermediate scattering function, $F_s(q,t)$. $F_s(q,t)$ for $\phi = 0.68$ (○), $\phi = 0.71$ (◁), $\phi = 0.74$ (▽), $\phi = 0.75$ (◇), $\phi = 0.76$ (■) and $\phi = 0.79$ (△).

versus ϕ, which as predicted by MCT is observed to be linear and yields $\phi_{MCT} = 0.76 \pm 0.01$ (Fig. 3.9a). We have also repeated this analysis for data in the presence of wall at region far away from the wall. Even in this case, we find the same ϕ_{MCT} within experimental certainities. These estimates of ϕ_{MCT} indeed confirm that the non-monotonicty occurs in the vicinity of MCT crossover.

This suggests that our observation corresponds to the same dynamic crossover seen in (Hocky *et al.* 2014; Kob *et al.* 2012; Flenner *et al.* 2014). It has been speculated in ref. Kob *et al.* (2012) that the observed non-monotonicty is a result of a change in the relaxation mechanisms and is therefore consistent with RFOT. Within RFOT it has been predicted that the relaxation mechanisms and hence the morphology of cooperatively rearranging regions (CRRs), localized areas which govern structural relaxation, changes from string-like to compact across the dynamic cross over temperature. According to ref. Kob *et al.* (2012), the spatial inhomogeneity introduced by the wall makes ξ_{dyn} sensitive not only to the number of particles in a CRR, but also to their arrangement thus giving rise to a non-monotonicity and providing an indirect evidence for the change in the relaxation mechanism across the dynamic cross over.

3.3.3 CRR Morphology

Preliminary indication in support of multiple relaxation mechanisms can be obtained from the decay profiles of $\tau_s(z)$. While the profiles for $\phi < 0.76$ as well as for $\phi = 0.79$ are well described by a single exponential decay, $\tau_s(z)$ exhibits two slopes for $\phi = 0.76$ (Fig. 3.6b), which indicates the presence of multiple relaxation mechanisms associated with the morphology and internal structure of CRRs (Kob *et al.* 2012). To test if the non-monotonicity indeed stems from a change in the shapes of CRRs, we examined the nature of the dynamical heterogeneities at various ϕs. For this we used data captured in the absence of the wall. To define CRRs, we first identified the top 10% most mobile particles over various time intervals Δt and clustered them based on nearest neighbour distances. As expected, we find that the average cluster size, $\langle N \rangle$,

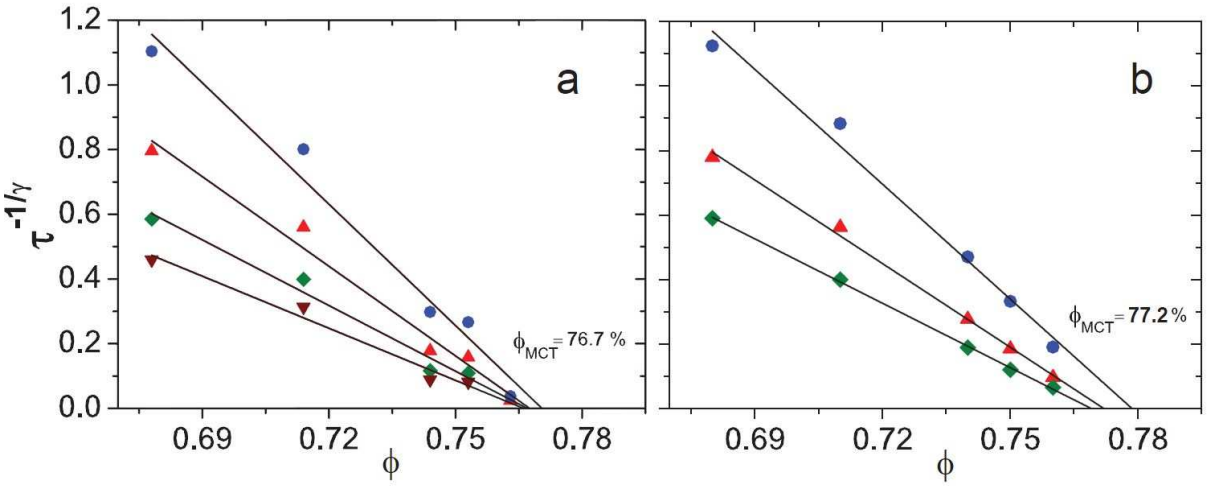

Figure 3.9: Mode coupling crossover area fraction, ϕ_{MCT}. $\tau^{-\frac{1}{\gamma}}$ versus ϕ for wave vectors $q = 2\pi/0.75\sigma$ (●), $q = 2\pi/\sigma$ (▲) and $q = 2\pi/1.25\sigma$ (◆), where σ is the mean diameter of the big and small particles. (b) $\tau^{-\frac{1}{\gamma}}$ versus ϕ for the region far away from the pinned wall.

shows a peak at a characteristic time, t^* (Fig. 3.10a-b). We have used the following definition for $\langle N \rangle$

$$\langle N \rangle = \frac{N^2 \mathcal{P}(N)}{N \mathcal{P}(N)} \tag{3.7}$$

Here, $\mathcal{P}(N)$ is the probability distribution of cluster sizes over a time t. Over the range of ϕs investigated, we find that $\langle N \rangle$ and t^* increase with increasing ϕ (Fig. 3.10a-b).

The increase in $\langle N \rangle$ with ϕ confirms that the non-monotonicity observed here is not due to the change in the size CRRs. Now it remains to check for the shape of CRRs. On observing the shapes of CRRs defined over t^*, remarkably, we notice that the morphology indeed changes from string-like to compact on approaching the glass transition (Fig. 3.11).

To quantify this change in morphology, we have computed the distribution $P(NN)$ of number of mobile nearest neighbours, NN, (Weeks *et al.* 2000; Zhang *et al.* 2011). To plot $P(NN)$, for every mobile particle in a given cluster we counted the number of nearest mobile neighbours NN. A mobile particle j is called a nearest neighbour of i if it lies within a distance of 1.4σ. Since very small clusters bias the distribution towards smaller values of NN, we only considered clusters having more than 4 particles. Also, to minimize the influence of large clusters which are rare, we restricted our analysis to cluster sizes, N, for which $\mathcal{P}(N)$, satisfies the following condition $\mathcal{P}(N)/\mathcal{P}(N) > 10^5$. In order to obtain error bars, we divided the entire experimental data into 3 equal intervals and computed $P(NN)$ for each of these. Intriguingly, for all $\phi < 0.76$ we observed a string-like morphology indicated by peak at $NN = 2$ in $P(NN)$ (Fig. 3.12a). But for $\phi \geq 0.76$, $P(NN)$ becomes broader and the peak shifts to $NN = 3$ clearly demonstrating that the morphology is becoming more compact like across the dynamic cross over (Fig. 3.12a). This change in morphology of CRRs can also be captured in $\int_3^\infty P(NN)dNN$. The trend in this quantity directly reflects the change in morphology of CRRs (Inset to Fig. 3.12a). We also computed $P(NN)$ and $\int_3^\infty P(NN)dNN$ for the data in the presence of pinned wall and observed similar trends (Inset to Fig. 3.12b). However, to allow comparisons with the unpinned case, we used region located beyond a distance of 20σ from the wall. This distance is 3-4σ larger than

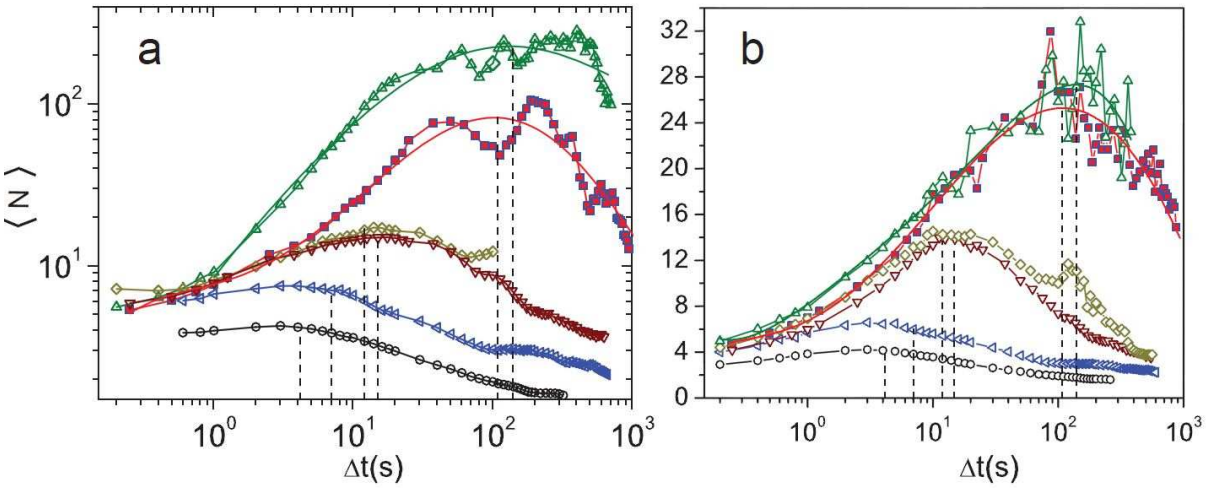

Figure 3.10: Dependence of average cluster size on ϕ. Average cluster size, $\langle N_c \rangle$, as a function of Δt for data in the absence of pinning for (a) all cluster sizes (b) only those cluster sizes for which $\mathcal{P}(N)/\mathcal{P}(1) \geq 2 \times 10^{-5}$ for $\phi = 0.68$ (○), $\phi = 0.71$ (◁), $\phi = 0.74$ (▽), $\phi = 0.75$ (◇), $\phi = 0.76$ (■) and $\phi = 0.79$ (△). In a and b, the dotted lines correspond to the Δt at which P(NN) was computed. The solid curves are polynomial fits to the data.

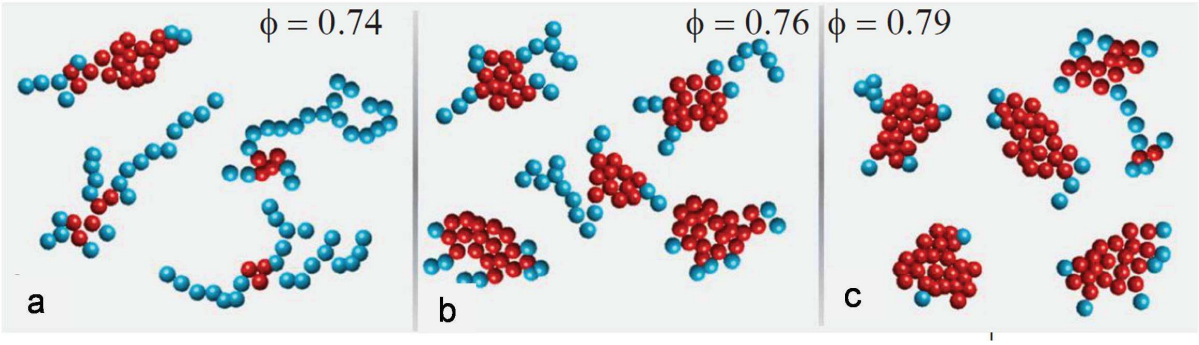

Figure 3.11: Representative cluster morphologies for 25-particle clusters. (a) $\phi = 0.74$ (b) $\phi = 0.76$ and (c) $\phi = 0.79$. Core-like particles are shown in red and string-like particles are shown in light blue.

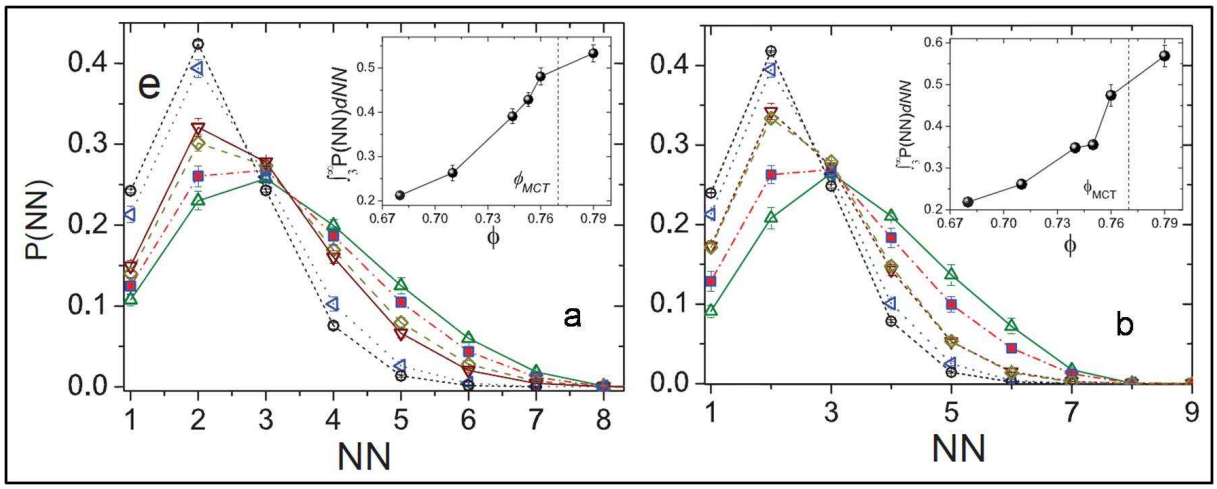

Figure 3.12: Distribution of the number of mobile nearest neighbours, $P(NN)$. (a) In the absence of the wall (b) In the presence of the pinned wall for a region located beyond a distance of $\sim 20\sigma$ from the wall. For $\phi = 0.68$ (○), $\phi = 0.71$ (◁), $\phi = 0.74$ (▽), $\phi = 0.75$ (◇), $\phi = 0.76$ (■) and $\phi = 0.79$ (△). In a-b inset: $P(NN)$ integrated over for $NN \geq 3$. The dotted line corresponds to ϕ_{MCT}

the maximum in ξ_{dyn}. Together, these findings are consistent with RFOT, which predicts that string-like CRRs occur with greater frequency on decreasing ϕ and eventually become dominant below ϕ_{MCT} (Stevenson & Wolynes 2010).

To unambiguously show that CRRs become more compact with increasing ϕ, we consider a fixed cluster size across all ϕs and investigate their morphology based on the 'Fuzzy Sphere Model' which within RFOT is used to describe the shapes of CRRs. According to this model, CRR is a composite object that contains a compact core surrounded by a ramified string-like. Also, string-like shell dominates at low ϕ and compact core at large ϕ, with a smooth crossover between the activation barrier distributions for the two morphological types near ϕ_{MCT}. As shown in Fig. 3.11a-c, we observe that for a fixed cluster size, $N = 25$, CRRs indeed have a large fraction of string-particles which belong to string at low ϕ and a large fraction of core-like ones at high ϕ. To quantify this, we have developed a protocol based on number of nearest and next nearest neighbors to determine the string-like and the core-like particles within a CRR. In a given CRR, we first identified all particles which have more than two neighbours, $i_{NN>2}$, where i is the particle index. Such particles can form the core of the CRR as well as the particles that connect core to string emerging from it. A particle 'j' is labelled core-like, only if it has at least two $i_{NN>2}$ neighbours. The remaining particles are considered to be string-like. Once we labeled particles belonging to string and core, we extracted the fractions n_s and n_c of string-like and core-like particles, respectively. Fig. 3.13a shows the dependence of n_s and n_c on ϕ for CRRs containing $N = 25$ particles. Remarkably for all cluster sizes studied, $N = 25, 20, 30, 35$ we find that n_c increases whereas n_s decreases with increasing ϕ with a cross over in the vicinity of ϕ_{MCT} (Fig. 3.13a-b).

Having identified the string like and core-like particles we have also computed the average size of the string, $\langle N_s \rangle$, and core $\langle N_c \rangle$ for all ϕs. To measure $\langle N_s \rangle$ and $\langle N_c \rangle$, we have used a definition analogous to the one used to quantify $\langle N \rangle$. In this case $\mathcal{P}(N)$ is the probability distribution of string or core sizes. As expected we find that $\langle N_c \rangle$ increases whereas $\langle N_s \rangle$

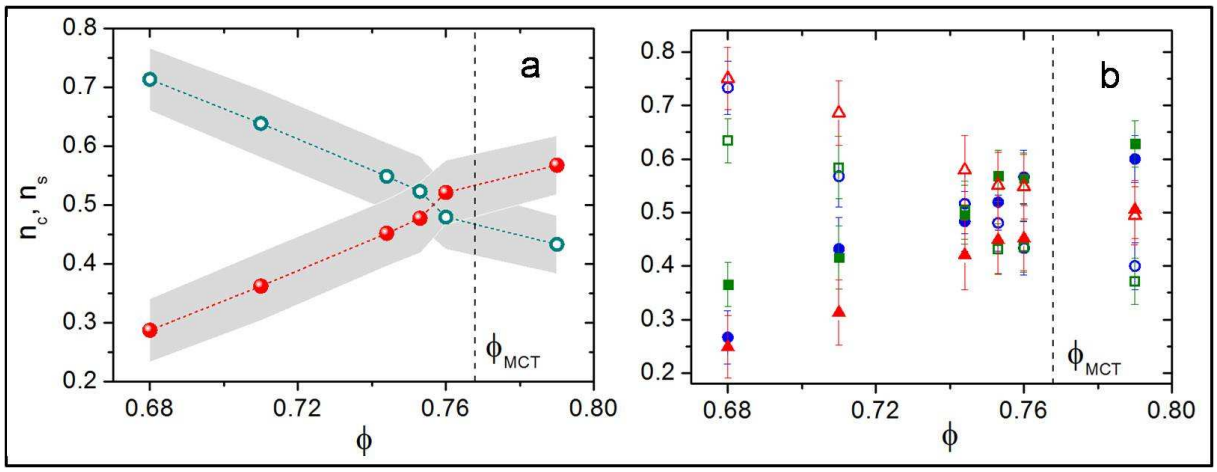

Figure 3.13: Fraction of string-like, n_s, and core-like, n_c, particles. (a) n_s, (○) and n_c (●) as a function of ϕ for 25-particle clusters. The grey shaded areas correspond to 50% confidence bands. (b) n_c and n_s as a function of ϕ for clusters containing 20 particles (red triangles), 30 particles (blue circles) and 35 particles (green squares). Here, the hollow and filled symbols correspond to string-like and core-like particles respectively. The error bars correspond to 50% confidence intervals.

decreases with increasing ϕ (Fig. 3.14). From all the above observations, it is evident that the non-monotonicity in ξ_{dyn} is due to the change in morphology and internal structure of CRRs. Also, this suggests that monotonically growing length scales like $\langle n \rangle$, are sensitive only to the number of particles in a CRR but not their arrangement. In a broader context, these results provide a direct verification of the Fuzzy sphere model of CRRs (Stevenson *et al.* 2006). In a broader context, our results provide the first direct verification for the change in morphology and internal structure of CRRs across the mode coupling crossover (Stevenson *et al.* 2006; Stevenson & Wolynes 2010).

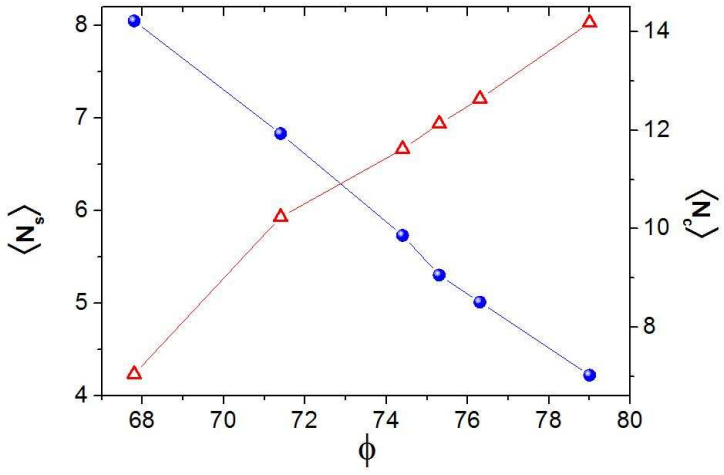

Figure 3.14: Average string size, $\langle N_s \rangle$, and core size, $\langle N_s \rangle$. $\langle N_s \rangle$ (●) and $\langle N_c \rangle$ (△) as a function of ϕ for clusters containing 25 particles.

3.3.4 Dynamic Facilitation Theory

As a final point, we discuss our findings in the context of dynamic facilitation approach (Chandler & Garrahan 2010; Keys *et al.* 2011), a purely kinetic theory of glass transition. Within DF, glass transition does not posses an underlying thermodynamic basis and the transition happens only at $T = 0$ K. Interestingly, a few important predictions of this theory have been recently verified by experiments on colloidal glass formers (Gokhale *et al.* 2014; Mishra *et al.* 2014). According to DF, structural relaxation takes place via the coordinated motion of localized mobile defects, whose concentration decreases on approaching the glass transition. Within DF, string like motion over t^* arises hierarchically from the dynamics of these defects. According to DF, string length increases with ϕ but in the current form it does not predict a cross over in the morphology of CRRs. A major difference between the RFOT and DF approaches is that the former emphasizes the importance of activated events that grow in size, whereas the in the latter relaxation is dominated by the facilitated dynamics of localized defects. The importance of facilitated dynamics can be quantified by evaluating the mobility transfer function $M(\Delta t)$ given by Vogel & Glotzer (2004)

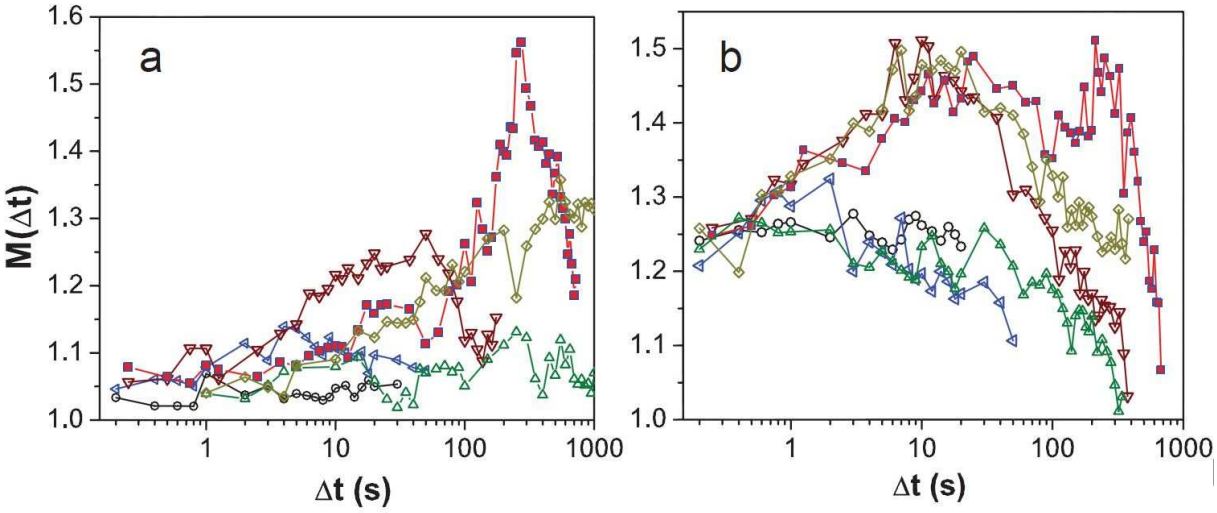

Figure 3.15: Mobility transfer function, M(Δt). M(Δt) for (a) big polystyrene particles and (b) small polystyrene particles for $\phi = 0.68$ (○), $\phi = 0.71$ (◁), $\phi = 0.74$ (▽), $\phi = 0.75$ (◇), $\phi = 0.76$ (■) and $\phi = 0.79$ (△) computed by considering the top 10% most mobile particles.

Briefly, given two successive time intervals Δt_1 and Δt_2 such that $\Delta t_1 = \Delta t_2 = \Delta t$, the mobility transfer function, $M(\Delta t)$, quantifies the probability of that the top 10% most mobile particles over Δt_2 lie in the vicinity of those over Δt_1, relative to the probability that they lie in the vicinity of the remaining immobile particles. (Vogel & Glotzer 2004; Gokhale *et al.* 2014). $M(\Delta t)$ is defined as follows:

$$M(\Delta t) = \frac{\int_0^{r_{min}} P_M(r, \Delta t) dr}{\int_0^{r_{min}} P_M^*(r, \Delta t) dr} \tag{3.8}$$

where r_{min} corresponds to the first minimum of the radial pair correlation function $g(r)$. Here, $P_M(r, \Delta t)$ is the distribution of the minimum distance between mobile particles in two successive time intervals of duration Δt. $P_M^*(r, \Delta t)$ is the reference distribution of the minimum distance between mobile particles in the second interval and randomly chosen immobile particles in

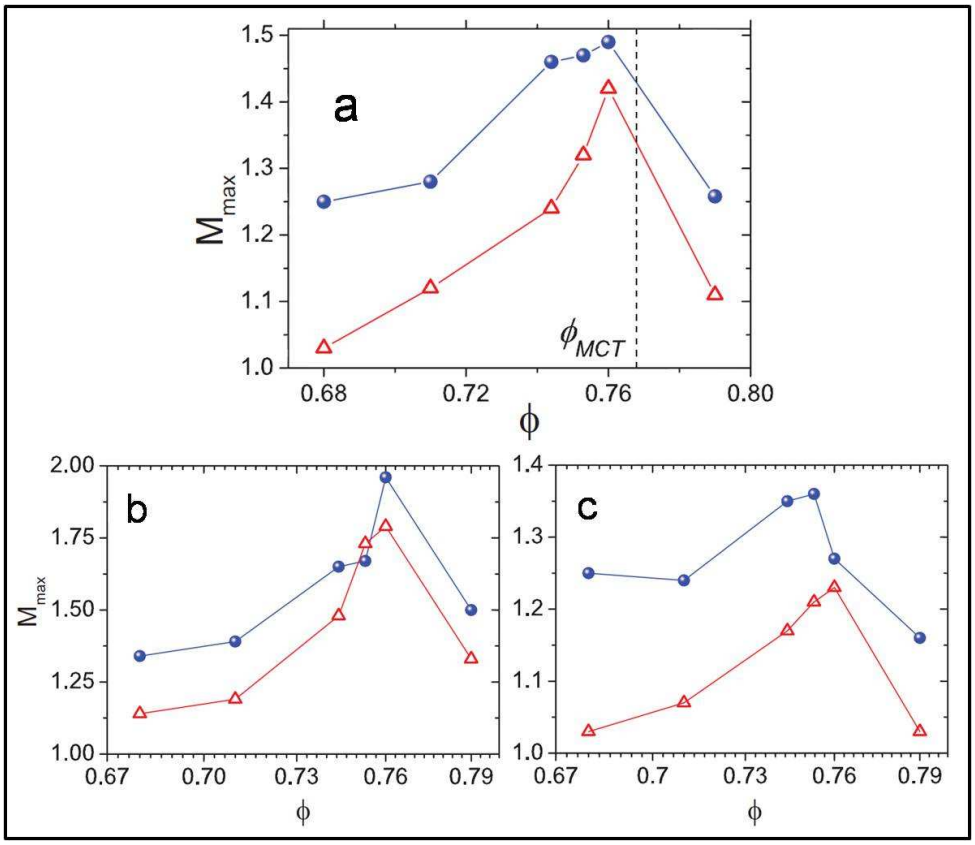

Figure 3.16: Maximum of the mobility transfer function $M(\Delta t)$, M_{max}. M_{max} for top (a) 10% most mobile particles, (b) 5% most mobile particles and (c) 15% most mobile particles. In a-c (●) corresponds to small particles and (△) corresponds to large ones.

the first interval. The peak of this function, M_{max} quantifies the importance of facilitated dynamics (Fig. 3.15). Thus, if facilitation is the dominant mechanism one expects M_{max} to grow monotonically with ϕ. On the contrary, we find that M_{max} exhibits a peak across $\phi = 0.76$. It has been shown in simulations that the presence of non-facilitated activated hops can give rise to a maximum in M_{max} at the ϕ corresponding to the crossover from the facilitation dominated regime to the activated hopping regime (Elmatad & Keys 2012). Also, they have shown that increasing the importance of activated events further shifts the peak to lower supercoolings. We note that a similar dependence of M_{max} on ϕ has been observed in a completely different colloidal system as well (Gokhale *et al.* 2014). The observed ϕ dependence of M_{max} is qualitatively consistent with RFOT, where facilitation is a secondary relaxation process that diminishes in importance on approaching the glass transition (Bhattacharyya *et al.* 2008), but is in stark contrast with predictions of the DF theory. To ensure that the behaviour of M_{max} is not effected by the choice of the percentage cut off used to identify mobile particle, we performed this analysis for top 5%, 10% and 15% most mobile particles. Remarkably, we find that the trend in M_{max} is identical in all cases (Fig. 3.16).

3.4 Conclusions

Our observation of a growing point-to-set correlation length, ξ_{PTS} (Fig. 3.7), is consistent with the prediction of RFOT, although it does not rule out competing theoretical scenarios (Jack & Garrahan 2005; Jack & Berthier 2012). However, at present, the non-monotonic density dependence of ξ_{dyn} (Fig. 3.7) and the concomitant change in the morphology and internal structure of CRRs (Fig. 3.11, Fig. 3.12, Fig. 3.13) can only be rationalized within the framework of RFOT. Crucially, the morphological crossover in CRRs as well as the maximum in the ϕ dependence of M_{max} do not find a natural explanation within the prominent competing framework of the DF theory. The non-monotonicity in M_{max} (Fig. 3.16) observed here as well as in (Gokhale *et al.* 2014) may be associated with the diminishing role of facilitated dynamics in governing structural relaxation, rather than finite size effects Elmatad & Keys (2012). Indeed, reconciling these findings within the facilitation paradigm poses an exciting challenge for future theory, experiments and simulations. A promising course in this direction would be to examine the influence of a pinned wall on facilitated dynamics of localized defects. Given that we see signatures of increasing cluster size of immobile particles with ϕ in the time averaged images shown in Fig. 3.2, it would be fascinating to explore connections between the regions of slow dynamics and the static and dynamic length scales extracted here. It would also be instructive to investigate whether our results are consistent with other thermodynamic frameworks such as geometric frustration-based models (Tarjus *et al.* 2005). We expect our findings to engender future research aimed at addressing these unresolved issues on the theoretical, numerical as well as experimental front.

Chapter 4

Experimental Signatures of an Absorbing Phase Transition Governing Yielding of a Colloidal Glass

4.1 Introduction

A wide variety of solids including atomic crystals, metallic glasses, dense suspensions, gels and foams yield and flow when subjected to external stresses beyond a threshold value - the yield stress (Miguel & Rubi 2006; Barnes 1999). Apart from representing an interesting class of non-equilibrium processes, these phenomena are routinely exploited in numerous industrial applications (Valiev 2004). Elucidating mechanisms that govern yielding and plasticity therefore assumes fundamental as well as technological significance. In the context of atomic systems, studies suggest the existence of a non-equilibrium phase transition centered at the yield point although a direct evidence is still lacking. By contrast, for soft solids which include dense colloidal suspensions, gels and foams, a holistic understanding of yielding is yet to emerge. A majority of the rheological studies on soft solids have been aimed at characterizing the bulk flow behaviour and examining its dependence on the nature of the inter particle interactions (Sollich 1998; Carrier & Petekidis 2009; Erwin *et al.* 2010; Rogers *et al.* 2011*a*,*b*; van der Vaart *et al.* 2013). However, most of these studies employed steady shear, where the continuous accumulation of strain precludes the characterization of steady states (Fall *et al.* 2010; Divoux *et al.* 2010) and hence they were unable to establish the exsistence of a critical phenomenon underlying yielding. On the other hand, oscillatory shear allows steady states to be probed at all applied strains. Despite its importance, yielding under oscillatory strain has received relatively less attention.

One of the first experimental studies in this direction was by Hebraud et.al (Hébraud *et al.* 1997), where diffusive wave spectroscopy was used to investigate periodically sheared concentrated emulsions. The authors showed the existence of a finite threshold for the onset of irreversibility. By employing the same technique, Petekidis and co-workers later showed that a similar threshold exists for hard sphere colloidal glasses as well (Petekidis *et al.* 2002). In addition, they found that the growth of irreversibility with strain beyond its onset is governed by the volume fraction. More importantly, they found the threshold strain for $\phi = 0.637$ to be 0.1. However, this value is significantly larger than the value estimated by calculating the rattle room available for a particle at this high ϕ. It was speculated that the large value of the

measured threshold strain could be due to the presence of collective motion of group of particles (Petekidis *et al.* 2002). Nevertheless, light scattering techniques are not well-suited either to probe directly the collective nature of local plastic events or to characterize them. These difficulties have been surmounted by optical microscopy based studies, which facilitate not only the identification of irreversible events but also the investigation of their spatio-temporal evolution down to the single-particle level. Recent optical microscopy studies on 2D jammed colloidal suspensions (Keim & Arratia 2013) have shown that irreversibility, characterized by the number of T1 events, decreases with time on approaching steady state. They have also observed that the that the steady state number approaches zero for very low applied strains, suggesting the existence of a completely reversible state at strains below yield strain. Further, they speculated that the steady state number to increase sharply across the transition from reversible to irreversible dynamics near the yield point. While all these studies suggest a threshold strain for microscopic irreversibility, it is as yet unclear if this value corresponds to bulk yield strain.

Indications for the presence of a phase transition underlying yielding using oscillatory shear, were also provided by computer simulations on amorphous solids. In this context, in simulation studies on soft sphere glasses (Mohan *et al.* 2013), the onset of yielding at the particle scale was characterized from the mean square displacement, a quantity proportional to the number of irreversible events. They observed that the mean squared displacement changes continuously with number of shear cycles and finally approaches a steady state for a given applied strain. Also the diffusion coefficient, a measure of steady state irreversibility, changes rapidly across the threshold strain. Similar trend in diffusion coefficient with strain was also observed in 3D simulations on binary Lennard-Jones mixture, a model amorphous solid (Fiocco *et al.* 2013). On the other hand, simulations on granular media have shown that yielding could be related to the onset to chaotic particle dynamics (Regev *et al.* 2013). At low oscillatory strains the system settles in a limit cycle on reaching a steady state indicating the presence of reversible steady states and at large strains the system is always chaotic. Further, these studies speculate that the onset of irreversibility may be associated with an absorbing phase transition, observed in periodically sheared dilute non-Brownian suspensions (Corte *et al.* 2008). Despite these advances in experiments and simulations, a few important issues remain unresolved. In all the experiments discussed above, the yield strain has been estimated from independent rheological measurements and it is therefore unclear whether or not the microscopic threshold for irreversibility corresponds to the bulk yield point. Moreover, quantitative measurements of the relaxation time associated with the evolution of irreversibility on approaching steady state are still lacking. As a consequence, whether the observed correlations between local plastic events lead to a non-equilibrium phase transition at the yield point still remains an open question.

Here, by combining particle scale imaging with bulk rheology we have investigated yielding of a prototypical soft solid - a binary colloidal glass.

4.2 Experimental Details

The experimental colloidal system comprised of an aqueous suspension of temperature-sensitive size-tunable poly N-isopropylacryl amide (PNIPAm) colloidal spheres of radii of 1 and 2 μm. The particles used for these experiments were synthesized using a standard emulsion polymerization

protocol (Chapter 2 (Table 2), Lawrence *et al.* (2007)). In addition to the dye incorporated into the particles during synthesis, we have added fluorophore Rhodamine 6G externally for better confocal imaging. The lower critical solution temperature for these particles is $\approx 38°$C and the experiments were performed at $\approx 24°$C. A number density ratio of 1:3 of large and small particles adequately suppressed crystallization, as confirmed by 3D confocal imaging. We have estimated the volume fraction by counting the number of big and small particles in a given 3-D confocal volume to be $\phi \approx 0.67$.

We have investigated the particle scale dynamics of colloidal glass under shear, by combining a fast confocal microscope with a rheometer (Fig. 4.1) (Chapter 2, Gokhale *et al.* (2012)). Our apparatus consisted of a commercial stress-controlled rheometer (MCR-301, Anton Paar), mounted on a fast confocal microscope (Visitech VT-Eye confocal scanner coupled to a Leica DMI 6000B microscope) using a home-made mechanical stage (for details see Chapter 2). Imaging was performed using a 100X N.A. 1.4, oil immersion Plan Apochromat Leica objective. The experiments were carried out in a home-made shear cell using a cone-plate geometry. A quartz cone of diameter 25 mm and cone angle 1° and a cover glass of thickness 170 μm were used as the top and the bottom plates respectively. In-order to prevent wall slip we have pinned a layer of particles on the top and the bottom surfaces. To stick particles irreversibly on the glass surface, we treated the plates with 2mg/ml of aqueous Poly(allylamine hydrochloride) (PAH) solution. For this, the plates were soaked in PAH solution for about 3 h. To ensure maximum coverage of PAH, during these 3 h of soaking PAH in the vial was replaced with fresh solution once every hour. These plates were then washed throughly with milli Q water (TKA, 18.2MΩ) to remove the excess PAH. We then dipped these plates in a suspension of PNIPAM particles for about 45 min. The glass surfaces were once again rinsed throughly with milli Q water to remove free particles. After this procedure, we found that the entire surface of the plates is covered with particles. This provided the roughness on the particle length scale needed to avoid slip at the boundaries. The stuck layer did not disassemble during the entire duration of the experiment which we confirmed from microscopy videos. After loading, the samples were subjected to a temperature quench to ensure homogenization and remove loading history. To maintain identical initial conditions for all measurements, the samples were pre-sheared at a constant strain rate of 5 s^{-1} for 3 min, following which a waiting time of 5 min was observed prior to every measurement. Following pre-shear, the bulk elastic and viscous moduli G' and G'', respectively, were measured by applying oscillatory strains $\gamma = \gamma_o \sin \omega t$, where γ_o is the strain amplitude and ω is the frequency. To ensure that the the sample's bulk rheological properties are identical thought the entire duration of the experiment, which is $\sim$ 40 h, we repeated the oscillatory amplitude experiment at regular intervals. We found identical viscoelastic behavior for all such runs. For characterizing the phase transition, we measured G' and G'' as a function of the oscillation cycle number τ for various γ_o's at $\omega = 1$ rad/s. For each γ_o, single-particle dynamics was quantified by imaging a 54 μm×54 μm 2D slice oriented parallel to the velocity-vorticity plane and located 7 μm away from the fixed bottom plate, at 60 frames per second. To visualize the 3D microstructure, we obtained image stacks (25 μm×25 μm×8 μm) along the velocity gradient direction at a few select γ_o's. The single-particle dynamics were quantified using standard particle tracking algorithms (Crocker & Grier 1996) as well as codes developed in-house.

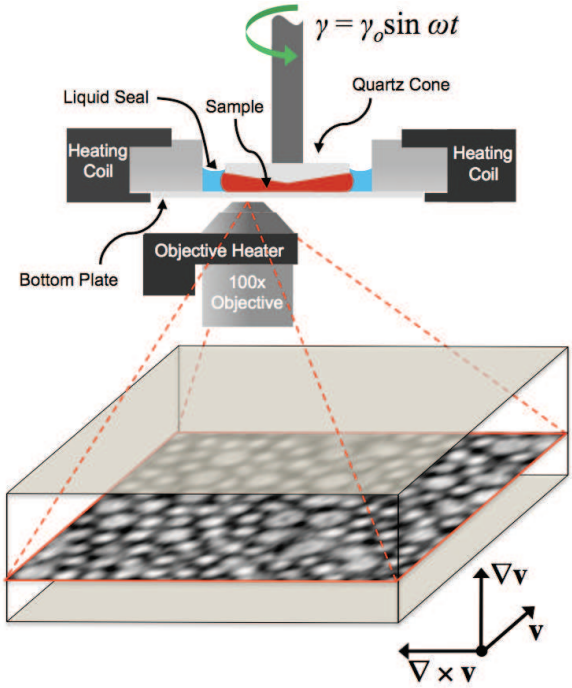

Figure 4.1: Schematic of the Confocal-rheometer.

4.3 Results and Discussion

4.3.1 Identifying Yield Strain

The rheological response of our sample is typical of a soft glass (Fig. 4.2a). (Sollich 1998; Carrier & Petekidis 2009; Erwin *et al.* 2010; Rogers *et al.* 2011*a*,*b*; van der Vaart *et al.* 2013). We found only a weak dependence of G' and G'' on ω, which independently confirmed that our samples were in the glassy state (inset to Fig. 4.2a) (Sollich 1998). From γ_o-sweep experiments, it is evident that for the volume fraction used here, the system is a viscoelastic solid in the zero strain limit. The plateau modulus G' observed here is low as compared to what is typically seen for microgels, suggesting that the major contribution to elasticity comes from particle caging and jamming (van der Vaart *et al.* 2013) rather than the interpenetration of the polymer chains themselves. With increasing γ_o we find that the system goes from a viscoelastic solid to a viscoelastic liquid with a well defined G'-G'' crossover. The γ_o corresponding to the crossover of G' and G'' was identified as the yield strain $\gamma_y = 0.2$ (van der Vaart *et al.* 2013). The ubiquitous G'' peak was located beyond γ_y (Fig. 4.2a). The Péclet number of our system, defined as $Pe = \omega\tau_B$ (Koumakis *et al.* 2013) is 1.92. Here, $\omega = 1$ rad/s is the frequency of applied strain and $\tau_B = R^2/D_o = 6\pi\eta R^3/k_BT$ is the Brownian time of the particles. Pe was estimated by taking R to be the mean radius of our particles (0.75 μm) and using the solvent viscosity $\eta = 0.001$ Pa.s. The high Pe combined with the position of the G'' peak, suggests that yielding in our system may be governed by shear-induced rearrangements rather than thermally assisted cage jumps (Koumakis *et al.* 2013). Moreover, from an independent set of experiments, we observed that in concord with ref. Koumakis *et al.* (2013), the G'' peak shifts further away from the crossover with increasing ω (Fig. 4.2b). This suggests that the location of the G'' is correlated

with the relative importance of thermally activated and shear-induced rearrangements.

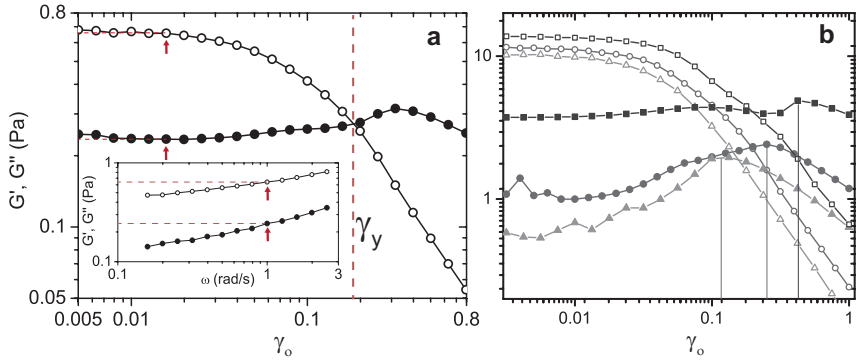

Figure 4.2: (a) γ_o-sweep measurements performed at $\omega = 1$ rad/s. Inset shows results from ω-sweep experiments at $\gamma_o = 0.015$. G' and G'' are denoted by (○) and (●), respectively. The red arrows and dotted lines in the figure and the inset highlight the values of G' and G'' for $\gamma_o = 0.015$ and $\omega = 1$ rad/s. (b) γ_o - sweep experiments for $\omega = 0.1$ rad/s (▲), $\omega = 1$ rad/s (●) and $\omega = 20$ rad/s (■). G' and G'' are denoted by open and filled symbols respectively. The solid lines highlight the γ_o corresponding to the G'' peak.

4.3.2 Evidence for a Phase Transition

Order-Parameter

We characterized the irreversible micro-structural changes that lead to yielding. A natural measure of irreversibility is the fraction, f_{IR}, of particles that do not return to their initial positions at the end of a strain cycle (Corte *et al.* 2008). Since f_{IR} is independent of the exact nature of local yield events, it should be generically applicable to ordered as well as disordered soft solids. We first identified the irreversible events (IRs) in 3-D. Here, the time resolution between two successive confocal z-stacks was too small to allow the construction of individual particle trajectories. We therefore used a protocol based on pattern matching to estimate macroscopic drift and to identify IRs. As the strain threshold for displacement of large particles is greater than that of the small ones, we used only large particles to estimate the drift. The drift was calculated by displacing one z-stack with respect to the other in both X and Y directions and finding the displacements X_d and Y_d for which the overlap between the two stacks is maximum. We then used the drift-corrected particle positions to identify IRs. A particle was labelled irreversible if at the end of the strain cycle, it did not return to its initial position within a distance of $\sigma/2$, where σ is the particle diameter. Confocal volumes with irreversible events highlighted show that f_{IR} exhibits an increase across γ_y (Lundberg *et al.* 2008) (Fig. 4.3). Further, f_{IR} predominantly comprises of small particles due to their lower strain threshold for irreversible rearrangements. However, as the displacement of large particles also becomes significant with increasing γ_o, this procedure is reliable only at small and moderate γ_o's.

Owing to the poor temporal resolution in 3D imaging at large γ_o's, we resorted to 2D to quantify $f_{IR}(\tau)$ for all γ_o's investigated. The high frame rate used to capture 2D slices is sufficient to track individual particles and hence standard procedures were used to obtain particle displacements (Crocker & Grier 1996). Here, to set the displacement threshold for

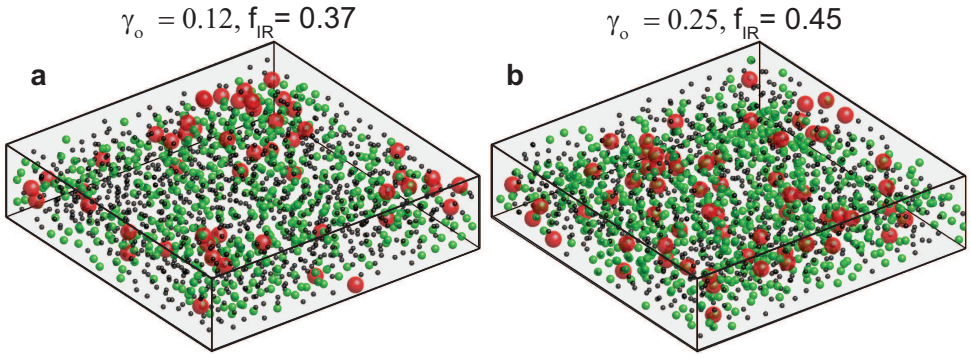

Figure 4.3: (a)-(b) Reconstruction of 3D volumes of the sample for $\gamma_o = 0.12$ and $\gamma_o = 0.25$, respectively. Large and small irreversible particles are rendered as red and green spheres, respectively and the reversible ones are shown as black spheres.

IRs, we plotted the distribution of displacements in the first cycle for each γ_o. The value of displacement beyond which the distributions exhibited deviations from Gaussian behavior was chosen as the threshold for identifying IRs. Also, as shear induces anisotropy in displacements, the threshold was chosen independently for X and Y directions. We find that for $\gamma_o < \gamma_y$, the thresholds in X and Y directions are $0.31 \pm 0.08\sigma$ and $0.32 \pm 0.08\sigma$ respectively, whereas for $\gamma_o > \gamma_y$, they are $0.39 \pm 0.1\sigma$ and $0.44 \pm 0.1\sigma$. Here, σ is the mean diameter of the big and the small particles. Further, we also checked the nearest-neighbour configurations for all the particles that underwent large displacements. Particles separated by a distance less than 1.4σ, which correspond to the first minimum of the radial pair correlation function, were identified as nearest-neighbours. Since we only tracked particles in the XY plane, we lack information about displacements in the Z- direction. However, it is likely that if a trajectory is terminated due to out-of-plane motion, then the particle made a large displacement. Hence, all such particles were also identified as lost neighbours. A particle was then labelled irreversible, if it made a displacement greater than the threshold and lost at least four neighbours at the end of the strain cycle. Studies on supercooled liquids and glasses have shown that configurational changes ensuing from such irreversible dynamics are permanent (Widmer-Cooper *et al.* 2008; Yunker *et al.* 2009).

For γ_o's far from γ_y, we did not observe any transients in $f_{IR}(\tau)$ implying that steady state was reached rapidly (Fig. 4.4a). Near γ_y, for $\gamma_o = 0.25$ however, $f_{IR}(\tau)$ shows a slow fall over the experimental duration. Similar long-lived transients near yielding have also been observed in recent simulations of periodically sheared amorphous solids (Fiocco *et al.* 2013; Regev *et al.* 2013). To investigate the onset and γ_o-dependence of irreversibility, we plotted the steady state fraction of irreversible particles after subtracting the thermal contribution, denoted by f_{IR}^{∞}, as a function of γ_o in Fig. 4.4b. f_{IR}^{∞} shows a modest rise up to a critical strain γ_c^{Mi} and increases more rapidly beyond γ_c^{Mi} (Petekidis *et al.* 2002). Here, the superscript 'Mi' signifies that the critical strain has been extracted from microscopy data. It is quite conceivable that f_{IR}^{∞} behaves as an order parameter for irreversibility. By fitting f_{IR}^{∞} with a power-law of the form $f_{IR}^{\infty} \propto (\gamma_o - \gamma_c^{Mi})^{\beta}$ for $\gamma_o > \gamma_c^{Mi}$, we extracted an 'order parameter exponent' $\beta = 0.67 \pm 0.09$ and a 'critical strain' γ_c^{Mi} of 0.16, which is close to γ_y (Inset to Fig. 4.4b). Remarkably, a marked change in f_{IR}^{∞}

across the yield strain was also observed in similar experiments on athermal amorphous bubble rafts, binary mixture of 1mm and 2mm bubbles (Neelima 2014). The procedure used to identify yield strain is identical to the one used here (Neelima 2014). Thus, we attribute the non-zero value and the small scatter in f_{IR}^{∞} observed at the low strain to thermal noise since the particles used in our studies are Brownian. In addition, they have also observed a completely reversible steady state, $f_{IR}^{\infty} = 0$ for $\gamma_o < \gamma_y$. However, this is in contrast with the recent observations on concentrated suspensions of emulsions, where a fully reversible state was not observed even at low γs. Moreover they suggest that the nature of the transition itself may also depend on ϕ (Knowlton *et al.* 2014).

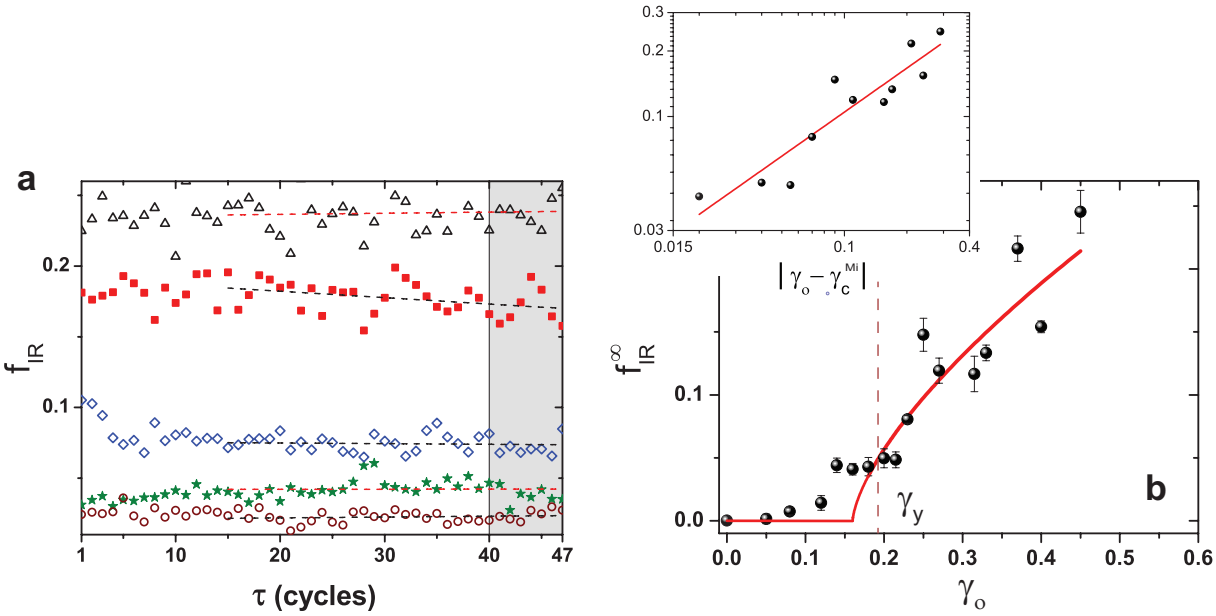

Figure 4.4: (a) $f_{IR}(\tau)$ for $\gamma_o = 0.05$ (○), $\gamma_o = 0.12$ (★), $\gamma_o = 0.215$ (◇), $\gamma_o = 0.25$ (■) and $\gamma_o = 0.37$ (△). The dashed lines are linear fits to the data. (b) f_{IR}^{∞} as a function of γ_o. Inset to B shows f_{IR}^{∞} versus $|\gamma_o - \gamma_c^{Mi}|$. $f_{IR}^{\infty}(\gamma_o) = f_{IR}^{ss}(\gamma_o) - f_{IR}(\gamma_o = 0)$, where f_{IR}^{ss} is the steady state fraction of irreversible rearrangements obtained by averaging over the shaded region in a. The thermal contribution to f_{IR}, $f_{IR}(\gamma_o = 0) = 0.023$. The red curve is a power-law fit to the data. γ_c^{Mi} and β were extracted by minimizing χ^2.

Relaxation Time

Transients in G'': The dependence of f_{IR}^{∞} on γ_o suggests a non-equilibrium phase transition governing yielding and it is therefore natural to wonder whether the long-lived transients in $f_{IR}(\tau)$ correspond to critical slowing down. Since irreversible dynamics leads to energy dissipation, the transients in f_{IR} are also evident in $G''(\tau)$ (Fig. 4.5a). Unlike $f_{IR}(\tau)$, $G''(\tau)$ is a bulk measure and therefore has a significantly better signal-to-noise ratio. Analogous to (Corte *et al.* 2008), the relaxation curves in Fig. 4.5a are well-fitted by the functional form $G''(\tau) = (G_o'' - G_\infty'')\frac{e^{-\tau/\tau_s}}{\tau^\delta} + G_\infty''$, where τ_s is the time taken to reach steady state and G_o'' and G_∞'' are the initial and steady state values of $G''(\tau)$, respectively. This functional form captures the crossover from exponential to power-law behaviour expected near a critical point. Remarkably, τ_s extracted from the fits appears to diverge at a critical strain $\gamma_c^{Rh} = 0.25$ close to γ_y

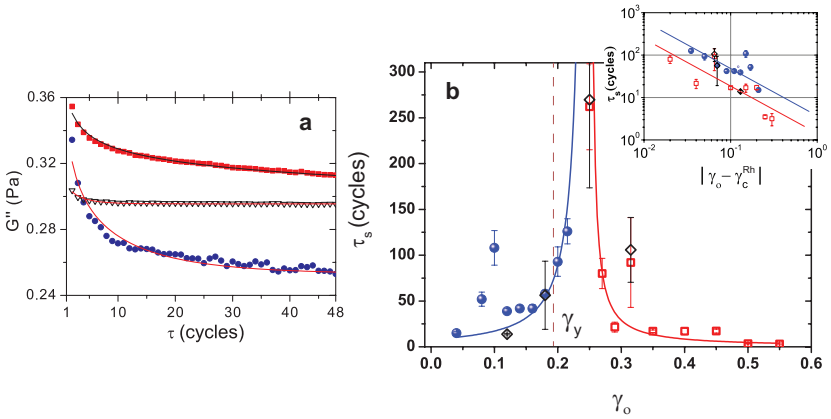

Figure 4.5: (a) $G''(\tau)$ for $\gamma_o = 0.04$ (●), $\gamma_o = 0.25$ (■) and $\gamma_o = 0.45$ (▽). The curves are best fits to the data. A power-law exponent $\delta = 0.27 \pm 0.02$ was found to give satisfactory fits for all γ_o's . (b) Relaxation time τ_s versus γ_o. The solid curves represent power-laws of the form $|\gamma_o - \gamma_c^{Rh}|^{-1.5}$ (blue) and $|\gamma_o - \gamma_c^{Rh}|^{-1.1}$ (red) and serve as guides to the eye. Inset to D shows τ_s versus $|\gamma_o - \gamma_c^{Rh}|$. Since $\gamma_o = 0.25$ corresponds to the critical strain γ_c^{Rh}, it cannot be represented on a double logarithmic plot and is therefore not shown in the inset. The red line is a fit to the data for $\gamma_o > \gamma_c^{Rh}$ (□). For $\gamma_o < \gamma_c^{Rh}$ (*bullet*), the presence of outliers precludes satisfactory linear fitting and hence, the blue line shown is a guide to the eye with the same slope as the red line. Black Diamonds (◇) correspond to τ_s obtained from independent measurements on the same sample.

(Fig. 4.5b). Here, the superscript 'Rh' denotes that the critical strain has been extracted from rheology data. By fitting τ_s with a power-law of the form $\tau_s \propto |\gamma_o - \gamma_c^{Rh}|^{-\alpha}$ for $\gamma_o > \gamma_c$, we obtained the relaxation time exponent $\alpha = 1.1 \pm 0.3$ (Inset to Fig. 4.5b). Although the dynamical range covered here is insufficient to extract reliable exponents, it is encouraging that a nearly identical relaxation time exponent was predicted in a recent theoretical study on periodically sheared amorphous solids (Perchikov & Bouchbinder 2014). A maximum in the time taken to attain a steady state was observed in the vicinity of yield strain in Bubble raft experiments as well(Neelima 2014). Collectively, from our observations (Fig. 4.4b & 4.5b) it is tempting to speculate that yielding of colloidal glasses is associated with a non-equilibrium critical point.

Transients in G': The observed decrease in f_{IR} with cycle number τ leads to a corresponding increase in the fraction of reversible particles $f_R = 1 - f_{IR}$, which should be reflected as a growth in the storage modulus G' with time. While this is certainly the case in the vicinity of γ_c, $G'(\tau)$ actually decreases monotonically for γ_o far from the critical strain. Even for γ_o close to γ_c, the slow rise in $G'(\tau)$ is preceded by an initial rapid decay, and $G'(\tau)$ goes through a minimum (Fig. 4.6).

We present a simple model to elucidate this peculiar time evolution of G'. The central idea is that the complex time evolution of G' results from a combination of two quite distinct processes. As mentioned before, the slow increase in G' at later times is a reflection of the transient in $f_{IR}(\tau)$, or alternatively, $G''(\tau)$. We conjecture that the initial rapid decay corresponds to the relaxation of elastic heterogeneity in the sample following pre-shear. Since our sample is

composed of deformable particles, some regions of it are likely to be over-compressed, which gives an excess elastic contribution. The relaxation of these regions does not require a change in particle configurations, and therefore leads to a fairly rapid decrease in $G'(\tau)$. Combining these two ingredients, we can split the time dependence of G' as

$$G'(\tau) = G'_{el}(\tau)(1 - f_{IR}(\tau)) \tag{4.1}$$

where G'_{el} captures the time dependence of the purely elastic transient. Assuming the time dependence of f_{IR} and G'' to be identical, we get

$$f_{IR}(\tau) = (f^0_{IR} - f^\infty_{IR})\frac{e^{-\tau/\tau_s}}{\tau^\delta} + f^\infty_{IR} \tag{4.2}$$

To model the time dependence of G'_{el}, we assume the system to be an elastically heterogeneous mosaic of domains of linear size ξ. The time dependence of G'_{el} follows from the relaxation of this local elastic heterogeneity. Intuitively, the rate of change of G'_{el}, $\frac{dG'_{el}}{d\tau}$ is proportional to the deviation of G'_{el} from its steady state value G'_s. Further, $\frac{dG'_{el}}{d\tau}$ is also proportional to the rate at which the stored energy is distributed. Here, we assume that this rate is given by v_s/ξ, where $v_s = \sqrt{G'_{el}/\rho}$ is the local sound velocity and ρ is the density. G'_{el} therefore satisfies a rate equation of the form

$$\frac{dG'_{el}}{d\tau} = \alpha\sqrt{G'_{el}}(G'_{el} - G'_s) \tag{4.3}$$

where α is a proportionality constant that depends on ξ, ρ and possibly other system parameters. Solving the above equation, one obtains

$$G'_{el}(\tau) = G'_s\coth^2(\alpha\sqrt{G'_s}\tau + C) \tag{4.4}$$

where C is the constant of integration defined through the relation $G'_{el}(0) = G'_s\coth^2(C)$. From Eqns. 4.2 and 4.4, after suitably adjusting the constants, we expect the transient behaviour of the storage modulus G' to be captured by the functional form

$$G'(\tau) = G'_\infty\coth^2(B\tau + C)(1 - D\frac{e^{-\tau/\tau_s}}{\tau^\delta}) \tag{4.5}$$

Although this equation has six parameters, δ and τ_s can be obtained from the corresponding $G''(\tau)$, and G'_∞ can be fixed from the saturation value of $G'(\tau)$. Further, B and C are not independent, as they are related through Eqn. 4.4. Thus, the model has only two free parameters, namely B, which depends on the length scale of elastic heterogeneity ξ, and D, which stems from the proportionality between f_{IR} and G''. This simplistic model correctly captures the complex temporal evolution of G' across the entire range of γ_o's investigated (Fig. 4.6).

Collectively, from our observations of f_{IR}, $G''(\tau)$ and $G'(\tau)$, it is tempting to speculate that yielding of colloidal glasses is associated with a non-equilibrium critical point. Yielding in hard materials has often been associated with the pinning-depinning transition (Tsekenis *et al.* 2013). However, quenched disorder, which is an important ingredient of pinning-depinning transitions, is absent in our system. The γ_o dependence of f^∞_{IR} observed here suggests a transition from reversible dynamics with $f^\infty_{IR} \approx 0$, to irreversible dynamics with $f^\infty_{IR} > 0$, which is character-

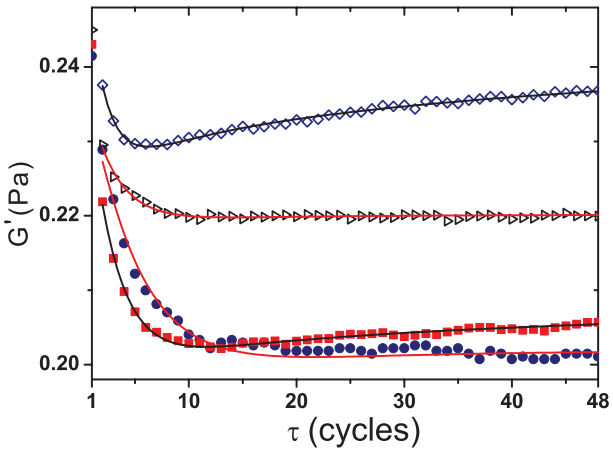

Figure 4.6: $G'(\tau)$ for $\gamma_o = 0.04$ (●), $\gamma_o = 0.215$ (◇), $\gamma_o = 0.25$ (■)and $\gamma_o = 0.4$ (▷). The curves are fits of the functional form given by Eqn. 4.5. The fit parameters δ and τ_s have been obtained from the corresponding $G''(\tau)$ and G'_∞ has been fixed from the saturation value of $G'(\tau)$. To facilitate comparison across γ_o's, $G'(\tau)$ has been scaled appropriately for $\gamma_o = 0.04$ and $\gamma_o = 0.4$.

istic of an absorbing phase transition (APT) (Corte *et al.* 2008). Most APTs belong to the directed percolation universality class (Hinrichsen 2000). However, the particle number density being conserved in our system, the putative non-equilibrium phase transition associated with yielding may belong to the conserved directed percolation (C-DP) universality class (Menon & Ramaswamy 2009). Further, in our cone-plate shear geometry, the diameter of the cone is ~ 200 times larger than the gap and hence, the critical exponents extracted here should therefore be in agreement with those observed for 2D C-DP (Menon & Ramaswamy 2009). Interestingly, we find that the relaxation time exponent $\alpha = 1.1 \pm 0.3$ (Fig. 4.5b) and the order parameter exponent $\beta = 0.67 \pm 0.09$ (Fig. 4.4b) are indeed very close to the C-DP universality class value in 2D (Menon & Ramaswamy 2009). While our experiments suggest that this transition belongs to C-DP universality class, more recent simulations suggest that it falls in the category of DP class of non-equilibrium phase transitions (Tjhung & Berthier 2015). However, within our experimental uncertainty, it is not possible to ascertain the universality class of the yielding transition.

Growing Length Scale

The observation of critical slowing down implies increasing spatial correlations between local irreversible rearrangements near yielding. In our system, these correlations can be probed using concepts developed to understand the dynamics of amorphous solids. Recent simulations suggest that local plastic events in glasses originate from spatially localized low frequency vibrational modes (Tanguy *et al.* 2010). Since these localised regions also posses low stiffness values, we identified them using a local measure of elasticity, namely, the Debye-Waller factor u_i (Tsamados *et al.* 2009) defined as $u_i = (r_i - \langle r_i \rangle)^2$ (Widmer-Cooper & Harrowell 2006). Here, r_i is the instantaneous position of particle i, and $\langle r_i \rangle$ is its mean position averaged over a suitable time window. To choose this window, we adopted a procedure analogous to the one routinely used for quantifying dynamical heterogeneities in supercooled liquids (Starr *et al.* 2013). Accordingly, for each γ_o, for different time windows Δt, with Δt being less than the cage-breaking time, we

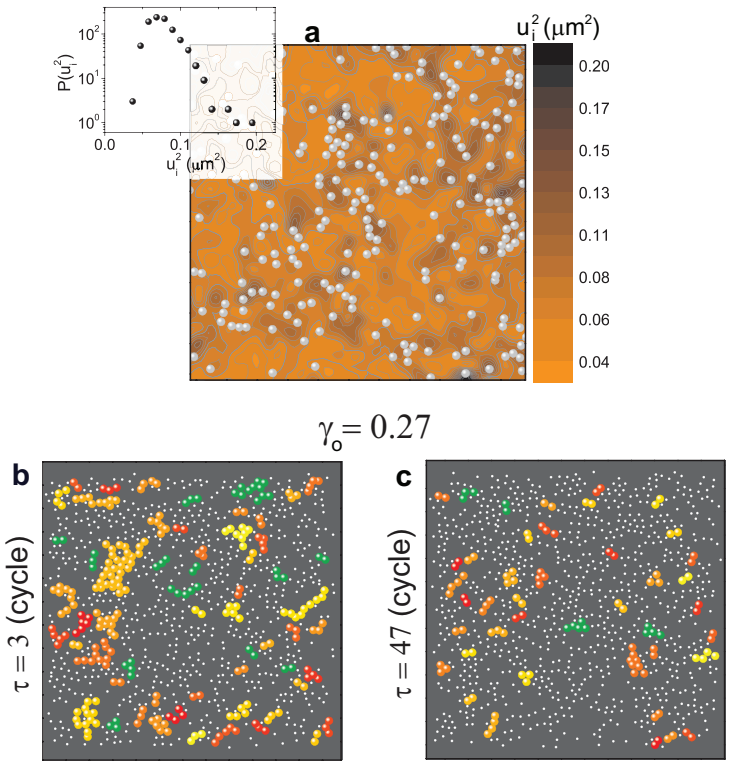

Figure 4.7: (a) Color map of u_i for $\tau = 2$. The solid spheres represent irreversible particles at the end of the same cycle. Inset shows the distribution of u_i. (b)-(c) Representative snapshots with the top 10% high u_i particles shown as big solid spheres and the remaining shown as small circles. The colors are a visual aid to help demarcate clusters.

clustered the top 10% high u_i particles based on nearest-neighbour distances. We find that the average cluster size as a function of time exhibits a maximum at $\Delta t = t_{max}$, which was chosen to be the appropriate time interval for computing u_i. Experimentally, u_i is a fairly accurate measure since it requires particles to be tracked only for a short duration. Figure 4.7a shows a color map of u_i averaged over an oscillation cycle, for $\gamma_o = 0.25$ and $\tau = 2$ and the inset shows its distribution $P(u_i)$. We find that regions of high u_i are spatially localised and correlated with subsequent irreversible rearrangements (grey circles in Fig. 4.7a). The transient dynamics of $f_{IR}(\tau)$ (Fig. 4.4a), should therefore stem from the spatio-temporal evolution of these high u_i regions. To show this, we first identified the top 10% high u_i particles for various γ_o's. Figure 4.7b & c show snapshots of these particles for $\gamma_o = 0.27$ at $\tau = 2$ and 47, respectively. The top 10% high u_i particles are spatially clustered and more importantly, there are fewer large clusters for $\tau = 47$. Figure 4.8a-c shows the cluster size distribution $P(n)$, where n is the number of particles in a cluster, for three different time intervals at various γ_o's. Analogous to $f_{IR}(\tau)$, $P(n)$ is stationary for γ_o far from γ_c^{Rh} and evolves steadily in the vicinity of γ_c^{Rh}. Further, near γ_c^{Rh}, $P(n)$ for $n > 20$ is significantly smaller at a larger τ. It is also evident that on average, clusters are larger for $\gamma_o \approx \gamma_c^{Rh}$ (Fig. 4.8b) as compared to γ_o far away from γ_c^{Rh} (Fig. 4.8a & c). Indeed, the average cluster size $\langle n \rangle = \frac{\sum n^2 P(n)}{\sum n P(n)}$, a commonly used measure of the correlation length (Weeks *et al.* 2000), shows a clear maximum near γ_c^{Rh} (Fig. 4.8c). The small increase in $\langle n \rangle$ could be due to the fact that this parameter was extracted from the precursors of the yield

events not these events themselves. Moreover, given that we are not sampling the events taking place in the velocity-vorticity plane, the value of $\langle n \rangle$ quoted here could be highly underestimated.

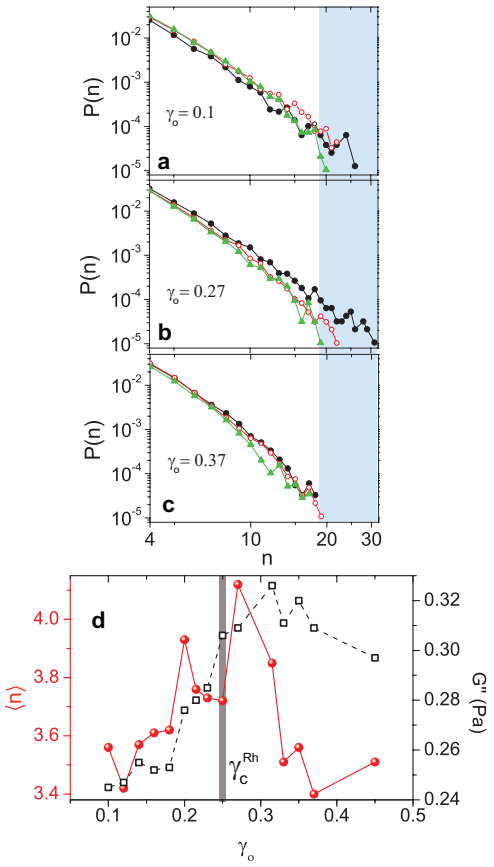

Figure 4.8: (a)-(c) Distribution of cluster size $P(n)$. In (a)-(c) $P(n)$ for $\tau = 2$ to 10 cycles (●), for $\tau = 20$ to 30 cycles (○) and for $\tau = 37$ to 47 cycles (▲). (d) $\langle n \rangle$ as a function of γ_o is shown as (●). G'' from bulk rheology is shown as (□).

4.4 Conclusions

Our results strongly suggest that correlations between local yield events not captured by mean field theories like Soft Glassy Rheology (SGR) (Sollich *et al.* 1997) lead to a non-equilibrium phase transition at the yield point. For γ_o less than a critical strain, yield events are rare and the system appears to self-organizes quickly into an 'absorbing' steady state ($f_{IR}^{\infty} \approx 0$), where the applied strain is insufficient to induce irreversible changes in particle configuration. For γ_o larger than the critical strain, the imposed strain facilitates many independent irreversible rearrangements, correlations between yield events are washed out, and the system rapidly reaches a 'fluctuating' steady state ($f_{IR}^{\infty} > 0$) (Sollich *et al.* 1997). Close to the critical strain, however, correlations between local yield events trigger a cascade of irreversible rearrangements, which is manifested as a growing length scale (Fig. 4.8d) and leads to critical slowing down (Fig. 4.5b). Further, it has not skipped our attention that the growing cluster sizes near γ_y may also have implications for the origin of the G'' peak (Fig. 4.8d). This is especially important when the G'' peak coincides with the yield strain, a scenario frequently observed in soft solids.

Through simultaneous quantification of single-particle dynamics and bulk viscoelastic moduli, we have uncovered signatures of a non-equilibrium critical phenomenon governing yielding of a colloidal glass (Fig. 4.4b & 4.5b). Unlike non-Brownian suspensions, our Brownian system has a finite threshold for irreversibility only at sufficiently large volume fractions where it behaves as a viscoelastic solid. This enabled us to identify the observed critical point with the yield strain. The surprising agreement between experimental (Fig. 4.5b) and theoretical (Perchikov & Bouchbinder 2014) value of the exponent characterizing the divergence in the relaxation time is worthy of further investigation. We found that the growing time scale in our experiments is accompanied by a growing length scale associated with clusters of particles with high Debye-Waller factor (Fig. 4.8d), which are precursors of local plastic events in amorphous solids (Fig. 4.7b). We therefore expect the correlations between local irreversible rearrangements observed here to have a correspondence with observations of avalanches in sheared amorphous solids (Lemaître & Caroli 2009). In the context of soft colloidal systems like star polymers and microgels, it would be interesting to study the influence of particle softness on the nature of the yielding transition. It would be interesting to investigate the presence of a growing length scale observed here in experiments on athermal amorphous bubble rafts as well. More generally, given that a wide range of soft materials such as gels, emulsions and foams also exhibit strikingly similar rheological properties, the transition observed here should be generic to soft solids and similar studies on diverse soft systems are required to verify this claim. Although the mechanical response of soft solids depends only weakly on frequency, it would be worthwhile to examine the frequency dependence of the onset of irreversibility in these materials. Our results exemplify the need for refining mean field theories like SGR. In particular, it might be possible to incorporate explicit interactions in SGR such that the local yielding of one element assists in the yielding of a neighbouring element. Connections of such an extended SGR model to theories that relate yielding to the percolation of a liquid phase within a deformed solid (Liu *et al.* 2013) may also be conceivable. Most importantly, our findings set the stage for developing a unified framework for yielding of soft solids.

Chapter 5

Confined Glassy Dynamics at Grain Boundaries in Colloidal Polycrystals

5.1 Introduction

Grain boundaries (GBs) are central to our understanding of deformation and fracture mechanisms (Shan *et al.* 2004), melting kinetics(Alsayed *et al.* 2005) and transport properties (Hilgenkamp & Mannhart 2002) in a wide class of natural and man-made materials. One of the active areas of materials research is to elucidate the spatio-temporal evolution of GBs and dynamics of their constituent atoms to better understand processes for enhancing material performance. Based on the value of the misorientation angle Θ, GBs are classified as Low angle and High angle (Chapter 1 Section 3). While low angle grain boundaries (LAGBs) that are composed of periodic discrete dislocations are relatively well understood, a majority of high angle grain boundaries (HAGBs) do not posses a well defined structure and continue to pose a challenge.

The structure of a GB is determined by the competing order indicated by its adjacent crystallites. Therefore, the particles at a grain boundary posses reduced packing efficiency and enhanced mobility as compared to their crystalline neighbors. Given that frustration due to packing results in the disordered structure of supercooled liquids, a simple assumption is that GBs share similarities with supercooled liquids. The amorphous structure of GBs was first put forth by Brillouin and Quincke (Quincke 1905) over 100 years ago, which was later developed by Rosenhain and Ewen (Rosenhain & Ewen 1913) and Rosenhain and Humphrey (Rosenhain & Humphrey 1913). They suggested that a GB in a polycrystal is like the amorphous cement which holds two grains together (Herman 1972). This model is popularly known as amorphous-cement model and has been used to rationalize processing characteristics of ferritic materials. Also, the soft and viscous nature of supercooled liquids at high temperatures and their hard and brittle nature at low temperatures was used to explain GB sliding at high temperature and GB embrittlement at low temperatures (Herman 1972). Further, all factors related to packing efficiency like confinement, impurities and external stress which effect amorphous solids are known to have an influence on GB properties as well. However, this model could not explain the Θ dependence of GB properties like mobility, diffusion, energy and GB corrosion (Upmanyu *et al.* 1999; Nomura & Adams 1992). Within the supercooled liquid model, owing to the isotropic structure of amorphous materials, these properties should in principle be independent of Θ (Gleiter 1971; Keblinski *et al.* 1996). Moreover, in contrast to a disordered structure, studies have shown that some GBs possess well defined structure such as special boundaries. In addition to the aforementioned reasons, this model was also neglected due to a lack of evidence for the amorphous nature of GBs either from simulations or direct experimental observations. Almost sixty years after Rosenhain and Ewen, Ashby studied grain boundary dynamics using

polycrystals made of macroscopic bubbles and provided the evidence for disordered structure of GBs (Ashby 1972). Since the system used was polycrystal made of bubbles, this evidence was not sufficient to establish the disordered structure of GBs. Later, simulations on real systems by D. Wolf and coworkers revealed a misorientation independent disordered structure of general HAGBs (Wolf 2001). They have quantified the structure through radial pair correlation function for various GBs. This study provided an initial hint from more realistic systems that supercooled liquid model of GBs could be true atleast for HAGBs. Strikingly, High Resolution Transmission Electro Microscopy (HRTEM) experiments on tilt boundaries have suggested the presence of cooperative motion of particles, a characteristic feature of supercooled liquids, in GBs (Deng & Schuh 2011). More recently, MD simulations on HAGBs under external driving force have shown that these boundaries exhibit dynamics analogous to that of glass forming liquids (Zhang *et al.* 2009).

While substantial support for the amorphous nature of HAGBs is obtained from simulations, it is to be noted that conventional simulation approaches access dynamics under an external stress and at high temperatures (Trautt *et al.* 2006; Gottstein & Shvindlerman 2009). Direct observation is beset by experimental limitations (Gottstein & Shvindlerman 2009; Deng & Schuh 2011) and hence evidence for supercooled liquid like dynamics at grain boundaries in the low temperature and zero driving force limit is still lacking. Moreover, the rationale for Θ dependent properties is also yet to be understood. Given that GBs are only few particle diameters wide at low temperatures, it is natural to expect confinement effects to play a key role in the dynamics. Here, by probing Θ dependent dynamics of GBs with single particle resolution at low temperatures and in the zero driving force limit in colloidal polycrystal we attempt to develop a microscopic picture which can rationalize the above observations.

5.2 Experimental Details

To mimic an atomic polycrystal closely, we have used a colloidal crystal composed of thermo-responsive Poly N-isopropyl acrylamide (PNIPAm) particles. This systems offers an advantage over other colloidal systems since the volume fraction and hence the phase behaviour can be tuned in-situ by changing temperature. Thus, colloidal polycrystals can be obtained by simply annealing the samples. Interestingly, annealing is routinely used for crystallizing metals. For our studies, we have synthesized PNIPAm colloidal particles of size $\sim$600 nm at 26 °C (Chapter 2, Table 1). These particles are negatively charged and interact via screened Coulomb repulsions. Above the lower critical solution temperature of 33 °C, the particles shrink to $\approx$300 nm. Samples with volume fraction $\phi > 70\%$ at 26°C were loaded in wedge-shaped cells (Gerbode *et al.* 2010). At these large volume fractions the particles self assemble into a random hexagonally close packed colloidal polycrystal even during the loading process. Thus to remove loading history, we have annealed the samples. Annealing at a rate of 0.09°C/min from 38°C where the sample is in a fluid state to 26 °C where the particles self-assemble to form a polycrystal (Fig. 5.1) resulted in an average grain size of $\sim 68\mu$m. This process also yielded a broad range of Θs as shown in Fig. 5.2a & b.

The GB planes are perpendicular to the walls of the cell and hence our studies are confined to tilt boundaries. Since HAGBs are least understood boundaries they are the primary focus of

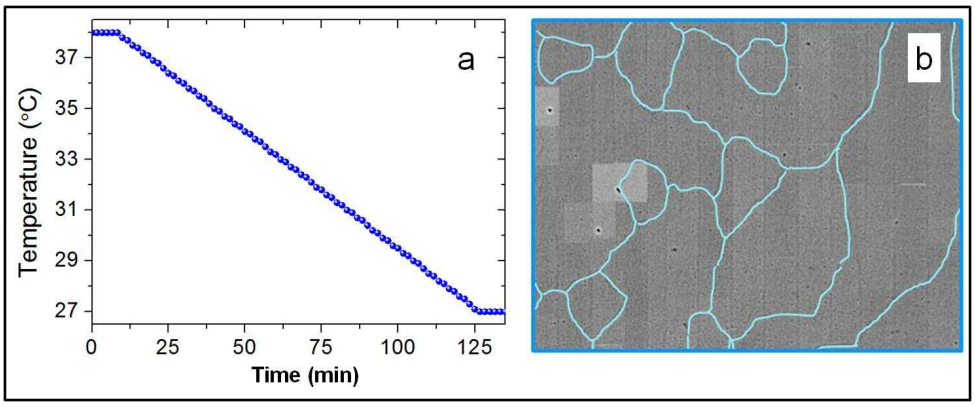

Figure 5.1: Formation of a Polycrystal. (a) Protocol used for cooling the colloidal system from 38° to 26°. (b) Grain boundary network of the polycrystal as a result of a. The cyan curves represent grain boundaries.

our study. In order to facilitate confocal imaging the particles were fluorescently labelled with a fluorophor, Rhodamine 6G (Chapter 2 (Table 1), Hu *et al.* (2000)). We used a wedge shaped cell and hence to avoid confinement effects, the sample was imaged at a thickness of ≈ 23 μm. All measurements were made 8 to 10 crystalline layers from the bottom of the cell to avoid wall effects. A Visitech VT-eye fast laser confocal scanner coupled to a Leica DMI 6000B optical microscope was used for confocal imaging. The samples were imaged using a Leica objective (Plan Apochromat 100X NA 1.4, oil immersion) with a laser excitation centered at 514 nm. The field of view was 20 μm x 20 μm and a 2-dimensional slice consisted of $\approx$ 1200 particles. An objective heater was used to maintain constant temperature through out the experiment.

Each experiment consisted of studying dynamics of GB colloids in a 2-D plane of a 3-D polycrystal for a fixed Θ and temperature, T. For Θ dependent studies we have considered HAGBs with $\Theta = 24.3°$, $18.4°$ and $17.6°$, LAGBs with $\Theta = 12.7°$ and $10.4°$ and for temperature dependent studies we have fixed $\Theta = 24.7°$ and investigated dynamics at $T = 25°$C and $T = 28°$C. Images were captured at 2 fps and 3.3 fps for experiments probing the effect of Θ and T, respectively. To facilitate local heating for experiments performed at high temperature, we have once again used the objective heater. Particles were tracked using standard algorithms (Gao & Kilfoil 2009; Crocker & Grier 1996) and GB dynamics were studied using codes developed in-house.

5.3 Results and Discussion

5.3.1 Identification of Grain Boundary Particles

In order to investigate the properties of GBs, we first identified the particles belonging to the boundary using the procedure described below. GB particles possess a lower coordination number compared to their crystalline counterparts and hence we used a method based on local bond-order parameter to identify them. For each particle j at each time step, we calculated the extent of the particle's local orientational order using the 2D Halperin-Nelson bond-order parameter, $\psi_6(j) = (1/N)\Sigma_k \exp(6i\theta_{jk})$. Here, N is the number of nearest-neighbors and θ_{jk} is the

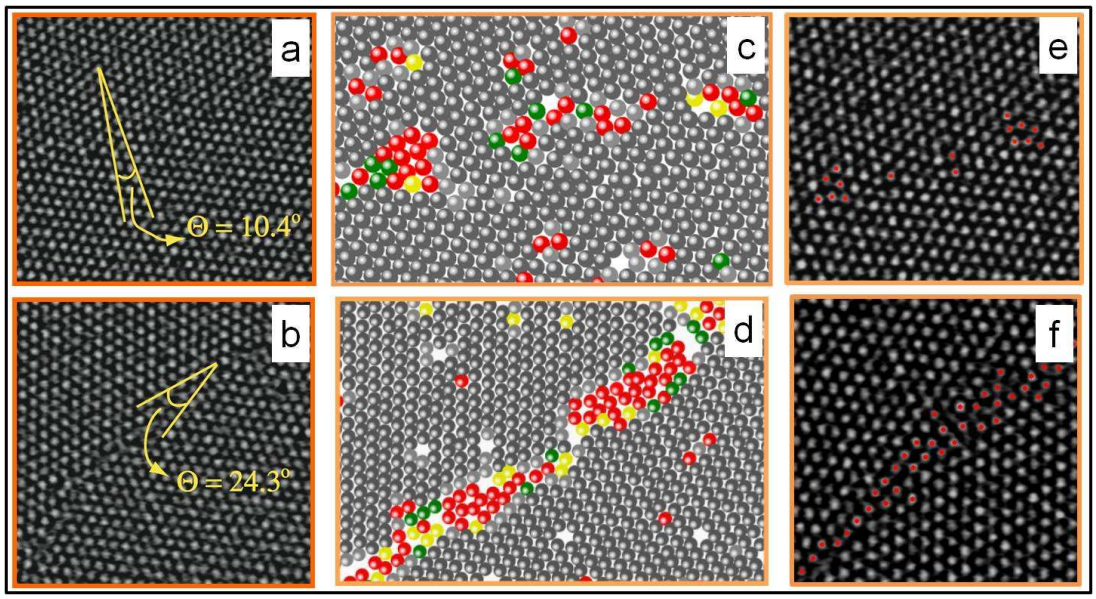

Figure 5.2: Representative images of GBs. Image of (a) LAGB and (b) HAGB. (c-d) Bond-order analysis of a and b respectively. The dark and light gray particles are crystal-like with ordered nearest-neighbors > 4, while the green to red colors correspond to ≤ 4 ordered nearest neighbors. Grain boundary particles highlighted in red (e) LAGB (f) HAGB.

angle between the $j-k$ bond and a reference axis. A particle k is a nearest-neighbor of j if it lies within 1.4σ, where σ is the lattice spacing. Typically, a particle having $\psi_6(j) > 0.7$ is considered to be an ordered particle. However, since GBs are dense amorphous regions they can posses a high degree of local orientational order and ψ_6 alone is insufficient to label GB colloids (Larsen & Grier 1996). In order to unambiguously determine crystal-like and amorphous-like particles, we set a cut-off on the number of ordered nearest-neighbors, $N_\circ$, for a particle j (Hernández-Guzmán & Weeks 2009). A particle k is an ordered nearest neighbor of particle j, if the complex inner product $\psi_6(j)\psi_6(k)^*$ exceeds a value 0.5 (Wu *et al.* 2009). Particles are termed amorphous-like if $N_\circ < 4$. The above procedure is similar in spirit to the Steinhardt bond-order parameter approach for identifying crystal-like clusters in 3D (Steinhardt *et al.* 1983). Fig. 5.2b&c show the particles color coded based on the number of ordered neighbors.

Further, we found that a colloid at the crystal-GB interface spends only a fraction of its time in the GB. Thus we have introduced an additional temporal cut-off for identifying a colloid as a part of a GB. For this we have plotted the distributions of the fraction of time a particle is amorphous-like. The sampling region included the GB as well as the adjacent crystallites such that at any given instant in time, the number of amorphous-like particles is nearly equal to the number of crystal-like particles. This ensures that the distribution is not biased due to one type of particles. Since particles within the bulk of the crystal remain crystal-like for most of the time, one would expect a peak in the distribution at small fractions. Also, one would expect particles in the grain GB to remain amorphous-like for most of the time and this would give rise to a peak at high fractions. In addition particles at the interface fluctuate between crystal-like and amorphous-like states. As expected, the profile of this distribution is nearly bimodal (Fig. 5.3). By fitting a fourth order polynomial to this distribution we estimated the minimum value to be close to 50%. Finally, particles which were amorphous-like for at least 50% of the duration

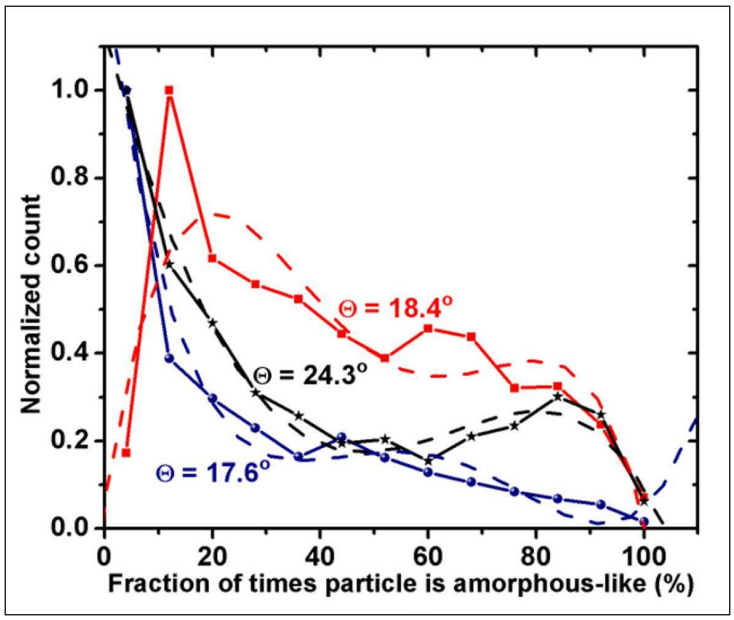

Figure 5.3: Distribution of amorphous-like and crystal-like particles. Fraction of particles that are amorphous like for Θ 24.3° (☆), 18.4° (◯) and 17.6° (■). The dashed curves are fourth order polynomial fits to the data.

of the experiment were identified as GB particles. Fig. 5.2e & f show representative snapshot of GB particles obtained by performing the aforementioned analysis highlighted. It is evident from the images that the procedure employed here, identifies GB particles unambiguously.

5.3.2 Structure of the Grain Boundaries

Having identified the GB particle, we first quantified their structure. The structure of LAGBs is evident from the Voronoi tessellation which shows periodic dislocation cores as pentagon-heptagon (5-7) dislocation pairs (Fig. 5.4a) (Read & Shockley 1950). For HAGBs the dislocation cores overlap resulting in a disordered structure and hence Voronoi tessellation cannot be used. Therefore to gain insights into the local order of HAGBs we have plotted the radial pair-correlation function, $\langle g(r)\rangle = \frac{1}{N}\sum_i \sum_{i\neq j}\langle \delta\,(r- \mid \mathbf{r}_i(0) - \mathbf{r}_j(0) \mid)\rangle$. Here, N is the total number of particles and $\mathbf{r}_i(t)$ is the position of the i^{th} particle at a time t. This quantity gives an estimate of the probability of finding a particle at a given distance, r. Because of the complex shape of the GB, the following procedure has been adopted to calculate $g(r)$. We first temporally average particle positions over a suitable time window in order to eliminate the effects due to thermal motion and to preserve the underlying structure. We have temporally averaged the particle positions over various time windows and we found that a window of 5 s is sufficient to prevent the smearing of peaks, while capturing the trend in $g(r)$. Using these time averaged particle positions we obtain the un-normalized $g(r)$. In the standard protocol, $g(r)$ is normalized by the area of the annulus formed by concentric circles of radii r and $r + dr$. However, here such an annulus is not entirely contained in the GB region for r greater than the grain boundary width, and hence will underestimate the number of GB particles contributing to the annulus. To circumvent this problem, we have modified the normalization procedure as follows. For a

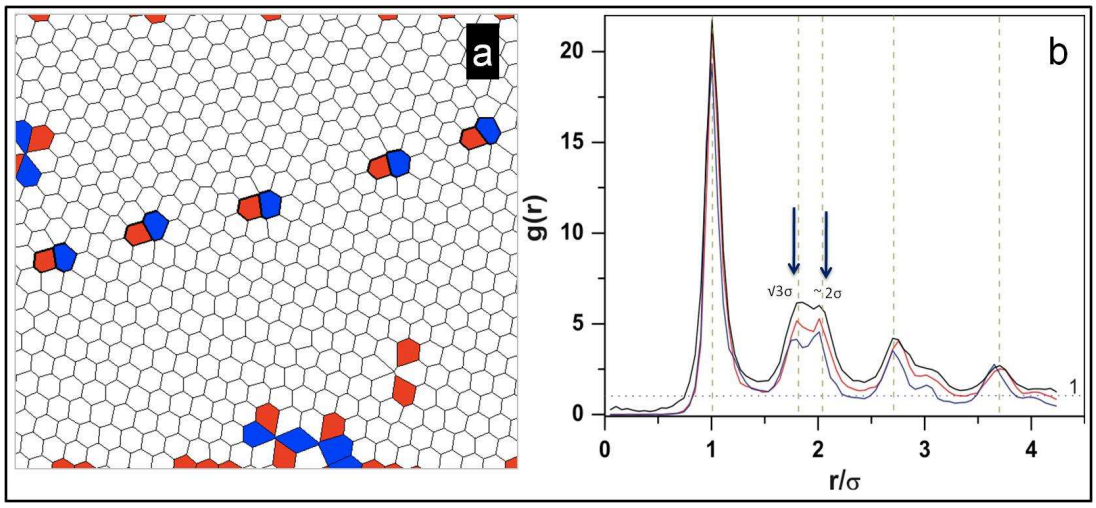

Figure 5.4: Structure of Grain Boundaries. (A) Voronoi analysis of LAGB with $\Theta = 10.4°$. The red and blue polygons correspond to pentagon-heptagon pairs of dislocations.(B) Radial pair correlation function for HAGBS. Black, red and blue curves correspond to $\Theta = 24.3°, 18.4°$ and $17.6°$ respectively. The vertical dashed lines represent crystal peaks.

conventional $g(r)$, the area under the first peak corresponds to the average number of nearest neighbors for a particle. We have determined this number independently by counting the number of nearest- neighbors of each GB particle and averaging over all particles in the GB region and over all times. We rescale the unnormalized $g(r)$ by a suitable multiplicative factor to ensure that the area under the first peak corresponds to the average number of nearest-neighbors counted. Also, as the number of particles increases linearly with r, we obtain the normalized $g(r)$ by further rescaling with $1/r$. The resulted $g(r)$ is shown in Fig. 5.4b.

An underlying feature of the $\langle g(r) \rangle$ for the three Θs investigated, is the presence of a split-second peak. The split-second peak has sub-peaks at 3σ and just below 2σ that coincide with the crystal peaks (dashed vertical lines) for an hcp lattice. This feature of $\langle g(r) \rangle$ has been observed in metallic (Yonezawa 1991) and colloidal glasses (van Blaaderen & Wiltzius 1995), random close packed granular media (Bernal 1964) and in computer simulations of HAGBs (Wolf 2001). We find that with decreasing Θ the splitting of the second peak becomes more pronounced which is indicative of a higher degree of particle localization. In addition, for HAGBs we find that the spatial and time averaged width of the GB interface extracted from the images decreases systematically from 2.1σ to 1.8σ to 1.5σ for Θ corresponding to $24.3°$, $18.4°$ and $17.6°$ respectively (Pennycook *et al.* 2000).

5.3.3 Dynamics of the HAGBs

In addition to the above mentioned structural attributes, there are prominent dynamical signatures associated with glass forming liquids and we seek them in GB dynamics (Weeks *et al.* 2000).

Mean-Squared Displacement, MSD

In glass forming liquids, particles are trapped in transient cages formed by neighboring particles at short-times. At long-times, thermally activated reconfiguration of the cage allows the

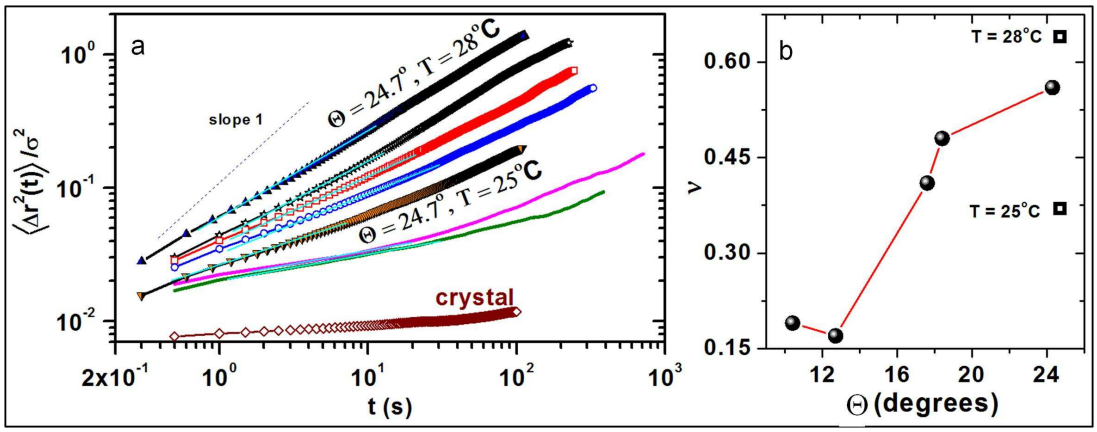

Figure 5.5: Mean Square Displacement of GB particles. (a) MSDs rescaled by σ^2. The hollow symbols are for HAGBs at $T = 26°$C, for $\Theta = 24.3°$ (☆), $\Theta = 18.4°$ (□)and $\Theta = 17.6°$ (○). The green and the pink lines correspond to LAGBs for $\Theta = 12.7°$ and $10.4°$, respectively. The solid triangles are for $\Theta = 24.7°$ at different T. The brown solid diamonds is the crystal MSD at $T = 26°$C. The intermediate time exponent, ν, is obtained from linear fits to the data which are shown by cyan lines. (b) ν as a function of Θ at $T = 26°$C (●) and for $\Theta = 24.7°$ at different T (□).

trapped particle to escape. This process is captured by the mean-squared displacement (MSD), $\langle \Delta r^2(t) \rangle \propto t^{\nu}$, of the particles which at short-to-intermediate times shows sub-diffusive behavior, ($\nu < 1$), indicative of trapping. The MSD approaches diffusive scaling ($\nu = 1$), also known as α-relaxation, at long-times due to cage breaking. In Fig. 5.5a we show $\langle \Delta r^2(t) \rangle / \sigma^2$ for all Θ values. For HAGBs, ν progressively increases with Θ at intermediate times (Fig. 5.5a hollow circles, Fig. 5.5b) which reflects the increasing mobility of the GB colloids with Θ. This increase in ν with Θ suggests a decrease in the degree of supercooling with increasing Θ. For LAGBs, there is lower packing frustration and the GB dynamics is governed only by the dislocation cores(Fig. 5.4a). Thus, as expected the intermediate time exponent is practically same for both the LAGBs studied although its greater than HAGBs (Fig. 5.5a lines, Fig. 5.5b). For HAGBs we observe that, with decreasing Θ the GB width decreases and the degree of supercooling increases. Experiments on hard-sphere colloids (Eral *et al.* 2009; Nugent *et al.* 2007) and computer simulations on polymeric fluids (Riggleman *et al.* 2006) have shown that spatial confinement can enhance the tendency of forming the glassy state (Scheidler *et al.* 2002; Alcoutlabi & McKenna 2005). Thus, we attribute the observed slowing down of particle dynamics in HAGBs with decreasing Θ to enhanced confinement of the amorphous phase by adjacent crystallites.

For confined supercooled liquids, it is also known that diffusion is anisotropic with it being slower along the confinement direction and we seek to look for this feature in GB dynamics. In the present case, this would imply slower dynamics along the direction perpendicular to the GB plane. To check this, we have plotted the MSDs of GB particles separately along directions parallel and perpendicular to the GB plane. Indeed for all HAGBs studied, we find that the intermediate time exponents, $\nu_{\parallel}$, for displacements parallel to the GB plane are indeed higher than the exponents, $\nu_{\perp}$, for displacements perpendicular to the GB plane as shown in Fig. 5.6. These results emphasize that the diffusion of GB particles is anisotropic and hence dynamics of HAGBs is influenced by geometric confinement.

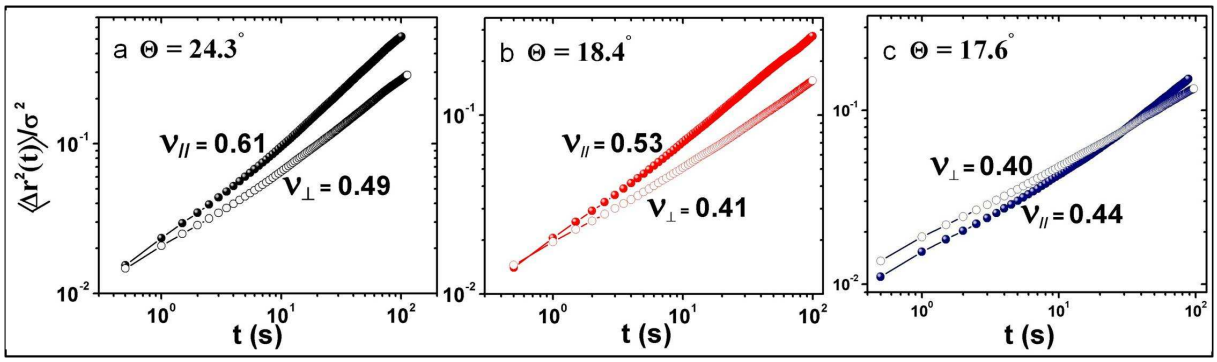

Figure 5.6: Anisotropic Diffusion in HAGBs. MSDs rescaled by σ^2 in the direction parallel to GB plane (solid symbols) and perpendicular to GB plane (hollow symbols) for (a) $\Theta = 24.3.7°$ (black symbols), (b) $\Theta = 18.4°$ (red symbols) and (C) $\Theta = 17.6°$ (blue symbols).

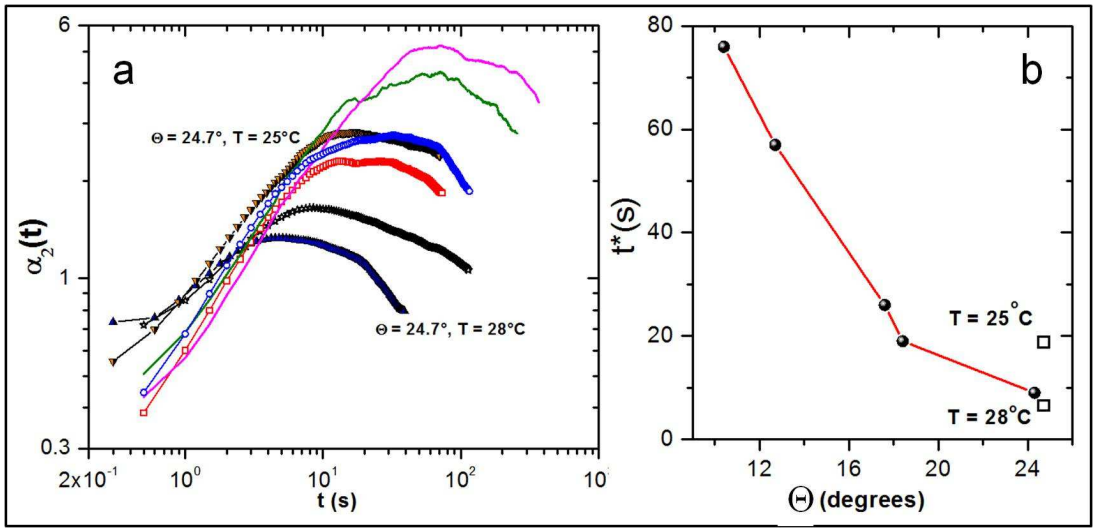

Figure 5.7: α_2 and cage breaking time, t^*. (a) α_2 for all GBs at all temperatures. The hollow symbols represent HAGBs at $T = 26°$C. (☆), (□) and (○) correspond to $\Theta = 24.3°$, $\Theta = 18.4°$ and $\Theta = 17.6°$, respectively. The green and the pink lines correspond to LAGBs for $\Theta = 12.7°$ and $10.4°$ respectively. The solid symbols are for $\Theta = 24.7°$ at different T. (b) t^* as a function of Θ at $T = 26°$C (●) and for $\Theta = 24.7°$ at different T (□)

To lend further support to the confinement argument, we exploit the size-tunable nature of PNIPAm colloids and study the GB dynamics for fixed Θ, as a function of temperature. On approaching the melting temperature ($\approx 33°$C), the GB width increases due to particle de-swelling as a result of which we expect reduced confinement and hence higher GB colloid mobility. Starting from T =25 °C, as we reach T =28 °C, we find that for $\Theta = 24.7°$ the GB width increases from 1.75σ to 1.95σ. We computed the MSDs of HAGB at these two temperatures. Consistent with the confinement picture, we find that $\langle \Delta r^2(t) \rangle_{28°\mathrm{C}} > \langle \Delta r^2(t) \rangle_{25°\mathrm{C}}$ (Fig. 5.5a upright triangles and inverted triangles respectively) with $\nu_{28°\mathrm{C}} > \nu_{25°\mathrm{C}}$ (Fig. 5.5b squares). It is evident from these results that the slowing down of dynamics with decreasing Θ is indeed due to increasing confinement.

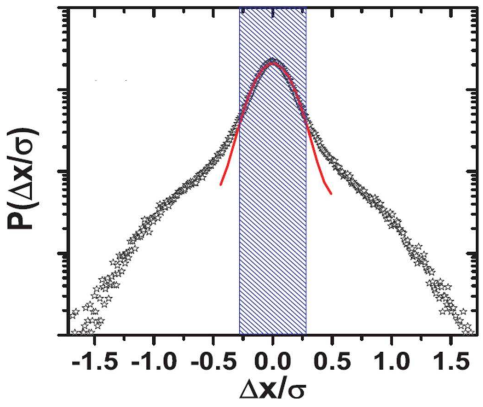

Figure 5.8: Non-Gaussian Displacements. Probability distribution of particle displacements, Δx, over $\Delta t = t^*$, for $\theta = 24.3°$ at T = 26°C. The red line is a Gaussian fit. Particles outside the shaded region are the top 10% most-mobile particles.

Non-Gaussian Parameter, α_2

For glasses, the particle dynamics in the vicinity of the cage-breaking time is expected to be non-Gaussian. To better quantify the cage-breaking dynamics, we plot the non-Gaussian parameter in 2-dimensions, defined as $\alpha_2(\Delta t) = (\langle \Delta r^4 \rangle / 2 \langle \Delta r^2 \rangle^2) - 1$. α_2 quantifies the deviation from the Gaussian nature. Accordingly, for diffusive behavior $\alpha_2(t) = 0$. For glasses, $\alpha_2(t)$ has a maximum at time t^* corresponding to the cage breaking time. Analogous to what is observed for supercooled liquids, even for the GB colloids (Fig. 5.7a) $\alpha_2(t)$ is large and goes through a maximum for all Θs studied. Further, we find that with decreasing Θ both t^* and the peak value of $\alpha_2(t)$ increase systematically (Fig. 5.7b) which once again confirms the confinement induced slowing down of GB particle dynamics. A similar trend in $\alpha_2(t)$ and t^* was also observed with decreasing temperature (Fig. 5.7b squares).

The presence of non-Gaussian displacements is also evident in the probability distribution of particle displacements, $P(\Delta x/\sigma)$, over t^* (Fig. 5.8). We find that while 90% of GB colloids display diffusive dynamics, the top 10% of the most-mobile particles are non-Gaussian, characterized by the tails of $P(\Delta x/\sigma)$. Such non-Gaussian displacements were also observed earlier in experiments as well as simulations on glass forming liquids.

Cooperatively Rearranging Regions

To unambiguously prove that GBs are dynamically similar to glasses, we check for signatures of cooperative particle dynamics. Cooperative motion of particles in the glassy state provides a pathway for structural relaxation and is, perhaps, the most striking feature of glass formers. This has been demonstrated in atomic simulations (Donati *et al.* 1998), experiments on colloidal (Weeks *et al.* 2000) and granular fluids (Berardi *et al.* 2010). To examine if similar dynamics exist in GBs, we employed methods developed to identify cooperative motion in supercooled liquids. As a first step towards this, we identify the top 10% most-mobile GB colloids over $\Delta t = t^*$ where the dynamics is maximally heterogeneous. In-order to verify the dynamics of these particles is indeed correlated, we plot the distinct part of the van Hove correlation function

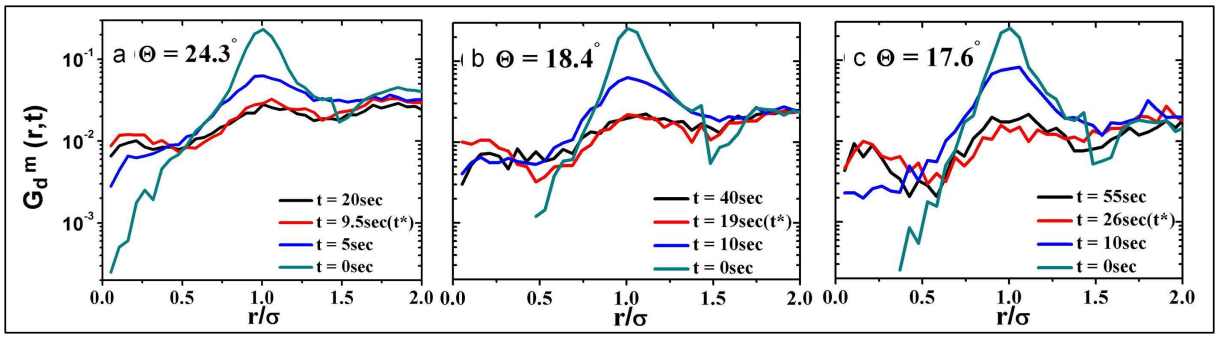

Figure 5.9: Cooperative Rearrangements - van Hove correlation function. Distinct part of the van Hove correlation function, $G_d^m(r,t)$, versus r rescaled by σ for most-mobile particles for (a) $\Theta = 24.3°$, (b) $\Theta = 18.4°$ and (c) $\Theta = 17.6°$. Different coloured lines correspond to different values of t.

$G_d^m(r,t)$.

$$G_d^m(r,t) = \frac{1}{N}\sum_i \sum_{i\neq j} \langle \delta\left(r - \mid \mathbf{r}_i(t) - \mathbf{r}_j(0) \mid\right)\rangle \tag{5.1}$$

Here, N is the number of mobile particles and $r_i(t)$ is the position of the i^{th} particle at a time t. $G_d^m(r,t)$ quantifies the time dependent probability of finding another mobile particle at a distance r from a randomly chosen mobile particle at time $t = 0$. For cooperative motion, one would expect that at later times the position of a mobile particle at $t = 0$ is occupied by another nearby mobile particle. This should be reflected as a peak in $G_d^m(r,t)$ at later times (Donati *et al.* 1998). Remarkably, we find that for all three HAGBs , $G_d^m(r,t)$ develops a peak at $r = 0$ at $t = t^*$ with a simultaneous decrease in the peak at $r = \sigma$ as t approaches t^* suggesting cooperative motion of mobile particles (Fig. 5.9).

While $G_d^m(r,t)$ indicates the presence of cooperative motion, given that we have access to single particle dynamics we can also quantify the shape and the size of these cooperatively rearranging regions. To this end, we have once again considered the top 10% most mobile particles over t^* and investigated their spatial arrangement. Interestingly, we observe that the mobile particles are indeed spatially clustered and we estimate the size of the clusters based on nearest neighbor distances. Here, a mobile particle belongs to a cluster only if it has a neighboring mobile particle within a distance of 1.4σ, the first minimum of $g(r)$ of a liquid. Fig. 5.10a shows GB colloids are spatially organized into strings. We have then plotted the probability distribution of cluster sizes $P_c(n_c)$ versus n_c, where n_c is the cluster size. For all three Θs and temperatures studied, the distribution of cluster size $P_c(n_c)$ decreases exponentially with n_c (Fig. 5.10b & c).

In addition to the above mentioned procedure where the mobile particles are clustered solely based on distances, we have also studied CRRs following the procedure described in ref. Donati *et al.* (1998). Here, the direction of displacement of a mobile particle is also taken into consideration. Within this protocol, two mobile particles i and j are said to be part of the same string if $\min[|\vec{r}_i(t^*) - \vec{r}_j(0)|, |\vec{r}_i(0) - \vec{r}_j(t^*)|] < \delta$, where $\delta = 1.0\sigma$. Physically, two particles belong to the same string if a particle i makes a hop and its position is occupied by particle j, with a position uncertainty δ and in a time interval t^*. Thus, this procedure captures very clearly cooperative motion. Representative images of strings are shown in Fig. 5.11a. From the positions of the

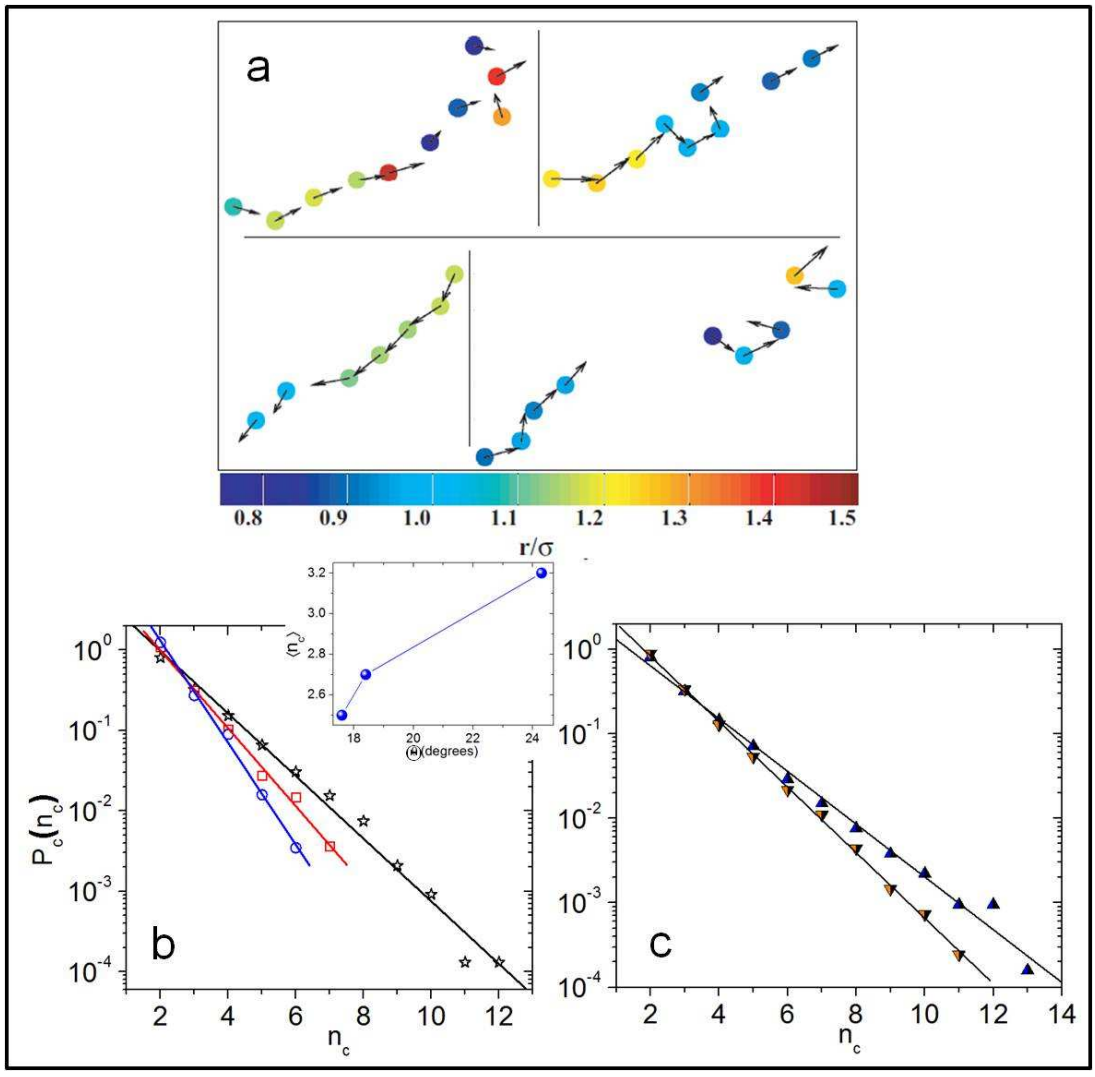

Figure 5.10: Cooperative Rearrangements - Morphology of clusters of most-mobile particles. (a) Snapshots of typical particle clusters observed for $\Theta = 24.3°$. Particles are drawn to 50% of their actual size. The length of the arrows and the particle color-code are based on the magnitude of their displacement. (b) $P_c(n_c)$ versus n_c for $\Theta = 24.3°$ (☆), $\Theta = 18.4°$ (□) and $\Theta = 17.6°$ (◯). Inset: $\langle n_c \rangle$ versus Θ at $T = 26°$C. (c) $P_c(n_c)$ versus n_c for $\Theta = 24.7°$ at $T = 25°$C (▼) and $T = 28°$C (▲). The straight lines in B and C are linear fits to the data.

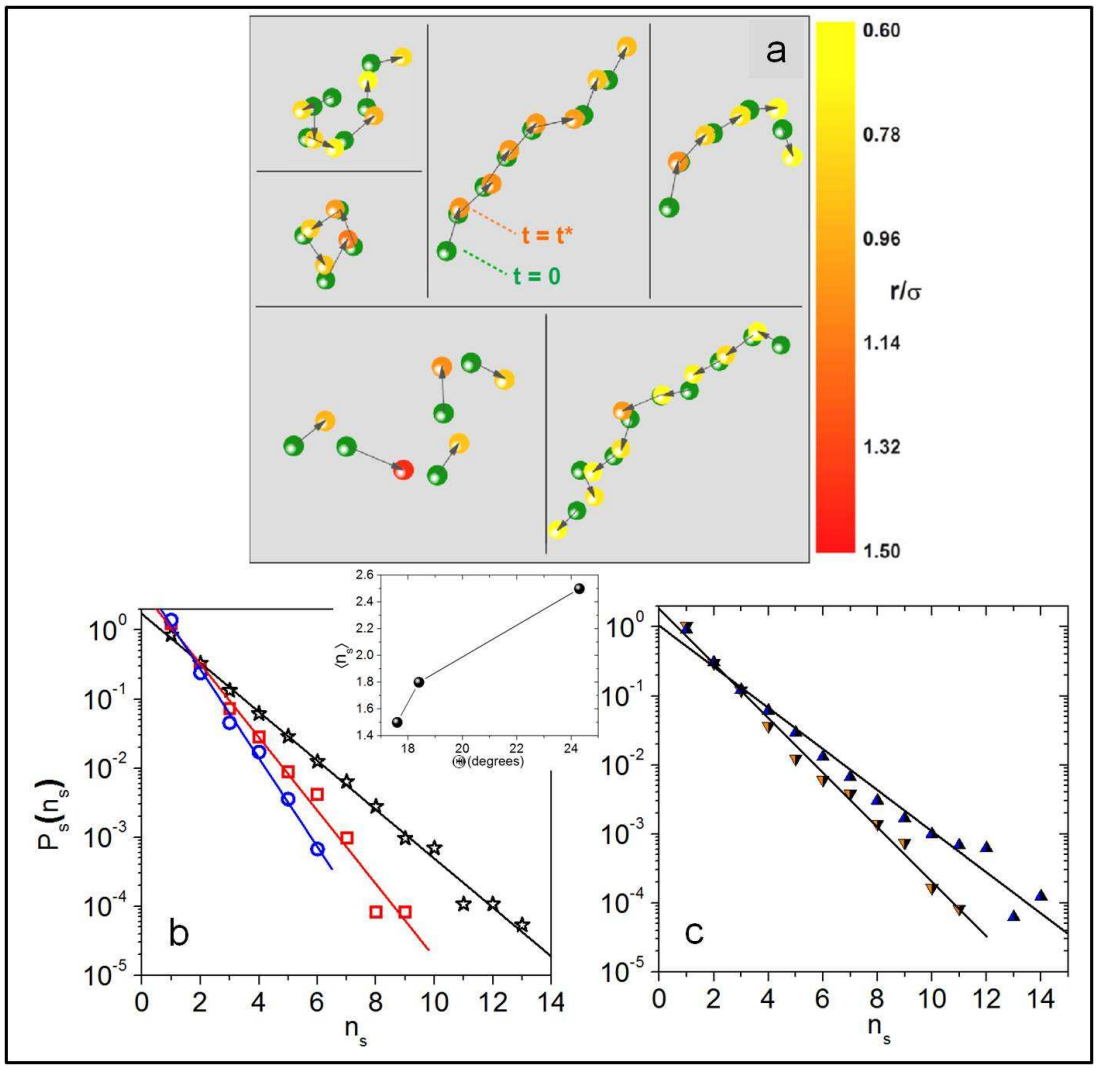

Figure 5.11: Cooperative Rearrangements - String like cooperative motion. (a) Snapshots of typical particle strings observed for $\Theta = 24.3°$. Particles are drawn to 50% of their actual size. Particle positions at $t = 0$ (shown by green circles) are linked to their positions at $t = t^*$ (shown by the color-coded circles) by arrows. The length of the arrows and the particle color-code are based on the magnitude of their displacement. Occasionally, we also see closed loops (middle image from left). (b) $P_s(n_s)$ versus n_s for $\Theta = 24.3°$ (☆), $\Theta = 18.4°$ (□) and $\Theta = 17.6°$ (◯). Inset: $\langle n_s \rangle$ versus Θ at $T = 26°$C. (c) $P_s(n_s)$ versus n_s for $\Theta = 24.7°$ at $T = 25°$C (▼) and $T = 28°$C (▲). The straight lines in B and C are linear fits to the data.

most-mobile particles at t (green spheres) and t^* (colored spheres) (Fig. 5.11a), it is evident that these particles indeed undergo rearrangements in a string-like manner. Similar to cluster sizes, we have plotted the distribution of string lengths $P_s(n_s)$ versus n_s, where n_s is the number of particles belonging to a string. Analogous to $P_c(n_c)$, we find that $P_s(n_s)$ also falls exponentially for all the Θs and Ts investigated. Such a dependence of cluster sizes and string lengths is in accordance with what has been observed for glass forming liquids (Keys *et al.* 2007).

More interestingly, we find that the maximum cluster size (string length), n_c^{max} (n_s^{max}), as well as average cluster size (string length), $\langle n_c \rangle (\langle n_s \rangle)$ increase with Θ (Inset Fig. 5.10b and Fig. 5.11b). Here, $\langle n \rangle = \frac{\sum n^2 P(n)}{\sum n P(n)}$. Further, we have performed the string analysis for different values of $\delta = 0.6\sigma$ & 1.4σ and we find that the trends in n_s^{max} and $\langle n_s \rangle$ do not dependent on the choice of δ. Moreover, similar trends of increasing $\langle n_c \rangle$ and $\langle n_s \rangle$ are also observed with decreasing temperature.

According to Adam-Gibbs hypothesis (Adam & Gibbs 1965) the size of CRRs increases with supercooling and hence one would expect the string length and the cluster size to decrease with Θ in our experiments. On the contrary, we observe an increase in the cluster size and string length with slowing down of dynamics i.e, with decreasing Θ. However, Adam-Gibbs hypothesis is not applicable here because geometric confinement is known to alter the very nature of the glass transition. Theory (Adam & Gibbs 1965) and simulations (Riggleman *et al.* 2006) on polymeric glass-forming fluids have shown that fragility decreases with confinement. Fragility is the parameter which characterizes the deviation from Arrhenius like/strong glass behavior of the structural relaxation time (Angell 1988). A decrease in fragility with confinement has also been experimentally seen in intercalated polymer films (Anastasiadis *et al.* 2000). Further, the decrease in the fragility is accompanied by a decrease in the size of the CRRs, as seen in experiments on bulk polymeric glass formers (Saiter *et al.* 2006) and simulations on confined polymeric glasses (Riggleman *et al.* 2006). In the light of these studies, the increase in n_c^{max} (n_s^{max}), and $\langle n_c \rangle$ ($\langle n_s \rangle$) with Θ, observed in our experiments, can be ascribed to the increase in the fragility of the glassy GB region. Experiments carried out at different temperatures are also in complete agreement with the confinement scenario. Our results illustrate that the behavior of HAGBs is strikingly similar to that of confined supercooled liquids and point to the crucial role played by misorientation angle-dependent fragility in the dynamics of GBs.

Viscoelastic Properties of HAGBs

An added advantage of our experiments is that the local viscoelastic properties of HAGBs can be quantified from the MSDs of the GB colloids. The dynamics of particles in viscoelastic media are sensitive to their local environment and the one-point microrheology technique (Mason & Weitz 1995) utilizes this fact to extract the frequency (ω) dependence of the storage (G') and loss moduli (G'').

We estimated $G'(\omega)$ and $G''(\omega)$ for a crystalline region far from the GB from the MSD shown in Fig.5 (brown diamonds). We have also performed bulk rheology measurements to compare the local moduli to bulk moduli. Bulk Rheology measurements were performed using an Anton Paar MCR 301 series stress-controlled rheometer. We used a parallel plate geometry with top and bottom plates made of glass. In-order to maintain identical conditions to that of microscopy experiments, we set the gap between the plates to 23μm and also performed a

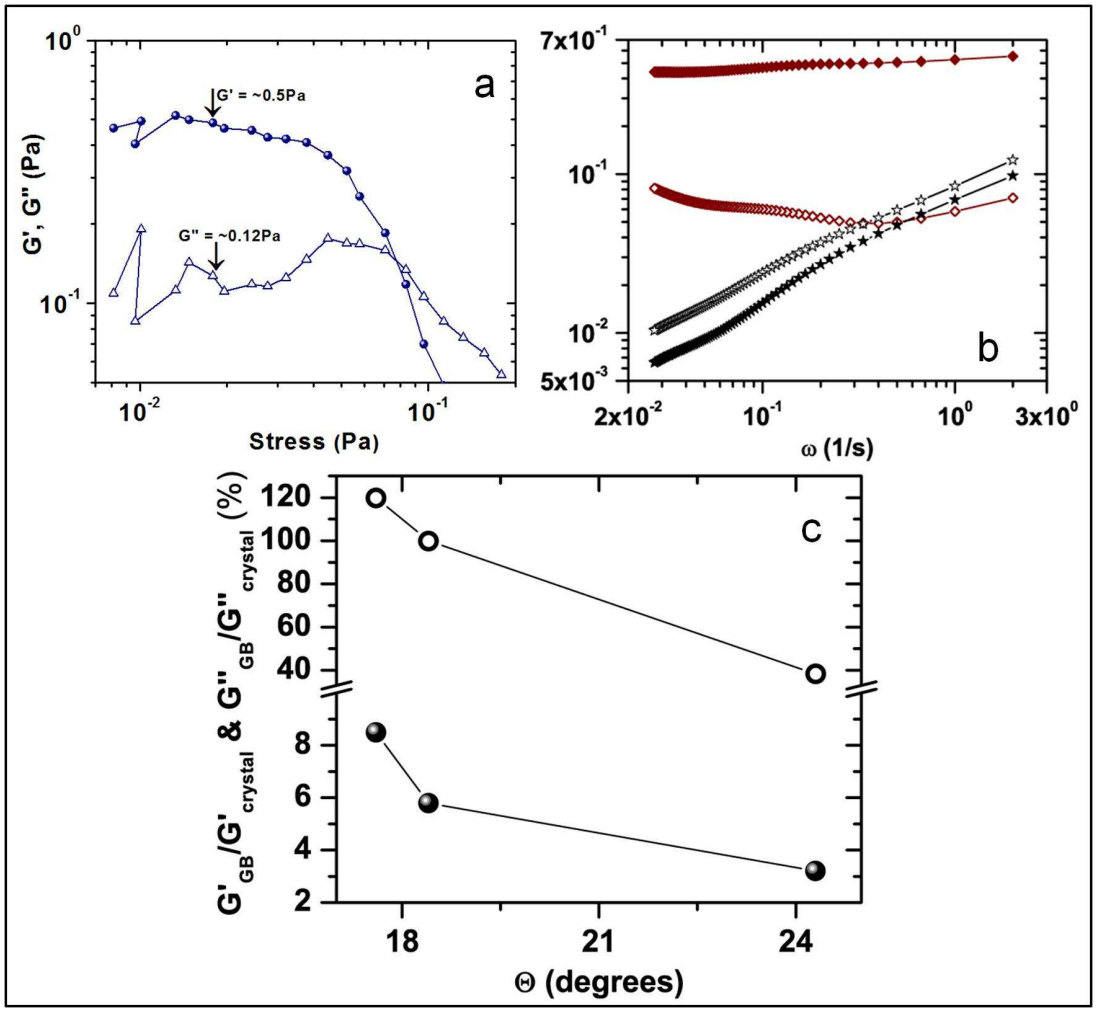

Figure 5.12: Viscoelastic Properties of Grain Boundaries. (a) Bulk storage modulus, G', (●) and loss modulus, G'', (△) of the polycrystal as a function of applied stress at an ω of 1 rad/s. (b) Local viscoelastic moduli for crystal G' (♦), G'' (◇) and for a HAGB ($\Theta = 24.3°$) G' (★), G'' (☆). (c) $\frac{G'_{GB}}{G'_{crystal}}$ (●) and $\frac{G''_{GB}}{G''_{crystal}}$ (○) as a function of Θ.

quench from 38 °C to 26 °C over two hours. To measure bulk viscoelastic properties, we have performed an amplitude sweep measurement by applying an oscillatory stress at a constant angular frequency of $\omega = 1$ rad/s. Fig. 5.12a shows G' and G'' for stresses varying from 0.003 Pa to 0.2 Pa. The linear response region extends up to a stress of about ~ 0.04 Pa above which the sample undergoes plastic deformation. In the linear response regime, $G' =\sim 0.5$ Pa and $G'' =\sim 0.12$ Pa. For the same ω, G' and G'' values obtained from microrheology measurements are 0.51 Pa and 0.06 Pa respectively (Fig. 5.12b, Brown diamonds). Remarkably, the moduli values estimated from micro rheology of the crystalline region are in good agreement with bulk rheology measurements. For HAGBs, $G'(\omega)$ and $G''(\omega)$ calculated from MSDs shown in (Fig. 5), show power law behaviour over a wide range of ω (Fig. 5.12b) (Sollich *et al.* 1997) as expected for systems exhibiting supercooled liquid dynamics. Fig. 5.12c shows the ratio of GB and crystal moduli with Θ for $\omega = 1$ rad/s. We find that both G' and G'' of GBs increase with decreasing Θ. From these measurements, it is evident that the spatial extent of confinement of the GB region has significant impact on the local mechanical response of HAGBs, which in turn should influence the bulk mechanical response of polycrystals.

5.4 Conclusions

Our model colloidal system has allowed us to investigate directly and with unprecedented detail the dynamics of GB in a 3-D colloidal polycrystal. We have shown conclusively that GBs display features that are hallmarks of glass forming liquids such as sub-diffusive MSD, non-Gaussian displacements and string-like cooperative rearrangements. Our experiments highlight the pivotal role of misorientation angle-dependent GB confinement in determining the dynamical properties of HAGBs. Notably, thermally induced changes in confinement by only a fraction of the particle diameter can also alter the behavior of HAGBs. Although a consensus on the behavior of confined glasses is yet to emerge, our experiments illustrate that the HAGBs, with a misorientation angle-dependent fragility, is a prototypical system where the rich physics of confined glasses can be directly applied. It is also tempting to speculate that the aging behavior ubiquitous in glassy systems may be relevant in the context of GBs. Our experiments offer a unique perspective on the current understanding of HAGBs and reiterate that colloids are an ideal test bed for addressing fundamental and technological problems such as GB diffusion mechanisms, GB migration under shear and grain growth.

Chapter 6

Outlook

The physical insights offered by systems as simple as micron size beads dispersed in water is invaluable. Here, by using spherical colloidal particles in combination with novel instrumentation techniques developed in-house, we have provided first experimental studies which help distinguishing between the two competing theories of the glass transition (Nagamanasa *et al.* 2014*a*). We have also demonstrated that yielding, a ubiquitous phenomenon of solids, is associated with an underlying non-equilibrium phase transition (Nagamanasa *et al.* 2014*b*). Further, we investigated dynamics of particles at grain boundaries which dictate mechanical properties of crystalline materials and showed that they share striking similarities with supercooled liquids (Nagamanasa *et al.* 2011).

Our studies on 2D binary colloidal glass forming liquids have provided an experimental verification for two key predictions of Random First Order Transition (RFOT) theory, a prominent thermodynamic theory of glass transition. We find evidence for a growing amorphous order on approaching the glass transition and change in the relaxation mechanisms across the mode coupling cross over area fraction (ϕ_{MCT}). Further, we show that the fuzzy-sphere model suggested by RFOT can well describe the morphology and internal structure of the cooperatively rearranging regions (CRRs). More importantly, our studies confirm that the non-monotonicity observed in dynamic correlations in the vicinity of ϕ_{MCT} in the presence of a wall is indeed due to the change in morphology of CRRs across ϕ_{MCT}. Furthermore, the peak in the maximum of the mobility transfer function M_{max} clearly indicates that activated events dominate relaxation close to the glass transition. Remarkably, all these results are consistent with the predictions of RFOT. Our experiments therefore suggest that the glass transition is thermodynamic in nature. In contrast to our findings, there exist recent experimental studies which show that dynamic facilitation (DF), a purely kinetic theory of the glass transition, is an important mechanism for the relaxation of supercooled liquids (Gokhale *et al.* 2014). By extending the methods developed for spherical particles to ellipsoidal particles, it has been shown that DF can predict the re-entrant transition for ellipsoidal systems with attractive interactions (Mishra *et al.* 2014). Such a re-entrant transition was also shown in colloidal experiments using MCT scaling (Mishra *et al.* 2013). Intriguingly, these studies suggest that DF is also an important mechanism for structural relaxation. However, it is to be noted that in both the aforementioned studies, all ϕs investigated are below ϕ_{MCT}. Taking this and the fact that we observe a peak in M_{max} around ϕ_{MCT} into consideration, it is tempting to speculate that DF governs relaxation processes for $\phi < \phi_{MCT}$ and activated hops, primary relaxation events within RFOT, for $\phi > \phi_{MCT}$. Nevertheless, proving that this is indeed the scenario necessitates more experiments and simulations. A promising approach towards this is to investigate facilitated dynamics in the presence of a wall. Furthermore, it would be fascinating to study the spatial organization of excitations - microscopic events responsible for facilitated dynamics - in the framework of core-shell mor-

phology developed for CRRs. Typically, colloid experiments are limited by the accuracy with which ϕ can be controlled. Thus, it is formidable to study wide range of supercoolings and their multiple realizations in colloid experiments. Nevertheless, simulations are not hindered by these factors, thus, a systematic study of facilitation and cluster morphology in simulations is crucial to establish the nature of the glass transition. We believe that such a comparative study which probes both the theories of the glass transition may help distinguishing between them. On the other hand, it is also necessary to reconcile our results within other thermodynamic frameworks of the glass transition.

By investigating bulk rheological response and single-particle dynamics under shear simultaneously in a prototypical soft system - colloidal glass, we provide direct connections between macroscopic and microscopic irreversibility. The trends in the relaxation time and the steady state fraction of irreversible particles with strain γ clearly show that yielding is associated with an underlying phase transition. We also find that the diverging relaxation time is accompanied by a growing length scale. Moreover, the relaxation time and the order parameter exponents suggest that yielding is an absorbing phase transition which belongs to conserved directed percolation universality class. However, to check the universality of this transition, it is necessary to probe these characteristic features in other soft systems as well. On the other hand, there exists an alternative approach according to which yielding could be transition to chaos (Regev *et al.* 2013). It would be interesting to check for the signatures of a chaotic transition in experiments on sheared colloidal glasses as well. Towards this end, by using individual particle trajectories, it is possible to compute Lyapunov exponent λ_L which is a characteristic measure of chaos. If yielding is indeed associated with a chaotic transition then across the threshold strain, λ_L will change from negative to positive. Also, recently Berthier and co-workers devised measures which can establish whether yielding is a non-equilibrium critical phenomenon or transition to chaos (Tjhung & Berthier 2015). Since these quantities are based on particle-dynamics, it would be interesting to compute them experimentally in 3D sheared colloidal glasses. Furthermore, they show that irreversibility transition shares qualitative analogies with the glass transition. Thus, it would also be fascinating to study observables developed for investigating the glass transition such as CRRs in the context of sheared amorphous solids.

Our studies on grain boundary (GB) dynamics demonstrate how concepts developed for glass forming liquids can be used for understanding other states of matter. We show that GBs share similarities with confined supercooled liquids and the degree of supercooling is governed by the confinement induced by the adjacent grains. The trends in the string length with misorientation angle observed here are due to confinement dependent fragility of grain boundaries. Our experiments also demonstrate that thermo-responsive colloidal crystals are ideal test beds to investigate fundamental phenomena like GB diffusion and impurity strengthening in polycrystalline materials. One of the easiest ways to introduce impurities is to add particles of sizes different from those which form the crystal (de Villeneuve *et al.* 2009). It would be interesting to study the effect of impurities on GB dynamics. Also, it is known that impurities segregate to GBs and pin them, thereby effecting their mobility and in-turn the strength of the crystal (Lejcek 2010). We feel that a holistic understanding of pinning and depinning can be achieved by coupling confocal microscope with tweezers and rheometer. This combination of instruments

will allow us to quantify local forces acting on an impurity while the grain boundary is driven against it. Thus such studies will greatly provide insights into the microscopic underpinnings of impurity pinning and depinning which may help engineer materials with enhanced functionalities.

References

Adam, G. & Gibbs, J. H. 1965 On the temperature dependence of cooperative relaxation properties in glass–forming liquids. *J. Chem. Phys.* **43** (1), 139.

Ahmadi, T. S., Wang, Z. L., Green, T. C., Henglein, A. & El-Sayed, M. A. 1996 Shape-controlled synthesis of colloidal platinum nanoparticles. *Science* p. 1924.

Alava, M. J., Laurson, L. & Zapperi, S. 2014 Crackling noise in plasticity. *Eur. Phys. J. Special Topics* **223** (11), 2353.

Alcoutlabi, M. & McKenna, G. B. 2005 Effects of confinement on material behaviour at the nanometre size scale. *J. Phys.: Condens. Matter* **17** (15), R461.

Alder, B. J. & Wainwright, T. E. 1957 Phase transition for a hard sphere system. *J. Chem. Phys.* **27** (5), 1208.

Alder, B. J. & Wainwright, T. E. 1960 Studies in molecular dynamics. ii. behavior of a small number of elastic spheres. *J. Chem. Phys.* **33** (5), 1439.

Alsayed, A. M. 2006 Melting in temperature sensitive suspensions .

Alsayed, A. M., Islam, M. F., Zhang, J., Collings, P. J. & Yodh, A. G. 2005 Premelting at defects within bulk colloidal crystals. *Science* **309** (5738), 1207.

Anastasiadis, S. H., Karatasos, K., Vlachos, G., Manias, E. & Giannelis, E. P. 2000 Nanoscopic-confinement effects on local dynamics. *Phys. Rev. Lett.* **84** (5), 915.

Andersen, H. C. 2005 Molecular dynamics studies of heterogeneous dynamics and dynamic crossover in supercooled atomic liquids. *Proc. Nat. Acad. Sci., USA* **102** (19), 6686.

Andersen, H. C., Chandler, D. & Weeks, J. D. 1976 Roles of repulsive and attractive forces in liquids: the equilibrium theory of classical fluids. *Adv. Chem. Phys* **34**, 105.

Angell, C. A. 1988 Perspective on the glass transition. *J. Phys. Chem. Solids* **49** (8), 863.

Angell, C. A. 1995 Formation of glasses from liquids and biopolymers. *Science* **267** (5206), 1924.

Angell, C. A., Ngai, K. L., McKenna, G. B., McMillan, P. F. & Martin, S. W. 2000 Relaxation in glassforming liquids and amorphous solids. *J. App. Phys.* **88** (6), 3113.

Antonaglia, J., Wright, J. W., Gu, X., Byer, R. R., Hufnagel, T. C., LeBlanc, M., Uhl, J. T. & Dahmen, K. A. 2014 Bulk metallic glasses deform via slip avalanches. *Phys. Rev. Lett.* **112** (15), 155501.

Argon, A. S. 1979 Plastic deformation in metallic glasses. *Acta Metall.* **27** (1), 47.

Argon, A. S. 1982 Mechanisms of inelastic deformation in metallic glasses. *J. Phys. Chem. Solids* **43** (10), 945–961.

Argon, A. S. & Kuo, H. Y. 1980 Free energy spectra for inelastic deformation of five metallic glass alloys. *J. Non-Cryst. Solids* **37** (2), 241.

Ashby, M. F. 1972 Boundary defects, and atomistic aspects of boundary sliding and diffusional creep. *Surf. Sci.* **31**, 498.

Ashkin, A. 1970 Acceleration and trapping of particles by radiation pressure. *Phys. Rev. Lett.* **24** (4), 156.

Ashkin, A. 1992 Forces of a single-beam gradient laser trap on a dielectric sphere in the ray optics regime. *Biophys. J.* **61** (2), 569.

Ashkin, A., Dziedzic, J. M., Bjorkholm, J. E. & Chu, S. 1986 Observation of a single-beam gradient force optical trap for dielectric particles. *Opt. Lett.* **11** (5), 288.

Ashkin, A., Dziedzic, J. M. & Yamane, T. 1987 Optical trapping and manipulation of single cells using infrared laser beams. *Nature* **330** (6150), 769.

Bailey, N. P., Schiøtz, J., Lemaître, A. & Jacobsen, K. W. 2007 Avalanche size scaling in sheared three-dimensional amorphous solid. *Phys. Rev. Lett.* **98** (9), 095501.

Barnes, H. A. 1999 The yield stress- a review-everything flows. *J. Non-Newtonian Fluid Mech.* **81** (1), 133.

Bässler, H. 1987 Viscous flow in supercooled liquids analyzed in terms of transport theory for random media with energetic disorder. *Phys. Rev. Lett.* **58** (8), 767.

Bates, F. S. & Fredrickson, G. H. 2008 Block copolymers-designer soft materials. *Physics Today* **52** (2), 32.

Bengtzelius, U., Gotze, W. & Sjolander, A. 1984 Dynamics of supercooled liquids and the glass transition. *J. Phys. C: Solid State Physics* **17** (33), 5915.

Berardi, C. R., Barros, K., Douglas, J. F. & Losert, W. 2010 Direct observation of stringlike collective motion in a two-dimensional driven granular fluid. *Phys. Rev. E* **81** (4), 041301.

Bernal, J. D. 1964 The bakerian lecture, 1962. the structure of liquids. *Proceedings of the Royal Society of London, Series A* p. 299.

Bernal, J. D. & Mason, J. 1960 Packing of spheres: Coordination of randomly packed spheres. *Nature* (188), 910.

Berndt, I. & Richtering, W. 2003 Doubly temperature sensitive core-shell microgels. *Macromolecules* **36** (23), 8780.

Berthier, L. & Biroli, G. 2011 Theoretical perspective on the glass transition and amorphous materials. *Rev. Mod. Phys.* **83** (2), 587.

Berthier, L., Biroli, G., Bouchaud, J.-P., Cipelletti, L., Masri, D. E., L'Hôte, D., Ladieu, F. & Pierno, M. 2005 Direct experimental evidence of a growing length scale accompanying the glass transition. *Science* **310** (5755), 1797.

Berthier, L., Biroli, G., Bouchaud, J. P., Cipelletti, L. & van Saarloos, W. 2011 *Dynamical heterogeneities in glasses, colloids, and granular media*. Oxford University Press.

Berthier, L. & Garrahan, J. P. 2003 Real space origin of temperature crossovers in supercooled liquids. *Phys. Rev. E* **68** (4), 041201.

Berthier, L. & Kob, W. 2012 Static point-to-set correlations in glass-forming liquids. *Phys. Rev. E* **85** (1), 011102.

Bhattacharyya, S. M., Bagchi, B. & Wolynes, P. G. 2008 Facilitation, complexity growth, mode coupling, and activated dynamics in supercooled liquids. *Proc. Nat. Acad. Sci., USA* **105** (42), 16077.

Binder, K. & Young, A. P. 1986 Spin glasses: Experimental facts, theoretical concepts, and open questions. *Rev. Mod. Phys.* **58** (4), 801.

Biroli, G. & Bouchaud, J.-P. 2012 The random first-order transition theory of glasses: a critical assessment. *Structural Glasses and Supercooled Liquids: Theory, Experiment, and Applications* p. 31.

Biroli, G., Bouchaud, J.-P., Cavagna, A., Grigera, T. S. & Verrocchio, P. 2008 Thermodynamic signature of growing amorphous order in glass-forming liquids. *Nat. Phys.* **4** (10), 771.

Biroli, G. & Garrahan, J. P. 2013 Perspective: The glass transition. *J. Chem. Phys.* **138**, 12A301.

van Blaaderen, A., Hoogenboom, J. P., Vossen, D. L. J., Yethiraj, A., van der Horst, A., Visscher, K. & Dogterom, M. 2003 Colloidal epitaxy: Playing with the boundary conditions of colloidal crystallization. *Faraday Discussions* **123**, 107.

van Blaaderen, A. & Wiltzius, P. 1995 Real-space structure of colloidal hard-sphere glasses. *Science* p. 1177.

Boitte, J.-B., Vizcaïno, C., Benyahia, L., Herry, J.-M., Michon, C. & Hayert, M. 2013 A novel rheo-optical device for studying complex fluids in a double shear plate geometry. *Rev. Sci. Instrum.* **84** (1), 013709.

Bouchaud, J. P. 1990 Anomalous diffusion in disordered media: statistical mechanisms, models and physical applications. *Phys. Rep.* **195** (4), 127.

Bouchaud, J. P. & Biroli, G. 2004 On the adam-gibbs-kirkpatrick-thirumalai-wolynes scenario for the viscosity increase in glasses. *J. Chem. Phys.* **121** (15), 7347.

Brinckmann, S., Kim, J.-Y. & Greer, J. R. 2008 Fundamental differences in mechanical behavior between two types of crystals at the nanoscale. *Phys. Rev. Lett.* **100** (15), 155502.

Brokman, A. & Balluffi, R. W. 1981 Coincidence lattice model for the structure and energy of grain boundaries. *Acta Metallurgica* **29** (10), 1703.

Brower-Toland, B. D., Smith, C. L., Yeh, R. C., Lis, J. T., Peterson, C. L. & Wang, M. D. 2002 Mechanical disruption of individual nucleosomes reveals a reversible multistage release of dna. *Proc. Nat. Acad. Sci., USA* **99** (4), 1960.

Bryngelson, J. D. & Wolynes, P. G. 1987 Spin glasses and the statistical mechanics of protein folding. *Proc. Nat. Acad. Sci., USA* **84** (21), 7524.

Budrikis, Z. & Zapperi, S. 2013 Avalanche localization and crossover scaling in amorphous plasticity. *Phys. Rev. E* **88** (6), 062403.

Bulatov, V. V. & Argon, A. S. 1994*a* Stochastic continuum simulations of structural relaxations in solids. *J. Non-Cryst. Solids* **172**, 876.

Bulatov, V. V. & Argon, A. S. 1994*b* A stochastic model for continuum elasto-plastic behavior. i. numerical approach and strain localization. *Modell. Simul. Mater. Sci. Eng.* **2** (2), 167.

Bulatov, V. V. & Argon, A. S. 1994*c* A stochastic model for continuum elasto-plastic behavior. ii. a study of the glass transition and structural relaxation. *Modell. Simul. Mater. Sci. Eng.* **2** (2), 185.

Bulatov, V. V. & Argon, A. S. 1994*d* A stochastic model for continuum elasto-plastic behavior. iii. plasticity in ordered versus disordered solids. *Modell. Simul. Mater. Sci. Eng.* **2** (2), 203.

Callister, W. D. & Rethwisch, D. G. 2007 *Materials science and engineering: an introduction*, , vol. 7. Wiley New York.

Cammarota, C. & Biroli, G. 2012*a* Ideal glass transitions by random pinning. *Proc. Nat. Acad. Sci., USA* **109** (23), 8850.

Cammarota, C. & Biroli, G. 2012*b* Patch-repetition correlation length in glassy systems. *Euro. Phys. Lett.* **98** (3), 36005.

Carrier, V. & Petekidis, G. 2009 Nonlinear rheology of colloidal glasses of soft thermosensitive microgel particles. *J. Rheol.* **53** (2), 245.

Cavagna, A. 2009 Supercooled liquids for pedestrians. *Physics Reports* **476** (4), 51.

Cayre, O., Paunov, V. N. & Velev, O. D. 2003 Fabrication of asymmetrically coated colloid particles by microcontact printing techniques. *J. Mater. Chem.* **13** (10), 2445.

Chandler, D. & Garrahan, J. P. 2010 Dynamics on the way to forming glass: Bubbles in space-time. *Ann. Rev. Phys. Chem.* **61**, 191.

Chandler, D., Garrahan, J. P., Jack, R. L., Maibaum, L. & Pan, A. C. 2006 Length-scale dependence of dynamic four-point susceptibilities in glass formers. *Phys. Rev. E* **74** (5), 051501.

Charbonneau, P. & Tarjus, G. 2013 Decorrelation of the static and dynamic length scales in hard-sphere glass formers. *Phys. Rev. E* **87** (4), 042305.

Chen, Q., Bae, S. C. & Granick, S. 2011 Directed self-assembly of a colloidal kagome lattice. *Nature* **469** (7330), 381.

Cheng, X., McCoy, J. H., Israelachvili, J. N. & Cohen, I. 2011 Imaging the microscopic structure of shear thinning and thickening colloidal suspensions. *Science* **333** (6047), 1276.

Chikkadi, V. & Schall, P. 2012 Nonaffine measures of particle displacements in sheared colloidal glasses. *Phys. Rev. E* **85** (3), 031402.

Chikkadi, V., Wegdam, G., Bonn, D., Nienhuis, B. & Schall, P. 2011 Long-range strain correlations in sheared colloidal glasses. *Phys. Rev. Lett.* **107** (19), 198303.

Chokshi, A. H., Rosen, A., Karch, J. & Gleiter, H. 1989 On the validity of the hall-petch relationship in nanocrystalline materials. *Scripta Metallurgica* **23** (10), 1679.

Corte, L., Chaikin, P. M., Gollub, J. P. & Pine, D. J. 2008 Random organization in periodically driven systems. *Nat. Phys.* **4** (5), 420.

Corté, L., Gerbode, S. J., Man, W. & Pine, D. J. 2009 Self-organized criticality in sheared suspensions. *Phys. Rev. Lett.* **103** (24), 248301.

Cosgrove, T. 2010 *Colloid science: principles, methods and applications*. John Wiley & Sons.

Cotterell, A. H. 1953 *Dislocation and plastic flow in crystals*. Clarendon Press.

Crocker, J. C. & Grier, D. J. 1996 Methods of digital video microscopy for colloidal studies. *J. Colloid Interface Sci.* **179** (1), 298.

Curtis, J. E., Koss, B. A. & Grier, D. G. 2002 Dynamic holographic optical tweezers. *Opt. Comm.* **207** (1), 169.

Dahmen, U., Hagege, S., Faudot, F., Radetic, T. & Johnson, E. 2004 Observations of interface premelting at grain-boundary precipitates of pb in al. *Philosophical Magazine* **84** (25), 2651.

Daisman, P. B. A., Hirata, A., Zhu, F., Pan, L., Reddy, K. M., Song, S., Liu, Y., Fujita, T., Shinji, K. & Chen, M. 2013 Ultrastrong and ultrastable metallic glass. *arXiv preprint arXiv:1306.1575* .

Das, S. P. 2004 Mode-coupling theory and the glass transition in supercooled liquids. *Rev. Mod. Phys.* **76** (3), 785.

Das, S. P. & Mazenko, G. F. 1986 Fluctuating nonlinear hydrodynamics and the liquid-glass transition. *Phys. Rev. A* **34** (3), 2265.

Dash, J. G. 1999 History of the search for continuous melting. *Rev. Mod. Phys.* **71** (5), 1737.

Dash, J. G., Fu, H. & Wettlaufer, J. S. 1995 The premelting of ice and its environmental consequences. *Reports on Progress in Physics* **58** (1), 115.

Dawson, K., Foffi, G., Fuchs, M., Götze, W., Sciortino, F., Sperl, M., Tartaglia, P., Voigtmann, T. & Zaccarelli, E. 2000 Higher-order glass-transition singularities in colloidal systems with attractive interactions. *Phys. Rev. E* **63** (1), 011401.

Debenedetti, P. G. & Stillinger, F. H. 2001 Supercooled liquids and the glass transition. *Nature* **410** (6825), 259.

Demkowicz, M. J. & Argon, A. S. 2005 Autocatalytic avalanches of unit inelastic shearing events are the mechanism of plastic deformation in amorphous silicon. *Phys. Rev. B* **72** (24), 245206.

Deng, C. & Schuh, C. A. 2011 Atomistic simulation of slow grain boundary motion. *Phys. Rev. Lett.* **106** (4), 045503.

Deshpande, A. P., Krishnan, J. M. & Kumar, S. 2010 *Rheology of complex fluids*. Springer Science & Business Media.

Dickman, R. 2002 Nonequilibrium phase transitions in epidemics and sandpiles. *Physica A* **306**, 90–97.

Dickman, R., Muñoz, M. A., A.Vespignani & Zapperi, S. 2000 Paths to self-organized criticality. *Braz. J. Phys.* **30** (1), 27–41.

Dimiduk, D. M., Uchic, M. D. & Parthasarathy, T. A. 2005 Size-affected single-slip behavior of pure nickel microcrystals. *Acta Mater.* **53** (15), 4065.

Dimiduk, D. M., Woodward, C., LeSar, R. & Uchic, M. D. 2006 Scale-free intermittent flow in crystal plasticity. *Science* **312** (5777), 1188.

Divoux, T., Tamarii, D., Barentin, C. & Manneville, S. 2010 Transient shear banding in a simple yield stress fluid. *Phys. Rev. Lett.* **104** (20), 208301.

Donati, C., Douglas, J. F., Kob, W., Plimpton, S. J., Poole, P. H. & Glotzer, S. C. 1998 Stringlike cooperative motion in a supercooled liquid. *Phys. Rev. Lett.* **80** (11), 2338.

Dufresne, E. R. & Grier, D. G. 1998 Optical tweezer arrays and optical substrates created with diffractive optics. *Rev. Sci. Instrum.* **69** (5), 1974.

Dunleavy, A. J., Wiesner, K. & Royall, C. P. 2012 Using mutual information to measure order in model glass formers. *Phys. Rev. E* **86** (4), 041505.

Duplantier, B., Halsey, T. C. & Rivasseau, V. 2011 *Glasses and Grains: Poincaré Seminar 2009*, , vol. 61. Springer Science & Business Media.

Dutta, S. K., Mbi, A., Arevalo, R. C. & Blair, D. L. 2013 Development of a confocal rheometer for soft and biological materials. *Rev. Sci. Instrum.* **84** (6), 063702.

Dyre, J. C., Hechsher, T. & Niss, K. 2009 A brief critique of the adam–gibbs entropy model. *J. Non-Cryst. Solids* **355** (10), 624.

Dziomkina, N. V. & Vancso, G. J. 2005 Colloidal crystal assembly on topologically patterned templates. *Soft Matter* **1** (4), 265.

Ediger, M. D. 2000 Spatially heterogeneous dynamics in supercooled liquids. *Ann. Rev. Phys. Chem.* **51** (1), 99.

Elmatad, Y. S., Chandler, D. & Garrahan, J. P. 2009 Corresponding states of structural glass formers. *J. Phys. Chem. B* **113** (16), 5563.

Elmatad, Y. S. & Keys, A. S. 2012 Manifestations of dynamical facilitation in glassy materials. *Phys. Rev. E* **85** (6), 061502.

Eral, H. B., van den Ende, D., Mugele, F. & Duits, M. H. G. 2009 Influence of confinement by smooth and rough walls on particle dynamics in dense hard-sphere suspensions. *Phys. Rev. E* **80** (6), 061403.

Eriksen, R., Daria, V. & Gluckstad, J. 2002 Fully dynamic multiple-beam optical tweezers. *Opt. Exp.* **10** (14), 597.

Erwin, B. M., Cloitre, M., Gauthier, M. & Vlassopoulos, D. 2010 Dynamics and rheology of colloidal star polymers. *Soft Matter* **6** (12), 2825.

Eshelby, J. D. 1957 The determination of the elastic field of an ellipsoidal inclusion, and related problems. In *Proceedings of the Royal Society of London A*, , vol. 241, p. 376. The Royal Society.

Evans, M. R. 2002 Anomalous coarsening and glassy dynamics. *J. Phys.: Condens. Matter* **14** (7), 1397.

Eyring, H. 1936 Viscosity, plasticity, and diffusion as examples of absolute reaction rates. *J. Chem. Phys.* **4** (4), 283.

Falk, M. L. & Langer, J. S. 1998 Dynamics of viscoplastic deformation in amorphous solids. *Phys. Rev. E* **57** (6), 7192.

Falk, M. L. & Langer, J. S. 2011 Deformation and failure of amorphous, solidlike materials. *Annu. Rev. Condens. Matter Phys.* **2**, 353.

Fall, A., Paredes, J. & Bonn, D. 2010 Yielding and shear banding in soft glassy materials. *Phys. Rev. Lett.* **105** (22), 225502.

Fällman, E. & Axner, O. 1997 Design for fully steerable dual-trap optical tweezers. *App. Opt.* **36** (10), 2107.

Fan, Y., Yildiz, B. & Yip, S. 2013 Analogy between glass rheology and crystal plasticity: yielding at high strain rate. *Soft Matter* **9** (40), 9511.

Fazal, F. M. & Block, S. M. 2011 Optical tweezers study life under tension. *Nature Photonics* **5** (6), 318.

Fiocco, D., Foffi, G. & Sastry, S. 2013 Oscillatory athermal quasistatic deformation of a model glass. *Phys. Rev. E* **88**, 020301.

Flenner, E., Staley, H. & Szamel, G. 2014 Universal features of dynamic heterogeneity in supercooled liquids. *Physical review letters* **112** (9), 097801.

Flenner, E. & Szamel, G. 2012 Characterizing dynamic length scales in glass-forming liquids. *Nat. Phys.* **8** (10), 696.

Foiles, S. M. & Hoyt, J. J. 2006 Computation of grain boundary stiffness and mobility from boundary fluctuations. *Acta Materialia* **54** (12), 3351.

Fournier, J.-M. R., Burns, M. M. & Golovchenko, J. A. 1995 Writing diffractive structures by optical trapping. In *IS&T/SPIE's Symposium on Electronic Imaging: Science & Technology*, p. 101. International Society for Optics and Photonics.

Frank, F. C. 1950 *Report of the symposium on the plastic deformation of crystalline solids*.

Fredrickson, G. H. & Andersen, H. C. 1984 Kinetic ising model of the glass transition. *Phys. Rev. Lett.* **53** (13), 1244.

Fredrickson, G. H. & Andersen, H. C. 1985 Facilitated kinetic ising models and the glass transition. *J. Chem. Phys.* **83** (11), 5822.

Fris, J. A. R., Appignanesi, G. A. & Weeks, E. R. 2011 Experimental verification of rapid, sporadic particle motions by direct imaging of glassy colloidal systems. *Phys. Rev. Lett.* **107** (6), 065704.

Fulcher, G. 1925 Analysis of recent measurements of the viscosity of glasses. *J. Am. Ceram. Soc.* **8** (12), 789.

Fusco, D. & Charbonneau, P. 2013 Crystallization of asymmetric patchy models for globular proteins in solution. *Phys. Rev. E* **88** (1), 012721.

Ganapathy, R., Buckley, M. R., Gerbode, S. J. & Cohen, I. 2010 Direct measurements of island growth and step-edge barriers in colloidal epitaxy. *Science* **327** (5964), 445.

Ganapathy, R. & Sood, A. K. 2006 Intermittency route to rheochaos in wormlike micelles with flow-concentration coupling. *Phys. Rev. Lett.* **96** (10), 108301.

Gao, Y. & Kilfoil, M. L. 2009 Accurate detection and complete tracking of large populations of features in three dimensions. *Opt. Exp.* **17** (6), 4685.

Garrahan, J. P. & Chandler, D. 2002 Geometrical explanation and scaling of dynamical heterogeneities in glass forming systems. *Phys. Rev. Lett.* **89** (3), 035704.

Garrahan, J. P. & Chandler, D. 2003 Coarse-grained microscopic model of glass formers. *Proc. Nat. Acad. Sci., USA* **100** (17), 9710.

Genzer, J. & Groenewold, J. 2006 Soft matter with hard skin: From skin wrinkles to templating and material characterization. *Soft Matter* **2** (4), 310.

Gerbode, S. J., Ong, D. C., Liddell, C. M. & Cohen, I. 2010 Dislocations and vacancies in two-dimensional mixed crystals of spheres and dimers. *Phys. Rev. E* **82** (4), 041404.

Ghofraniha, N., Tamborini, E., Oberdisse, J., Cipelletti, L. & Ramos, L. 2012 Grain refinement and partitioning of impurities in the grain boundaries of a colloidal polycrystal. *Soft Matter* **8** (23), 6214.

Ghosh, A., Mari, R., Chikkadi, V., Schall, P., Kurchan, J. & Bonn, D. 2010 Density of states of colloidal glasses and supercooled liquids. *Soft Matter* **6** (13), 3082.

Gleiter, H. 1971 The structure and properties of high-angle grain boundaries in metals. *Physica Status Solidi* **45** (1), 9.

Glotzer, S. C. 2000 Spatially heterogeneous dynamics in liquids: insights from simulation. *J. Non-Cryst. Solids* **274** (1), 342.

Glotzer, S. C. & Solomon, M. J. 2007 Anisotropy of building blocks and their assembly into complex structures. *Nat. Mater.* **6** (8), 557.

Gokhale, S., Nagamanasa, K. H., Ganapathy, R., & Sood, A. K. 2013 Grain growth and grain boundary dynamics in colloidal polycrystals. *Soft Matter* **9** (29), 6634.

Gokhale, S., Nagamanasa, K. H., Ganapathy, R. & Sood, A. K. 2014 Growing dynamical facilitation on approaching the random pinning colloidal glass transition. *Nat. Comm.* **5**.

Gokhale, S., Nagamanasa, K. H., Santhosh, V., Sood, A. K. & Ganapathy, R. 2012 Directional grain growth from anisotropic kinetic roughening of grain boundaries in sheared colloidal crystals. *Proc. Nat. Acad. Sci., USA* **109** (50), 20314.

Golestanian, R. 2012 Collective behavior of thermally active colloids. *Phys. Rev. Lett.* **108** (3), 038303.

Gottstein, G., Molodov, D. A., Shvindlerman, L. S., Srolovitz, D. J. & Winning, M. 2001 Grain boundary migration: misorientation dependence. *Current Opinion in Solid State and Materials Science* **5** (1), 9.

Gottstein, G. & Shvindlerman, L. S. 2009 *Grain boundary migration in metals: thermodynamics, kinetics, applications*. CRC press.

Götze, W. 2008 *Complex dynamics of glass-forming liquids: A mode-coupling theory*, , vol. 143. Oxford University Press.

Götze, W. & Sjögren, L. 1987 The glass transition singularity. *Zeitschrift für Physik B Condens. Matter* **65** (4), 415.

Götze, W. & Sjogren, L. 1988 Scaling properties in supercooled liquids near the glass transition. *J. Phys. C: Solid State Physics* **21** (18), 3407.

Götze, W. & Sjogren, L. 1992 Relaxation processes in supercooled liquids. *Reports on Progress in Physics* **55** (3), 241.

Goux, C. 1974 Observation of grain boundaries. *Journal of Microscopy* **102** (3), 241.

Greyson, E. C., Barton, J. E. & Odom, T. W. 2006 Tetrahedral zinc blende tin sulfide nano-and microcrystals. *Small* **2** (3), 368.

Grier, D. G. 1997 Optical tweezers in colloid and interface science. *Current Opinion in Colloid & Interface Science* **2** (3), 264.

Grier, D. G. 2003 A revolution in optical manipulation. *Nature* **424** (6950), 810.

Hansen, N. 2004 Hall–petch relation and boundary strengthening. *Scripta Materialia* **51** (8), 801.

Hansen, P. M., Bhatia, V. K., Harrit, N. & Oddershede, L. 2005 Expanding the optical trapping range of gold nanoparticles. *Nano lett.* **5** (10), 1937.

Harada, Y. & Asakura, T. 1996 Radiation forces on a dielectric sphere in the rayleigh scattering regime. *Opt. Comm.* **124** (5), 529.

Hébraud, P., Lequeux, F., Munch, J. P. & Pine, D. J. 1997 Yielding and rearrangements in disordered emulsions. *Phys. Rev. Lett.* **78** (24), 4657.

Hellweg, T., Dewhurst, C. D., Eimer, W. & Kratz, K. 2004 Pnipam-co-polystyrene core-shell microgels: structure, swelling behavior, and crystallization. *Langmuir* **20** (11), 4330.

Herman, H. 1972 *Treatise on Materials Science and Technology. Treatise Mat. Sci. and Tech.* v. 8. Academic Press.

Hernández-Guzmán, J. & Weeks, E. R. 2009 The equilibrium intrinsic crystal–liquid interface of colloids. *Proc. Nat. Acad. Sci., USA* **106** (36), 15198.

Hilgenkamp, H. & Mannhart, J. 2002 Grain boundaries in high-tc superconductors. *Rev. Mod. Phys.* **74** (2), 485.

Hinrichsen, H. 2000 Non-equilibrium critical phenomena and phase transitions into absorbing states. *Adv. Phys.* **49** (7), 815.

Hocky, G. M., Berthier, L., Kob, W. & Reichman, D. R. 2014 Crossovers in the dynamics of supercooled liquids probed by an amorphous wall. *Phys. Rev. E* **89** (5), 052311.

Hocky, G. M., Markland, T. E. & Reichman, D. R. 2012 Growing point-to-set length scale correlates with growing relaxation times in model supercooled liquids. *Phys. Rev. Lett.* **108** (22), 225506.

Hong, L., Cacciuto, A., Luijten, E. & Granick, S. 2006 Clusters of charged janus spheres. *Nano letters* **6** (11), 2510.

Hong, L., Cacciuto, A., Luijten, E. & Granick, S. 2008 Clusters of amphiphilic colloidal spheres. *Langmuir* **24** (3), 621.

Howe, J. M. 1997 *Interfaces in materials: atomic structure, thermodynamics and kinetics of solid-vapor, solid-liquid and solid-solid interfaces*. Wiley-Interscience.

Hu, Z., Lu, X., Gao, J. & Wang, C. 2000 Polymer gel nanoparticle networks. *Adv. Mat.* **12** (16), 1173.

Hull, D. & Bacon, D. J. 1984 *Introduction to dislocations*, , vol. 257. Pergamon Press Oxford.

Hunter, G. L. & Weeks, E. R. 2012 The physics of the colloidal glass transition. *Reports on Progress in Physics* . **75** (6), 066501.

Huo, F., Lytton-Jean, A. K. R. & Mirkin, C. A. 2006 Asymmetric functionalization of nanoparticles based on thermally addressable dna interconnects. *Advanced Materials* **18** (17), 2304.

Irvine, W. T. M., Hollingsworth, A., Grier, D. G. & Chaikin, P. M. 2013 Dislocation reactions, grain boundaries, and irreversibility in two-dimensional lattices using topological tweezers. *Proc. Nat. Acad. Sci., USA* **110** (39), 15544.

Ispánovity, P. D., Laurson, L., Zaiser, M., Groma, I., Zapperi, S. & Alava, M. J. 2014 Avalanches in 2d dislocation systems: Plastic yielding is not depinning. *Phys. Rev. Lett.* **112** (23), 235501.

Israelachvili, J. N. 2010 *Intermolecular and Surface Forces*. Elsevier Science.

Jack, R. L. & Berthier, L. 2012 Random pinning in glassy spin models with plaquette interactions. *Phys. Rev. E* **85** (2), 021120.

Jack, R. L. & Garrahan, J. P. 2005 Caging and mosaic length scales in plaquette spin models of glasses. *J. Chem. Phys.* **123** (16), 164508.

Jäckle, J. & Eisinger, S. 1991 A hierarchically constrained kinetic ising model. *Zeitschrift für Physik B Condens. Matter* **84** (1), 115.

Jaishankar, A. & McKinley, G. H. 2013 Power-law rheology in the bulk and at the interface: quasi-properties and fractional constitutive equations. *Proceedings of the Royal Society A: Mathematical, Physical and Engineering Science* **469** (2149), 20120284.

Jensen, I. 1993 Critical behavior of the pair contact process. *Phys. Rev. Lett.* **70** (10), 1465.

Johnson, P. M., van Kats, C. M. & van Blaaderen, A. 2005 Synthesis of colloidal silica dumbbells. *Langmuir* **21** (24), 11510.

Jones, R. A. L. 2002 *Soft Condensed Matter*. OUP Oxford.

Karmakar, S., Lerner, E. & Procaccia, I. 2012 Direct estimate of the static length-scale accompanying the glass transition. *Physica A* **391** (4), 1001.

van Kats, C. M., Johnson, P. M., van den Meerakker, J. E. & van Blaaderen, A. 2004 Synthesis of monodisperse high-aspect-ratio colloidal silicon and silica rods. *Langmuir* **20** (25), 11201.

Kauzmann, W. 1948 The nature of the glassy state and the behavior of liquids at low temperatures. *Chem. Rev.* **43** (2), 219.

Kaya, D., Green, N. L., Maloney, C. E. & Islam, M. F. 2010 Normal modes and density of states of disordered colloidal solids. *Science* **329** (5992), 656.

Keblinski, P., Phillpot, S. R., Wolf, D. & Gleiter, H. 1996 Thermodynamic criterion for the stability of amorphous intergranular films in covalent materials. *Phys. Rev. Lett.* **77** (14), 2965.

Keim, N. C. & Arratia, P. E. 2013 Yielding and microstructure in a 2d jammed material under shear deformation. *Soft Matter* **9** (27), 6222.

Kelton, K. & Greer, A. L. 2010 *Nucleation in condensed matter: applications in materials and biology*, , vol. 15. Elsevier.

Kerssemakers, J. W. J., Janson, M. E., van der Horst, A. & Dogterom, M. 2003 Optical trap setup for measuring microtubule pushing forces. *App. Phys. Lett.* **83** (21), 4441.

Keys, A. S., Abate, A. R., Glotzer, S. C. & Durian, D. J. 2007 Measurement of growing dynamical length scales and prediction of the jamming transition in a granular material. *Nat. Phys.* **3** (4), 260.

Keys, A. S., Garrahan, J. P. & Chandler, D. 2013 Calorimetric glass transition explained by hierarchical dynamic facilitation. *Proc. Nat. Acad. Sci., USA* **110** (12), 4482.

Keys, A. S., Hedges, L. O., Garrahan, J. P., Glotzer, S. C. & Chandler, D. 2011 Excitations are localized and relaxation is hierarchical in glass-forming liquids. *Phys. Rev. X* **1** (2), 021013.

Kim, S. H., Lee, S. Y., Yang, S.-M. & Yi, G. R. 2011 Self-assembled colloidal structures for photonics. *NPG Asia Materials* **3** (1), 25.

Kirkpatrick, S., Gelatt, C. D. & Vecchi, M. P. 1983 Optimization by simmulated annealing. *science* **220** (4598), 671.

Kirkpatrick, T. R. & Thirumalai, D. 1987*a* Dynamics of the structural glass transition and the p-spin-interaction spin-glass model. *Phys. Rev. Lett.* **58** (20), 2091.

Kirkpatrick, T. R. & Thirumalai, D. 1987*b* p-spin-interaction spin-glass models: Connections with the structural glass problem. *Phys. Rev. B* **36** (10), 5388.

Kirkpatrick, T. R., Thirumalai, D. & Wolynes, P. G. 1989 Scaling concepts for the dynamics of viscous liquids near an ideal glassy state. *Phys. Rev. A* **40** (2), 1045.

Kirkpatrick, T. R. & Wolynes, P. G. 1987*a* Connections between some kinetic and equilibrium theories of the glass transition. *Phys. Rev. A* **35** (7), 3072.

Kirkpatrick, T. R. & Wolynes, P. G. 1987*b* Stable and metastable states in mean-field potts and structural glasses. *Phys. Rev. B* **36** (16), 8552.

Knowlton, E. D., Pine, D. J. & Cipelletti, L. 2014 A microscopic view of the yielding transition in concentrated emulsions. *Soft Matter* **10** (36), 6931.

Kob, W. 1997 The mode-coupling theory of the glass transition. *arXiv preprint cond-mat/9702073* .

Kob, W. 1999 Computer simulations of supercooled liquids and glasses. *J. Phys.: Condens. Matter* **11** (10), R85.

Kob, W. 2003 Course 5: Supercooled liquids, the glass transition, and computer simulations. In *Slow relaxations and nonequilibrium dynamics in condensed matter*, p. 199. Springer.

Kob, W. & Andersen, H. C. 1994 Scaling behavior in the β-relaxation regime of a supercooled lennard-jones mixture. *Phys. Rev. Lett.* **73** (10), 1376.

Kob, W. & Andersen, H. C. 1995 Testing mode-coupling theory for a supercooled binary lennard-jones mixture. ii. intermediate scattering function and dynamic susceptibility. *Phys. Rev. E* **52** (4), 4134.

Kob, W., Donati, C., Plimpton, S. J., Poole, P. H. & Glotzer, S. C. 1997 Dynamical heterogeneities in a supercooled lennard-jones liquid. *Phys. Rev. Lett.* **79** (15), 2827.

Kob, W., Roldán-Vargas, S. & Berthier, L. 2012 Non-monotonic temperature evolution of dynamic correlations in glass-forming liquids. *Nat. Phys.* **8** (2), 164.

Kohlrausch, R. 1854 Theorie des elektrischen rückstandes in der leidener flasche. *Annalen der Physik* **167** (2), 179.

Koumakis, N., Brady, J. F. & Petekidis, G. 2013 Complex oscillatory yielding of model hard-sphere glasses. *Phys. Rev. Lett.* **110** (17), 178301.

Kraft, D. J., Groenewold, J. & Kegel, W. 2009 Colloidal molecules with well-controlled bond angles. *Soft Matter* **5** (20), 3823.

Kraft, D. J., Vlug, W. S., van Kats, C. M., van Blaaderen, A., Imhof, A. & Kegel, W. K. 2008 Self-assembly of colloids with liquid protrusions. *J. Am. Chem. Soc.* **131** (3), 1182.

Ladavac, K. & Grier, D. G. 2004 Microoptomechanical pumps assembled and driven by holographic optical vortex arrays. *Opt. Exp.* **12** (6), 1144.

Larsen, A. E. & Grier, D. G. 1996 Melting of metastable crystallites in charge-stabilized colloidal suspensions. *Phys. Rev. Lett.* **76** (20), 3862.

Larson, R. G. 1998 *The structure and rheology of complex fluids*, , vol. 688. Oxford University Press: New York.

Lawrence, D. B., Cai, T., Hu, Z., Marquez, M. & Dinsmore, A. D. 2007 Temperature-responsive semipermeable capsules composed of colloidal microgel spheres. *Langmuir* **23** (2), 395.

Leach, J., Wulff, K., Sinclair, G., Jordan, P., Courtial, J., Thomson, L., Gibson, G., K. Karunwi and, J. C., Laczik, Z. J. *et al.* 2006 Interactive approach to optical tweezers control. *App. Opt.* **45** (5), 897.

Lee, S.-H., Ladavac, K., Polin, M. & Grier, D. G. 2005 Observation of flux reversal in a symmetric optical thermal ratchet. *Phys. Rev. Lett.* **94** (11), 110601.

Lejcek, P. 2010 *Grain boundary segregation in metals*, , vol. 136. Springer Science & Business Media.

Lemaître, A. & Caroli, C. 2009 Rate-dependent avalanche size in athermally sheared amorphous solids. *Phys. Rev. Lett.* **103** (6), 065501.

Leonardo, R. D., Ianni, F. & Ruocco, G. 2007 Computer generation of optimal holograms for optical trap arrays. *Opt. Exp.* **15** (4), 1913.

Leunissen, M. E., Christova, C. G., Hynninen, A.-P., Royall, C. P., Campbell, A. I., Imhof, A., Dijkstra, M., Rene, R. V. R. & van Blaaderen, A. 2005 Ionic colloidal crystals of oppositely charged particles. *Nature* **437** (7056), 235.

Leutheusser, E. 1984 Dynamical model of the liquid-glass transition. *Phys. Rev. A* **29** (5), 2765.

Li, F., Josephson, D. P. & Stein, A. 2011 Colloidal assembly: the road from particles to colloidal molecules and crystals. *Angew. Chem. Int. Ed.* **50** (2), 360.

Liberatore, M. W., Nettesheim, F., Wagner, N. J. & Porcar, L. 2006 Spatially resolved small-angle neutron scattering in the 1-2 plane: A study of shear-induced phase-separating wormlike micelles. *Phys. Rev. E* **73** (2), 020504.

Liesener, J., Reicherter, M., Haist, T. & Tiziani, H. J. 2000 Multi-functional optical tweezers using computer-generated holograms. *Opt. Comm.* **185** (1), 77.

Lin, J., Saade, A., Lerner, E., Rosso, A. & Wyart, M. 2014 On the density of shear transformations in amorphous solids. *Europhys. Lett.* **105** (2), 26003.

Lipowsky, R. 1986 Melting at grain boundaries and surfaces. *Phys. Rev. Lett.* **57** (22), 2876.

Liu, J. 2003 Colloidal soft sphere crystallisation and phase behaviour. PhD thesis, Dissertation, Universität Mainz.

Liu, S. T., Jiao, W., Sun, B. A. & Wang, W. H. 2013 A quasi-phase perspective on flow units of glass transition and plastic flow in metallic glasses. *J. Non-Cryst. Solidis* **376**, 76.

Löwen, H. 1994 Melting, freezing and colloidal suspensions. *Phys. Rep.* **237** (5), 249.

Lubchenko, Vassiliy & Wolynes, P. G. 2007 Theory of structural glasses and supercooled liquids. *Annu. Rev. Phys. Chem* **58** (1), 235.

Lundberg, M., Krishan, K., Xu, N., Hern, C. S. O. & Dennin, M. 2008 Reversible plastic events in amorphous materials. *Phys. Rev. E* **77** (4), 041505.

Macosko, C. W. & Larson, R. G. 1994 Rheology: principles, measurements, and applications .

Malins, A., Eggers, J., Royall, C. P., Williams, S. R. & Tanaka, H. 2013*a* Identification of long-lived clusters and their link to slow dynamics in a model glass former. *J. Chem. Phys.* **138** (12), 12A535.

Malins, A., Eggers, J., Tanaka, H. & Royall, C. P. 2013*b* Lifetimes and lengthscales of structural motifs in a model glassformer. *Faraday Discussions* **167**, 405.

Maloney, C. & Lemaitre, A. 2004 Subextensive scaling in the athermal, quasistatic limit of amorphous matter in plastic shear flow. *Phys. Rev. Lett.* **93** (1), 016001.

Maloney, C. E. & Lemaitre, A. 2006 Amorphous systems in athermal, quasistatic shear. *Phys. Rev. E* **74** (1), 016118.

Mason, T. G. & Weitz, D. A. 1995 Optical measurements of frequency-dependent linear viscoelastic moduli of complex fluids. *Phys. Rev. Lett.* **74** (7), 1250.

Mattsson, J., Wyss, H. M., Fernandez-Nieves, A., Miyazaki, K., Hu, Z., Reichman, D. R. & Weitz, D. A. 2009 Soft colloids make strong glasses. *Nature* **462** (7269), 83.

Mazolli, A., Neto, P. A. M. & Nussenzveig, H. M. 2003 Theory of trapping forces in optical tweezers. *Proceedings of the Royal Society of London, Series A* **459** (2040), 3021.

McGloin, D. 2006 Optical tweezers: 20 years on. *Philosophical Transactions of the Royal Society of London A* **364** (1849), 3521.

Meister, M. & Winfield, R. J. 2002 Novel approaches to direct search algorithms for the design of diffractive optical elements. *Opt. Comm.* **203** (1), 39.

Meng, G., Arkus, N., Brenner, M. P. & Manoharan, V. N. 2010 The free-energy landscape of clusters of attractive hard spheres. *Science* **327** (5965), 560.

Menon, G. I. & Ramaswamy, S. 2009 Universality class of the reversible-irreversible transition in sheared suspensions. *Phys. Rev. E* **79** (6), 061108.

Merkle, K. L., Thompson, L. J. & Phillipp, F. 2002 Collective effects in grain boundary migration. *Phys. Rev. Lett.* **88** (22), 225501.

Miguel, C. & Rubi, M. 2006 *Jamming, yielding, and irreversible deformation in condensed matter*. Springer.

Miguel, M.-C., Vespignani, A., Zapperi, S., Weiss, J. & Grasso, J.-R. 2001 Intermittent dislocation flow in viscoplastic deformation. *Nature* **410** (6829), 667.

Minsky, M. 1988 Memoir on inventing the confocal scanning microscope. *Scanning* **10** (4), 128.

Mishra, C. K., Nagamanasa, K. H., Ganapathy, R., Sood, A. K. & Gokhale, S. 2014 Dynamical facilitation governs glassy dynamics in suspensions of colloidal ellipsoids. *Proc. Nat. Acad. Sci., USA* **111** (43), 15362.

Mishra, C. K., Rangarajan, A. & Ganapathy, R. 2013 Two-step glass transition induced by attractive interactions in quasi-two-dimensional suspensions of ellipsoidal particles. *Phys. Rev. Lett.* **110** (18), 188301.

Moffitt, J. R., Chemla, Y. R., Smith, S. & Bustamante, C. 2008 Recent advances in optical tweezers. *Annu. Rev. Biochem.* **77**, 205.

Mohan, L., Pellet, C., Cloitre, M. & Bonnecaze, R. 2013 Local mobility and microstructure in periodically sheared soft particle glasses and their connection to macroscopic rheology. *J. Rheol.* **57** (3), 1023.

Montanari, A. & Semerjian, G. 2006 Rigorous inequalities between length and time scales in glassy systems. *J. Stat. Phys.* **125** (1), 23.

Mrowec, S. & Marcinkiewicz, S. 1980 *Defects and diffusion in solids: an introduction*. Elsevier Amsterdam.

Nabarro, F. R. N. & Duesbery, M. S. 2002 *Dislocations in solids*, , vol. 11. Elsevier.

Nagamanasa, K. H., Gokhale, S., Ganapathy, R. & Sood, A. K. 2011 Confined glassy dynamics at grain boundaries in colloidal crystals. *Proc. Nat. Acad. Sci., USA* **108** (28), 11323.

Nagamanasa, K. H., Gokhale, S., Sood, A. K. & Ganapathy, R. 2014*a* Direct measurements of growing amorphous order and non-monotonic dynamic correlations in a colloidal glass-former. *arXiv preprint arXiv:1408.5485* .

Nagamanasa, K. H., Gokhale, S., Sood, A. K. & Ganapathy, R. 2014*b* Experimental signatures of a nonequilibrium phase transition governing the yielding of a soft glass. *Phys. Rev. E* **89** (6), 062308.

Neelima, K. 2014 *Exploring the Connections between Yielding and Microscopic Irreversibility in Athermal Amorphous Rafts*. JNCASR.

Neto, P. A. M. & Nussenzveig, H. M. 2000 Theory of optical tweezers. *Euro. Phys. Lett.* **50** (5), 702.

Nieh, T. G., Wadsworth, J. & Sherby, O. D. 2005 *Superplasticity in metals and ceramics*. Cambridge university press.

Nomura, M. & Adams, J. B. 1992 Self-diffusion along twist grain boundaries in cu. *J. Mat. Res.* **7** (12), 3202.

Nugent, C. R., Edmond, K. V., Patel, H. N. & Weeks, E. R. 2007 Colloidal glass transition observed in confinement. *Phys. Rev. Lett.* **99** (2), 025702.

Nugent-Glandorf, L. & Perkins, T. T. 2004 Measuring 0.1-nm motion in 1 ms in an optical microscope with differential back-focal-plane detection. *Opt. lett.* **29** (22), 2611.

Ojeda, J. F., Xie, C., Li, Y.-Q., Bertrand, F. E., Wiley, J. & McConnell, T. J. 2006 Chromosomal analysis and identification based on optical tweezers and raman spectroscopy. *Opt. Exp.* **14** (12), 5385.

Padgett, M. & Leonardo, R. D. 2011 Holographic optical tweezers and their relevance to lab on chip devices. *Lab on a Chip* **11** (7), 1196.

Palberg, T., Härtl, W., Wittig, U., Versmold, H., Würth, M. & Simnacher, E. 1992 Continuous deionization of latex suspensions. *J. Phys. Chem.* **96** (20), 8180.

Palberg, T., Mönch, W., Schwarz, J. & Leiderer, P. 1995 Grain size control in polycrystalline colloidal solids. *J. Chem Phys.* **102** (12), 5082.

Panine, P., Gradzielski, M. & Narayanan, T. 2003 Combined rheometry and small-angle x-ray scattering. *Rev. Sci. Instrum.* **74** (4), 2451.

Pawar, A. B. & Kretzschmar, I. 2009 Multifunctional patchy particles by glancing angle deposition. *Langmuir* **25** (16), 9057.

Pawar, A. B. & Kretzschmar, I. 2010 Fabrication, assembly, and application of patchy particles. *Macromol. Rapid Commun.* **31** (2), 150.

Peng, Y., Wang, F., Wang, Z., Alsayed, A. M., Zhang, Z., Yodh, A. G. & Han, Y. 2015 Two-step nucleation mechanism in solid–solid phase transitions. *Nat. Mater.* **14** (1), 101.

Pennycook, S. J. *et al.* 2000 Studies of high temperature superconductors: Microstructural studies in htsc. *Nova Science Publishers, New York* **30**, 145.

Perchikov, N. & Bouchbinder, E. 2014 Variable-amplitude oscillatory shear response of amorphous materials. *Phys. Rev. E* **89** (6), 062307.

Percus, J. K. & Yevick, G. J. 1958 Analysis of classical statistical mechanics by means of collective coordinates. *Phys. Rev.* **110** (1), 1.

Pertsinidis, A. & Ling, X. S. 2005 Video microscopy and micromechanics studies of one-and two-dimensional colloidal crystals. *New J. Phys.* **7** (1), 33.

Petekidis, G., Moussaid, A. & Pusey, P. N. 2002 Rearrangements in hard-sphere glasses under oscillatory shear strain. *Phys. Rev. E* **66** (5), 051402.

Pham, K. N., Puertas, A. M., Bergenholtz, J., Egelhaaf, S. U., Moussaid, A., Pusey, P. N., Schofield, A. B., Cates, M. E., Fuchs, M. & Poon, W. C. K. 2002 Multiple glassy states in a simple model system. *Science* **296** (5565), 104.

Pine, D. J., Gollub, J. P., Brady, J. F. & Leshansky, A. M. 2005 Chaos and threshold for irreversibility in sheared suspensions. *Nature* **438** (7070), 997.

Pluis, B., der Gon, A. W. D. V., Frenken, J. W. M. & van der Veen, J. F. 1987 Crystal-face dependence of surface melting. *Phys. Rev. Lett.* **59** (23), 2678.

Pomeau, Y. 1986 Front motion, metastability and subcritical bifurcations in hydrodynamics. *Physica D* **23** (1), 3.

Poon, W. 2004 Colloids as big atoms. *Science* **304** (5672), 830.

Porcar, L., Pozzo, D., Langenbucher, G., Moyer, J. & Butler, P. D. 2011 Rheo–small-angle neutron scattering at the national institute of standards and technology center for neutron research. *Rev. Sci. Instrum.* **82** (8), 083902.

Prasad, V., Semwogerere, D. & Weeks, E. R. 2007 Confocal microscopy of colloids. *J. Phys.: Condens. Matter* **19** (11), 113102.

Pusey, P. N. & van Megan, W. 1986 Phase behaviour of concentrated suspensions of nearly hard colloidal spheres. *Nature* **320** (6060), 340.

Pusey, P. N. & van Megen, W. 1987 Observation of a glass transition in suspensions of spherical colloidal particles. *Phys. Rev. Lett.* **59** (18), 2083.

Pusey, P. N. & van Megen, W. 1989 Dynamic light scattering by non-ergodic media. *Physica A* **157** (2), 705.

Pusey, P. N., van Megen, W., Bartlett, P., Ackerson, B. J., Rarity, J. G. & Underwood, S. M. 1989 Structure of crystals of hard colloidal spheres. *Phys. Rev. Lett.* **63** (25), 2753.

Quake, S. R. & Scherer, A. 2000 From micro-to nanofabrication with soft materials. *Science* **290** (5496), 1536.

Quincke, G. 1905 The formation of ice and the grained structure of glaciers. *Proceedings of the Royal Society of London, Series A* **76** (512), 431.

Rahmani, Y., Koopman, R., Denisov, D. & Schall, P. 2013 Probing incipient plasticity by indenting colloidal glasses. *Sci. Rep.* **3**.

Rahmani, Y., Koopman, R., Denisov, D. & Schall, P. 2014 Visualizing the strain evolution during the indentation of colloidal glasses. *Phys. Rev. E* **89** (1), 012304.

Ramsteiner, I. B., Weitz, D. A. & Spaepen, F. 2010 Stiffness of the crystal-liquid interface in a hard-sphere colloidal system measured from capillary fluctuations. *Phys. Rev. E* **82** (4), 041603.

Randle, V. 2010 Grain boundary engineering: an overview after 25 years. *Mat. Sci. and Tech.* **26** (3), 253.

Read, W. T. & Shockley, W. 1950 Dislocation models of crystal grain boundaries. *Phys. Rev.* **78** (3), 275.

Regev, I., Lookman, T. & Reichhardt, C. 2013 Onset of irreversibility and chaos in amorphous solids under periodic shear. *Phys. Rev. E* **88** (6), 062401.

Reicherter, M., Haist, T., Wagemann, E. U. & Tiziani, H. J. 1999 Optical particle trapping with computer-generated holograms written on a liquid-crystal display. *Opt. Lett.* **24** (9), 608.

Reichman, D. R. & Charbonneau, P. 2005 Mode-coupling theory. *J. Stat. Mech.* **2005** (05), P05013.

Richert, R. & Angell, C. A. 1998 Dynamics of glass-forming liquids. v. on the link between molecular dynamics and configurational entropy. *J. Chem. Phys.* **108**, 9016.

Richeton, T., Weiss, J. & Louchet, F. 2005 Breakdown of avalanche critical behaviour in polycrystalline plasticity. *Nat. Mater.* **4** (6), 465.

Riggleman, R. A., Yoshimoto, K., Douglas, J. F. & de Pablo, J. J. 2006 Influence of confinement on the fragility of antiplasticized and pure polymer films. *Phys. Rev. Lett.* **97** (4), 045502.

Ritort, F. & Sollich, P. 2003 Glassy dynamics of kinetically constrained models. *Adv. Phys.* **52** (4), 219.

Rodrigo, P. J., Daria, V. R. & Glückstad, J. 2004 Real-time three-dimensional optical micromanipulation of multiple particles and living cells. *Op. Lett.* **29** (19), 2270.

Rogers, S. A., Erwin, B. M., Vlassopoulos, D. & Cloitre, M. 2011*a* Oscillatory yielding of a colloidal star glass. *J. Rheol.* **55** (4), 733.

Rogers, S. A., Erwin, B. M., Vlassopoulos, D. & Cloitre, M. 2011*b* A sequence of physical processes determined and quantified in laos: Application to a yield stress fluid. *J. Rheol.* **55** (2), 435.

Rollett, A., Humphreys, F. J., Rohrer, G. S. & Hatherly, M. 2004 *Recrystallization and related annealing phenomena*. Elsevier.

Romanczuk, P., Bär, M., Ebelin, W., Lindner, B. & Schimansky-Geier, L. 2012 Active brownian particles. *Eur. Phys. J. Special Topics* **202** (1), 1.

Rosenhain, W. & Ewen, D. 1913 The intercrystalline cohesion of metals. *Journal of the Institute of Metals* **10**, 119.

Rosenhain, W. & Humphrey, J. 1913 The tenacity, deformations and fracture of soft steel at high temperatures. *Journal of the Steel Inst* **87**, 219–314.

Rossi, L., Sacanna, S., Irvine, W. T. M., Chaikin, P. M., Pine, D. J. & Philipse, A. P. 2011 Cubic crystals from cubic colloids. *Soft Matter* **7** (9), 4139.

Royall, C. P., Poon, W. C. K. & Weeks, E. R. 2013 In search of colloidal hard spheres. *Soft Matter* **9** (1), 17.

Sacanna, S., Irvine, W. T. M., Chaikin, P. M. & Pine, D. J. 2010 Lock and key colloids. *Nature* **464** (7288), 575.

Sacanna, S. & Pine, D. J. 2011 Shape-anisotropic colloids: Building blocks for complex assemblies. *Curr. Opin. Colloid Interface Sci.* **16** (2), 96.

Saiter, A., Saiter, J. M. & Grenet, J. 2006 Cooperative rearranging regions in polymeric materials: Relationship with the fragility of glass-forming liquids. *Euro. Poly. J.* **42** (1), 213.

Salje, E. K. H. & Dahmen, K. A. 2014 Crackling noise in disordered materials. *Annu. Rev. Condens. Matter Phys.* **5** (1), 233.

Sasa, L. A., Yearley, E. J., Welch, C. F., Taylor, M. A., Gilbertson, R. D., Hammeter, C., Majewski, J. & Hjelm, R. P. 2010 The los alamos neutron science center neutron rheometer in the cone and plate geometry to examine tethered polymers/polymer melt interfaces via neutron reflectivity. *Rev. Sci. Instrum.* **81** (5), 055102.

Savage, J. R., Hopp, S. F., Ganapathy, R., Gerbode, S. J., Heuer, A. & Cohen, I. 2013 Entropy-driven crystal formation on highly strained substrates. *Proc. Nat. Acad. Sci., USA* **110** (23), 9301.

Schall, P., Cohen, I., Weitz, D. A. & Spaepen, F. 2004 Visualization of dislocation dynamics in colloidal crystals. *Science* **305** (5692), 1944.

Schall, P., Cohen, I., Weitz, D. A. & Spaepen, F. 2006 Visualizing dislocation nucleation by indenting colloidal crystals. *Nature* **440** (7082), 319.

Schall, P., Weitz, D. A. & Spaepen, F. 2007 Structural rearrangements that govern flow in colloidal glasses. *Science* **318** (5858), 1895.

Scheidler, P., Kob, W. & Binder, K. 2002 Cooperative motion and growing length scales in supercooled confined liquids. *Euro. Phys. Lett.* **59** (5), 701.

Schmitz, C., Spatz, J. & Curtis, J. 2005 High-precision steering of multiple holographic optical traps. *Opt. Exp.* **13** (21), 8678.

Schweitzer, F. 2007 *Brownian agents and active particles: collective dynamics in the natural and social sciences*. Springer Science & Business Media.

Scott, G. D. 1960 Packing of spheres: Packing of equal spheres. *Nature* (188), 908.

Semwogerere, D. & Weeks, E. R. 2005 Confocal microscopy. *Encycl. Biomat. and Biomed. Engg.* p. 1.

Shan, Z., Stacha, E. A., Wiezorek, J. M. K., Knapp, J. A., Follstaedt, D. M. & Mao, S. X. 2004 Grain boundary-mediated plasticity in nanocrystalline nickel. *Science* **305** (5684), 654.

Shan, Z. W., Li, J., Cheng, Y. Q., Minor, A. M., Asif, S. A. S., Warren, O. L. & Ma, E. 2008 Plastic flow and failure resistance of metallic glass: Insight from in situ compression of nanopillars. *Phys. Rev. B* **77** (15), 155419.

Sheppard, C. J. R. & Shotton, D. M. 1997 *Confocal laser scanning microscopy*. BIOS Scientific Publishers.

Shevchenko, E. V., Talapin, D. V., Kotov, N. A., O'Brien, S. & Murray, C. B. 2006 Structural diversity in binary nanoparticle superlattices. *Nature* **439** (7072), 55.

Singh, M., Haverinen, H. M., Dhagat, P. & Jabbour, G. E. 2010 Inkjet printing-process and its applications. *Adv. Mater.* **22** (6), 673.

Singh, S., Ediger, M. D., & de Pablo, J. J. 2013 Ultrastable glasses from in silico vapour deposition. *Nat. Mater.* **12** (2), 139.

Skinner, T. O. E., Aarts, D. G. A. L. & Dullens, R. P. A. 2010 Grain-boundary fluctuations in two-dimensional colloidal crystals. *Phys. Rev. Lett.* **105** (16), 168301.

Skinner, T. O. E., Aarts, D. G. A. L. & Dullens, R. P. A. 2011 Supercooled dynamics of grain boundary particles in two-dimensional colloidal crystals. *J. Chem Phys.* **135** (12), 124711.

Smallenburg, F., Filion, L. & Sciortino, F. 2014 Erasing no-man's land by thermodynamically stabilizing the liquid-liquid transition in tetrahedral particles. *Nat. Phys.* **10**, 653.

van der Sman, R. G. M. 2012 Soft matter approaches to food structuring. *Adv. Colloid Interface Sci.* **176**, 18.

Smith, S. B., Cui, Y. & Bustamante, C. 1996 Overstretching b-dna: the elastic response of individual double-stranded and single-stranded dna molecules. *Science* **271** (5250), 795.

Snoeks, E., van Blaaderen, A., van Dillen, T., van Kats, C. M., Brongersma, M. L. & Polman, A. 2000 Colloidal ellipsoids with continuously variable shape. *Adv. Mater.* **12** (20), 1511.

Sollich, P. 1998 Rheological constitutive equation for a model of soft glassy materials. *Phys. Rev. E* **58** (1), 738.

Sollich, P., Lequeux, F., Hébraud, P. & Cates, M. E. 1997 Rheology of soft glassy materials. *Phys. Rev. Lett.* **78** (10), 2020.

Starr, F. W., Douglas, J. F. & Sastry, S. 2013 The relationship of dynamical heterogeneity to the adam-gibbs and random first-order transition theories of glass formation. *J. Chem .Phys.* **138** (12), 12A541.

Steinhardt, P. J., Nelson, D. R. & Ronchetti, M. 1983 Bond-orientational order in liquids and glasses. *Phys. Rev. B* **28** (2), 784.

Stevenson, J. D., Schmalian, J. & Wolynes, P. G. 2006 The shapes of cooperatively rearranging regions in glass-forming liquids. *Nat. Phys.* **2** (4), 268.

Stevenson, J. D. & Wolynes, P. G. 2010 A universal origin for secondary relaxations in supercooled liquids and structural glasses. *Nat. Phys.* **6** (1), 62.

Sun, B. A., Yu, H. B., Jiao, W., Bai, H. Y., Zhao, D. Q. & Wang, W. H. 2010 Plasticity of ductile metallic glasses: A self-organized critical state. *Phys. Rev. Lett.* **105** (3), 35501.

Suresh, S. 2006 Crystal deformation: Colloid model for atoms. *Nat. Mater.* **5** (4), 253.

Swallen, S. F., Kearns, K. L., Mapes, M. K., Kim, Y. S., McMahon, R. J., Ediger, M. D., Wu, T., Yu, L. & Satija, S. 2007 Organic glasses with exceptional thermodynamic and kinetic stability. *Science* **315** (5810), 353.

Tammann, G. & Hesse, W. Z. 1926 Die abhangigkeit der viscositat von der temperatur bie unterkuhlten flussigkeiten. *Z. Anorg. Allg. Chem.* **156**.

Tanaka, H., Kawasaki, T., Shintani, H. & Watanabe, K. 2010 Critical-like behaviour of glass-forming liquids. *Nat. Mater.* **9** (4), 324.

Tanguy, A., Mantisi, B. & Tsamados, M. 2010 Vibrational modes as a predictor for plasticity in a model glass. *Euro. Phys. Lett.* **90** (1), 16004.

Tarjus, G., Kivelson, S. A., Nussinov, Z. & Viot, P. 2005 The frustration-based approach of supercooled liquids and the glass transition: a review and critical assessment. *J. Phys.: Condens. Matter* **17** (50), R1143.

Thiele, E. 1963 Equation of state for hard spheres. *J. Chem. Phys.* **39** (2), 474.

Tjhung, E. & Berthier, L. 2015 Suppressed density fluctuations and diverging dynamic correlations in periodically driven colloidal suspensions. *arXiv preprint arXiv:1501.05633* .

Trautt, Z. T. & Upmanyu, M. 2005 Direct two-dimensional calculations of grain boundary stiffness. *Scripta Materialia* **52** (11), 1175.

Trautt, Z. T., Upmanyu, M. & Karma, A. 2006 Interface mobility from interface random walk. *Science* **314** (5799), 632.

Tsamados, M., Tanguy, A., Goldenberg, C. & Barrat, J.-L. 2009 Local elasticity map and plasticity in a model lennard-jones glass. *Phys. Rev. E* **80** (2), 026112.

Tsekenis, G., Uhl, J. T., Goldenfeld, N. & Dahmen, K. A. 2013 Determination of the universality class of crystal plasticity. *Euro. Phys. Lett.* **101** (3), 36003.

Turnbull, D. & Cohen, M. H. 1970 On the free-volume model of the liquid-glass transition. *J. Chem. Phys.* **52** (6), 3038.

Ubbink, J., Burbidge, A. & Mezzenga, R. 2008 Food structure and functionality: a soft matter perspective. *Soft Matter* **4** (8), 1569.

Uchic, M. D. & Dimiduk, D. M. 2005 A methodology to investigate size scale effects in crystalline plasticity using uniaxial compression testing. *Materials Science and Engineering: A* **400**, 268.

Uchic, M. D., Dimiduk, D. M., Florando, J. N. & Nix, W. D. 2004 Sample dimensions influence strength and crystal plasticity. *Science* **305** (5686), 986.

Upmanyu, M., Srolovitz, D. J., Shvindlerman, L. S. & Gottstein, G. 1999 Misorientation dependence of intrinsic grain boundary mobility: simulation and experiment. *Acta Materialia* **47** (14), 3901.

van der Vaart, K., Rahmani, Y., Zargar, R., Z. Hu, D. B. & Schall, P. 2013 Rheology of concentrated soft and hard-sphere suspensions. *J. Rheol.* **57**, 1195.

Valiev, R. 2004 Nanostructuring of metals by severe plastic deformation for advanced properties. *Nat. Mater.* **3** (8), 511.

Velikov, K. P., Christova, C. G., Dullens, R. P. A. & van Blaaderen, A. 2002 Layer-by-layer growth of binary colloidal crystals. *Science* **296** (5565), 106.

Villain, J. 1985 Equilibrium critical properties of random field systems: new conjectures. *Journal de Physique* **46** (11), 1843.

de Villeneuve, V. W. A., Derendorp, L., Verboekend, D., Vermolen, E. C. M., Kegel, W. K., Lekkerkerker, H. N. W. & Dullens, R. P. A. 2009 Grain boundary pinning in doped hard sphere crystals. *Soft Matter* **5** (12), 2448.

de Villeneuve, V. W. A., Dullens, R. P. A., Aarts, D. G. A. L., Groeneveld, E., Scherff, J. H., Kegel, W. K. & Lekkerkerker, H. N. W. 2005 Colloidal hard-sphere crystal growth frustrated by large spherical impurities. *Science* **309** (5738), 1231.

Vlasov, Y. A., Bo, X.-Z., Sturm, J. C. & Norris, D. J. 2001 On-chip natural assembly of silicon photonic bandgap crystals. *Nature* **414** (6861), 289.

Vogel, H. 1921 The law of the relation between the viscosity of liquids and the temperature. *Phys. Z* **22**, 645.

Vogel, M. & Glotzer, S. C. 2004 Spatially heterogeneous dynamics and dynamic facilitation in a model of viscous silica. *Phys. Rev. Lett.* **92** (25), 255901.

Vogel, N., Weiss, C. K. & Landfester, K. 2012 From soft to hard: the generation of functional and complex colloidal monolayers for nanolithography. *Soft Matter* **8** (15), 4044.

Vossen, D. L. J., van der Horst, A., Dogterom, M. & van Blaaderen, A. 2004 Optical tweezers and confocal microscopy for simultaneous three-dimensional manipulation and imaging in concentrated colloidal dispersions. *Rev. Sci. Instrum.* **75** (9), 2960.

W. Götze, J. P. Hansen, D. L. & Zinn-Justin, J. 1991 Liquids, freezing and the glass transition (les houches session li, 1989).

Wang, G., Chan, K. C., Xia, L., Yu, P., Shen, J. & Wang, W. H. 2009 Self-organized intermittent plastic flow in bulk metallic glasses. *Acta Mater.* **57** (20), 6146–6155.

Wang, Y., Wang, Y., Breed, D. R., Manoharan, V. N., Feng, L., Hollingsworth, A. D., Weck, M. & Pine, D. J. 2012*a* Colloids with valence and specific directional bonding. *Nature* **491** (7422), 51.

Wang, Z., Wang, F., Peng, Y., Zheng, Z. & Han, Y. 2012*b* Imaging the homogeneous nucleation during the melting of superheated colloidal crystals. *Science* **338** (6103), 87.

Weeks, E. R., Crocker, J. C., Levitt, A. C., Schofield, A. & Weitz, D. A. 2000 Three-dimensional direct imaging of structural relaxation near the colloidal glass transition. *Science* **287** (5453), 627.

Weeks, J. D., Chandler, D. & Andersen, H. C. 1971 Role of repulsive forces in determining the equilibrium structure of simple liquids. *J. Chem. Phys.* **54** (12), 5237.

Weiss, J. & Grasso, J.-R. 1997 Acoustic emission in single crystals of ice. *J. Phys. Chem. B* **101** (32), 6113.

Weiss, J. & Marsan, D. 2003 Three-dimensional mapping of dislocation avalanches: clustering and space/time coupling. *Science* **299** (5603), 89.

Wertheim, M. S. 1963 Exact solution of the percus-yevick integral equation for hard spheres. *Phys. Rev. Lett.* **10** (8), 321.

Whitelam, S., Berthier, L. & Garrahan, J. P. 2004 Dynamic criticality in glass-forming liquids. *Phys. Rev. Lett.* **92** (18), 185705.

Widmer-Cooper, A. & Harrowell, P. 2006 Predicting the long-time dynamic heterogeneity in a supercooled liquid on the basis of short-time heterogeneities. *Phys. Rev. Lett.* **96** (18), 185701.

Widmer-Cooper, A., Perry, H., Harrowell, P. & Reichman, D. R. 2008 Irreversible reorganization in a supercooled liquid originates from localized soft modes. *Nat. Phys.* **4** (9), 711.

Williams, G. & Watts, D. C. 1970 Non-symmetrical dielectric relaxation behaviour arising from a simple empirical decay function. *T. Faraday Soc.* **66**, 80.

Wolf, D. 2001 High-temperature structure and properties of grain boundaries: long-range vs. short-range structural effects. *Current Opinion in Solid State and Material Science* **5** (5), 435.

Wood, W. W. & Jacobson, J. U. D. 1957 Preliminary results from a recalculation of the monte carlo equation of state of hard spheres. *J. Chem. Phys.* **27** (5), 1207.

Wu, J., Zhou, B. & Hu, Z. 2003 Phase behavior of thermally responsive microgel colloids. *Phys. Rev. Lett.* **90** (4), 048304.

Wu, Y. L., Derks, D., van Blaaderen, A. & Imhof, A. 2009 Melting and crystallization of colloidal hard-sphere suspensions under shear. *Proc. Nat. Acad. Sci., USA* **106** (26), 10564.

Xia, X. & Wolynes, P. G. 2001 Microscopic theory of heterogeneity and nonexponential relaxations in supercooled liquids. *Phys. Rev. Lett.* **86** (24), 5526.

Xu, X., Rosi, N. L., Wang, Y., Huo, F. & Mirkin, C. A. 2006 Asymmetric functionalization of gold nanoparticles with oligonucleotides. *J. Am. Chem. Soc.* **128** (29), 9286.

Yin, Y., Lu, Y., Gates, B. & Xia, Y. 2001 Template-assisted self-assembly: a practical route to complex aggregates of monodispersed colloids with well-defined sizes, shapes, and structures. *J. Am. Chem. Soc.* **123** (36), 8718.

Yip, S. 2007 *Handbook of materials modeling*. Springer Science & Business Media.

Yonezawa, F. 1991 Solid state physics vol. 45.

Yoshizawa, K., Okuzono, T., Koga, T., Taniji, T. & Yamanaka, J. 2011 Exclusion of impurity particles during grain growth in charged colloidal crystals. *Langmuir* **27** (22), 13420.

Yunker, P., Zhang, Z., Aptowicz, K. B. & Yodh, A. G. 2009 Irreversible rearrangements, correlated domains, and local structure in aging glasses. *Phys. Rev. Lett.* **103** (11), 115701.

Zaiser, M., Marmo, B. & Moretti, P. 2005 The yielding transition in crystal plasticity-discrete dislocations and continuum models. In *Proceedings of the International Conference on Statistical Mechanics of Plasticity and Related Instabilities*.

Zhang, G., Wang, D., Dayang, H. & Möhwald, H. 2005 Decoration of microspheres with gold nanodots-giving colloidal spheres valences. *Angew. Chem. Inter. Ed.* **44** (47), 7767.

Zhang, H., Srolovitz, D. J., Douglas, J. F. & Warren, J. A. 2009 Grain boundaries exhibit the dynamics of glass-forming liquids. *Proc. Nat. Acad. Sci., USA* **106** (19), 7735.

Zhang, Z., Yunker, P. J., Habdas, P. & Yodh, A. G. 2011 Cooperative rearrangement regions and dynamical heterogeneities in colloidal glasses with attractive versus repulsive interactions. *Phys. Rev. Lett.* **107** (20), 208303.

Zheng, Z., Ni, R., Wang, F., Dijkstra, M., Wang, Y. & Han, Y. 2014 Structural signatures of dynamic heterogeneities in monolayers of colloidal ellipsoids. *Nat. Comm.* **5**.

Zheng, Z., Wang, F. & Han, Y. 2011 Glass transitions in quasi-two-dimensional suspensions of colloidal ellipsoids. *Phys. Rev. Lett.* **107** (6), 065702.

Ziff, M. R., Gulari, E. & Barshad, Y. 1986 Kinetic phase transitions in an irreversible surface-reaction model. *Phys. Rev. Lett.* **56** (24), 2553.

List of Publications

Publications from the Thesis:

1. K Hima Nagamanasa, Shreyas Gokhale, A. K. Sood & Rajesh Ganapathy. Direct measurements of growing amorphous order and non-monotonic dynamic correlations in a colloidal glass-former.
   Nature Phys. (accepted 2015); arXiv:1408.5485 (2014).
   Chapter: 3

2. K Hima Nagamanasa, Shreyas Gokhale, A. K. Sood & Rajesh Ganapathy. Experimental signatures of a nonequilibrium phase transition governing the yielding of a soft glass.
   Phys. Rev. E, 89(6), 062308 (2014).
   Chapter: 4

3. K Hima Nagamanasa, Shreyas Gokhale, Rajesh Ganapathy & A. K. Sood. Confined glassy dynamics at grain boundaries in colloidal crystals.
   Proc. Natl. Acad. Sci. USA, 108(28), 11323-11326 (2011).
   Chapter: 5

4. Shreyas Gokhale, K Hima Nagamanasa, Rajesh Ganapathy & A. K. Sood. Grain growth and grain boundary dynamics in colloidal polycrystals.
   Soft Matter, 9(29), 6634-6644 (2013).
   Chapter: 5

Other Publications:

1. Shreyas Gokhale, K Hima Nagamanasa, A. K. Sood & Rajesh Ganapathy. Directional grain growth from anisotropic kinetic roughening of grain boundaries in sheared colloidal crystals.
   Proc. Natl. Acad. Sci. USA, 109(50), 20314-20319 (2012).

2. Shreyas Gokhale, K Hima Nagamanasa, Rajesh Ganapathy & A. K. Sood . Growing dynamical facilitation on approaching the random pinning colloidal glass transition.
   Nat. Commun, 5, 4685 (2014).

3. Chandan K. Mishra, K Hima Nagamanasa, Rajesh Ganapathy, A. K. Sood & Shreyas Gokhale. Dynamical facilitation governs glassy dynamics in suspensions of colloidal ellipsoids.
   Proc. Natl. Acad. Sci. USA, 111, 15362-15367 (2014).

4. Giridhar U. Kulkarni, Ritu Gupta, K. Hima Nagamanasa & Rajesh Ganapathy. Viscoelastic nature of Au nanoparticle-PDMS nanocomposite gels.
   Submitted, 2015.

5. Shreyas Gokhale, Rajesh Ganapathy, A. K. Sood & K Hima Nagamanasa . Direct evidence of a crossover from facilitation to hopping in a colloidal glass-former.
Under preparation.